Environmental Public Health Surveillance of Freshwater Harmful Algal Blooms in Washington State Using Drone Technology

Joseph Teresi

A thesis

submitted in partial fulfillment of the

requirements for the degree of

Master of Science, Environmental Health Sciences

University of Washington

2024

Committee:

Tania Busch Isaksen

Scott Meschke

Stefan Grozev

Program Authorized to Offer Degree:

Environmental and Occupational Health Sciences

School of Public Health

University of Washington

Abstract

Environmental Public Health Surveillance of Freshwater Harmful Algal Blooms in Washington State Using Drone Technology

Joseph Teresi

Chair of the Supervisory Committee:

Dr. Tania Busch Isaksen, PhD, MPH

Department of Environmental and Occupational Health Sciences

Freshwater harmful cyanobacterial blooms (HCBs) present a mounting threat to public health outcomes and lake ecosystem services. The current climate crisis is expected to intensify the occurrence of freshwater HCBs in recreational water bodies, their formation of potent toxins, and resultant human exposures. Novel technological approaches like remote sensing are increasingly applied as an environmental monitoring tool for timely detection of HCBs. For this study, we used remotely piloted drones equipped with high-resolution cameras to capture aerial imagery at an urbanized lake in Washington State. Color band manipulation of the drone imagery was leveraged to estimate levels of chlorophyll a—the photosynthetic pigment found in all algae and cyanobacteria—as a proxy for phytoplankton biomass at the lake surface. Using simple linear regression models, we tested ten vegetation indices against lake water samples collected for chlorophyll a validation. The best estimates of chlorophyll a variation were provided by the Color Index of Vegetation Extraction (CIVE) index ($R^2 = 0.45$, $p < 0.001$). Challenges associated with this drone application were documented and insights into optimal field operation

and environmental conditions needed for successful implementation were incorporated into a guidance document for local practitioners. Drones represent a relatively inexpensive, user-friendly, and time-efficient monitoring tool to estimate phytoplankton biomass in smaller-scale lakes. These findings suggest remote sensing capabilities will help freshwater resource managers better anticipate the development of HCBs and more rapidly communicate this environmental public health risk.

Table of Contents

List of Appendices

List of Tables

List of Figures

List of Equations

Equation 1. Jeffrey and Humphrey's Trichromatic Equations (Arar, 1997):

$C_{E,a}$ = 11.85 (Abs 664) - 1.54 (Abs 647) - 0.08 (Abs 630)

$C_{E,b}$ = 21.03 (Abs 647) - 5.43 (Abs 664) - 2.66 (Abs 630)

$C_{E,c}$ = 24.52 (Abs 630) - 7.60 (Abs 647) - 1.67 (Abs 664)

where:

$C_{E,a}$ = concentration (mg/L) of chlorophyll a in the extraction solution analyzed.

$C_{E,b}$ = concentration (mg/L) of chlorophyll b in the extraction solution analyzed.

$C_{E,c}$ = concentration (mg/L) of chlorophyll c_1 + c_2 in the extraction solution analyzed.

Abs = 750 nm-corrected absorbance value (difference between the uncorrected absorbance value at 664, 647, and 630 nm with the absorbance value at 750 nm, representing turbidity).

Equation 2. Lorenzen's Modified Monochromatic Equations (Arar, 1997):

$C_{E,a}$ = 26.7 (Abs 664_b - Abs 665_a)

$P_{E,a}$ = 26.7 [1.7 * (Abs 665_a) - (Abs 664_b)]

where:

$C_{E,a}$ = concentration (mg/L) of chlorophyll a in the extraction solution analyzed.

$P_{E,a}$ = concentration (mg/L) of pheophytin a in the extraction solution analyzed.

Abs 664_b = absorbance at 664 nm (minus absorbance at 750 nm) measured before acidification.

Abs 665_a = absorbance at 665 nm (minus absorbance at 750 nm) measured after acidification.

Equation 3. Generalized Equation for Whole Water Sample Pigment Concentration (Arar, 1997):

$C_s = [(C_{E(a,b, or\ c)} * \text{Extract Volume (L)} * DF) / (\text{Sample Volume (L)} * \text{Cell Length (cm)})]$

where:

C_s = concentration (mg/L) of pigment in the whole water sample.

$C_{E(a,b, or\ c)}$ = concentration (mg/L) of pigment in extract measured in the cuvette.

Extract Volume = volume (L) of extract (before any dilutions).

DF = any dilution factors.

Sample Volume = volume (L) of whole water sample that was filtered.

Cell Length = optical path length (cm) of cuvette used.

Abbreviations and Acronyms

APHA: American Public Health Association

CDC: Centers for Disease Control and Prevention

cm: centimeters

DEOHS: Department of Environmental and Occupational Health Sciences

DI: deionized

DOH: Washington State Department of Health

DSM: Digital Surface Model

DUP: Duplicate

Ecology: Washington State Department of Ecology

ELNA: Echo Lake Neighborhood Association

EOHML: Environmental and Occupational Health Microbiology Lab

EXIF: Exchangeable Image File Format

FAA: Federal Aviation Administration

GCP: Ground Control Point

GNSS: Global Navigation Satellite System

HASP: Health and Safety Plan

HCB: Harmful Cyanobacterial Bloom

HPLC: High-Performance Liquid Chromatography

L: liters

LCMP: Lake Cyanobacteria Management Plan

LHJ: Local Health Jurisdiction

m: meters

mg/L: milligrams per liter

mL: milliliters

N HCl: Normalized Hydrochloric Acid

NALMS: North American Lake Management Society

NHERI: Natural Hazards Engineering Research Infrastructure

NIR: Near Infrared

nm: nanometers

NRDC: Natural Resources Defense Council

OD: Optical Density

OHHABS: One Health Harmful Algal Bloom System

PHI: Population Health Initiative

ppb: parts per billion

QA/QC: Quality Assurance/Quality Control

QALYs: Quality-Adjusted Life Years

QQ: Quantile-Quantile

qPCR: Quantitative Polymerase Chain Reaction

r: Pearson's Correlation Coefficient

R^2: Coefficient of Determination

RAPID: University of Washington Natural Hazards Reconnaissance Facility

RGB: Red-Green-Blue

RFC: Relative Centrifugal Force

RTK: Real Time Kinematic

SE: standard error

SfM: Structure from Motion

SSS: Stock Standard Solution

SW: Surface Water

TSI: Trophic State Index

µg/L: micrograms per liter

µL: microliters

USEPA: United States Environmental Protection Agency

UTM: Universal Transverse Mercator

UW: University of Washington

VFR: Visual Flight Rules

VI: Vegetation Index

WGS: World Geodetic System

WHO: World Health Organization

95% CI: 95% Confidence Interval

Acknowledgments

Funding for this thesis project was acquired through the University of Washington Population Health Initiative (PHI), a program that fosters interdisciplinary research across human health, environmental resilience, and social and economic equity. A Tier I pilot research grant was awarded by PHI in May 2023 to facilitate a proof-of-concept project relating ecological health and public health. The PHI grant application and final report are provided in Appendices A and B, respectively. In addition, the Department of Environmental and Occupational Health Sciences (DEOHS) generously provided matching funds for this pilot project.

I want to thank my advisor Dr. Tania Busch Isaksen for encouraging me to pursue a research project specific to my interests and for the constant support throughout this process. Our frequent check-ins and her reassurance to set lofty goals for my efforts were influential in helping me get to the finish line. I also want to thank Dr. Scott Meschke for his technical support, connections with pertinent contacts, and for challenging me to think critically about the different aspects of this project. Stefan Grozev and the members of the Friends of Echo Lake community group were instrumental in providing on-the-ground assistance and feedback for this work and I am very grateful for their support. Special thanks also to Dr. Gordon Holtgrieve of the School of Aquatic & Fishery Sciences for his support in facilitating this pilot project as well as providing technical support and constructive feedback along the way.

I also want to thank members of the Environmental and Occupational Health Microbiology Lab (EOHML), including Nicky Beck, Rachel Swan, Lisa Stutz, and Stella Christoforou for their technical support with water sampling and analysis activities as well as taking the time to troubleshoot issues. Additionally, I want to thank members of the UW RAPID staff: Dr. Mike Grilliot, Andrew Lyda, Karen Dedinsky, Jaqueline Zdebski, and Kandai

Shimada. Their assistance with drone operation and photogrammetry analysis, as well as generous use of their lab space, were very much appreciated throughout the project period.

In addition, I want to acknowledge lab members of the Collaborative on Extreme Event Resilience for their support and feedback throughout this research project's development. I am thankful for the constructive feedback given for this work by faculty and students of the UW Future Rivers Program as well. I also want to thank DEOHS administrative staff that supported my graduate experience and professional development. Trina Sterry, Janet Hang, Amy Gundlach Ritter, Dan Poux, and Kylie Milano provided critical administrative support and check-ins during my graduate career. I also want to acknowledge Helen Lee and Caroline Deurwarder for project budgeting support. I owe a lot of gratitude to Brian High and Dr. Chris Zuidema for their critical support with R programming and statistical analysis for this project as well.

My DEOHS cohort, friends, and family provided non-stop support throughout this entire process and I am forever in their debt. A special thank you to my partner Jessica Lechtenberg for the constant support and insight and for always believing in me.

Introduction

Freshwater cyanobacterial harmful algal blooms (HCBs) are an emerging hazard in environmental public health. Commonly referred to as “blue-green algae,” cyanobacteria are in fact prokaryotic, gram-negative bacteria with the ability to photosynthesize—structurally related to bacteria and functionally related to algae (Graham et al., 2008). Cyanobacteria are among the earth’s oldest and most widespread organisms, greatly contributing to the oxygenation of the planet’s atmosphere billions of years ago and maintaining the global nitrogen cycle through nitrogen fixation today (Merel et al., 2013; Zepernick et al., 2023). Despite these apparent benefits, cyanobacteria have the potential to grow out of control in freshwater bodies and cause ecological damage and human health risks. Cyanobacterial blooms, or high phytoplankton cell densities [typically 20,000 to 100,000 cells per milliliter (mL)] dominated by cyanobacteria species, can accumulate at the water surface and become harmful when they produce undesirable metabolic byproducts (Graham et al., 2008). These metabolites include taste-and-odor compounds like 2-methylisoborneol and geosmin as well as cyanotoxins—notably hepatotoxins like microcystins and cylindrospermopsins, and neurotoxins like anatoxins and saxitoxins (Merel et al., 2013). These compounds can negatively impact human health through consumption of contaminated drinking water or swimming in HCB-impacted recreational water bodies.

Cyanobacteria species thrive under specific environmental factors, including elevated nutrient concentrations (mainly nitrogen and phosphorus), increased light intensities, higher water temperatures, higher turbidity, reduced water flow and mixing, and longer lake residence times with lower flushing rates (Merel et al., 2013; Bormans et al., 2016). These factors are likely to increase in the face of global climate change, with meteorological and hydrological fluctuations increasing the distribution, frequency, duration, and magnitude of HCBs (Zepernick

et al., 2023). Along with elevated atmospheric temperatures and carbon dioxide concentrations, an increase in rainstorms can facilitate nutrient loading to lakes and cause eutrophication. Nutrient sources include stormwater, wastewater, and agricultural discharges. This nutrient over-enrichment can create conditions in which toxic blooms are preferentially selected over non-toxic blooms (Otten & Paerl, 2015). Nutrient pollution currently impacts more than one-third of lakes and about half of all rivers and streams in the U.S. (NRDC, 2019). In addition, once cyanobacteria begin to dominate a lake, they can become self-sustaining. As cyanobacteria cells decompose, they consume dissolved oxygen in the process and promote anoxic waters; consequently, this change in water chemistry can release nutrients such as phosphorus from lake sediments—termed internal loading—and fuel continued growth (Bormans et al., 2016). This oxidation-reduction reaction acts as a negative feedback loop for HCBs (Bormans et al., 2016)

Furthermore, cyanobacteria possess unique traits that make them competitive and successful over other phytoplankton. This includes the ability to regulate their position in the water column through the use of gas vesicle structures (Zepernick et al., 2023). This buoyancy mechanism allows cyanobacteria to migrate to more favorable light or nutrient conditions in a lake at different times of day, such as from the air-water interface to the soil-water interface. High uptake efficiency of carbon dioxide, nitrogen, and phosphorus also make cyanobacteria opportunistic over other phytoplankton (Zepernick et al., 2023). While not all species of cyanobacteria are able to fix nitrogen from the atmosphere, the species that can effectively eliminate this nutrient limitation, conferring an additional evolutionary advantage (Zepernick et al., 2023). The production of toxic metabolites is another survival strategy, preventing cyanobacteria consumption by herbivorous organisms. Environmental factors that may influence these toxic compounds include nutrient levels, water chemistry and flow characteristics, light

intensity, allelopathy and competition (e.g., biochemical inhibition), zooplankton grazing, and biomass growth rates (Merel et al., 2013). Due to these complex environmental and biological interactions within lake ecosystems, formation of HCBs and their expressed cyanotoxins are quite variable in time and space. This is made more complicated by the fact that not all HCB-forming species will produce toxins since these metabolites are strain-specific and gene-controlled (Merel et al., 2013). In the context of environmental public health surveillance, understanding the timing, location, and toxicity of an HCB becomes a significant challenge.

Moreover, the human health effects of cyanotoxins cannot be overstated. The most common routes of exposure are through direct consumption, dermal contact, and inhalation of aerosolized water spray (Otten & Paerl, 2015). The wide array of cyanotoxins primarily target the hepatic, neurological, and cellular systems and can cause both acute (e.g., liver failure, paralysis) and chronic (e.g., endocrine disruption, cancer) health impacts (Otten & Paerl, 2015). The skin, gastrointestinal tract, kidney, lungs, and heart are also considered target organs (Abdallah et al., 2021). While reports of cyanotoxicosis are rare in developed countries—with the exception of animals and livestock—this health hazard disproportionately impacts human populations in developing countries with tropical and subtropical climates (Pírez et al., 2013; Abdallah et al., 2021). Reliance on local drinking water reservoirs that are vulnerable to climate change and nutrient pollution, lack of adequate surveillance or analytical testing capabilities, and insufficient or nonexistent water treatment technologies result in higher exposures and resultant diseases (Otten & Paerl, 2015; Pírez et al., 2013; Abdallah et al., 2021). Furthermore, a narrative literature review on the health risks of HCBs was conducted, incorporating a risk assessment framework. The purpose of the review was to understand the current state of knowledge on the

human health risks of freshwater HCBs and to identify knowledge gaps and research needs expressed in the current literature. The narrative literature review is provided in Appendix C.

Historical occurrence of HCBs and adverse human health effects is well documented, with recorded observations as far back as one thousand years before the present (Steffen et al., 2014). One modern example is Lake Erie, one of the most developed of the Laurentian Great Lakes. In early August 2014, prevailing winds forced a toxic bloom into a water treatment facility's nearshore intake in Toledo, Ohio; as a result, cyanotoxin levels in finished drinking water were detected at 2.5 micrograms per liter (μg/L), exceeding the World Health Organization (WHO) limit of 1 μg/L (Bullerjahn et al., 2016). Subsequently, a "do not drink" advisory was issued to more than 400,000 residents and hundreds of businesses (Bullerjahn et al., 2016). Despite prompt risk notification and water treatment by the city, at least 110 people became ill, with no hospitalizations or deaths reported (Benedict, 2017). Lake Erie is surrounded by urbanized developments, underground septic systems, agriculture, and animal farming, which contribute sizable nutrient pollution to the lake (Steffen et al., 2014). On top of this, the lake's morphology favors HCBs, with a shallow average depth of 19 meters (m), a lake retention time of less than three years, and regular summer water temperatures above 25°C (Steffen et al., 2014). This public health incident exemplifies the need to anticipate disastrous HCB events.

Furthermore, HCBs constitute a major economic challenge to tourism, water recreation, property values, drinking water infrastructure, aquacultures, and subsistence livelihoods. The U.S. Environmental Protection Agency (USEPA) provides estimates on the multi-faceted costs of nutrient pollution-related source reduction and environmental impacts, based on national case studies (USEPA, 2015). HCBs have even been estimated to cost the U.S. economy 2.2 to 4.6 billion dollars annually (Hudnell, 2010). Moreover, a systematic review by Kouakou & Poder

(2019) assessed the human health costs of HCB exposures based on reported illnesses. These costs included expenses for healthcare and medication, loss of income from being sick, cost of death, and the intangible costs of pain and suffering, approximated by presenteeism—reduced productivity at work—by the study authors. The authors calculated direct, indirect, and intangible costs and quality-adjusted life-years (QALYs) lost for different severities of digestive and respiratory illnesses. Digestive illness costs were approximated to be $86 (mild case), $1,015 (moderate case), and $12,605 (severe case) and respiratory illness costs were $86 (mild case), $1,235 (moderate case), and $14,600 (severe case) (Kouakou & Poder, 2019). The individual and societal costs of HCBs are significant and expected to increase with a warming climate.

At the federal level, the USEPA lists cyanobacteria and several cyanotoxins on their Contaminant Candidate List under the Safe Drinking Water Act. Although the USEPA has not set federally enforceable standards for cyanotoxins, they have provided both recreational (USEPA, 2023a) and drinking water (USEPA, 2023b) guideline values, as well as general monitoring guidelines for states. In addition, the Centers for Disease Control and Prevention (CDC) provides information on human and animal illnesses from HCB events through their One Health Harmful Algal Bloom System (OHHABS) online platform, which provides annual summaries of voluntarily reported public health data (CDC, 2021). A One Health approach to managing HCBs is critical since toxic blooms threaten human and animal health as well as biodiversity and critical ecosystem services. On November 27, 2023, a bipartisan U.S. Senate bill—the Harmful Algal Bloom and Hypoxia Research and Control Amendments Act of 2023—was introduced and aims to improve monitoring, forecasting, prevention, and mitigation of HCBs and hypoxia through intra and interagency coordination at all levels of government

(S.3348, 2023). The dangers of HCBs represent a national risk to environmental public health and actions are being taken to minimize this hazard and address it accordingly.

In Washington, the State Department of Health (DOH) and State Department of Ecology (Ecology) often work together to manage the risks of HCBs. The state follows USEPA's drinking water guidelines for cyanotoxins and DOH has provided recreational guidance values for select freshwater cyanotoxins, including provisional values for anatoxin-a and saxitoxin (DOH, 2021). Washington has been proactive in implementing HCB monitoring programs and communicating risk to the public during bloom events. In 2005, the state legislature funded the Freshwater Algae Control Program, which provides funding support for local health agencies, water resource managers, and residents to test their lake water at an analytical testing laboratory (DOH, 2021; Trainer and Hardy, 2015). This passive surveillance program connects state resources with Washington's 39 counties, including 35 local health jurisdictions (LHJs), and incorporates observations from citizens and trained volunteers alike. This integrative approach works to prevent the occurrence of HCB-related illnesses, which have been well documented in the state (Trainer and Hardy, 2015). Risk notification typically includes mailers, emails, or list serves. Additionally, statewide toxin results along with toxic lake notifications are provided on Ecology's freshwater toxic algae online database (Ecology, 2024). This is especially useful since the only way to determine whether a bloom is toxic is through testing the water for the presence of cyanotoxins. While LHJs make the final determination on public risk notification for their jurisdiction, DOH has provided an updated two-tiered approach to follow when managing HCBs, including posting "Warning" and "Danger" signs at the lake dependent on toxicity results, reports of illness or death, or historical occurrence of HCBs (DOH, 2021). Furthermore, due to the lack of standardized outreach approaches, Hardy et al. (2016) generated a framework for

appropriate HCB education and notification strategies tailored to specific audiences—namely technical professionals, lake users, and lake residents. The study authors found that establishing HCB toxicity guidelines and advisory protocols were essential starting points for effective agency collaboration and public risk communication (Hardy et al. 2016). By implementing a robust HCB monitoring program and finding targeted ways to raise public awareness and communicate risk, Washington state provides excellent resources to deal with the risks posed by toxic blooms.

Study Background

It is important to understand the conceptual foundations for this research project. The dynamics of HCBs are complex and must be monitored comprehensively—no single tool or approach is appropriate to understand their occurrence or health risk. In addition to in-situ sampling, tools like remote sensing offer a complimentary source of data to integrate with traditional surveillance methods. By incorporating layers of information, water resource managers and public health practitioners can begin to fill the knowledge gaps associated with HCBs and the threats they pose.

A number of knowledge gaps on HCBs currently exist. Notably, there is a lack of universal indicators for monitoring and modelling blooms regarding their cell volume, toxin concentration, genetic characteristics, and environmental data (e.g., temperature, precipitation, nutrient concentrations); likewise, a lack of standardized sampling and analysis methods complicates comparison of studies and surveillance efforts (O'Keeffe, 2019). In addition, time delays and costs limit the number of samples collected, the frequency of sampling, and the ability to translate sample results into action (O'Keeffe, 2019). For example, many water utilities in the U.S. reported low reliability of monitoring programs to provide prompt HCB alerts (Almuhtaram et al., 2021). Real-time monitoring tools like continuous measurement sensors or remote sensing can provide timely detection and risk quantification along with enhanced public risk communication, as with guidance on when to lift a bloom advisory (O'Keeffe, 2019). There are also many unknowns on health impacts, including low-level chronic exposure to cyanotoxins, bioaccumulation, toxin levels and mechanisms of toxicity, mixture interactions (e.g., additive, synergistic effects), target organ systems, and health effects on more vulnerable populations (O'Keeffe, 2019). Consideration of knowledge gaps in Washington state was also warranted.

In preparation for this study, our research team met with representatives from Washington jurisdictions to gather information on potential research needs and knowledge gaps surrounding HCBs. Based on these meetings, the following concerns were summarized: insufficient resources on testing and decision making for different counties, improvements needed for community engagement, a need for more rapid indicators to communicate risks to the public, a need for additional surveillance and diagnostic tools for HCBs, risks from septic systems to nearby water bodies, and increased HCB risks to drinking water sources due to the effects of climate change. Concerns for the use of drones as an HCB monitoring tool were also identified. Many jurisdictions do not currently use drones for environmental surveillance of HCBs due to a variety of reasons ranging from costs and technical difficulties to liability issues and a lack of standardized methods. Specifically, costs associated with training, insurance, and requiring third party consultants for operation; logistical difficulties with drone-based sampling; place-based flight restrictions; inclement weather conditions hindering flights; challenges with determining the best time of day to avoid sun glare; time constraints for aerial image processing and technical difficulties with mapping water surfaces; necessity for accurate ground control points; and the lack of knowledge surrounding the implementation of drones as an environmental monitoring tool for HCBs. Some counties in Washington currently employ drones for public safety, emergency management, and construction-related activities. One notable exception was Pierce County, Washington, which uses drones for a variety of use cases, including for water resource visual assessment, sampling, and monitoring support (Pierce County, n.d.).

In addition, our research team identified several challenges involving the specific use of drone-based water sampling, whereby a tether was used to connect a water sampling container (housed in a 3D-printed apparatus) to the drone platform's housing. Based on previous studies

describing this methodology (Graham et al., 2022; Hanlon et al., 2022; Benson et al., 2019), our team conducted preliminary research and development to evaluate this method and encountered the following difficulties: logistical issues with flight operation near power lines, tall trees, and territorial birds; stabilization time needed for tether swinging after drone movement; poor and inconsistent water volume collection efficiency; limitations with drone battery life and payload for water volume desired; and unreliability of collecting surface water composite samples. These revelations prompted the research team to shift its focus to drone-based aerial image collection to supplement visual monitoring and detection for HCBs.

Almuhtaram et al. (2021) provided a comprehensive review of current cyanobacteria detection methods, including traditional water quality indicators, satellite remote sensing, fluorescence-based probes, drones, biosensors, and quantitative polymerase chain reaction (qPCR). The study's authors summarized these methods and categorized them into whether they detected biological or bloom activity (Tier I tools), confirmed the presence of cyanobacteria (Tier II tools), or confirmed the presence of cyanotoxins (Tier III tools). Accordingly, they devised this three-tier framework to provide practitioners with a cost-saving, multi-barrier approach for HCB monitoring (Almuhtaram et al., 2021). One widely used Tier I tool in monitoring programs is the analysis of chlorophyll a concentrations. Chlorophyll a, the green pigment present in all photosynthetic organisms, comprises 1.5% dry weight of algal organic matter, representing an indirect estimation of algal biomass (Almuhtaram et al., 2021). Generally, higher concentrations of chlorophyll a indicate both a higher rate of photosynthesis and a higher concentration of phytoplankton, which may include cyanobacteria. The WHO provides guidance levels for chlorophyll a concentrations in water bodies dominated by cyanobacteria, including 1 microgram per liter (µg/L) (Alert Level 1) and 12 µg/L (Alert Level

2), but this metric is often contextualized with other water quality parameters (Almuhtaram et al., 2021). Furthermore, drone technology may be used as either a Tier I or Tier II monitoring tool, depending on their measurement target (Almuhtaram et al., 2021). This research project primarily focused on assessing the incorporation of drones as a Tier I visual assessment tool that compliments other monitoring strategies (e.g., in-situ sampling). To determine how effective drone-based aerial imaging could be for routine HCB monitoring, we assessed the remote sensing capabilities of different drone platform sensors (visible light and multispectral) to estimate chlorophyll a concentrations. This type of remote sensing stands in contrast to more powerful remote sensing platforms, such as satellites and drones outfitted with hyperspectral sensors (considered Tier II tools). While the selection of tools discussed in Almuhtaram et al. (2021) vary depending on local geography and monitoring goals, we were interested in the use of drone imagery to monitor recreational lakes in Washington.

It is important to understand the fundamentals of remote sensing and how this technology can be applied to environmental public health applications. Remote sensing generally consists of the following components: an energy source; interaction with a target; sensors and platforms; and downstream transmission, processing, and analysis (Abd El-Ghany et al., 2020). An energy source (e.g., the sun) emits electromagnetic radiation toward a target (e.g., the ground surface, a water molecule, a tree, a microbe). Once the solar radiation reaches the target, it will interact based on the target's unique properties (e.g., via absorption, scattering, emittance, etc.). Next, the scattered or emitted light is recorded by a remote sensor (e.g., camera sensor, multispectral or hyperspectral sensors) that is typically housed within a ground-based, airborne, or spaceborne instrument (e.g., handheld camera, drone, airplane, satellite). Once a platform acquires this data, the imagery may be saved directly to the device or transmitted to a receiving station, error-

corrected, and further processed until analysis and interpretation (Abd El-Ghany et al., 2020). The evolution of remote sensing has resulted in multifaceted applications today, with the basic principle that all natural objects uniquely reflect, emit, and absorb radiation and can be diagnostically identified based on these spectral characteristics. Furthermore, remote sensing and public health applications abound in the academic literature. Remote sensing has been used to understand the link between air quality and the built environment (Tian et al., 2023; Wang et al., 2022); to track airborne atmospheric dust causing health hazards like asthma, meningitis, and Valley fever (Tong et al, 2023); and for the management of weeds, insect pests, and plant diseases on fruit orchards and crops (Abd El-Ghany et al., 2020).

Reviews on the use of remote sensing for HCB monitoring have also been extensively documented (Wu et al., 2019; Kislik et al., 2018; Rolim et al., 2023). These review articles have shown a rise in remote sensing applications as technological capabilities improve the ability to track blooms spatially and temporally in real or near real time. Satellite remote sensing has especially become a major tracking tool for larger lakes. Schaeffer et al. (2024) generated a promising forecasting model that was able to predict HCBs with high accuracy, sensitivity, and specificity using satellite remote sensing technology. The research team compared timely data of predictive variables like water surface temperature, precipitation, and lake morphometry against chlorophyll a in over 2,000 large-scale lakes and reservoirs with cyanobacteria dominance, across the U.S. (Schaeffer et al., 2024). For smaller-scale lakes, however, satellites are inhibited by low-resolution imagery, interferences by cloud cover and other atmospheric particles, inflexibility in flight scheduling, and generally higher costs compared to drones (Kislik et al. 2018; Rolim et al., 2023). Moreover, high-resolution drone optical imagery is able to capture color change differences in a water body. The presence of chlorophyll a in cyanobacteria

strongly absorbs blue and red regions of the visible spectrum while green and near infrared (NIR) wavelengths are strongly reflected (Merwe & Price, 2015). Drones provide many practical benefits for implementation at small scale lakes, including accessibility and ease of use, relatively lower costs, more frequent and flexible data collection, customizable data acquisition setups, greater spatial resolution of imagery, applicability in cloudy or hazy weather conditions, allowing access to previously inaccessible areas, and improving safety by minimizing investigator exposure to HCBs (Wu et al., 2019; Kislik et al., 2018; Rolim et al., 2023). As opposed to satellites, drones also allow synchronization between the collection of imagery and water samples for quantitative modelling (Wu et al., 2019). For instance, combinations of Red-Green-Blue (RGB) bands from true color camera images have been used to monitor offshore floating green tide in eastern China (Wu et al., 2019) and multispectral imagery, including NIR wavelengths, was used to estimate cyanobacterial densities in Kansas (Merwe & Price, 2015). In addition, Tan et al. (2023) applied multi-step machine learning models to identify HCBs from RGB imagery at a lake in China, reporting accurate, real-time detection.

For this research project, water samples were collected from a western Washington lake and analyzed for chlorophyll a in tandem with aerial photo collection using two different drone platforms, one housing an RGB sensor and the other a multispectral sensor. Methodologies and working hypotheses were adapted from similar work conducted at recreational, research, and aquaculture lakes in Alabama by Fernandez-Figueroa et al. (2021); at recreational lakes and ponds in New Hampshire by Bunyon et al. (2023); and at a recreational lake and reservoir in southern Illinois by Wu et al. (2023). These studies were successful in implementing drone-based HCB monitoring. We hypothesized that implementing drone surveillance at an HCB-vulnerable lake offered a more comprehensive visual assessment, as opposed to a limited view

from the shoreline. Chlorophyll a concentrations were estimated from the drone sensors using software for image processing and color band manipulations, which were validated with in-situ water samples. Field conditions were recorded to better understand this remote sensing tool.

Study Aims

The overarching research question for this study was, "is the incorporation of drones for small scale lake monitoring of HCBs effective for local agencies?" Our first study objective included reviewing the academic literature on freshwater HCBs and their human health risks as well as understanding the local context for their management and control. This was accomplished through a narrative literature review and meeting with pertinent agency stakeholders. To date, we have engaged with representatives from DOH, Ecology, King and Snohomish Counties, and the City of Shoreline. Based on our review of current literature, we found that remote sensing applications are an emerging HCB monitoring tool that can supplement current monitoring strategies for small-scale lakes. However, their successful application and associated challenges in Washington State lakes were not identified. Our second objective was to conduct drone-based aerial imaging and manual water sample collection at a Washington lake to assess implementation of this remote sensing technology. This method was evaluated by conducting a simple linear regression analysis on the variables collected. Based on the results of this work, our third objective was to create a guidance document detailing lessons learned to be provided to pertinent local agencies. Project aims are summarized below.

- Aim 1: Understand the current state of knowledge on the human health risks of HCBs and the local context for their monitoring, surveillance, and risk notification.
    - Complete a narrative literature review on the health risks of HCBs to identify knowledge gaps and research needs from the academic literature.
    - Conduct meetings with local, county, and state professionals with experience in HCB monitoring and response to understand current research needs.

- Aim 2: Perform drone-based aerial photo collection and manual water sample collection to assess the use of drones as a supplemental HCB monitoring tool.
    - Evaluate the strength of drone imagery to estimate lake chlorophyll a concentrations using simple linear regression analyses.
    - Compare this method to status quo techniques of regular lake monitoring.
- Aim 3: Communicate findings to local water resource management and public health agencies through a drone-based data collection guidance document.
    - Provide a deliverable summarizing optimal conditions needed for field performance as well as challenges and facilitators encountered with this method.
    - Collaborate with a representative from the City of Shoreline for iterative feedback to provide a final deliverable.

Study Setting

Field work activities were conducted at Echo Lake, an approximately 12-acre freshwater recreational lake measuring approximately 1,200 feet in length and 600 feet in width, in the City of Shoreline, King County, Washington. Residential complexes, single-family residences, and a public access park adjoin the perimeter of the lake. Aurora Avenue North/U.S. Route 99 is located to the west and the surrounding area is highly urbanized. Echo Lake has a mean depth of 14 feet and a maximum depth of 30 feet with a watershed area of approximately 288 acres (King County, 2002; King County, 2015). Sampling activities were conducted at four locations along the perimeter of the lake, including at the public beach and at private docks located on the northern and western portions of the lake. A general site map with dedicated sample locations is provided in Figure 1. Site access was facilitated in collaboration with the City of Shoreline and Friends of Echo Lake, an advocacy group affiliated with the Echo Lake Neighborhood Association (ELNA) that conducts volunteer lake sampling work in the summer months. A summary table of the sample locations and their geographic coordinates is provided in Table 1.

Echo Lake was selected since it was deemed representative of an urbanized, small-scale lake in western Washington that has experienced HCBs, notably a 2021 bloom that measured anatoxin concentrations 114 times higher than state guidelines and led to a lake closure (King County, 2021). In 2023, the City of Shoreline was awarded a grant from Ecology's Freshwater Algae Control Program to create a Lake Cyanobacteria Management Plan (LCMP) for Echo Lake (Washington State, n.d.). Also, Echo Lake has been characterized by the University of Washington since the early 1900s (Scheffer, 1933). Water sample lab analysis activities were conducted at the Environmental and Occupational Health Microbiology Lab (EOHML) on the University of Washington Seattle campus. Aerial imagery and data processing activities were

conducted at the Natural Hazards Engineering Research Infrastructure (NHERI) Reconnaissance Facility (the "RAPID") lab within the UW Department of Civil and Environmental Engineering.

Figure 1. Study Setting Map and Sample Locations of Echo Lake (King County, 2024).

Table 1. Sample Locations

Sample Number	Location Description	GPS Coordinates
SW01 / SW05 / SW09 / SW13 / SW17 / SW21 / SW25	Public Beach	47.77270046, -122.3414122
SW02 / SW06 / SW10 / SW14 / SW18 / SW22 / SW26	North Dock	47.77279744, -122.3423559
SW03 / SW07 / SW11 / SW15 / SW19 / SW23 / SW27	West Docks - North	47.77157037, -122.3440734
SW04 / SW08 / SW12 / SW16 / SW20 / SW24 / SW28	West Docks - South	47.77127324, -122.3443405

Notes:

GPS coordinates were collected using an Emlid Reach RS2+ multi-band RTK GNSS receiver.

SW = Surface Water

Methods

The methodologies for Aim 1 are included as part of Appendix C. This section will solely discuss the methods employed for Aim 2. Different methodologies were employed at each stage of the project for this aim. The following section will first describe water sampling collection procedures and laboratory sample analysis. This will be followed by a discussion of chlorophyll a calculations and quality assurance and quality control (QA/QC) procedures. Next, procedures for aerial image acquisition, photogrammetric analysis, and spectral index calculations are discussed. The section will conclude with discussion on the specific index equations used and applicable statistical analyses. Figure 2 below provides a summary flowchart for the overall methods employed as well as specific methods for the environmental sample analysis and aerial image analysis steps. A more detailed workflow for the environmental sample lab materials and procedures is found in Appendix D. A site health and safety plan (HASP) was generated prior to conducting field work to anticipate potential hazards at the site and specifies actions to eliminate or reduce those hazards. The site HASP can be found in Appendix E.

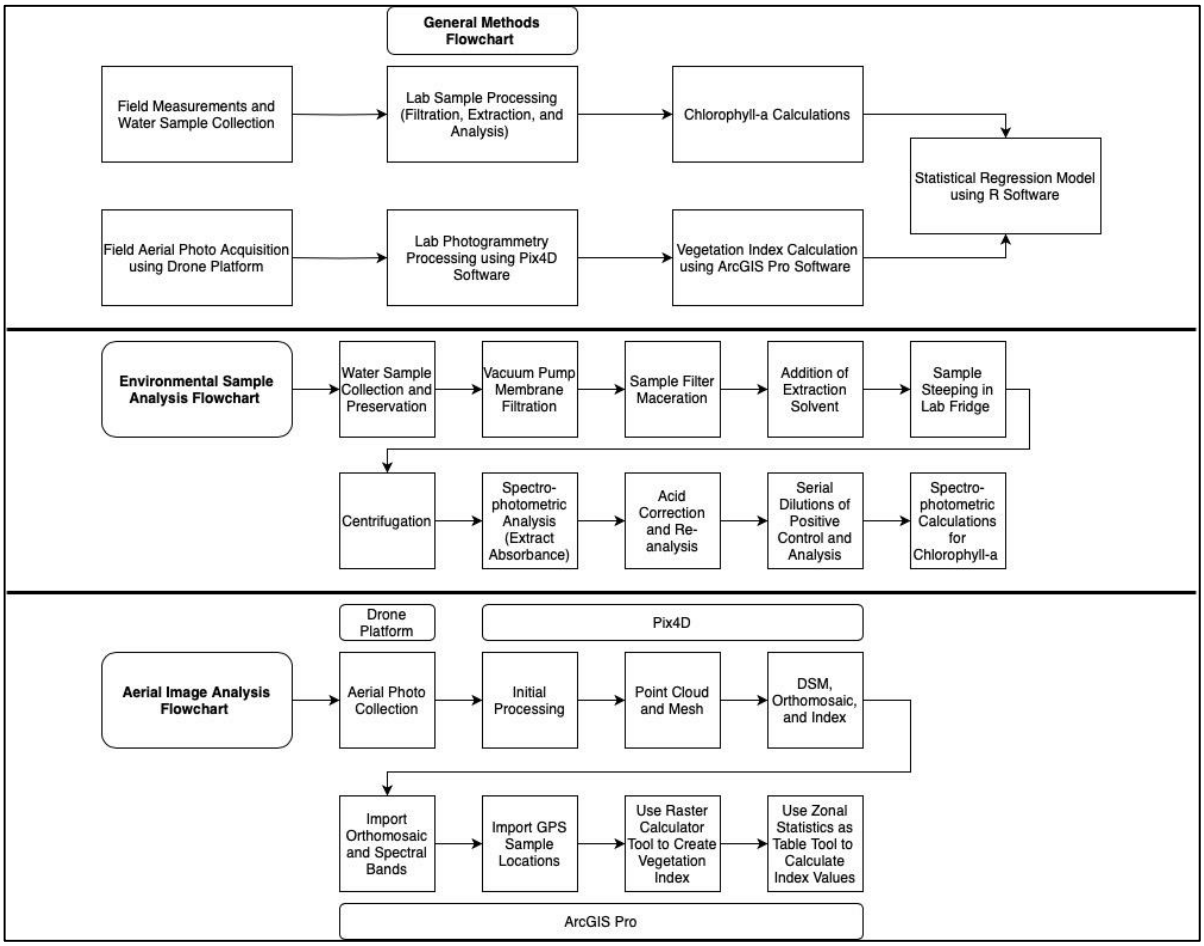

Figure 2. Flow Diagrams of Study Protocols.

Water Sample Field Collection

Collection of water samples for chlorophyll a analysis were completed generally following USEPA (USEPA, 2013) and state standard operating field procedures (Oklahoma Water Resources Board, 2018). All dedicated sampling locations were recorded using an Emlid Reach RS2+ multi-band Real Time Kinematic (RTK) global navigation satellite system (GNSS) receiver. Equipment with GNSS capabilities can use satellite navigation from other networks beyond GPS. After donning a high-visibility vest, nitrile gloves, and hip waders, 1 L opaque Nalgene bottles were primed by rinsing in lake water three times. Water samples were then collected by slowly submerging the bottle upside down/nose-down to a depth of 0.5m, inverting

it slightly, and allowing the bottle to fill slowly until completely full. The pre-labelled containers were capped and immediately placed on ice in a sample cooler and kept at an approximate temperature of 4°C until delivered to the lab. It is important to ensure that the water samples are kept out of sun exposure and chilled to avoid chlorophyll pigment degradation. Lastly, a field blank was collected. Samples were labelled “SW” for surface water, followed by the sample number, and their respective duplicates were labelled “DUP.” Seven water sampling events occurred on July 24, August 7 and 21, September 2 and 11, and October 7 and 23, 2023.

In addition to water sample collection for chlorophyll a analysis, the research team acquired a Turner Designs FluoroSense Handheld Fluorometer with phycocyanin optics, including a 200 parts per billion (ppb) Rhodamine water tracer calibration solution. Phycocyanin is a unique photosynthetic pigment specific to all cyanobacteria. The battery-powered probe uses excitation light from the fluorometer to target phycocyanin within the cyanobacterial cells, causing them to fluoresce, and then converts the reading to a digital value that is correlated to a known concentration (Turner Designs, 2023). The probe has a linear range of 0 to 199 μg/L and a resolution of 1 μg/L (Turner Designs, 2023). This probe was acquired to determine the presence of cyanobacteria in particular since chlorophyll a is only diagnostic for all photosynthetic phytoplankton, including brown algae and green algae. The probe was utilized for the sixth (10/07/2023) and seventh (10/23/2023) sampling events and compared to chlorophyll a results. Briefly, the probe was calibrated in the field with the calibration solution, the sensor was dipped into the designated sampling areas, and three measurements were recorded and averaged. The probe was decontaminated with distilled water between samples.

Chlorophyll a Lab Analysis and Calculations

Lab sample processing generally followed USEPA Method 446.0 (Arar, 1997) and American Public Health Association (APHA) Method 10200H (Baird et al., 2017) for the determination of chlorophyll a from freshwater samples using visible spectrophotometry. Visible spectrophotometry uses ultraviolet and visible light to measure concentrations of proteins, nucleic acids, and various molecules based on how light interacts with the analyte. For this work, a SPECTRAmax^{TM} PLUS microplate spectrophotometer was used to measure the optical density (OD) of chlorophyll a extracts at preferential wavelengths (Molecular Devices Corporation, 1997). The OD measures the transmission of light through these substances. Once water samples were collected in the field and stored on ice, they were transported to the UW EOHML 4°C field lab fridge. For the filtration step, a lab vacuum pump with an operating flow rate below six inches mercury was used. Prior to filtration, samples were homogenized by carefully inverting the container several times. A measured volume of sample water was filtered using 0.7 µm glass fiber membrane filters. Glass fibers efficiently break the phytoplankton cells during grinding (Baird et al., 2017). Sample volumes were poured in 100 mL increments until the filter was sufficiently strained with visible algae. Care was taken to ensure sample filters were not overloaded. Filters were then stored in pre-labelled Petri dishes wrapped in aluminum foil and placed into a -20°C freezer for preservation until extraction. Filters can be stored frozen for up to 3.5 weeks without significant chlorophyll a degradation (Arar, 1997). Each sample was analyzed in duplicate following identical procedures and volumes and a lab blank was also collected.

For the extraction step, frozen filters were cut into pieces—to facilitate the extraction process—and made into a slurry by adding aqueous acetone. The filter slurry was added to pre-labelled 50 mL centrifuge tubes and manually macerated with a metal spatula for five minutes.

Once sufficiently macerated, the slurry was transferred to pre-labelled, 15 mL centrifuge tubes wrapped in aluminum foil, vigorously shaken, and left to steep in the dark at 4°C for approximately 24 hours. After steeping was completed, the samples were centrifuged for 15 minutes with a relative centrifugal force (RFC) of 700 G to allow the filtrate to separate. After centrifugation, 2 mL of the supernatant was transferred to 3.5 mL glass cuvette cells, which were then inserted into the spectrophotometer. The SPECTRAmax^{TM} PLUS spectrophotometer used SoftMax Pro (Version 5.2) software for data analysis.

In addition to the water samples, their duplicates, and the blanks, serial dilutions of a positive control of known concentration was also inserted into the measuring instrument. The optical densities of the analytes were analyzed at four wavelengths—750, 664, 647, and 630 nanometers (nm)—to determine turbidity, chlorophylls a, b, and $c_1 + c_2$, respectively. These values were applied to Jeffrey and Humphrey's Trichromatic Equations and Lorenzen's Modified Monochromatic Equations to calculate the respective analyte concentrations (Arar, 1997). See the List of Equations for equation explanations. Calculations were performed using Microsoft Excel (Version 16.77.1) and Google Sheets software. It is important to note that the Trichromatic equations are considered an "uncorrected" method since they overestimate the concentration of chlorophyll a in the presence of pheophytin a, a non-photosynthetic degradation product of chlorophyll a with a similar wavelength absorbance (Arar, 1997; Baird et al., 2017). Likewise, the Modified Monochromatic equations are considered "acid-corrected" to account for the sample's pheophytin a concentration. In addition to pheopigments, a number of other pigments in lake waters may have minor interferences, including the phaeophorbides, chlorophyllides, bacteriochlorophylls, and phycobiliprotein (NALMS, n.d.-a). In order to determine whether the collected samples were preserved properly and that natural pheopigment concentrations were

low, we reanalyzed the “uncorrected” samples with acid-corrected extractions for the last three sampling events (09/11/2023, 10/07/2023, and 10/23/2023). This step was completed successfully only for these events. This was performed by adding 60 microliters (µL) of 0.1 Normalized (N) hydrochloric acid (HCl) to the 2 mL supernatant to obtain an acid concentration of 0.003 N, pipette mixing for 90 seconds, and then re-running the sample. Once OD measurements were acquired, they were applied to Lorenzen's Modified Monochromatic Equations to correct for the pheo-a pigment. Sample and duplicate chlorophyll a concentrations were calculated from the extract solutions to yield whole sample chlorophyll a values, converted from milligrams per liter (mg/L) to µg/L. Blank measurements were used to identify potential points of contamination during lab and field procedures. Serial dilution concentrations from the stock standard solution were compared to the sample results by generating calibration curves for each sampling event and are further discussed below and in the Results and Discussion sections.

Sample Quality Assurance and Quality Control

Quality assurance and control procedures were completed to ensure that environmental samples were collected and analyzed precisely, accurately, and without cross contamination or significant degradation. All water samples were collected in 1 L opaque Nalgene bottles and later homogenized and split into duplicate samples for lab analysis. These subsamples of the independent sample were analyzed to confirm analytical measurement consistency. In addition, a field blank containing either deionized (DI) laboratory water or steam-distilled water was collected in the field by transferring these contents from a clean, 1 L container into a 1 L opaque bottle and stored along with the other sample containers until lab analysis. This “trip blank” was collected to check that field equipment was being effectively decontaminated between sampling

events to avoid cross contamination, as well as to check for any contamination in the DI or distilled water being used. Furthermore, a laboratory blank consisting of a blank membrane filter was filtered by DI or distilled water and processed to check against contamination of lab equipment or reagents used. In the order of sample analysis, the field blank was analyzed first to account for cross-contamination in the field and the lab blank was analyzed last to account for any lab contamination.

To ensure the chlorophyll a did not significantly degrade from factors such as sunlight exposure, elevated temperatures, acidity, or time, a variety of controls and checks were implemented. Samples were collected in opaque bottles and immediately stored on ice in sample coolers to avoid sun exposure and warmer temperatures. Samples were then transported to the laboratory where they were stored in a lab fridge preceding filtration. Sample collection and processing proceeded in as timely a fashion as was feasible, with collection and filtration activities occurring on the same day. In addition, all analysis was performed in subdued light by turning off overhead lights in the lab and by transferring samples in a small sample cooler where applicable. Furthermore, the approximate acidity of the lake water near the sample areas was determined during several field events using pH test paper strips, which indicated that the lake water was not below a pH of 6, a critical level that will degrade chlorophyll a (Baird et al., 2017). During the filtration process, 2 mL of saturated magnesium carbonate ($MgCO_3$) solution were added to the sample filters as a pH buffer to prevent acid degradation (Baird et al., 2017). This buffering solution was added to each sample's duplicate for the last two sampling events (10/07/2023 and 10/23/2023); however, differences in final chlorophyll a concentrations between each sample and its duplicate were found to be negligible when adding the $MgCO_3$. This indicated that the lake water samples were not problematically acidic in the first place.

In addition to duplicates and negative controls, a positive control was used by acquiring a powdered pellet of pure chlorophyll a from an independent laboratory. A chlorophyll a stock standard solution (SSS) was created by diluting one milligram (mg) of pure chlorophyll a pigment in 25 mL of 90% aqueous acetone to yield a known concentration of 40 mg of pigment per liter of aqueous acetone. The subsequent positive control included serial dilutions using an aqueous acetone solvent. For the first sampling event (07/24/2023), a 1:10 dilution was prepared from the SSS and serially diluted into the following ratios: 1:100, 1:1,000, 1:10,000, and 1:100,000. For the remaining events, separate 1:25 dilutions were prepared from the SSS and serially diluted into the following ratios: 1:50, 1:100, 1:200, and 1:500. These latter dilutions were optimal as they better accounted for the range of chlorophyll a extract concentrations expected from the actual samples. Dilutions were prepared and analyzed in triplicate for each event and averaged values were used to create a standardized calibration curve comparing chlorophyll a extract concentrations to their OD absorbance measurements at 664 nm (the peak absorbance for chlorophyll a), for both the positive controls and the field samples. A calibration curve was generated for all sampling events to understand the upper and lower limits of the spectrophotometer's range of detection and to check that the field data was consistent with expected values. Lastly, all samples analyzed by the spectrophotometer itself were run three times by the instrument and averaged to capture any variations in instrument measurement.

To ensure that the SSS itself did not degrade over time, its glass container was covered in aluminum foil and placed in a -20°C lab freezer; in addition, all work with the SSS was performed in subdued light. For the last three sampling events, the dilution standards were also acid-corrected and reanalyzed by the spectrophotometer. According to Baird et al. (2017), when a solution of pure chlorophyll a is converted to pheophytin a through acidification, the quotient

of the absorbance at 664 nm before acidification and the absorbance at 665 nm after acidification, or the absorption-peak ratio (664b:665a), is used to correct the apparent concentration of chlorophyll a for pheophytin a. Essentially, this ratio accounts for the absorption of the unacidified mixture of chlorophyll a and pheophytin a compared with the acidified mixture primarily containing pheophytin a. Solutions with an absorption peak ratio of 1.70 are considered to contain no pheophytin a with chlorophyll a pigments in exceptional physiological condition whereas solutions with an absorption peak ratio of 1.0 are considered to contain pure pheophytin (i.e., total degradation) with no reductions after acidification (Baird et al., 2017). These absorption peak ratios are based on the use of a 90% aqueous acetone solvent but a higher percentage of acetone used (closer to 100%) can result in absorption peak ratios closer to 2.0 (Baird et al., 2017). Absorption peak ratios are further discussed in the following main sections.

Finally, disposable containers and Nitrile gloves were replaced and dedicated equipment was decontaminated between samples and sample events. Decontamination procedures involved the use of tap water and Alconox detergent, a scrub brush, deionized and distilled water, and acetone rinses. Between sampling events, applicable equipment was run through an autoclave dry cycle at 123.0°C for one hour to rid equipment of bacterial contamination and residue.

Aerial Imagery Acquisition

Prior to flight planning and drone operation, the project team acquired a Federal Aviation Administration (FAA) Part 107 Remote Pilot Certificate (Certification #4823551) in order to remain compliant with FAA remote pilot rules and safety regulations. In addition, the research team accessed Visual Flight Rules (VFR) Sectional Aeronautical Charts for the local geographical area in order to review flight regulations and maintain compliance while operating

within the airspace of Echo Lake. We used the following drone platforms and camera models for this project: DJI Phantom 4 Pro+ RTK (DJI, 2020) equipped with an RGB optical camera and DJI Matrice 210 (DJI, 2019) equipped with a Micasense Altum multispectral sensor (MicaSense, Inc., 2020), which includes RGB, NIR, red edge, and thermal spectral bands. Drone platform and sensor specifications used in this project are summarized in Table 2 and shown in Figure 3.

Table 2. Drone Platform and Camera Sensor Summary

Parameter	DJI Phantom 4 Pro+ RTK[1]	DJI Matrice 210[2]
Approximate Weight with Batteries	1.391 kg	4.8 kg
Diagonal Length	350 mm	643 mm
Vertical Position Accuracy	±0.1 m	±0.5 m
Horizontal Position Accuracy	±0.1 m	±1.5 m
Max Payload Capacity	0.5 kg	1.34 kg
Max Speed	31 mph	50.3 mph
Max Wind Speed Resistance	10 m/s	12 m/s
Max Flight Time (per battery)	30 min.	34 min.
Retail Value	$6,600 USD	$12,000 USD
Sensor Type	1" CMOS RGB Camera	Micasense Altum Multispectral Sensor
Spatial Resolution	20 MP	2064 x 1544 pixels (3.2 MP x 5 imagers)
Focal Length	24 mm	8 mm
Field of View	84° 8.8 mm/24 mm	48° x 36.8°
Retail Value	(included with platform)	$16,000 USD

Notes:
[1]DJI (2020), [2]DJI (2019)
CMOS = Complementary Metal-Oxide-Semiconductor
kg = kilograms
m = meters, mm = millimeters
m/s = meters per second
MP = Megapixels
mph = miles per hour

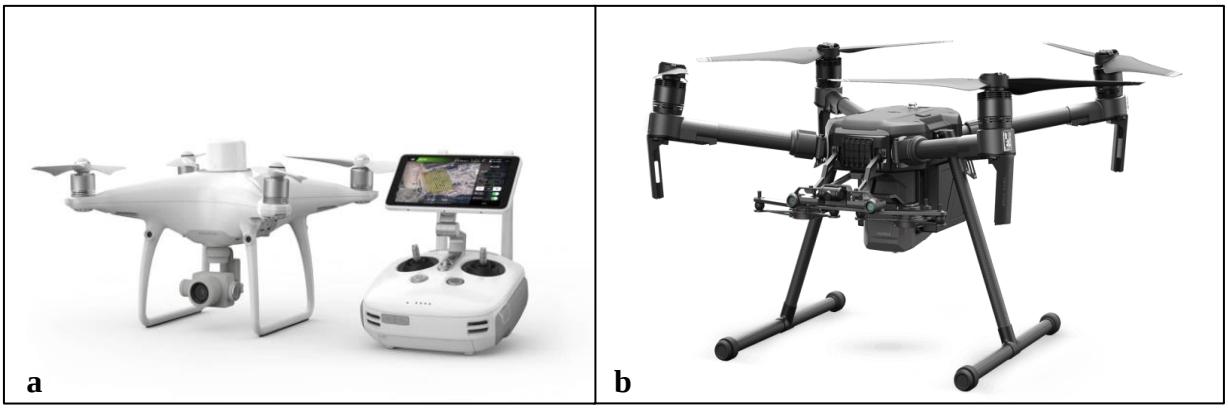

Figure 3. Drone platforms used for this project, including the DJI Phantom 4 Pro+ RTK (a) and the DJI Matrice 210 (b).

The Phantom 4 Pro+ RTK (Phantom) was used for all seven sampling events and the Matrice 210, operated by RAPID staff, was used for two sampling events (09/11/2023 and 10/23/2023). Safety precautions were made prior to each flight by assessing weather forecasts, using mobile apps to check local flight restrictions, and by periodically scanning the operational airspace for other aircraft and structures. Using the drone controllers, each drone was pre-programmed to follow a "lawnmower pattern" across the lake surface, flying back and forth in equally spaced flight lines. Three flight altitudes were selected at 60m, 90m, and 120m above ground level in order to assess the most optimal conditions for flight operation and downstream photo analysis. This included comparing different spatial resolutions and how well the imagery was able to stitch together at each height. Also, for the same sized lake, lower altitude flights consume more battery life than higher altitude flights since more photos are collected to account for the entire lake surface. The 60m altitude was chosen since it was high enough to clear the lake's surrounding treetops. Based on FAA regulations, drones are not allowed to be flown above 121m (limit of 400 feet) so 120m was chosen as the highest altitude. The 90m height fell between these extremes. Various default camera settings were also selected (e.g., the white balance was adjusted to match cloudy or sunny climatological conditions). In addition to onboard GPS units, Phantom flights were supported by a high precision GNSS mobile station with centimeter-level accuracy and the Matrice 210 flights utilized three manually placed ground control points (GCPs) for improved locational accuracy. The GCPs include numbered, easily identified mats with their locations recorded using a handheld GPS unit. Each drone launched from and landed on the North Dock platform and were operated using tablet devices connected to their controllers. Constant surveillance of the drone's position and its operational airspace was maintained during the automated flights. In addition to the three flight altitudes, additional flights

were conducted to better understand various drone and camera settings (e.g., different times and sun positions, camera settings, etc.).

For each flight, images were collected by the drone camera at nadir (vertically downward) every few seconds during the entire flight in order to capture any visible algal formation on the lake surface. Hundreds to thousands of images were collected per flight and saved to a memory card housed within the drone platform. Flights were scheduled in the mid-morning (when the sun was not highest in the sky) to avoid sun glare and a shimmering water surface. To determine optimal environmental conditions for flight operation, weather and sky conditions, temperature and humidity, wind speed, sun angle and shadow length, and other characteristics were recorded using several mobile applications (SunCalc, n.d.; UAV Forecast, n.d.). For example, sun angle was recorded as the solar altitude (measured in degrees), representing the angular position between the horizon and the sun's center (SunCalc, n.d.). This also affects the shadow length, measured in meters, which represents the distance of an object's shadow cast by the sun, calculated as the object's height divided by the solar altitude. In other words, for a particular object's height such as a tree, the shadow length may have a value equal to the tree's height or slightly less than or greater than this value depending on the sun angle (SunCalc, n.d.). A summary of the drone flight details and various environmental conditions for each sampling event is provided in Table 3. Note that the table was arranged to match the optical and multispectral flights side by side. Flights and sample events were conducted generally every two weeks with scheduling based on changing weather conditions and personnel availability. Sunny, overcast, slightly rainy, and even hazy sky conditions were captured during the project period. Takeaways from this table will be discussed in further detail in the Discussion section.

Table 3. Drone Flight Details Summary									
Parameter	**Flight Description**								
Sampling Event and Drone Platform	**7-24-23 1st Event - P4P+ RTK**			**8-7-23 2nd Event - P4P+ RTK**			**8-21-23 3rd Event - P4P+ RTK**		
Flight Altitude (m)	60	90	120	60	90	120	60	90	120
Start/End Time	0955/1007	1013/1021	0931/0938	1012/1024	0949/0959	0853/0901	0826/0843	0857/0907	0918/0927
Total Time (min.)	13:21	8:17	7:47	12:45	10:02	8:57	17:34	10:49	9:13
Flight Plan Area (m^2)	49,814	49,730	50,598	49,814	49,730	50,598	49,814	49,730	50,598
Average GSD (cm/pixel)	1.73	2.60	3.43	1.75	2.62	3.46	1.76	2.62	3.48
Speed (m/s)	9.0	9.0	9.0	9.0	9.0	9.0	9.0	9.0	9.0
Image Overlap (%)	75	75	75	75	75	75	80	80	80
Temperature (°F)	59	59	59	63	63	61	57	58	59
Dew Point (°F)	54	54	54	61	61	61	51	51	52
Wind Speed and Gust (mph)	10G20	11G22	10G20	1G3	1G3	1G4	4G9	4G9	4G9
Wind Direction	S-SW	S-SW	S-SW	S	SW	SW	NE	NE	NE
Sky Conditions	Overcast, Light Rain			Overcast			Sunny, Hazy Sky		
Cloud Cover (%)	97	97	97	89	91	88	13	53	57
Solar Altitude (°)	40.98	47.05	36.07	40.66	36.83	27.63	20.52	26.00	30.10
Shadow Length (m)	1.15	0.93	1.37	1.16	1.34	1.91	2.67	2.05	1.73
Sampling Event and Drone Platform	**9-2-23 4th Event - P4P+ RTK**			**9-11-23 5th Event - P4P+ RTK**			**9-11-23 5th Event - Matrice 210**		
Flight Altitude (m)	60	90	120	60	90	120	60	90	120^
Start/End Time	0733/0747	0754/0804	0810/0819	1143/1157	1207/1217	1224/1232	1242/1321	1335/1348	NA
Total Time (min.)	14:44	10:32	9:02	14:42	10:31	8:57	30:00	13:00	NA
Flight Plan Area (m^2)	49,814	49,730	50,598	49,814	49,730	50,598	118,827	151,161	NA
Average GSD (cm/pixel)	1.75	2.61	3.44	1.74	2.62	3.46	2.72	4.19	NA
Speed (m/s)	9.0	9.0	9.0	9.0	9.0	9.0	12.0	12.0	NA
Image Overlap (%)	75	75	75	75	75	75	75	75	NA
Temperature (°F)	61	61	61	62	63	63	63	63	NA
Dew Point (°F)	54	54	54	58	58	58	58	58	NA
Wind Speed and Gust (mph)	1G1	1G4	2G4	2G6	2G7	2G7	2G7	2G7	NA
Wind Direction	SW	SW	SW	SE	SE	SE	SE	SE	NA
Sky Conditions	Mostly Sunny, Partly Cloudy			Overcast			Overcast		
Cloud Cover (%)	68	72	72	94	94	92	92	92	NA
Solar Altitude (°)	9.40	13.30	16.08	43.09	44.82	45.70	46.64	46.04	NA
Shadow Length (m)	6.04	4.23	3.47	1.07	1.01	0.98	0.94	0.96	NA
Sampling Event and Drone Platform	**10-7-23 6th Event - P4P+ RTK**			**10-23-23 7th Event - P4P+ RTK**			**10-23-23 7th Event - Matrice 210**		
Flight Altitude (m)	60	90	120	60	90	120	60	90	120
Start/End Time	1158/1212	1015/1025	1108/1117	1029/1043	1010/1019	0954/1003	1250/1336	1230/1243	1214/1222
Total Time (min.)	14:55	10:36	9:03	14:46	10:33	9:05	46:00	13:00	8:00
Flight Plan Area (m^2)	49,814	49,730	50,598	49,814	49,730	50,598	115,354	131,993	178,484
Average GSD (cm/pixel)	1.76	2.62	3.44	1.75	2.62	3.44	2.78	4.10	5.49
Speed (m/s)	9.0	9.0	9.0	9.0	9.0	9.0	12.0	12.0	9.0
Image Overlap (%)	75	75	75	75	75	75	75	75	75
Temperature (°F)	67	61	64	51	51	51	54	53	53
Dew Point (°F)	53	51	52	47	47	48	47	47	47
Wind Speed and Gust (mph)	1G5	1G4	1G5	8G15	8G15	8G15	6G12	6G12	7G13
Wind Direction	SE	SE	SE	N-NE	N-NE	N-NE	N	N-NE	N-NE
Sky Conditions	Sunny, Mostly Clear Sky			Overcast			Overcast		
Cloud Cover (%)	8	12	9	87	91	92	78	80	80
Solar Altitude (°)	35.03	25.87	31.43	22.61	20.36	17.40	30.20	30.71	30.55
Shadow Length (m)	1.43	2.06	1.64	2.40	2.69	3.19	1.72	1.68	1.69

Notes:

P4P+ RTK = DJI Phantom 4 Pro+ Real Time Kinematic Platform with RGB Sensor

Matrice 210 = DJI Matrice 210 Platform with Micasense Altum Multispectral Sensor

GSD = Ground Sampling Distance

m/s = meters per second

mph = miles per hour

NA = Not Applicable

120^ = 120m Matrice 210 flight was aborted due to mechanical issues

Aerial Imagery Processing

Processing of aerial imagery was completed using Pix4Dmapper (Version 4.8.4) photogrammetry software (Pix4D). This program processes the Phantom RGB camera images and the Matrice 210 Altum multispectral images similarly, with some additional steps needed for the latter (e.g., deletion of redundant images collected, calibration of GCP points, etc.). Pre-processing involved uploading the image files into the program where it extracted exchangeable image file format (EXIF) metadata from the images and identified the camera model used, as well as its georeferencing system—in this case the World Geodetic System (WGS) 84 / Universal Transverse Mercator (UTM) zone 10N (Washington North) coordinate system was the final georeferencing system used.

Pix4D image processing occurs in three main steps: initial processing; point cloud and mesh generation; and digital surface model (DSM), orthomosaic, and index generation. During initial processing, the geolocated imagery and GCPs were used to create keypoints—unique features of interest in each image—and tie points—points that connect or "stitch" together images with the same keypoints. Dependent on each flight, tens of thousands of keypoints were identified. In addition, the program optimized the camera model used by calibrating its internal parameters (e.g., focal length, aperture, resolution) and external parameters (e.g., orientation, location) (Pix4D, n.d.-b).

Next, a model of the scene where aerial photos were collected is created by using the tie points to create a densified point cloud and a 3D textured mesh. A densified point cloud is a collection of 3D points containing each image's x, y, and z position information as well as color information to create a 3D model; this model provides accurate distance, surface, and volume measurements (Pix4D, n.d.-a). The densified point cloud generates the 3D textured mesh, which

represents the model's shape and consists of vertices, edges, faces, and textures from the image data (Pix4D, n.d.-a). These were generated using Pix4D's proprietary algorithms and the process of Structure from Motion (SfM), which involves the creation of 3D models from 2D images.

For the final step, a DSM was created and represents a topographic model of the earth's surface based on elevation data (Pix4D, n.d.-a). The DSM is used to generate two end products: an orthomosaic and a reflectance map. The orthomosaic image product is a 2D map of the lake's extent, mosaicked from the hundreds (RGB camera) and thousands (Altum sensor) of raw image files, and orthorectified to remove perspective distortions (Pix4D, n.d.-a). The reflectance map is a 2D map where the value of each pixel represents the actual reflectance of the object, for each spectral band (Pix4D, n.d.-a). Finally, Pix4D has the option to generate index maps that compute pixel values of different bands of the reflectance maps into a new map with new pixel values (Pix4D, n.d.-a). This last step is completed in Pix4D using their proprietary software so this step was instead performed manually in ArcGIS Pro after transferring files. To ensure consistency for all of these steps, default processing settings were used for each flight image acquisition.

After orthomosaics were generated from Pix4D, they were uploaded to ArcGIS Pro (Version 3.1.0) software for further processing. Both the orthomosaic image products (.TIFF files) and the individual RGB, NIR, red edge, and thermal bands were uploaded as map layers into the ArcGIS workspace. Once uploaded, ArcGIS assigns integer values to each individual pixel comprising the images; each pixel value is associated with a color defined by RGB values. In addition, GPS coordinates for the sampling locations were uploaded to the workspace as point features. We used the Raster Calculator Image Analyst tool to generate a Vegetation Index (VI) raster dataset for each flight's orthomosaic image. A VI is an image transformation product in which the individual spectral bands of the original image are manipulated to highlight vegetation

properties in the new image; in this case, it was used to highlight any visible algal formation. As discussed further below, we used several VIs found in the academic literature to approximate chlorophyll a concentrations at the site. Note that, based on these VI equations, the output spectral pixel values may become positive or negative values. We then used the Zonal Statistics as Table Spatial Analyst tool to average the nine pixel values around and including the sample location for the selected VI. The average of these spectral index values was calculated for each sample location and compared to the corresponding chlorophyll a results for each sample event. It is important to note that since the resolution of this imagery is at the centimeter-level, the nine pixels do not represent a very large surface area of the lake. Since averaging 100 pixels yielded similar spectral index averages and due to the water being in constant flux, the nine pixel values were deemed representative of the general area that the sample was collected from. Fernandez-Figueroa et al. (2021) also followed this procedure for their VI calculations.

Selection of Vegetation Indices

A wide variety of VIs exist for environmental remote sensing applications and they vary depending on the platform and sensor used, application, and measurement target (Xue & Su, 2017; Sunoj et al., 2021). This study prioritized VIs commonly used to determine algal biomass and chlorophyll a concentrations. Namely, we utilized the Color Index of Vegetation Extraction (CIVE), Excess Green Index (EXG), KIVU (named for its geographic region of use), Normalized Green-Red Difference Index (NGRDI), and Visible Band Difference VI (VDVI) for the RGB optical imagery. Based on the literature, the CIVE index is inversely correlated with chlorophyll a concentrations while the remaining indices are directly correlated. The CIVE index was originally developed by Kataoka et al. (2003) to differentiate between vegetation and

surrounding soil to estimate crop growth without the need to measure the NIR wavelength but has also been more recently used to approximate algal biomass (Fernandez-Figueroa et al., 2022; Kataoka et al., 2003). The EXG, NGRDI, and VDVI indices have been used with RGB drone imagery to identify green algae growing on rafts and the KIVU index was generated from Landsat 5 images to determine chlorophyll a levels in inland aquatic ecosystems (Fernandez-Figueroa et al., 2022).

For the multispectral imagery, we utilized the Normalized Difference Vegetation Index (NDVI), Band Ratio (B/G), Ratio Vegetation Index (RVI), Green Normalized Difference Vegetation Index (GNDVI), and 2-Band Enhanced Vegetation Index (EVI2) based on their reported applications in the literature. Based on the literature, the B/G index is inversely correlated with chlorophyll a concentrations while the remaining indices are directly correlated. The NDVI index is widely used in agricultural applications to measure crop health and was originally developed to monitor terrestrial vegetation using satellites (Fernandez-Figueroa et al., 2022). Importantly, chlorophyll a concentrations reflect NIR light more strongly than green light (Fernandez-Figueroa et al., 2022). The NDVI index measures the difference between the reflectance of NIR wavelengths and absorption of red wavelengths; consequently; as chlorophyll a concentrations increase, the NDVI will also increase (Wu et al., 2023) The B/G index was originally developed from satellite imagery to estimate chlorophyll a concentrations from ocean color changes in Antarctica (Zeng et al., 2016). While it can also be used with the RGB VIs, we used it for the multispectral VIs only, following Wu et al. (2023). The RVI index was one of the first VIs generated and is considered a sensitive indicator for green plant biomass (Xue & Su, 2017). This index was also reportedly used to measure chlorophyll a levels in small drinking water reservoirs (Fernandez-Figueroa et al., 2022). The GNDVI and EVI2 indices also factor in

the NIR band to estimate terrestrial chlorophyll a concentrations and have been implemented in similar phytoplankton applications (Fernandez-Figueroa et al., 2022). While additional band combinations could be analyzed, analysis of these ten indices was determined to be within the scope of this project. A summary of the ten VIs used is provided in Table 4.

Table 4. Vegetation Index Summary

Vegetation Index	Equation	Application
Color Index of Vegetation Extraction (CIVE)[1,2,3]	(0.441 * R) - (0.881 * G) + (0.385 * B) + 18.787	Agricultural crop health
Excess Green Index (EXG)[1,3,4]	(2 * G) - R - B	Green algae biomass
KIVU[1,*]	(B - R) / G	Lake phytoplankton chlorophyll concentration
Normalized Green-Red Difference Index (NGRDI)[1,4,5]	(G - R) / (G + R)	Green algae biomass
Visible Band Difference VI (VDVI)[1,4]	(2 * G - R - B) / (2 * G + R + B)	Green algae biomass
Normalized Difference Vegetation Index (NDVI)[1,4,6]	(NIR - R) / (NIR + R)	Terrestrial vegetation chlorophyll
Band Ratio (B/G)[6,7]	B / G	Ocean color changes of chlorophyll
Ratio Vegetation Index (RVI)[1,4,6]	NIR / R	Drinking water reservoir chlorophyll concentration
Green Normalized Difference Vegetation Index (GNDVI)[1,4,6]	(NIR - G) / (NIR + G)	Terrestrial vegetation chlorophyll
2-Band Enhanced Vegetation Index (EVI2)[1,4]	2.5*[(NIR - R) / (NIR + 2.4 * R + 1)]	Terrestrial vegetation chlorophyll

Notes:

[1]Fernandez-Figueroa et al. (2022); [2]Kataoka et al. (2003); [3]Sunoj et al. (2021); [4]Xue & Su (2017); [5]Bunyon et al. (2023); [6]Wu et al. (2023); [7]Zeng et al. (2016)

*KIVU was named for its geographic location of use

Red (R), Green (G), Blue (B), Near Infrared (NIR)

Statistical Data Analysis

Descriptive and inferential statistical analysis was completed using RStudio (Version 2023.03.0+386) and R (Version 4.2.3) statistical software. Descriptive summary tables and boxplots were generated for the chlorophyll a results. Boxplots visually represent the locality, spread, and skewness of the data. Calibration curves (scatterplots) comparing chlorophyll a extract concentrations to their absorbance measurements at 664 nm for both the positive controls and the field samples were also generated in R for each sample event. This was done to validate the accuracy of the field samples. In addition, inferential analysis was conducted by generating a simple linear regression model for each flight altitude (60m, 90m, and 120m) for each of the 10 VIs, including for both the RGB and multispectral imagery (30 linear regression models total). The regression models used the method of least squares to estimate the relationship between the average spectral index values (independent variable, X) and chlorophyll a values (dependent variable, Y). We tested the coefficient of the independent variable (average spectral index value)

at the 95% confidence level (5% significance level) using naïve standard error (SE) for all the regression models. While robust SE is typically used to account for violations to model assumptions (e.g., heteroscedasticity), its use is not encouraged for smaller sample sizes since it can dramatically change the models' Confidence Interval (CI) and p-values. This estimation error can lead to misleading model results and interpretations and so was avoided for this analysis. In addition, the strength of the linear relationship was assessed by calculating the Coefficient of Determination (R^2), which is the square of Pearson's Correlation Coefficient (r). The R^2 value assesses the strength of a linear regression model while r measures the strength and direction of the relationship between two variables. We hypothesized that there would be a moderate strength R^2 value between the two variables across the different VIs and that the lower altitude flights will have stronger R^2 values due to their higher spatial resolutions. In addition, model checking was conducted to test the assumptions of the linear regression models, namely by checking the linearity, independence, normality, and equal variance of each model. Respectively, these assumptions state that the relationship between the predictor and the outcome variables is linear, that the residual error terms are independent, that the residual errors are normally distributed, and that the residuals have a constant variance (i.e., homoscedasticity). Residual plots and Quantile-Quantile (QQ) plots were generated to assess these model assumptions in R. All R data analysis code is found in Appendix F as an R Markdown file. This original code also includes an equation sourced from Ramnath (2011) on Stack Overflow, an online resource for computer programmers.

Results

Aim 1

For Aim 1, a narrative literature review was conducted to understand the breadth of the problem that HCBs pose to human health. The review synthesized 15 review articles and 5 experimental studies published across 14 academic journals discussing freshwater cyanobacteria issues across the globe. Major findings included recommendations for future research directions into the less studied cyanotoxins, exploration with new monitoring tools and technologies, improved public education and outreach, and a need for community-based interventions and interdisciplinary collaboration. The lesser known threat of freshwater benthic cyanobacteria, the chronic effects of low-dose cyanotoxin exposure, and the need for a One Health approach to management and risk communication are a few examples of knowledge gaps and future needs identified. This review afforded proper context for this project's case study at the highly populated Echo Lake since blooms are occurring there with higher frequency and measures to better monitor comparable lakes in the state are warranted. Findings from the literature review are discussed in greater depth in Appendix C. In addition, communication with Washington local and state agencies prompted considerations for the evaluation of different environmental factors (e.g., meteorological conditions, solar altitude) and flight settings (e.g., camera sensors, different altitudes) to understand optimal field conditions for drone operation. Table 3 provides a summary of the drone flights and variables measured. These meetings also aided the project team's understanding of how HCBs are currently monitored in Washington State and where there may be opportunities to improve on current surveillance practices.

Aim 2

The results for Aim 2 will include summaries for the calibration curves, chlorophyll a results, phycocyanin results, orthomosaic and VI imagery products, regression models, and model checking in R. Table 5 provides a summary of the spectrophotometer's absorbance readings at 664 nm (the peak absorption for chlorophyll a) and the resultant chlorophyll a values for the extract solutions. Samples are shown in black and serial dilutions are shown in green. Note that this data reflects averages of the duplicate samples and triplicate dilutions.

Table 5. Average Chlorophyll a Extract and Absorbance Measurements - Dilutions and Samples

Sample or Dilution	Average Chl-a (µg/L) - Extract	Average Abs 664 nm	Sample or Dilution	Average Chl-a (µg/L) - Extract	Average Abs 664 nm
7-24-23 1st Sampling Event					
SW01	382.56	0.034			
SW02	445.38	0.039			
SW03	462.31	0.041			
SW04	483.62	0.043			
1:10	2961.11	0.258			
1:100	313.77	0.027			
1:1,000	27.11	0.002			
1:10,000	0	0.000			
1:100,000	0	0.000			
8-7-23 2nd Sampling Event			**8-21-23 3rd Sampling Event**		
SW05	813.40	0.071	SW09	144.33	0.013
SW06	893.92	0.078	SW10	162.92	0.015
SW07	692.99	0.061	SW11	123.87	0.011
SW08	732.80	0.064	SW12	128.99	0.012
1:25	1448.74	0.126	1:25	1459.36	0.127
1:50	733.99	0.064	1:50	731.66	0.064
1:100	378.82	0.033	1:100	336.33	0.029
1:200	195.08	0.021	1:200	146.15	0.012
1:500	77.40	0.007	1:500	39.50	0.003
9-2-23 4th Sampling Event			**9-11-23 5th Sampling Event**		
SW13	333.54	0.030	SW17	293.56	0.026
SW14	482.69	0.043	SW18	324.77	0.029
SW15	512.39	0.045	SW19	351.96	0.031
SW16	346.24	0.031	SW20	232.48	0.021
1:25	1501.65	0.131	1:25	1564.51	0.136
1:50	751.33	0.065	1:50	776.87	0.068
1:100	369.64	0.032	1:100	401.95	0.035
1:200	181.95	0.016	1:200	202.98	0.018
1:500	62.69	0.005	1:500	83.71	0.007
10-7-23 6th Sampling Event			**10-23-23 7th Sampling Event**		
SW21	805.82	0.071	SW25	953.55	0.084
SW22	822.82	0.072	SW26	689.79	0.061
SW23	491.16	0.043	SW27	691.37	0.061
SW24	547.17	0.048	SW28	690.60	0.061
1:25	1536.86	0.134	1:25	1538.43	0.134
1:50	775.84	0.068	1:50	777.38	0.068
1:100	393.59	0.034	1:100	398.03	0.035
1:200	199.03	0.017	1:200	199.57	0.017
1:500	79.79	0.007	1:500	81.38	0.007

Notes:

All samples (black) were run in duplicate and all positive controls (green) were run in triplicate

Abs 664 nm = Absorbance (in Absorbance Units) measured at a wavelength of 664 nanometers

µg/L = micrograms per liter

This data was used to generate the calibration curves presented in Figure 4. The samples (indicated in black) align well between the highest and lowest dilutions of positive controls (indicated in green). This indicates that the sample absorbance readings were agreeable with typically expected absorbances for a range of known chlorophyll a concentrations. In addition, lines of best fit were plotted and the R^2 values are approximately 1.0, indicating a strong fit for the sample and positive control dilution data points. Error bars showing standard deviation for the dilution points are not shown in Figure 4 since they are too small to present graphically. A supplemental table (Table A1) includes all results for the triplicate serial dilutions, including averages and standard deviations for measurements within each sampling event as well as across all sample events, and is provided in Appendix H. The absorbance values in Table A1 indicate that the spectrophotometer measured the extract solution positive controls consistently for the three dilutions in the same event as well as across the sample events. Additionally, acidification of the SSS dilutions was performed to understand the condition of the SSS and whether it was significantly degrading over time. For the last three sampling events, the absorption peak ratios calculated for the SSS dilutions were consistently, approximately 1.70, indicating that the chlorophyll a remained in excellent condition with minimal degradation. These results were tabulated in Table A2 and are also provided as a supplemental table in Appendix H. For each event, results are reported for the first of the three dilutions analyzed in triplicate as these values were deemed representative for the remaining two values and since averaging the values would be less appropriate for this portion of the dilution analysis.

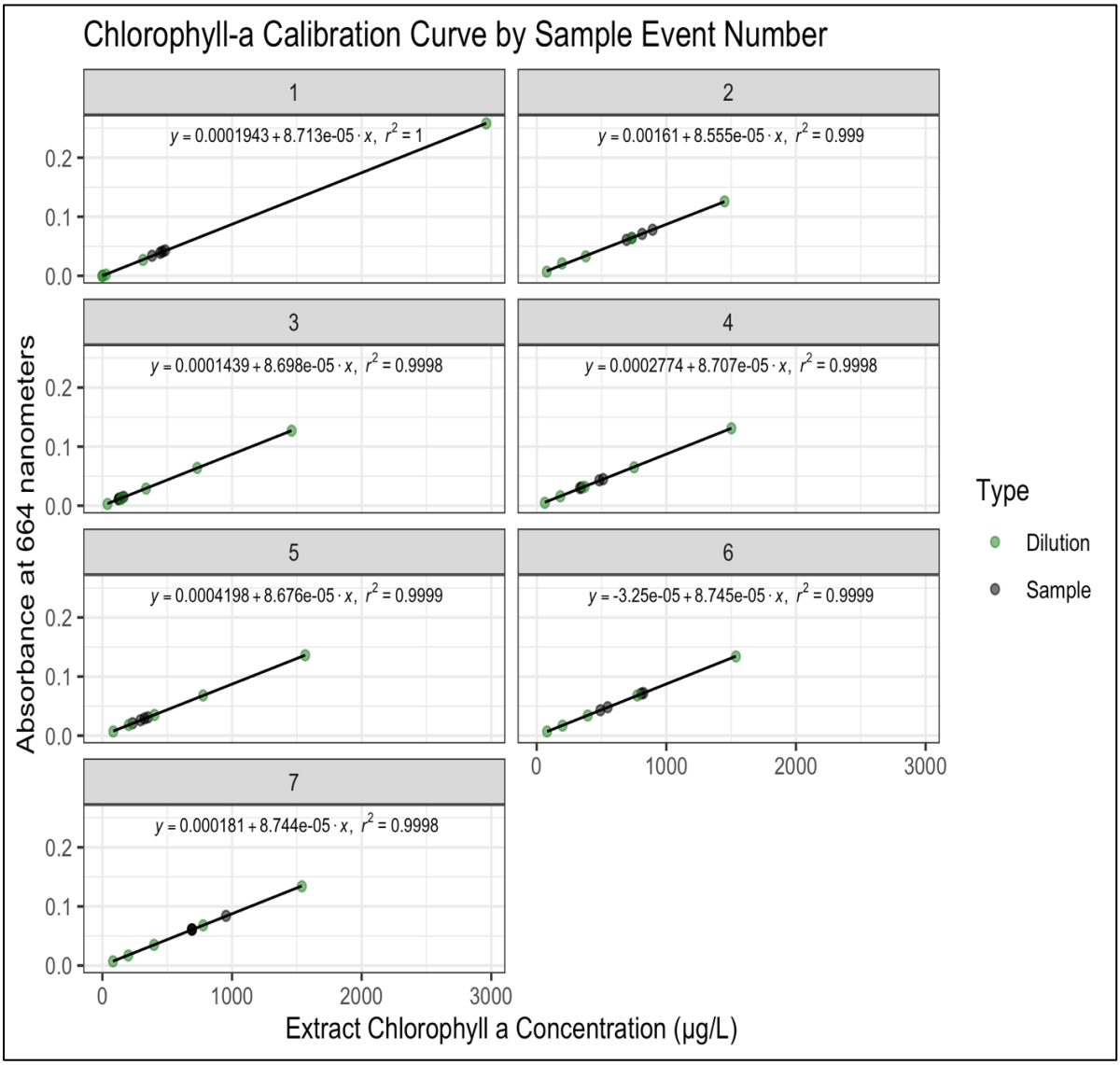

Figure 4. Calibration Curves – Dilutions and Samples.

Between July and October 2023, a total of 28 samples were collected from the public beach and private docks around Echo Lake across seven sampling events. Depending on the event, samples were collected in the late morning or afternoon immediately after drone operation was completed. Water volume filtered for both the samples and their duplicates ranged from 100 mL to 300 mL. More turbid samples required less water to filtrate to prevent overloading of the filter media. Sample collection times and filtration volumes are provided in Table 6.

Table 6. Sample Collection Times and Filter Volumes					
Sample	**Collection Time**	**Volume Filtered (mL)**	**Sample**	**Collection Time**	**Volume Filtered (mL)**
7-24-23 1st Sampling Event			**8-7-23 2nd Sampling Event**		
SW01	1101	200	SW05	1128	200
SW02	1126	200	SW06	1140	200
SW03	1151	200	SW07	1202	200
SW04	1158	200	SW08	1207	200
8-21-23 3rd Sampling Event			**9-2-23 4th Sampling Event**		
SW09	1043	200	SW13	1013	300
SW10	1056	200	SW14	1029	300
SW11	1115	200	SW15	1048	300
SW12	1121	200	SW16	1055	300
9-11-23 5th Sampling Event			**10-7-23 6th Sampling Event**		
SW17	1553	300	SW21	1325	100
SW18	1529	300	SW22	1254	100
SW19	1619	300	SW23	1354	200
SW20	1615	300	SW24	1402	200
10-23-23 7th Sampling Event					
SW25	1412	200			
SW26	1345	200			
SW27	1442	200			
SW28	1448	200			
Notes:					
mL = milliliters					

Table 7 provides a summary of the chlorophyll a concentrations for both the samples and their duplicates, including averaged values. A descriptive summary table for the overall chlorophyll a results and stratified by sample location and event is found in Table 8. The overall average concentration of chlorophyll a was 26.26 µg/L, ranging from 6.19 µg/L to 82.28 µg/L. The sample with the highest average concentration was collected from the North Dock and during the sixth sampling event (10/07/2023), while the sample with the lowest average concentration was collected from the West Docks – South location and during the third sampling event (08/21/2023). Calculated values for chlorophylls b and $c_1 + c_2$ are not reported since these results were negligible or even negative when entered into the Trichromatic and Modified Monochromatic equations, indicating minor amounts of these photosynthetic pigments.

Table 7. Chlorophyll a Sample Results					
Sample	Chl-a (µg/L) - Whole Sample	Chl-a (µg/L) - Average	Sample	Chl-a (µg/L) - Whole Sample	Chl-a (µg/L) - Average
7-24-23 1st Sampling Event			**8-7-23 2nd Sampling Event**		
SW01	18.24	19.13	**SW05**	39.53	40.67
SW01-DUP	20.02		**SW05-DUP**	41.81	
SW02	22.23	22.27	**SW06**	44.70	44.70
SW02-DUP	22.31		**SW06-DUP**	44.70	
SW03	22.90	23.12	**SW07**	34.95	34.65
SW03-DUP	23.33		**SW07-DUP**	34.35	
SW04	23.93	24.18	**SW08**	36.64	36.64
SW04-DUP	24.44		**SW08-DUP**	36.64	
8-21-23 3rd Sampling Event			**9-2-23 4th Sampling Event**		
SW09	7.22	7.22	**SW13**	10.92	11.12
SW09-DUP	7.22		**SW13-DUP**	11.32	
SW10	8.40	8.15	**SW14**	18.55	16.09
SW10-DUP	7.89		**SW14-DUP**	13.63	
SW11	6.19	6.19	**SW15**	17.08	17.08
SW11-DUP	6.19		**SW15-DUP**	17.08	
SW12	6.19	6.45	**SW16**	11.71	11.54
SW12-DUP	6.71		**SW16-DUP**	11.37	
9-11-23 5th Sampling Event			**10-7-23 6th Sampling Event**		
SW17	9.79	9.79	**SW21**	80.07	80.58
SW17-DUP	9.78		**SW21-DUP**	81.10	
SW18	11.02	10.83	**SW22**	81.10	82.28
SW18-DUP	10.63		**SW22-DUP**	83.47	
SW19	11.71	11.73	**SW23**	23.41	24.56
SW19-DUP	11.76		**SW23-DUP**	25.70	
SW20	7.18	7.75	**SW24**	27.40	27.36
SW20-DUP	8.31		**SW24-DUP**	27.32	
10-23-23 7th Sampling Event					
SW25	48.44	47.68			
SW25-DUP	46.91				
SW26	35.81	34.49			
SW26-DUP	33.17				
SW27	35.37	34.57			
SW27-DUP	33.76				
SW28	35.30	34.53			
SW28-DUP	33.76				
Notes:					
µg/L = micrograms per liter					
DUP = Duplicate					

Table 8. Chlorophyll a Results - Overall and Stratified Descriptive Statistics Summary					
Category	**Mean**	**SD**	**Median**	**Min**	**Max**
All Samples (n=28)	26.26	19.95	22.69	6.19	82.28
Beach (n=7)	30.88	27.02	19.13	7.22	80.58
North Dock (n=7)	31.26	26.00	22.27	8.15	82.28
West Docks - North (n=7)	21.70	10.84	23.12	6.19	34.65
West Docks - South (n=7)	21.21	12.61	24.18	6.45	36.64
First Event (n=4)	22.17	2.18	22.69	19.13	24.18
Second Event (n=4)	39.16	4.46	38.66	34.65	44.70
Third Event (n=4)	7.00	0.88	6.83	6.19	8.15
Fourth Event (n=4)	13.96	3.07	13.82	11.12	17.08
Fifth Event (n=4)	10.02	1.71	10.31	7.75	11.73
Sixth Event (n=4)	53.70	32.06	53.97	24.56	82.28
Seventh Event (n=4)	37.82	6.57	34.55	34.49	47.68
Notes:					
All results reported in micrograms per liter					
SD = Standard Deviation					

To visually represent this data, boxplot diagrams were created for the overall chlorophyll a results (Figure 5), stratified by sample location (Figure 6), and stratified by sample event (Figure 7). The outlier points in Figure 5 represent the two highest chlorophyll a concentrations measured (SW21 and SW22) during the sixth sampling event (10/07/2023) when an HCB occurred at Echo Lake. Figure 6 represents very similar results between each sample location

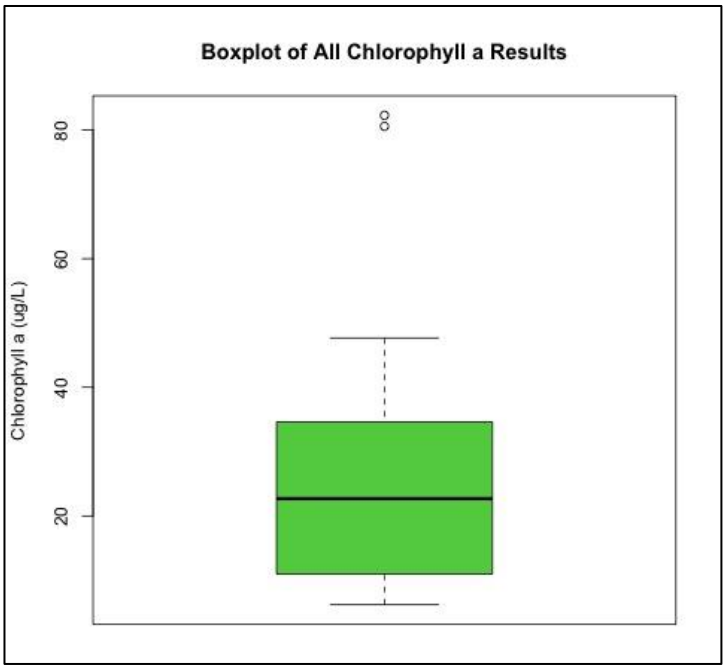

Figure 5. Boxplot of All Chlorophyll a Results.

due to the overlap of the boxplots. In Figure 7, however, differences can be gleamed across the sample events. The chlorophyll a concentrations fluctuated across the field season with moderate levels measured in late July and early August, relatively lower levels in late August and September, and relatively higher levels in October. Chlorophyll a concentrations at the surface of a lake can differ over time based on the level of photosynthetic activity, dependent on available sunlight and nutrients. Chlorophyll a concentrations are typically integrated with other water quality lake indicators to understand the trophic state, or biological activity, of a lake and benchmark values vary based on jurisdiction, with higher values indicating bloom conditions.

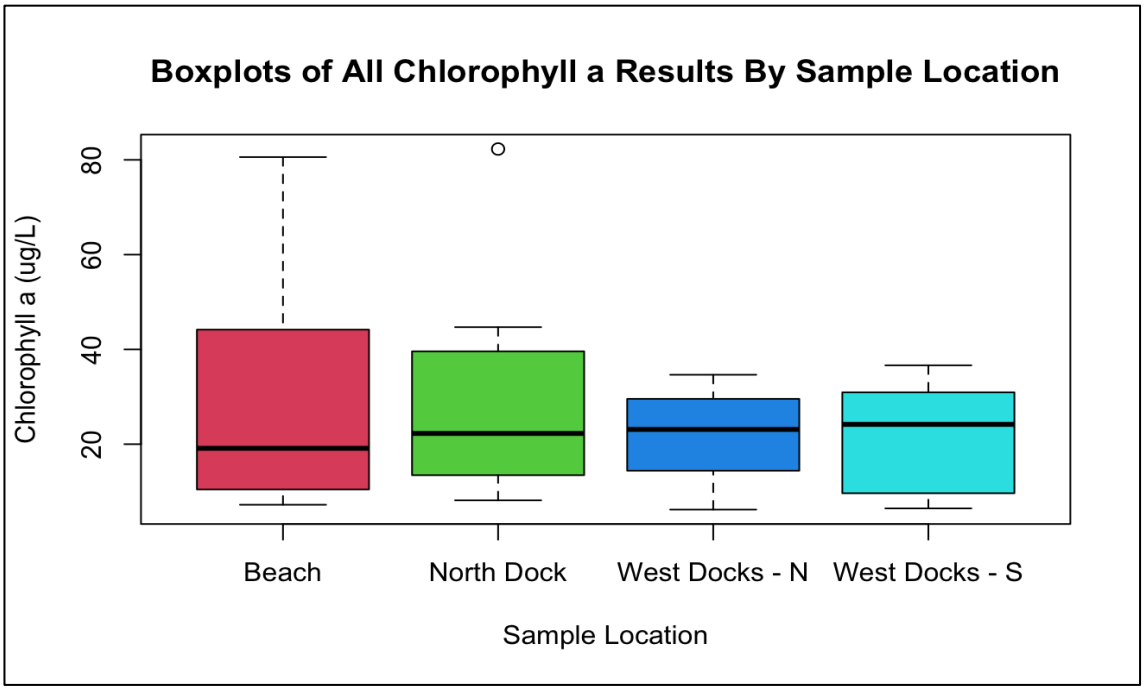

Figure 6. Boxplots of All Chlorophyll a Results Stratified by Sample Location.

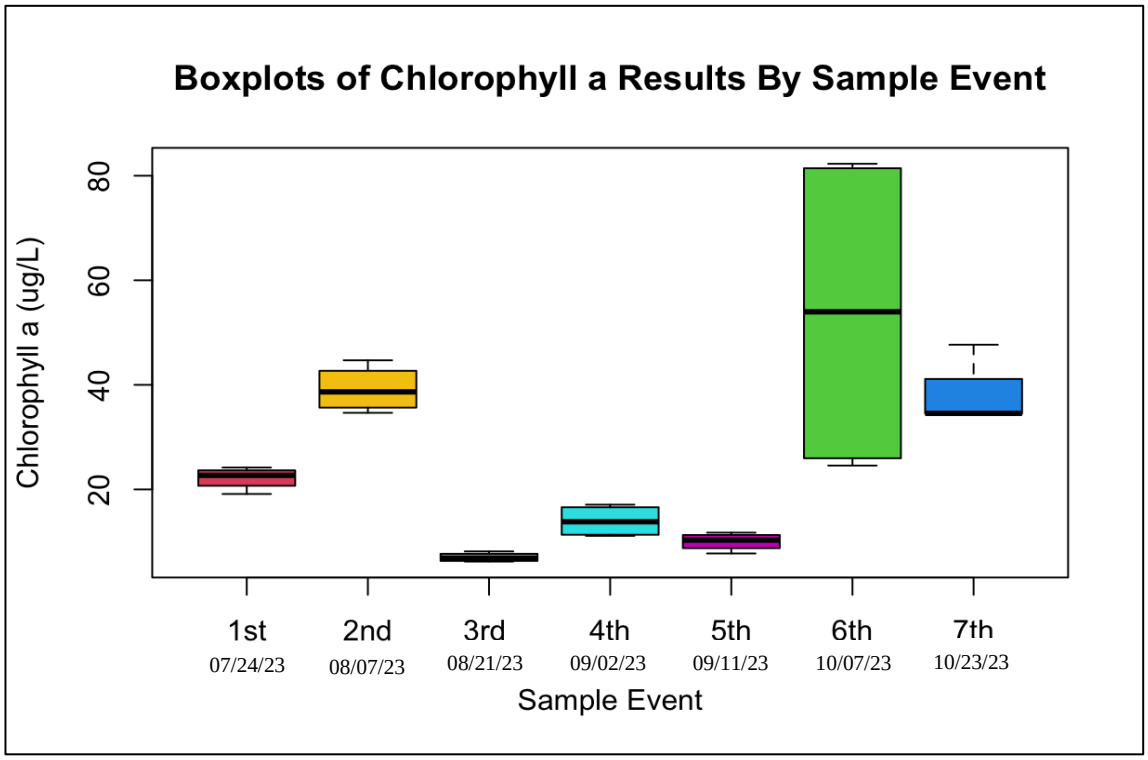

Figure 7. Boxplots of All Chlorophyll a Results Stratified by Sample Event.

These chlorophyll a results represent unacidified values for all sampling events and were compared with acidified values for the last three sampling events. This was done to compare "uncorrected" and "acid-corrected" values. Results are recorded in Table A3, provided as a supplementary table in Appendix H. The acidified sample results generally reduced chlorophyll a by a few µg/L compared to their unacidified counterparts, with the greatest differences observed in SW21 and SW22. Despite the differences observed in these side by side results, the samples generally did not appear to have contained significant pheophytin degradation products and so were properly preserved during the collection and analysis process. Nevertheless, the lack of acidification data for the first four events represents a study limitation and will be discussed in more detail in the Discussion section. In addition, Table 9 provides results for the field and lab blank filters analyzed for QA/QC purposes. Impurities in the filtered deionized or distilled water may absorb in the same peak wavelength as chlorophyll a by the spectrophotometer, resulting in the values shown in Table 9 when applied to the equations.

Table 9. Field Blank and Lab Blank Results

Sample	Chl-a (µg/L) - Whole Sample
7-24-23 1st Sampling Event	
FB	0.10
LB	0.94
8-7-23 2nd Sampling Event	
FB	0.09
LB	1.02
8-21-23 3rd Sampling Event	
FB	0.09
LB	0.94
9-2-23 4th Sampling Event	
FB	0.19
LB	0.28
9-11-23 5th Sampling Event	
FB	0.27
LB	1.02
10-7-23 6th Sampling Event	
FB	0.10
LB	0
10-23-23 7th Sampling Event	
FB	0.29
LB	0.94

Notes:
FB = Field Blank
LB = Lab Blank
Lab deionized water was used for the first two events and distilled water was used for the last five events

Table 10 shows the results for the phycocyanin readings measured using the phycocyanin handheld fluorometer. Readings were taken from each sample collection point immediately after water sample collection. Of the eight, averaged sample readings for phycocyanin during the sixth (10/07/2023) and seventh (10/23/2023) sample events, the fluorometer showed levels that generally aligned with the measured chlorophyll a readings, in that higher concentrations of phycocyanin were recorded with higher concentrations of chlorophyll a. Results for SW21 and SW22 during the bloom event indicated readings that represented the upper limit of detection of the instrument (199 µg/L). These results are further examined in the Discussion section.

Table 10. Phycocyanin Fluorescense Probe Readings

Sample	Collection Time	Readings (µg/L)	Average Readings (µg/L)
10-7-23 6th Sampling Event			
SW21	1325	199, 199, 199	199
SW22	1254	199, 199, 199	199
SW23	1354	31, 24, 57	37
SW24	1402	30, 17, 28	25
10-23-23 7th Sampling Event			
SW25	1412	59, 27, 26	37
SW26	1345	22, 28, 29	26
SW27	1442	22, 25, 22	23
SW28	1448	28, 17, 27	24

Notes:
In-situ readings were measured three times using a Turner Designs FluoroSense Handheld Fluorometer with phycocyanin optics during the last two sampling events.

Simple linear regression models were generated to understand how predictive the aerial image-derived VIs were in estimating chlorophyll a levels. It is important to first note that the sample location at the public beach was obscured by a tree shadow during the sixth sampling event (10/07/2023) and led to a misrepresentative VI index average for SW21. Consequently, this data point, which measured 80.58 µg/L chlorophyll a, was omitted from the regression analysis to avoid bias. This resulted in one less sample point for the regression analyses. The sample size for the RGB VIs is 27 for each flight altitude and the sample size for the

multispectral VIs is 8 for the 60m and 90m flights and 4 for the 120m flight. The 120m multispectral flight for the fifth event (09/11/2023) was not conducted due to technical difficulties. Furthermore, the CIVE, EXG, and VDVI VIs resulted in low to moderate strength R^2 values, with higher R^2 values at lower flight altitudes. These models were found to be statistically significant with p-values less than the significance level of 0.05 for each of the flight altitudes tested. Moreover, the R^2 values and p-values for the remaining RGB-derived VIs and altitudes were found to be weakly correlated, explaining little of the data's variation, and not statistically significant ($p > 0.05$). Likewise, the R^2 values for the multispectral VIs were all found to be weaker with p-values greater than the 0.05 significance level, due to low sample size and other considerations reported in the Discussion section.

Table 11 provides an analysis summary for all VIs tested for each of the flight altitudes and includes model coefficient estimates, 95% CIs for the slope estimate, R^2 values, and p-values. The following interpretations for the model coefficient estimates and hypothesis testing are made for the CIVE 60m regression model. Based on the CIVE 60m data, the estimated mean of chlorophyll a was 27.45 µg/L at a CIVE index value of 0. With a one-unit difference (upward) in the CIVE index value, we estimated the mean of chlorophyll a to be lower by 1.066 µg/L. There is a statistically significant association between the CIVE 60m index and chlorophyll a. We reject the null hypothesis (i.e., no association, slope estimate of 0) at the 5% significance level because the p-value is less than the significance value and because the 95% CI does not contain the null value of 0. Moreover, we are 95% confident that the interval (-1.549, -0.5844) contains the true population slope coefficient. For the coefficient of determination, the regression on the CIVE 60m spectral index values accounts for approximately 45% of the total variation in chlorophyll a, based on this data.

Table 11. Simple Linear Regression Model Analysis Summary				
Flight Altitude	**60m**			
Vegetation Index	**Intercept Estimate**	**Slope Estimate**	**95% CI**	**R^2 value (p value)**
CIVE	27.45	-1.066	[-1.549, -0.5844]	**0.4537 (0.0001*)**
EXG	16.07	0.4192	[0.2029, 0.6356]	**0.3892 (0.0005*)**
KIVU	29.38	-40.25	[-88.02, 7.511]	0.1075 (0.095)
NGRDI	17.78	87.59	[-41.95, 217.1]	0.0720 (0.176)
VDVI	17.38	178.7	[63.32, 294.2]	**0.2892 (0.004*)**
NDVI	2.638	-70.86	[-249.3, 107.5]	0.136 (0.369)
B/G	47.78	-19.90	[-103.3, 63.55]	0.0537 (0.581)
RVI	53.98	-55.29	[-198.5, 87.93]	0.1295 (0.381)
GNDVI	11.80	-41.94	[-143.6, 59.71]	0.1452 (0.352)
EVI2	0.9801	-58.74	[-208.7, 91.25]	0.1327 (0.375)
Flight Altitude	**90m**			
Vegetation Index	**Intercept Estimate**	**Slope Estimate**	**95% CI**	**R^2 value (p value)**
CIVE	27.51	-0.9967	[-1.622, -0.3715]	**0.3013 (0.003*)**
EXG	17.11	0.3882	[0.1192, 0.6572]	**0.2611 (0.006*)**
KIVU	27.52	-25.00	[-82.65, 32.64]	0.0309 (0.380)
NGRDI	15.89	113.2	[-8.086, 234.4]	0.1288 (0.066)
VDVI	17.64	178.0	[54.18, 301.9]	**0.2596 (0.007*)**
NDVI	-2.397	-85.40	[-346.1, 175.3]	0.0968 (0.453)
B/G	17.76	5.266	[-132.9, 143.4]	0.0014 (0.929)
RVI	59.96	-67.81	[-295.2, 159.6]	0.0815 (0.493)
GNDVI	-1.802	-83.58	[-308.1, 140.9]	0.1215 (0.397)
EVI2	-4.663	-71.30	[-298.8, 156.2]	0.0893 (0.472)
Flight Altitude	**120m**			
Vegetation Index	**Intercept Estimate**	**Slope Estimate**	**95% CI**	**R^2 value (p value)**
CIVE	27.05	-0.8513	[-1.412, -0.2908]	**0.2813 (0.004*)**
EXG	17.89	0.3431	[0.09489, 0.5913]	**0.2448 (0.009*)**
KIVU	28.62	-33.28	[-76.22, 9.663]	0.0925 (0.123)
NGRDI	20.74	48.22	[-68.32, 164.8]	0.0282 (0.402)
VDVI	17.83	181.4	[53.10, 309.6]	**0.2533 (0.007*)**
NDVI	64.48	97.39	[-453.8, 648.6]	0.2242 (0.527)
B/G	-37.48	65.17	[-143.6, 274.0]	0.4741 (0.311)
RVI	-8.773	81.59	[-373.3, 536.5]	0.2295 (0.521)
GNDVI	19.70	-61.43	[-426.3, 303.4]	0.2079 (0.544)
EVI2	67.92	83.28	[-384.7, 551.3]	0.2267 (0.524)

Notes:

95% CI = 95% Confidence Interval for the slope estimate

The p value has a significance level (α) of 0.05.

BOLD and * indicate p values less than 0.05

The top five listed vegetation indices were calculated for the RGB imagery (n = 27 for each flight altitude) and the bottom five listed vegetation indices were calculated for the multispectral imagery (n = 8 for the 60m and 90m flights; n = 4 for the 120m flight due to technical difficulties during this flight event).

Orthomosaic imagery products were generated from ArcGIS Pro for each sampling event and are presented as supplemental figures in Appendix H. Figures A1a-g include orthomosaics for the RGB imagery and Figures A2a-b include orthomosaics for the multispectral imagery, by sample event. For the first five sampling events, the formation of algae on the lake was minimal but an HCB occurred during the month of October 2023 for the sixth and seventh events. The orthomosaic images were used to generate new maps highlighting vegetation in the lake and surrounding area using the different VI equations. Selected site photographs from the drone platforms before and after this bloom event are provided in Appendix I.

Figure 8 presents RGB orthomosaic images and the associated CIVE index maps generated for the first sampling event (07/24/2023). Green areas (lower CIVE index values) represent vegetated areas while red areas (higher CIVE index values) represent unvegetated areas, such as pavement and other darker surfaces. Recall that the CIVE index has a negative association with chlorophyll a concentrations. These index values are based on the reflection of green light at the surface of the lake (upper photic zone). In addition, the quality of the orthomosaic image stitching and the calculated VI values changed slightly between flight altitudes. For instance, various streaks on the images, representing imperfect image stitching, generally decrease in appearance with higher altitude flights. Also note that the outer edges of the orthomosaics appear distorted due to reduced imagery collection on the perimeter of the defined flight area. The Figure 8 VI maps are fairly representative of low-bloom event maps for most of the RGB VIs used in this study.

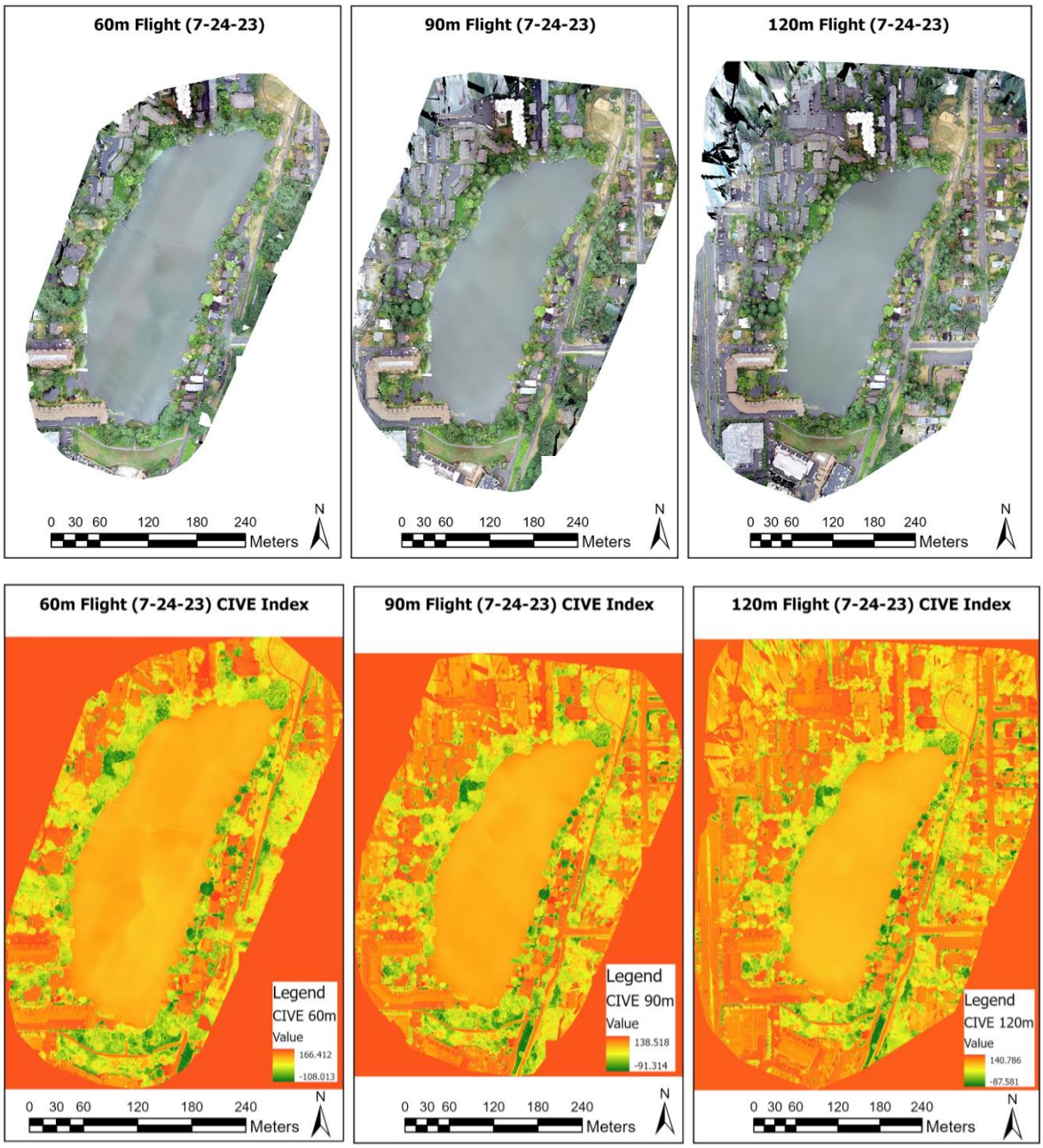

Figure 8. First Sampling Event RGB Orthomosaics and CIVE Index Maps.

In contrast to this event, Figure 9 shows RGB orthomosaics for the sixth sampling event (10/07/2023) and the associated CIVE index maps when a bloom was present. Nearly the entire lake surface was covered by an algal bloom. The CIVE index maps were able to assign different spectral values for the chlorophyll a levels across the lake surface, notably for the swirling

feature of the bloom shown in the images. The different time of day of image collection and effects of tree shadowing bias the true color and subsequent VI calculation for these images. As mentioned, sample SW21 was omitted due to the impacts of tree shadowing.

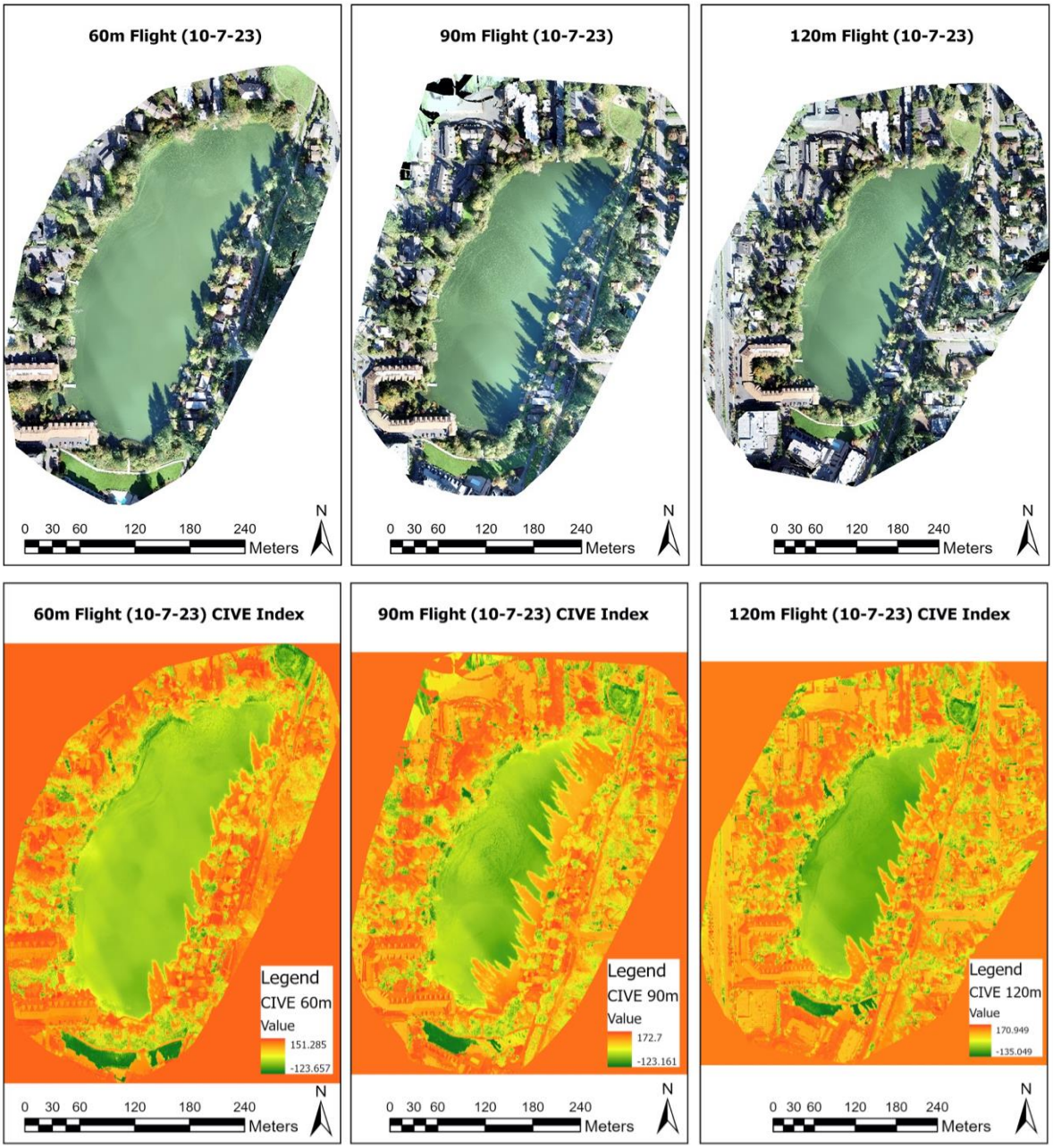

Figure 9. Sixth Sampling Event RGB Orthomosaics and CIVE Index Maps.

Figure 10 shows RGB orthomosaics for the seventh sampling event (10/23/2023) and associated CIVE index maps after the bloom began to dissipate. Surface scum was still present in the northeast portion of the lake and was captured by the CIVE index maps.

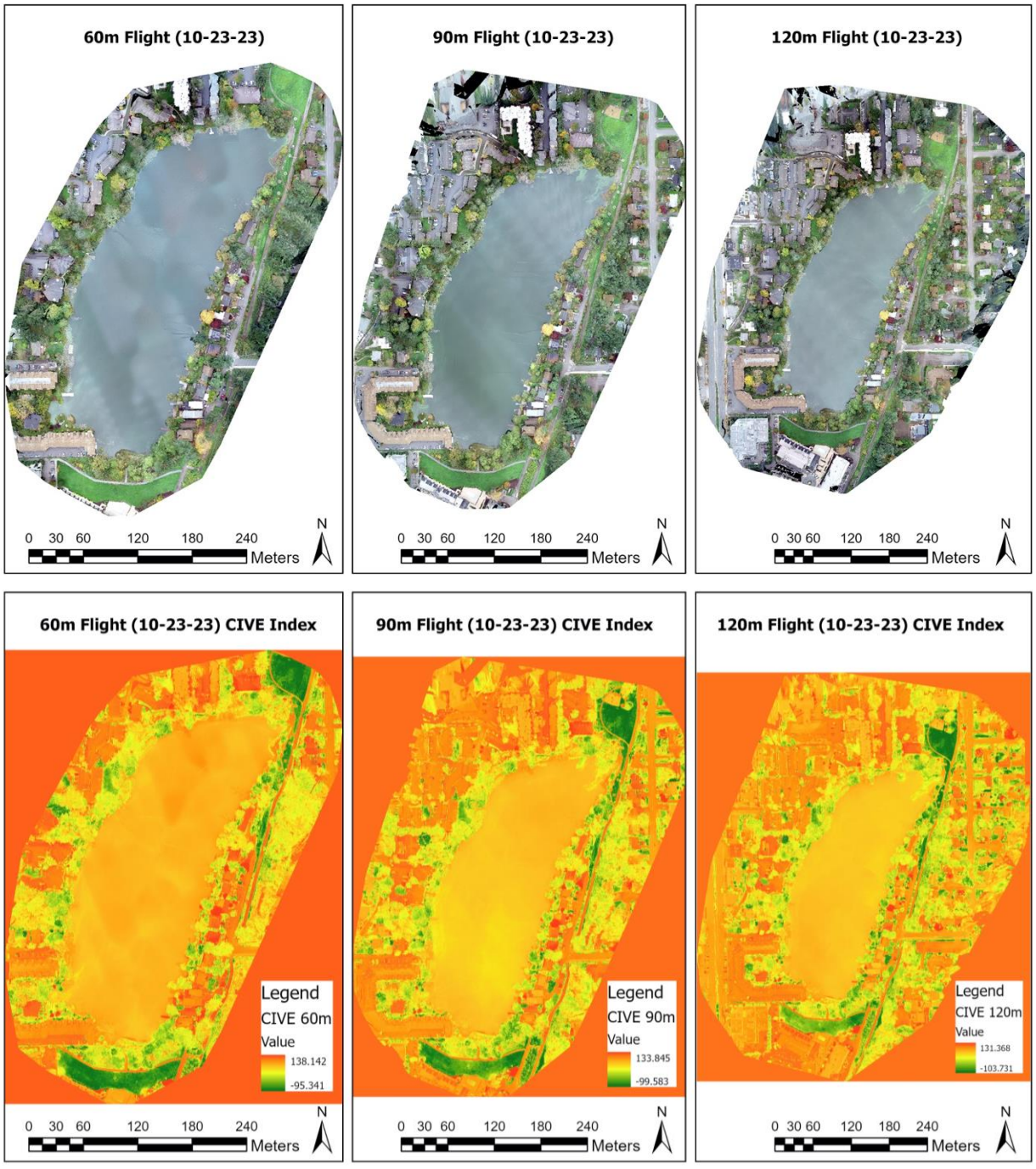

Figure 10. Seventh Sampling Event RGB Orthomosaics and CIVE Index Maps.

The orthomosaics presented in Figures 8 and 9 are fairly representative of the extremes of algal scum observed during no bloom and bloom events, respectively, while Figure 10 shows a minimal amount of surface scum present. In addition, the CIVE index maps presented in these figures are fairly representative in appearance to the other RGB indices analyzed as they all used the same color ramp symbology in ArcGIS Pro to portray vegetated and unvegetated areas, albeit with varying pixel spectral values.

Figure 11 presents orthomosaics generated from the multispectral imagery and associated NDVI index maps for the seventh sampling event (10/23/2023). Stitching of the water surface using the multispectral sensor was not as successful as the RGB optical camera due to expected difficulties with stitching constantly changing water surfaces as well as limitations of the Matrice drone platform. However, stitching did improve with higher flight altitudes. In addition, the multispectral composite orthomosaics generated appear to not match the lake surface's true color. This is a result of the nature of how multispectral sensors measure each wavelength of light, but the resultant VI maps do account for the lake's true color. For the VI maps, the green areas (higher NDVI index values) represent vegetated areas while red areas (lower NDVI index values) represent unvegetated areas, such as pavement and other darker surfaces. Sample events using the multispectral drone and sensor experienced either no-bloom (fifth event) or low-bloom (seventh event) conditions with minimal surface scum on the lake surface. The maps presented in this figure are representative of the orthomosaics and NDVI index maps for the fifth sample event (09/11/2023). The fifth event orthomosaic images are included as Figure A2a in Appendix H. The NDVI index maps presented in Figure 11 are fairly representative in appearance to the other multispectral indices analyzed as they all used the same color ramp symbology in ArcGIS Pro to portray vegetated and unvegetated areas, albeit with varying pixel spectral values.

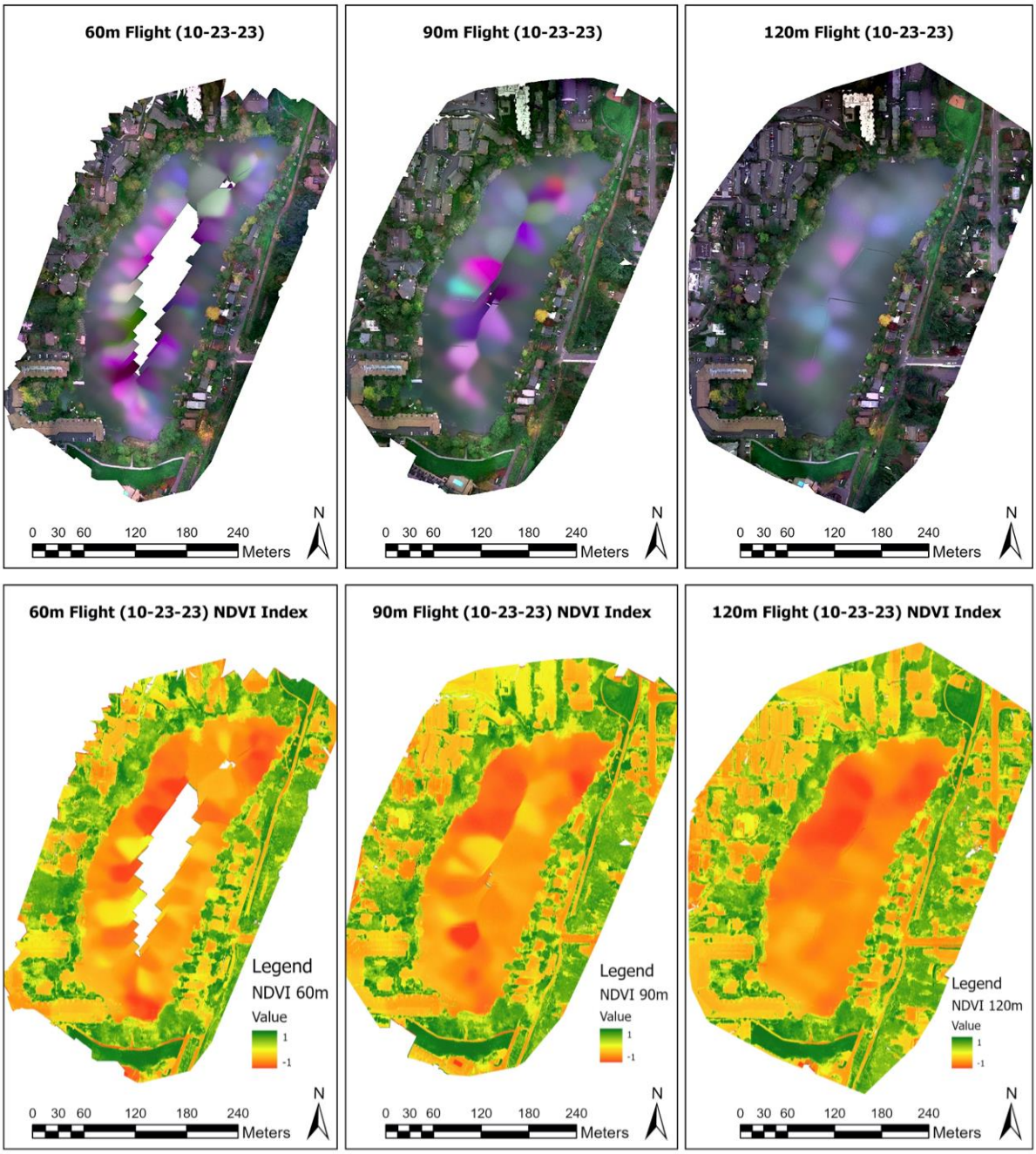

Figure 11. Seventh Sampling Event Multispectral Orthomosaics and NDVI Index Maps.

Furthermore, Figure 12 presents the regression models for the CIVE index at each flight altitude, including the regression equation and R^2 value. Confidence intervals are shown in gray. The R^2 values decreased with increasing altitude. Linear regression models for all the RGB (Figure A3) and multispectral (Figure A4) indices are provided as supplemental figures in Appendix H. As expected, the CIVE index had an inverse relationship with chlorophyll a and the EXG, NGRDI, and VDVI VIs evidenced a direct relationship, for all altitudes. However, the KIVU index showed a negative relationship with chlorophyll a at all altitudes rather than a positive one, based on the literature. For the multispectral VIs, all the 60m and 90m curves showed either an inverse or no relationship with chlorophyll a while the 120m curves showed negative relationships for all VIs except for NGRDI, which was positive. The direction of these associations was less definitive due to the low sample sizes obtained while using the multispectral drone platform.

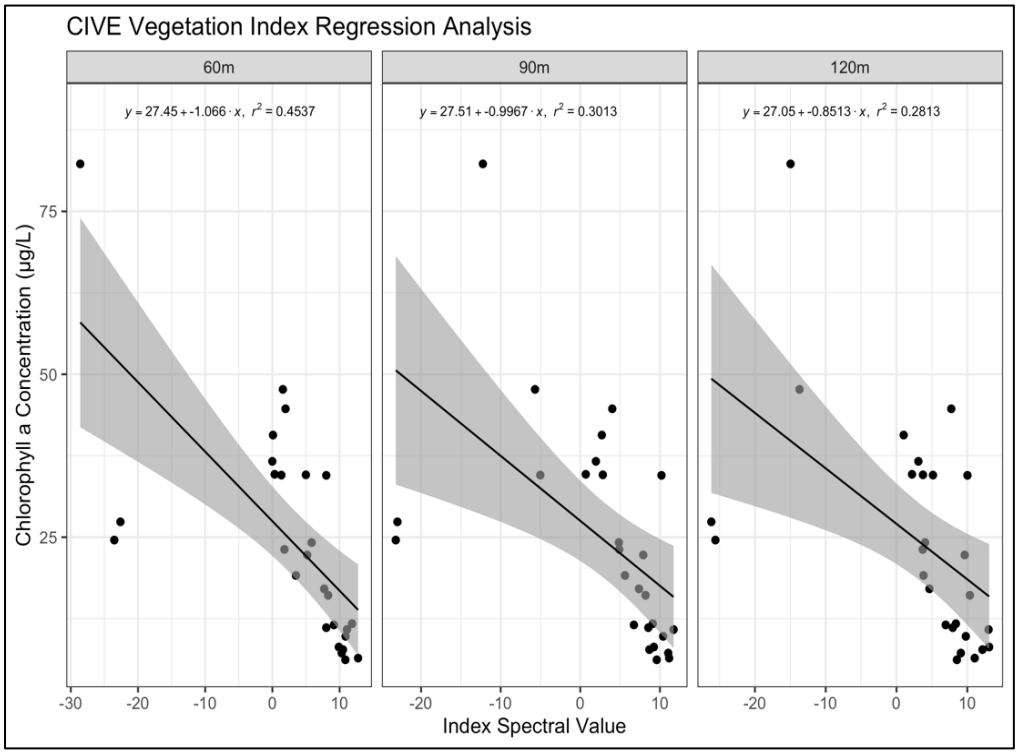

Figure 12. CIVE Linear Regression Models.

The project team also conducted model checking by assessing the linearity, equal variance, independence, and normality assumptions of all the regression models. To this end, residual plots and QQ plots were generated using R. The following describes a typical model check conducted for the CIVE 60m linear regression model. The CIVE 60m residual plot (Figure 13) suggests possible non-linearity in the conditional mean of chlorophyll a concentration given the mean CIVE 60m spectral index value. This is due to the behavior of the lowess line on the right side of the graph. It is important to note that since the lowess line averages over nearby points, it is more susceptible to the outliers on the right side of the plot (the curve is more dominated by these points). However, the residuals on the left side of the plot appear to be an unstructured, mostly horizontal band of points centered around zero. Based on this, evidence for non-linearity is somewhat equivocal; however, it appears that the linearity assumption has been violated when accounting for these outlier values. Moreover, the residual points of the graph appear to be placed nicely around the horizontal line at zero on the left side of the plot but

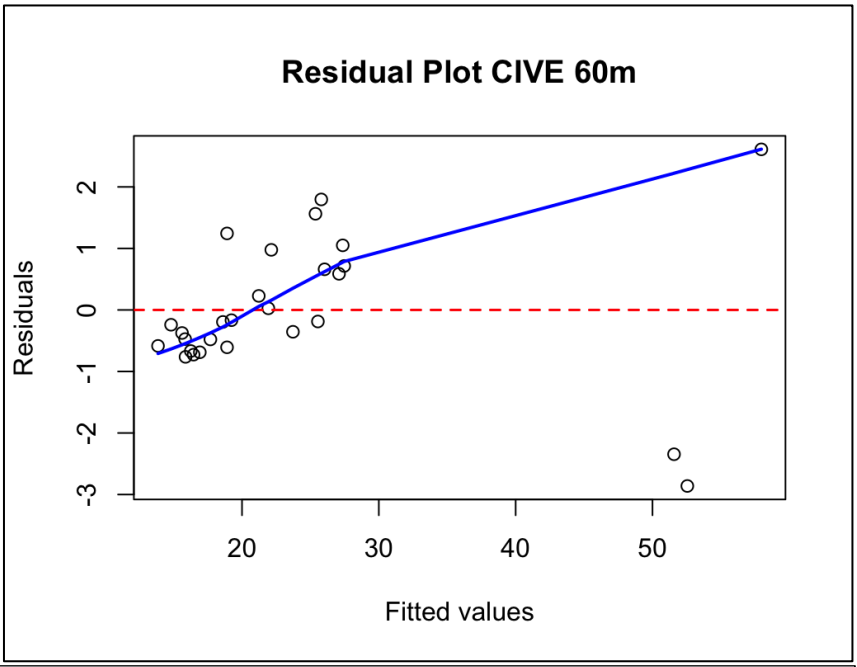

Figure 13. CIVE 60m Linear Regression Model Residual Plot.

deviate on the right side of the plot. Based on the behavior of the outliers, the assumption of equal variance is also equivocal. Even accounting for the outliers, we conclude that there is evidence of heteroscedasticity, meaning our assumption of homoscedasticity or equal/constant variance has not been met. We can conclude from this residual analysis that our confidence interval of the mean may be impacted due to some limited evidence of nonlinearity and heteroscedasticity, based on the presence of outliers.

Independence is based on the study design and since the water samples and drone flight data were collected independently from each other for each sampling event, the assumption of independence has been met. For normality, the CIVE 60m QQ plot (Figure 14) shows that the dataset values are normally distributed since most residual points lie approximately along the diagonal line. There are, however, several points on the tails that deviate from the diagonal line. This suggests a small deviation from normality, most likely as a result of the small sample size and presence of outlier points. The normality assumption is determined to have been met.

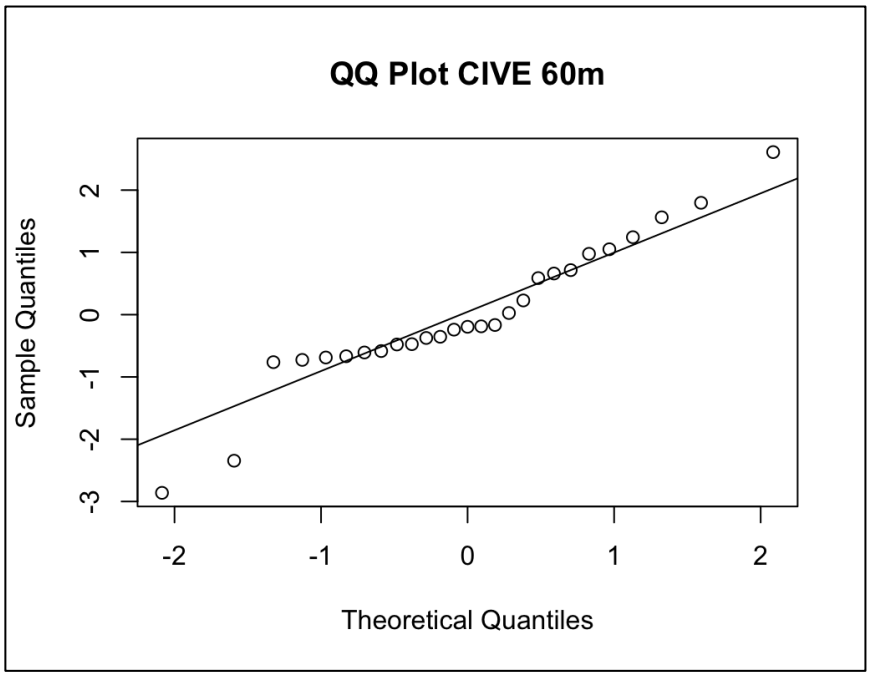

Figure 14. CIVE 60m Linear Regression Model QQ Plot.

To summarize, model checking showed that assumptions for the CIVE 60m regression model have been violated for linearity and equal variance, but not for independence or normality. This is due to a small sample size and the presence of outliers, notably from the sixth sample event (10/07/2023). This overall finding represents a study limitation and will be discussed in more detail in the Discussion Section. Besides the CIVE 60m regression model, residual plots and QQ plots were generated for all VI regression models derived from the RGB imagery and are included in the R Markdown report in Appendix F. The overall results and interpretations of the model checks for the CIVE 90m and CIVE 120m models were similar to the CIVE 60m model. This was generally also the case when reviewing these plots for the EXG, KIVU, NGRDI, and VDVI VIs for all their altitudes. The implications of these model checks on the final regression results are discussed more in the Discussion section. Furthermore, model checking was not completed for the VI regression models derived from the multispectral imagery because of very low sample sizes. This also represents a study limitation.

Aim 3

For Aim 3, a deliverable was generated highlighting considerations for conducting similar lake surveillance work using drones. The purpose of this document is to provide information to water resource managers and public health practitioners on best practices using remotely piloted drones for the monitoring of HCBs in small inland lakes. Considerations for certification and training, drone platforms and operation, camera sensors and settings, environmental conditions, site access and logistics, data storage and safety, costs, and other parameters are discussed based on the findings of this pilot research project. The guidance document is provided in Appendix G and will be disseminated to pertinent local agencies.

Findings from this research study were presented at the Washington State Environmental Health Association (WSEHA) Annual Education Conference (AEC) in May 2024, held in Yakima, Washington. Research findings will also be presented in a poster format at the National Environmental Health Association (NEHA) AEC in July 2024, held in Pittsburgh, Pennsylvania. The audience for these conferences generally includes environmental health professionals, academics, and students in Washington State and across the U.S. The goal of these presentations is to inform water resource managers and public health practitioners of the use of drones as an emerging environmental monitoring tool for HCBs as well as the findings from this pilot work.

Discussion

The use of drone imaging to estimate chlorophyll a concentrations in Echo Lake was most successful using the Phantom platform and while employing the CIVE 60m index (R^2 = 0.45, $p < 0.001$). The CIVE 90m and 120m regression models, as well as the EXG and VDVI models at all altitudes, were statistically significant as well (Table 11). These results were agreeable with Fernandez-Figueroa (2021), which also found the CIVE index to generate the best estimate of chlorophyll a concentration collected from the same Phantom 4 Pro platform (R^2 = 0.35, $p < 0.0001$) (Fernandez-Figueroa, 2021). In addition, their EXG index ($R^2 = 0.33$, $p < 0.0001$) and VDVI index ($R^2 = 0.24$, $p < 0.0001$) results also generated statistical significance despite weak R^2 values. While these models used water surface color changes in the lake's upper photic zone to explain some of the variability within the chlorophyll a values measured, other sources of variability include meteorological and water quality parameters influencing photosynthesis (e.g., sun exposure, nutrient levels, turbidity), the phytoplankton composition of the lake and growth rates, phytoplankton mobility in the water column, pigment interferences, variations of the drone's flight path, light reflection at different times of day and sun angle, and unknown factors. Factors like total phosphorus levels, for instance, are an important predictor of HCBs in addition to chlorophyll a levels. These other factors limit the predictive ability of these models. In addition, it is important to note that the confidence intervals for the statistically significant indices are very wide, meaning the uncertainty is greater. This is a major limitation for the interpretation of the regression model estimates and statistical tests. Nevertheless, use of the CIVE VI allows a reasonable estimation of lake chlorophyll a levels using a relatively inexpensive, user-friendly, and time-efficient drone platform. In practice, the use of a drone for frequent monitoring of a lake may provide additional information on the whole lake's relative

chlorophyll a levels where a single sample may only offer a limited snapshot of the lake's biological productivity.

Major limitations for the multispectral linear regression analyses included low sample size and data collection during non-peak bloom events. Attaining a higher sample size for these models was less feasible due to the higher costs of rental equipment. There was also difficulty with anticipating time-sensitive bloom conditions due to their intermittent nature, especially factoring in scheduling conflicts since a RAPID staff member was required to operate the multispectral equipment. Acquiring additional funding to collect more water samples and schedule more multispectral flights is necessary for future work. Furthermore, although the multispectral VIs yielded insignificant results for this study, incorporation of VIs using the NIR wavelength has been found to generate accurate chlorophyll a estimates (Fernandez-Figueroa, 2021; Wu et al., 2023). For instance, correlation with chlorophyll a using the NDVI index was reported with an R^2 value of 0.79 ($p < 0.0001$) for 70 water samples collected from 54 ponds of varying trophic status by Fernandez-Figueroa (2021) and an R^2 value of 0.49 ($p < 0.05$) for 12 water samples collected at a single lake by Wu et al. (2023). However, Wu et al. (2023) found the strength of the correlation for two of its most predictive indices—NDVI and B/G—to vary substantially with each of the two lakes they sampled. Increased sample power and sampling lakes of different size and biological productivity are crucial considerations when employing these VIs. In addition, the use of multispectral imagery in precision agriculture and crop management may also be useful for water resource managers to identify nutrient sources near water bodies. Agrahari et al. (2021) used the NDVI index to identify higher and lower amounts of nitrogen fertilizer in an agricultural setting (Figure 1, Agrahari et al., 2021). This technology

may be useful to identify areas with excess nutrients around a lake and for local jurisdictions to conduct outreach and recommend source control measures.

Furthermore, the use of a multispectral drone was incorporated based on its widespread application in the literature and to understand its logistical and image processing challenges. This study found that stitching of water surfaces to generate true color composite orthomosaics and subsequent VI analyses was less successful than the Phantom platform but improved with higher altitude flights. At higher flight altitudes, the sensor's field of view increases and captures more surface features, which improves image overlap and consequent stitching of the images. This finding was consistent with previous work using drones equipped with multispectral sensors (Figure 7, Bunyon et al., 2023). Both sets of multispectral orthomosaics in Figure A2 were collected when the lake did not exhibit much algal growth and sky conditions were overcast; consequently, the water surface lacked distinguishable features and did not stitch well. Future research with drones equipped with multispectral cameras will need to account for the requirement of landmark features such as buoys, docks, or established vegetation to facilitate image stitching of keypoints. Different photogrammetric processing settings may also be explored to improve imagery outputs and subsequent analysis.

For the RGB imagery, photo stitching of the entire lake surface improved with higher altitude flights but overall was quite successful for all altitudes. This may have been due to the smaller size of this particular lake (approximately 12 acres) and this drone platform's ability to tie image keypoints together. However, several exceptions were observed. During the third sampling event (08/21/2023), the orthomosaic did not stitch properly due to a lack of tie points and has a white box displayed (Figure A1c). This may have been due to the presence of particulate matter in the atmosphere due to recent wildfire activity in the region during the month

of August, which created slightly hazy conditions that impacted the photographs. The least successful photo stitching occurred during the fourth sampling event (09/02/2023) when the sky was mostly sunny with passing clouds (see Figure A1d). The imagery appeared to stitch more successfully on events when it was either overcast or sunny with a clear sky, while the events with sunny skies and the presence of clouds generated lower quality orthomosaics. This may have been a result of the lake reflecting too many clouds across the sky, creating a "moving terrain" that impeded image stitching as the lake surface appeared to change. Interestingly, the presence of the bloom appeared to help image stitching as it resembled a recognizable water surface feature. Moreover, since the R^2 values improved with lower altitude flights for the CIVE, EXG, and VDVI indices but image stitching appeared to improve with higher altitude flights, a balance may need to be considered for these two factors. Flying at too low an altitude inhibits successful photo stitching but improves the image resolution and resultant VI association while flying too high up improves stitching albeit with less strong VI-chlorophyll a associations.

A closer look at the chlorophyll a results is also appropriate. The highest concentrations were observed during the second (08/07/2023), sixth (10/07/2023), and seventh (10/23/2023) sampling events. One possible explanation for the elevated levels during the second event may have been the result of an influx of nutrients from the surrounding area via stormwater outfalls. Utilizing the City of Shoreline's City Surface Water Assets Interactive Map, a number of outfalls were identified around Echo Lake (City of Shoreline, n.d.-a). According to the City, the majority of Echo Lake's water inflow comes from outfalls on the southern portion of the lake, with smaller outfalls around the lake perimeter draining impervious areas of the residential complexes. Surface discharges can contribute excess nutrients and help fuel cyanobacteria growth. Outfall tracing is one technique that can help pinpoint outfalls that are draining excess

nutrient loads. This drone application may be useful to distinguish areas of the lake with higher or lower biological activity; however, these areas are subject to wind movements and may migrate or dissipate. In an effort to prevent stormwater pollution of natural waterways, the City of Shoreline's Source Control program aims to inspect and educate businesses and public properties, recommending best management practices such as the use of spill kits and other site-specific controls (City of Shoreline, n.d.-b).

For the sixth and seventh sampling events, a major HCB occurred at the lake. Cyanobacteria blooms often occur during late summer and early fall when water temperatures, sunlight, and nutrient levels are at their highest. King County records routine lake monitoring data on their "Water Quality Data" online search tool. Based on this resource, Echo Lake measured peak total nitrogen and total phosphorus values in August and October 2023, coinciding with the highest chlorophyll a values measured (King County, 2023b). Additionally, King County integrates its data on chlorophyll a, Secchi disk depth (a measure of water clarity), and total phosphorus into a Trophic State Index (TSI), an overall metric for biological productivity calculated from each of these variables. The TSI produces the same index value for a given combination of these variables because they are correlated by linear regression models; in addition, the TSI requires minimal data to calculate, is easy to interpret, and is suitable for citizen lake monitoring programs (NALMS, n.d.-b). According to the July 2023 *King County Lake Stewardship Program: 2022 Monitoring Update*, the most recent water quality report available for Echo Lake, the chlorophyll a and total phosphorus TSI values were in the eutrophic range, a trend that appears to have continued into 2023 (King County, 2023a). Based on this report, eutrophic lakes are defined as having a TSI index greater than 50, less clear water with

higher nutrient concentrations and consequent algal growth, and are more likely to have more frequent, and potentially more toxic, algal blooms (King County, 2023a).

On October 2, 2023, the City of Shoreline collected a scum sample from Echo Lake's public beach, measuring a concentration of 10 µg/L for Microcystin, above the state recreational guideline of 8 µg/L, and finding no level detected for Anatoxin-a, per the state toxic algae website (Ecology, 2024). On October 4, when these test results by King County became available, the City of Shoreline posted a Tier I Warning sign on the lake and notified residents of these results (Swim Guide, n.d.). The lake continued to be sampled approximately weekly until October 30, 2023, with all subsequent sample results measured as either "non-detect" or below the state guidance level (Ecology, 2024). Based on the state toxic algae website, water samples were also collected from Echo Lake on October 9, 2023 for phytoplankton identification and indicated the presence of species for the following cyanobacteria: Aphanizomenon, Dolichospermum (formerly Anabaena), Microcystis, Phormidium, Planktothrix, and Woronichinia (Ecology, 2024). Water samples collected from Echo Lake in the past for phytoplankton identification have indicated dominant species present of Aphanizomenon, Woronichinia, and Dinobryon (Ecology, 2024). Cyanobacteria management options will be recommended based on Echo Lake's LCMP.

Furthermore, surface algal scum was present throughout the month of October and overlapped with the sixth (10/07/2023) and seventh (10/23/2023) sampling events. During the peak bloom event (10/07/2023), the two samples collected at the West Docks sample locations (SW23 and SW24) had much lower chlorophyll a concentrations—24.56 and 27.36 µg/L, respectively— relative to samples collected from the northern portion of the lake (SW21 and SW22), which measured 80.58 and 82.27 µg/L, respectively. We believe that the West Docks

concentrations were lower due to the northward movement of the water pushing and concentrating the bloom toward the northern portion of the lake. This provided a valuable lesson in ensuring that samples are collected as close in time as possible to the planned flights to account for the temporal and spatial variability of HCBs. In addition, due to the effect of the tree shadow at the Public Beach sample location during this event, SW21 had its average spectral index value mischaracterized, so this data point was omitted. We believe that had this extreme sample point been included in the regression analyses, and if the West Docks sample concentrations had been more reflective of apparent bloom concentrations, we would have observed improved regression model R^2 values. This presents a limitation for future work in that chlorophyll a concentrations and green, scummy water surfaces may not always correlate well. Future applications may consider collecting additional samples during an HCB event and to align sample collection timing with drone imagery acquisition.

The measurement of phycocyanin is an incredibly useful metric to quantify developing HCBs since this pigment is primarily associated with cyanobacteria. Fernandez-Figueroa (2021) found a statistically significant association between phycocyanin and the GNDVI index (R^2 = 0.64, $p < 0.0001$). The researchers used a Turner Designs Trilogy fluorometer combined with laboratory procedures to measure phycocyanin levels. While this parameter is a powerful predictor for cyanobacterial blooms and multispectral imagery is well-poised to estimate their concentrations, phycocyanin can be costly and labor-intensive to analyze. For this project, we tested the use of a Turner Designs FluoroSense Handheld Fluorometer, which provided a relatively inexpensive alternative with a rapid turnaround time for an approximate value of phycocyanin. The incorporation of this instrument validated the presence of cyanobacteria in Echo Lake during the October HCB by measuring positive readings that matched the magnitude

of measured chlorophyll a concentrations (Table 10). Notably, the sensor was able to distinguish different levels of phycocyanin—and hence cyanobacteria—from areas of the lake that were visibly similar in appearance. This instrument, albeit with lower specificity and sensitivity than traditional microscopy, can be implemented in future projects to assess the association between multispectral-derived VIs and more rapidly collected phycocyanin readings. Caution in interpreting results is needed since ambient light conditions for the probe and the drone imagery to estimate phycocyanin may differ based on sun angle, sample timing, and other factors. Moreover, Thomson-Laing et al. (2020) evaluated the performance of a portable handheld fluorometer with much higher sensitivity, the Turner Designs CyanoFluor, and found a significant association between phycocyanin measurements and cyanobacterial biomass, accurate enough to use for recreational guidelines worldwide (Thomson-Laing et al., 2020). Other researchers have utilized in-situ phycocyanin fluorometer probes to accurately measure cyanobacteria abundance (Loisa et al., 2015) while others are testing the performance of chlorophyll a portable fluorometers as well (Hamdhani et al., 2021). Use of these fluorometers to validate phycocyanin levels estimated by multispectral sensors can be an instrumental tool.

In addition, the phycocyanin sensor used in this study can help guide field staff on where to collect samples for cyanotoxin or even genetic analysis during an HCB event. This is an important consideration in public health since it can be difficult to discern where the highest concentrations of cyanotoxins are located in a lake. Water resource managers typically collect water samples from public access areas as it represents the greatest risk to public exposure, but potentially higher toxin levels can occur elsewhere on the lake and migrate to higher or lower traffic areas. For the City of Shoreline, a sample is collected any time there is visible scum or a bloom, samples are sent to King County's Environmental Laboratory, and both results and

recommendations (e.g., lake signage, next steps) are communicated by King County to the City and Department of Health. Prior to an official closure of the lake, the precautionary principle is generally followed in that lake residents avoid contact with the lake when visible scum is present. With this quick and simple, semi-quantitative instrument, investigators can target priority areas in a lake based on relative phycocyanin readings that may indicate more consequential sample results with regard to toxin concentration or genetic composition.

Data on meteorological, environmental, and flight parameters is provided in Table 3. Average flight times were 14.6 minutes (60m Phantom), 10.2 minutes (90m Phantom), 8.9 minutes (120m Phantom), 38 minutes (60m Matrice 210), and 13 minutes (90m Matrice 210), along with a total flight time of 8 minutes for the 120m Matrice 210 flight. Higher altitude flights were faster than lower altitude flights since they collected less photos of the lake area. One key measurement was the solar altitude, which generally measures 0 degrees at sunrise and 90 degrees when the sun is highest in the sky, though the maximum altitude can vary depending on geography and time of year. Following Fernandez-Figueroa (2021), we strived to schedule flights when the solar altitude was 43 degrees or lower to avoid sun glint. The solar altitude at 43 degrees at the study site coincided with approximately 10:00 am in mid-July, 10:30 am in mid-August, and 12:00 pm in mid-September, with a maximum solar altitude of 33 degrees at 13:00 pm in mid-October (SunCalc, n.d.). Flights were conducted between 07:30 am and 14:00 pm during the project period depending on weather delays, technical difficulties, and other factors. Since most flights occurred with overcast conditions, the solar altitude was less of a concern. However, the third (08/21/2023), fourth (09/02/2023), and sixth (10/07/2023) sampling events included sunshine but the recorded solar altitudes were between 9 and 30 degrees. With minimal sun glints effects observed in the orthomosaic images, 43 degrees appears to be an ideal

benchmark value for conducting flights. Moreover, Mount (2005) describes the photographic impacts of sun glint, reflection, refraction, and wind speed in more technical detail and how these factors determine the optimal window of time to collect nadir imagery of shallow water bodies. Generally, solar altitudes below 20 to 25 degrees risk low light transmittance and limit subsurface illumination while solar altitudes greater than 30 to 35 degrees are more likely to have sun glint effects (Mount, 2005). While these values were derived from models generated for marine environments, this study still provides valuable insights for this drone application regarding the complex water surface effects on aerial imagery. Additional lessons learned from this project on optimal flight operation are further summarized and presented in the form of a guidance document in Appendix G.

Finally, the benefits of using drone platforms to monitor lakes were also identified. Drones can collect data for an entire lake in a short period of time, are flexible in terms of flight scheduling and customizable data collection, and are able to have their imagery processed in shorter timeframes than traditional sampling and thus provide faster decision making. For this work, the following approximate timing was recorded for each methodological step: field water sample collection (1 hour), lab water sample processing (8 to 10 hours over three days), calculation of chlorophyll a results (1 hour), field photo acquisition using drone platforms (30 minutes for equipment setup and calibration with 10 to 40 minutes per flight), lab photogrammetry processing using Pix4D (1 hour for initial processing and between 1 to 3 hours of processing per flight), and vegetation index calculations using ArcGIS Pro (1 hour per orthomosaic). These estimates do not account for travel time to and from the study setting and may not account for Internet connectivity and computer memory speeds. Based on the study by Bunyon et al. (2023), they found that water sample collection and processing for chlorophyll a

and cell concentrations took more than 4.5 times longer than the collection and processing of drone-acquired data (Figure 6, Bunyon et al., 2023). In addition, drones are able to access previously inaccessible portions of a lake, minimize the health risks of sample collection from HCB-impacted areas, are a cheaper option over manual sampling, provide the appropriate image resolution for small-scale lakes that satellite imagery cannot provide, are an accessible technology that is easy to learn, and greatly enhance routine visual inspections of a lake surface. Based on these advantages, more frequent flights across a lake can help lake managers monitor for bloom conditions with greater temporal and spatial frequency. Integrated with traditional monitoring strategies, drones can act as early warning tools for the onset of a bloom by quantifying increasing levels of chlorophyll a or phycocyanin over time. This can help pinpoint areas of higher risk around the lake and by extension higher priority areas to sample. Similar to the USEPA's bloomWatch mobile application, which crowdsources data from citizen scientists to track and document HCBs in lakes across the world, drone imagery may be similarly crowdsourced and uploaded to an online database to better understand trends in HCB development and occurrence (Cyanobacteria Monitoring Collaborative, n.d.). Citizen scientists able to capture drone imagery would also require the ability to geolocate the images and send the data to an agency capable of downstream storage and processing.

Study Limitations

This project has a number of limitations that should be addressed. Despite the QA/QC procedures followed to ensure precision and accuracy of water sample collection and analysis, opportunities for bias or inaccuracies exist. Possible sample degradation from exposure to heat or light, insufficient preservation in the field or lab, cross contamination, the timing of sample

collection and filtration, appropriate filter volumes, instrument or human measurement error, and interferences from dissolved organic matter or chlorophyll degradation products are all factors. Also, standard settings for the drone flights and photogrammetry analysis software were chosen for this project although more optimized configurations may have been warranted. The research team chose processing settings suited to this research application to the best of their knowledge. Also, while this study only assessed 10 VIs, a multitude exist that can be investigated to estimate levels of chlorophyll a or phycocyanin.

Regarding the dilution analyses, results showed that the spectrophotometer generated fairly consistent absorbance readings for the SSS within and across sample events and was able to bracket the sample absorbance readings (Table A1). In addition to checking instrument measurement precision, acidification of the pure chlorophyll a dilutions resulted in absorption peak ratios indicating that the SSS remained in robust physiological condition with minimal degradation over the project period (Table A2). However, this data was limited to the last three sampling events and generalizations were made for the first four sampling events without this acidification data. Similarly, acidification of the field sample results was only completed for the last three sampling events. While differences in the "uncorrected" and "acid-corrected" chlorophyll a concentrations appeared small for this data—with the exception of the highest chlorophyll a readings—the lack of information for the first four events raises questions on the accuracy of the "uncorrected" results (Table A3). It is important to adhere to the "acid-corrected" analysis method to account for pheophytin a degradation biases. We contend that the findings of this project are not meaningfully impacted by the lack of the acidification data since the lake water was not problematically acidic to cause excess degradation, preservation methods were adhered to, and since pheophytin a amounts are typically minimal with actively growing algae

(King County, 2023a). In addition, King County reported measurements of pheophytin a below the method detection limit or reporting detection limit during the project period (King County, 2023b). Although the chlorophyll a values used in this analysis were slightly overestimated, the uniform decrease brought about by acidification, at least observed for the last three sampling events, would not substantially alter the linear regression analysis results.

In terms of the linear regression model checking, all of the RGB-derived models were found to have violated the assumptions of linearity and equal variance. This was caused primarily by a low sample size (27 total water samples with the omission of SW21) as well as outlier points, including the high chlorophyll a concentration measured for SW22. While these data points were valuable in capturing chlorophyll a extremes during the HCB event, they introduced a right skew in the sample distribution. Based on the residual plot analyses for these models, a violation of linearity makes the model less accurate and less predictive of non-linear data. The violation of equal variance also compromises the results and interpretations of the confidence intervals and statistical tests for these models. It is critical that future studies applying this methodology collect larger sample sizes and perhaps apply a logarithmic transformation to the response variable (i.e., chlorophyll a) before statistical analysis to reduce heteroscedasticity, as was done by Fernandez-Figueroa (2021). These decisions would improve the linearity, normality, and equal variance of the models and resultant findings. For the purposes of this Tier I project, we were interested in identifying the limitations of this drone application and recommend follow-up projects address the statistical shortcomings of this work. Furthermore, for the multispectral VI models, the low sample size disallowed an appropriate check of the model assumptions, making a meaningful interpretation of these models not possible.

Limitations for the use drones were also encountered with this project and have been well documented in the literature (Almuhtaram et al., 2021; Kislik et al., 2018). Weather conditions constituted a limitation for the flights except in cases of overcast skies or sunny skies with few clouds; however, hazy and partly sunny skies hindered water stitching. The timing of day and shadows cast by tall objects such as trees also inhibited downstream analysis. In the case of Echo Lake, site accessibility and flight restrictions were not an issue but this is generally not the case for other water bodies, which require research and notification to ensure safe and acceptable flight operation. The major limitations for the Matrice 210 drone were the higher cost associated with the multispectral sensor as well as difficulties with imaging the water surface. Initial training and costs to use this equipment along with the inherent liability of flying unmanned aerial vehicles can inhibit their use by local jurisdictions. As Kislik et al. (2018) also found, the lack of standardized methodologies for this research application introduced difficulties, leading to the research team relying on similar work presented in the academic literature. These challenges must be balanced with the benefits drones offer in monitoring HCB-impacted lakes.

Concluding Remarks and Future Directions

Toxic algal blooms represent a mounting threat to the environment and to public health. Cyanotoxicosis presents myriad human health issues and HCBs are projected to worsen over the coming decades as a result of the climate crisis. Novel technological approaches like satellite remote sensing are already proving effective for HCB monitoring but implementation at smaller geographic scales are still developing. Integration of drones with routine HCB surveillance strategies at the sub-state level provides additional information for local public health and environmental resource agencies to act. This study incorporated drone imaging to monitor a local lake in Washington State and validated chlorophyll a estimations with in-situ water sample analysis. Future work may address the use of different drone platforms and spectral sensors, collection of additional samples along the shoreline or further offshore, additional lakes with varying sizes and trophic levels, experimenting with different platform settings and environmental conditions, application of additional VIs, incorporation of methods to compare multispectral imagery to phycocyanin measurements, more robust statistical analysis, and additional collaborations. This work may be expanded by applying machine learning algorithms to detect HCBs from the spectral imagery or by experimenting with different approaches in which drones can enhance HCB surveillance. In order to protect our limited freshwater resources, we must meet the challenge of HCBs as we head toward an unknown future.

References

Abd El-Ghany, N. M., Abd El-Aziz, S. E., & Marei, S. S. (2020). A review: Application of remote sensing as a promising strategy for insect pests and diseases management. *Environmental Science and Pollution Research, 27*(27), 33503–33515. https://doi.org/10.1007/s11356-020-09517-2.

Abdallah, M. F., Van Hassel, W. H. R., Andjelkovic, M., Wilmotte, A., & Rajkovic, A. (2021). Cyanotoxins and Food Contamination in Developing Countries: Review of Their Types, Toxicity, Analysis, Occurrence and Mitigation Strategies. *Toxins, 13*(11), Article 11. https://doi.org/10.3390/toxins13110786.

Agrahari, R. K., Kobayashi, Y., Tanaka, T. S. T., Panda, S. K., & Koyama, H. (2021). Smart fertilizer management: The progress of imaging technologies and possible implementation of plant biomarkers in agriculture. *Soil Science and Plant Nutrition*, *67*(3), 248–258. https://doi.org/10.1080/00380768.2021.1897479.

Almuhtaram, H., Kibuye, F. A., Ajjampur, S., Glover, C. M., Hofmann, R., Gaget, V., Owen, C., Wert, E. C., & Zamyadi, A. (2021). State of knowledge on early warning tools for cyanobacteria detection. *Ecological Indicators, 133*, 108442. https://doi.org/10.1016/j.ecolind.2021.108442.

Arar, E. J. 1997. *Method 446.0: In Vitro Determination of Chlorophylls a, b, c + c and Pheopigments in 1 2Marine And Freshwater Algae by Visible Spectrophotometry*. U.S. Environmental Protection Agency, Washington, DC, EPA/600/R-15/005. Retrieved from https://cfpub.epa.gov/si/si_public_record_report.cfm?Lab=NERL&dirEntryId=309415.

Baird, R. B., Bridgewater, L. L., Eaton, A. D., & Rice, E. W. (2017). *Standard Methods for the Examination of Water and Wastewater (23rd ed., pp. 10-22–10-30).* American Public Health Association.

Benedict, K. M. (2017). Surveillance for Waterborne Disease Outbreaks Associated with Drinking Water—United States, 2013–2014. *MMWR. Morbidity and Mortality Weekly Report*, *66*. https://doi.org/10.15585/mmwr.mm6644a3.

Benson, J., Hanlon, R., Seifried, T. M., Baloh, P., Powers, C. W., Grothe, H., & Schmale, D. G. (2019). Microorganisms Collected from the Surface of Freshwater Lakes Using a Drone

Water Sampling System (DOWSE). *Water*, *11*(1), Article 1. https://doi.org/10.3390/w11010157.

Bormans, M., Maršálek, B., & Jančula, D. (2016). Controlling internal phosphorus loading in lakes by physical methods to reduce cyanobacterial blooms: A review. *Aquatic Ecology*, *50*(3), 407–422. https://doi.org/10.1007/s10452-015-9564-x.

Bullerjahn, G. S., McKay, R. M., Davis, T. W., Baker, D. B., Boyer, G. L., D'Anglada, L. V., Doucette, G. J., Ho, J. C., Irwin, E. G., Kling, C. L., Kudela, R. M., Kurmayer, R., Michalak, A. M., Ortiz, J. D., Otten, T. G., Paerl, H. W., Qin, B., Sohngen, B. L., Stumpf, R. P., … Wilhelm, S. W. (2016). Global solutions to regional problems: Collecting global expertise to address the problem of harmful cyanobacterial blooms. A Lake Erie case study. *Harmful Algae, 54*, 223–238. https://doi.org/10.1016/j.hal.2016.01.003.

Bunyon, C. L., Fraser, B. T., McQuaid, A., & Congalton, R. G. (2023). Using Imagery Collected by an Unmanned Aerial System to Monitor Cyanobacteria in New Hampshire, USA, Lakes. *Remote Sensing*, *15*(11), Article 11. https://doi.org/10.3390/rs15112839.

City of Shoreline. (n.d.-a). *Shoreline Surface Water Assets*. Retrieved April 5, 2024, from https://shoreline.maps.arcgis.com/apps/webappviewer/index.html?id=b54b046d8b894440b62406f0245a10d8.

City of Shoreline. (n.d.-b). *Source Control Program*. Retrieved April 6, 2024, from https://www.shorelinewa.gov/government/departments/public-works/surface-water-utility/services/business-pollution-prevention.

CDC. (2021, September 30). *One Health Harmful Algal Bloom System (OHHABS)*. Harmful Algal Bloom (HAB)-Associated Illness. https://www.cdc.gov/habs/ohhabs.html.

Cyanobacteria Monitoring Collaborative. (n.d.). *bloomWatch*. https://cyanos.org/bloomwatch/.

DJI. (2019 June). *Matrice 200 Series V2 M210 V2 / M210 RTK V2 User Manual V1.4*. https://dl.djicdn.com/downloads/m200_v2/20190617/M210_V2_M210_RTK_V2_User_Manual_v1.4_EN.pdf.

DJI. (2020 July). *Phantom 4 RTK User Manual v2.4*. https://dl.djicdn.com/downloads/phantom_4_rtk/20200721/Phantom_4_RTK_User_Manual_v2.4_EN.pdf.

DOH. (2021). *Washington State Recreational Guidance for Microcystins, Anatoxin-a, Cylindrospermopsin and Saxitoxin*. Publication Number 333-279.

https://doh.wa.gov/sites/default/files/legacy/Documents/4300/333-279-GuidanceFreshwaterToxins.pdf?uid=644aacf2a2330.

Ecology. (2024). *Washington State Toxic Algae, Freshwater Algae Bloom Monitoring Program*. https://www.nwtoxicalgae.org.

Fernandez-Figueroa, E. G., Wilson, A. E., & Rogers, S. R. (2022). Commercially available unoccupied aerial systems for monitoring harmful algal blooms: A comparative study. *Limnology and Oceanography: Methods, 20*(3), 146–158. https://doi.org/10.1002/lom3.10477.

Graham, J.L., Loftin, K.A., Ziegler, A.C., & Meyer, M.T. (2008). *Guidelines for Design and Sampling for Cyanobacterial Toxin and Taste-And-Odor Studies in Lakes and Reservoirs*. U.S. Geological Survey Scientific Investigations Report 2008–5038. https://pubs.usgs.gov/sir/2008/5038/pdf/SIR2008-5038.pdf.

Graham, C. T., O'Connor, I., Broderick, L., Broderick, M., Jensen, O., & Lally, H. T. (2022). Drones can reliably, accurately and with high levels of precision, collect large volume water samples and physio-chemical data from lakes. *Science of The Total Environment, 824*, 153875. https://doi.org/10.1016/j.scitotenv.2022.153875.

Hamdhani, H., Eppehimer, D. E., Walker, D., & Bogan, M. T. (2021). Performance of a Handheld Chlorophyll-a Fluorometer: Potential Use for Rapid Algae Monitoring. *Water, 13*(10), Article 10. https://doi.org/10.3390/w13101409.

Hanlon, R., Jacquemin, S. J., Birbeck, J. A., Westrick, J. A., Harb, C., Gruszewski, H., Ault, A. P., Scott, D., Foroutan, H., Ross, S. D., González-Rocha, J., Powers, C., Pratt, L., Looney, H., Baker, G., & Schmale, D. G. (2022). Drone-based water sampling and characterization of three freshwater harmful algal blooms in the United States. *Frontiers in Remote Sensing, 3*. https://doi.org/10.3389/frsen.2022.949052.

Hardy, F. J., Bouchard, D., Burghdoff, M., Hanowell, R., LeDoux, B., Preece, E., Tuttle, L., & Williams, G. (2016). Education and notification approaches for harmful algal blooms (HABs), Washington State, USA. *Harmful Algae, 60*, 70–80. https://doi.org/10.1016/j.hal.2016.10.004.

Hudnell, H. K. (2010). The state of U.S. freshwater harmful algal blooms assessments, policy and legislation. *Toxicon, 55*(5), 1024–1034. https://doi.org/10.1016/j.toxicon.2009.07.021.

Kataoka, T., Kaneko, T., Okamoto, H., & Hata, S. (2003). Crop growth estimation system using machine vision. *Proceedings 2003 IEEE/ASME International Conference on Advanced Intelligent Mechatronics (AIM 2003), 2*, b1079-b1083 vol.2. https://doi.org/10.1109/AIM.2003.1225492.

King County. (2002). *Volunteer Lake Monitoring Results for the Water Year 2001. King County Lake Monitoring Report: Volunteer Lake Monitoring Results for Water Year 2000-2001*. https://your.kingcounty.gov/dnrp/library/archive-documents/wlr/waterres/smlakes/LMRep_01.pdf.

King County. (2015, December 15). *Echo-Shoreline Lake. Lake Information Page - King County*. https://green2.kingcounty.gov/smalllakes/LakePage.aspx?SiteID=10.

King County. (2021). *Echo Lake 2021 Lake Stewardship Monitoring Report*. https://your.kingcounty.gov/dnrp/library/water-and-land/science/stewardship/2022-Echo-Shoreline-2021.pdf.

King County. (2023a). *King County Lake Stewardship Program: 2022 Monitoring Update*. Prepared by Wafa Tafesh and Daniel Nidzgorski, Water and Land Resources Division. Seattle, Washington. https://your.kingcounty.gov/dnrp/library/2023/kcr3000-2022/kcr3000-2022.pdf.

King County. (2023b). *Water Quality Data*. https://green2.kingcounty.gov/smalllakes/WQData.aspx.

King County. (2024). *King County iMap Interactive mapping tool*. https://kingcounty.gov/en/legacy/services/gis/maps/imap.

Kislik, C., Dronova, I., & Kelly, M. (2018). UAVs in Support of Algal Bloom Research: A Review of Current Applications and Future Opportunities. *Drones, 2*(4), Article 4. https://doi.org/10.3390/drones2040035.

Kouakou, C. R. C., & Poder, T. G. (2019). Economic impact of harmful algal blooms on human health: A systematic review. *Journal of Water and Health, 17*(4), 499–516. https://doi.org/10.2166/wh.2019.064.

Loisa, O., Kääriä, J., Laaksonlaita, J., Niemi, J., Sarvala, J., & Saario, J. (2015). From phycocyanin fluorescence to absolute cyanobacteria biomass: An application using in-situ fluorometer probes in the monitoring of potentially harmful cyanobacteria

blooms. *Water Practice and Technology*, *10*(4), 695-698. https://doi.org/10.2166/wpt.2015.083.

Merel, S., Walker, D., Chicana, R., Snyder, S., Baurès, E., & Thomas, O. (2013). State of knowledge and concerns on cyanobacterial blooms and cyanotoxins. *Environment International, 59*, 303–327. https://doi.org/10.1016/j.envint.2013.06.013.

MicaSense, Inc. (2020 June). *MicaSense Altum™ and DLS 2 Integration Guide*. Revision 10, MSPN 900-00021-01. https://support.micasense.com/hc/article_attachments/360073921173/AltumDLS2IntegrationGuideRev10.pdf.

Molecular Devices Corporation. (1997). *SPECTRAmax® PLUS Microplate Spectrophotometer Operator's Manual*. https://mdc.custhelp.com/euf/assets/content/User%20Manual%20-%20Plus.pdf.

Mount, R. (2005). Acquisition of through-water aerial survey images: Surface effects and the prediction of sun glitter and subsurface illumination. *Photogrammetric Engineering and Remote Sensing, 71*, 1407–1415. https://doi.org/10.14358/PERS.71.12.1407.

NALMS. (n.d.-a). *Chlorophyll Analysis*. Retrieved July 2023, from http://www.nalms.org/secchidipin/monitoring-methods/chlorophyll-analysis/.

NALMS. (n.d.-b) *Trophic State Equations*. Retrieved April 5, 2024, from http://www.nalms.org/secchidipin/monitoring-methods/trophic-state-equations/.

NRDC. (2019, August 28). *Freshwater Harmful Algal Blooms 101*. https://www.nrdc.org/stories/freshwater-harmful-algal-blooms-101.

O'Keeffe, J. (2019). *Cyanobacteria and drinking water: Occurrence, risks, management and knowledge gaps for public health*. https://ccnse.ca/sites/default/files/Cyanobacteria%20and%20Drinking%20Water-%20Occurrence%20Risks%20Management%20and%20Knowledge%20Gaps%20for%20Public%20Health%20EN.pdf.

Oklahoma Water Resources Board. (2018). *Standard Operating Procedure for the Collection and Processing of Chlorophyll-a Samples in Lakes*. https://www.owrb.ok.gov/quality/monitoring/bump/pdf_bump/Lakes/SOPs/Collection_of_Water_Quality_Samples.pdf.

Otten, T. G., & Paerl, H. W. (2015). Health Effects of Toxic Cyanobacteria in U.S. Drinking and Recreational Waters: Our Current Understanding and Proposed Direction. *Current Environmental Health Reports, 2*(1), 75–84. https://doi.org/10.1007/s40572-014-0041-9.

Pierce County. (n.d.). *Pierce County Drone Program | Remotely Piloted Aircraft Systems (RPAS)*. https://www.piercecountywa.gov/5998/PC-Drone-Program.

Pírez, M., Gonzalez-Sapienza, G., Sienra, D., Ferrari, G., Last, M., Last, J. A., & Brena, B. M. (2013). Limited analytical capacity for cyanotoxins in developing countries may hide serious environmental health problems: Simple and affordable methods may be the answer. *Journal of Environmental Management, 114*, 63–71. https://doi.org/10.1016/j.jenvman.2012.10.052.

Pix4D. (n.d.-a). P*hotogrammetry Knowledge: What is... (a densified point cloud? an orthomosaic? etc.)*. https://support.pix4d.com/hc/en-us/articles/206455126-What-is-a-densified-point-cloud-an-orthomosaic-etc#label2.

Pix4D. (n.d.-b). *Pix4D Documentation: Processing Steps*. https://support.pix4d.com/hc/en-us/articles/115002472186-Processing-steps.

Ramnath. (2011, September 26). Answer to: "Add regression line equation and Rˆ2 on graph." Edited by MrFlick. (2019, July 2). Meta Stack Exchange. https://stackoverflow.com/questions/7549694/add-regression-line-equation-and-r2-on-graph/7549819#7549819.

Rolim, S. B. A., Veettil, B. K., Vieiro, A. P., Kessler, A. B., & Gonzatti, C. (2023). Remote sensing for mapping algal blooms in freshwater lakes: A review. *Environmental Science and Pollution Research, 30*(8), 19602–19616. https://doi.org/10.1007/s11356-023-25230-2.

S.3348 - 118th Congress (2023-2024): Harmful Algal Bloom and Hypoxia Research and Control Amendments Act of 2023. (2023, November 27). https://www.congress.gov/bill/118th-congress/senate-bill/3348/text?s=1&r=7.

Schaeffer, B. A., Reynolds, N., Ferriby, H., Salls, W., Smith, D., Johnston, J. M., & Myer, M. (2024). Forecasting freshwater cyanobacterial harmful algal blooms for Sentinel-3 satellite resolved U.S. lakes and reservoirs. *Journal of Environmental Management, 349*, 119518. https://doi.org/10.1016/j.jenvman.2023.119518.

Scheffer, V. B. (1933). Biological Conditions in a Puget Sound Lake. *Ecology, 14*(1), 15–30. https://doi.org/10.2307/1932572.

Shoreline Area News. (2023, October 6). *Echo Lake closed for fishing, swimming, dogs due to toxic algae bloom*. https://www.shorelineareanews.com/2023/10/echo-lake-closed-for-fishing-swimming.html.

Steffen, M. M., Belisle, B. S., Watson, S. B., Boyer, G. L., & Wilhelm, S. W. (2014). Status, causes and controls of cyanobacterial blooms in Lake Erie. *Journal of Great Lakes Research, 40*(2), 215–225. https://doi.org/10.1016/j.jglr.2013.12.012.

SunCalc. (n.d.). *Suncalc.org Torsten Hoffman 2015-2024*. https://www.suncalc.org/#/27.6936,-97.5195,3/2024.03.27/15:41/1/3.

Sunoj, S., Hammed, A., Igathinathane, C., Eshkabilov, S., & Simsek, H. (2021). Identification, quantification, and growth profiling of eight different microalgae species using image analysis. *Algal Research, 60*, 102487. https://doi.org/10.1016/j.algal.2021.102487.

Swim Guide. (n.d.). *Echo Lake Shoreline, Washington*. https://www.theswimguide.org/beach/6438.

Tan, Z., Yang, C., Qiu, Y., Jia, W., Gao, C., & Duan, H. (2023). A three-step machine learning approach for algal bloom detection using stationary RGB camera images. *International Journal of Applied Earth Observation and Geoinformation, 122*, 103421. https://doi.org/10.1016/j.jag.2023.103421.

Thomson-Laing, G., Puddick, J., & Wood, S. A. (2020). Predicting cyanobacterial biovolumes from phycocyanin fluorescence using a handheld fluorometer in the field. *Harmful Algae, 97*, 101869. https://doi.org/10.1016/j.hal.2020.101869.

Tian, Y., Duan, M., Cui, X., Zhao, Q., Tian, S., Lin, Y., & Wang, W. (2023). Advancing application of satellite remote sensing technologies for linking atmospheric and built environment to health. *Frontiers in Public Health, 11*, 1270033. https://doi.org/10.3389/fpubh.2023.1270033.

Tong, D. Q., Gill, T. E., Sprigg, W. A., Van Pelt, R. S., Baklanov, A. A., Barker, B. M., Bell, J. E., Castillo, J., Gassó, S., Gaston, C. J., Griffin, D. W., Huneeus, N., Kahn, R. A., Kuciauskas, A. P., Ladino, L. A., Li, J., Mayol-Bracero, O. L., McCotter, O. Z., Méndez-Lázaro, P. A., … Vimic, A. V. (2023). Health and Safety Effects of Airborne Soil Dust in

the Americas and Beyond. *Reviews of Geophysics, 61*(2), e2021RG000763. https://doi.org/10.1029/2021RG000763.

Trainer, V. L., & Hardy, F. J. (2015). Integrative Monitoring of Marine and Freshwater Harmful Algae in Washington State for Public Health Protection. *Toxins, 7*(4), Article 4. https://doi.org/10.3390/toxins7041206.

Turner Designs. (2023 January 7). *FluoroSense™ User's Manual*. http://docs.turnerdesigns.com/t2/doc/manuals/998-2852.pdf.

UAV Forecast. (n.d.). https://www.uavforecast.com.

USEPA. (2013). *Standard Operating Procedure for Chlorophyll a Sampling Method Field Procedure. LG404, Revision 07*. Retrieved from https://www.epa.gov/sites/default/files/2017-01/documents/sop-for-chlorophyll-a-201303-5pp.pdf.

USEPA. (2015). *A Compilation of Cost Data Associated with the Impacts and Control of Nutrient Pollution*. EPA 820-F-15-096. Retrieved from https://www.epa.gov/sites/default/files/2015-04/documents/nutrient-economics-report-2015.pdf.

USEPA. (2023a, October 4). *Monitoring and Responding to Cyanobacteria and Cyanotoxins in Recreational Waters*. Cyanobacterial HABs. https://www.epa.gov/cyanohabs/monitoring-and-responding-cyanobacteria-and-cyanotoxins-recreational-waters.

USEPA. (2023b, October 10). *EPA Drinking Water Health Advisories for Cyanotoxins. Cyanobacterial HABs*. https://www.epa.gov/cyanohabs/epa-drinking-water-health-advisories-cyanotoxins.

Van der Merwe, D., & Price, K. P. (2015). Harmful Algal Bloom Characterization at Ultra-High Spatial and Temporal Resolution Using Small Unmanned Aircraft Systems. *Toxins, 7*(4), Article 4. https://doi.org/10.3390/toxins7041065.

Wang, C., Sheng, Y., Wang, J., Wang, Y., Wang, P., & Huang, L. (2022). Air Pollution and Human Health: Investigating the Moderating Effect of the Built Environment. *Remote Sensing, 14*(15), Article 15. https://doi.org/10.3390/rs14153703.

Washington State Department of Ecology. (n.d.). *Freshwater algae control grant program*. https://ecology.wa.gov/About-us/Payments-contracts-grants/Grants-loans/Find-a-grant-or-loan/Freshwater-algae-program-grants.

Wu, D., Li, R., Zhang, F., & Liu, J. (2019). A review on drone-based harmful algae blooms monitoring. *Environmental Monitoring and Assessment, 191*(4), 211. https://doi.org/10.1007/s10661-019-7365-8.

Wu, D., Li, R., Liu, J., & Khan, N. (2023). Monitoring Algal Blooms in Small Lakes Using Drones: A Case Study in Southern Illinois. *Journal of Contemporary Water Research & Education, 177*(1), 83–93. https://doi.org/10.1111/j.1936-704X.2022.3383.x.

Xue, J., & Su, B. (2017). Significant Remote Sensing Vegetation Indices: A Review of Developments and Applications. *Journal of Sensors, 2017*, e1353691. https://doi.org/10.1155/2017/1353691.

Zeng, C., Xu, H., & Fischer, A. M. (2016). Chlorophyll-a Estimation Around the Antarctica Peninsula Using Satellite Algorithms: Hints from Field Water Leaving Reflectance. *Sensors, 16*(12), Article 12. https://doi.org/10.3390/s16122075.

Zepernick, B. N., Wilhelm, S. W., Bullerjahn, G. S., & Paerl, H. W. (2023). Climate change and the aquatic continuum: A cyanobacterial comeback story. *Environmental Microbiology Reports, 15*(1), 3–12. https://doi.org/10.1111/1758-2229.13122.

Appendix A. PHI Grant Application

POPULATION HEALTH INITIATIVE
UNIVERSITY of WASHINGTON

Tier 1 Pilot Grant Application: Laying the Foundation
Spring 2023 Cover Sheet

Project Information

Project Title	Improving Public Health Surveillance and Communication for Freshwater Harmful Algal Blooms in Washington State: A Pilot Study using Drone Technology
Budget Request from Initiative	25,000 USD
Budget Match (if applicable)	5,000 USD
Total Project Budget	30,000 USD

Applicant Information

- Joey Teresi, MS Student, Department of Environmental and Occupational Health Sciences (DEOHS), School of Public Health, University of Washington, jteresi@uw.edu
- Dr. Tania M. Busch Isaksen, PhD, MPH, Associate Teaching Professor, DEOHS, School of Public Health, University of Washington, tania@uw.edu
    - Principle Investigator
    - Finance Point-of-Contact: Ms. Helen Lee, happylee@uw.edu
- Dr. Scott Meschke, PhD, JD, Professor and Associate Chair, Graduate Program Coordinator for DEOHS, School of Public Health, University of Washington, jmeschke@uw.edu
    - Co-investigator
- Dr. Gordon Holtgrieve, PhD, Associate Professor, Director of Future Rivers, School of Aquatic and Fishery Sciences, College of the Environment, University of Washington, gholt@uw.edu
    - Co-investigator

Abstract

As climate change warms the planet, freshwater harmful algal blooms (HABs) will continue to increase and threaten access to drinking and recreational waters, leading to adverse public health outcomes. Freshwater HABs are mainly caused by photosynthetic microorganisms called cyanobacteria, or "blue-green algae," that accumulate in excessive amounts and impair freshwater ecosystem services, including potable drinking water, recreation, and subsistence-based and sport fishing. According to the Centers for Disease Control, exposure to cyanotoxins can result in negative health outcomes including dermatologic, gastrointestinal, respiratory, or neurologic symptoms. In Washington State, freshwater HABs are a growing public health concern to residents, pets, livestock, and other animals as blooms increase in frequency and severity.

Remotely piloted drones can be an effective tool for environmental monitoring of smaller-scale freshwater bodies. Drones with high-resolution cameras offer a more comprehensive visual assessment of a HAB's spatial extent and migration over time, as opposed to a limited view from the shoreline or boat. Additionally, drones can be outfitted to facilitate quicker and more frequent water sample collection, enabling additional data collection to understand bloom dynamics. This pilot study aims to develop a protocol for drone-based water sampling of lake cyanotoxins and aerial photo collection, specific to the needs of Washington State local environmental resource management and health agencies. We posit that drone technology will improve local jurisdiction's ability to characterize HAB health risks and communicate risk to the public. This multidisciplinary study will result in a standard operating and sampling procedure document to be adopted by health agencies.

POPULATION HEALTH INITIATIVE
UNIVERSITY of WASHINGTON

Tier 1 Project Research Plan

Freshwater HABs pose a significant public health threat to the world's freshwater supply and have been estimated to cost the United States up to 4.6 billion dollars annually.[1] Excessive nutrient pollution combined with a warmer climate has, and will continue to result in, increased HAB formation; cyanobacterial blooms and climate change can also have synergistic consequences for freshwater systems, like hypoxia and acidification.[2] The health effects of HAB biotoxins are well documented and have the potential to cause outbreaks in Washington State.[3,4] Exposure routes include dermal contact, ingestion, and aerosol inhalation and may result in a wide array of symptomology, including skin irritation, rash, swelling, sores; ear and eye irritation; fever; headache; and gastrointestinal, respiratory, or neurologic distress.[4] Despite the recognition of this environmental hazard and its public health urgency, freshwater HABs are not well understood and novel methods to characterize their occurrence, development, and toxicity are needed. Drone-based methods show potential for enhanced HAB sampling and monitoring.[5,67] In preparation of this application's submission, we sought to understand current research priorities and knowledge gaps by conducting key informant interviews with representatives from the Washington State Department of Health, King County Department of Natural Resources, and the City of Shoreline. Key agreement from these discussions were that 1) there is a need for innovative monitoring strategies; 2) there is enthusiastic interest in using drones to improve environmental health decision making; and 3) there is an anticipation that the kind of data collected could result in more timely and effective public risk communication. These conversations have resulted in a collaboration with the City of Shoreline to develop and test a drone sampling protocol, as they are currently in the process of developing a cyanobacteria management plan for Echo Lake (Figure 1). *The specific aims for this proposed project are*:

Figure 1. Echo Lake (Source: Google Earth)

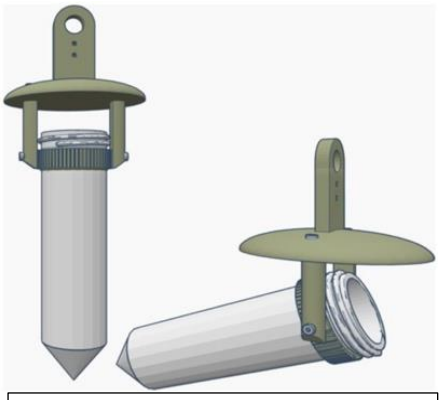

Figure 2. Water Sampling Apparatus[6]

Aim 1: Perform drone-based aerial photo and water sample collection at Echo Lake, including cyanotoxin analysis, to establish drones as an effective environmental monitoring tool for local freshwater HAB monitoring and response. One member of our research team will acquire a remote pilot certification and work directly with UW's Natural Hazards Reconnaissance Facility (known as the "RAPID") to operate their DJI Phantom 4 drone. Aerial photos will be collected by the drone's camera and the extent of visible algal formation across the lake surface will be recorded during the study period. These photos will be compared to water quality data collected (temperature, total nitrogen, cyanotoxin levels, etc.) to understand the effect of environmental conditions on bloom distribution, as well as potential high nutrient input areas. Photographic data aids resource management's decision making by pinpointing bloom hotspots and their potential migration to public spaces given wind conditions. In addition, a water sampling apparatus (similar to Figure 2) will be attached to the drone. The drone will collect water samples along a transect of Echo Lake, returning the sample container to the shore each time to be replaced. Samples will be analyzed using laboratory benchtop methods for water quality parameters and EPA Method 546 to quantify specific cyanotoxin concentrations (e.g., Microcystin), employing Enzyme-Linked Immunosorbent Assay (ELISA) test kits. Algal counts using microscopy methods will also be used to assess the general microbial community structure. Sampling will be conducted biweekly from July-Sept. 2023. Descriptive statistics will be analyzed using R programming software. **Aim 2: Create a drone-based data collection protocol specific to the needs of local resource management and health agency audiences.** We will produce a generalizable guidance document for drone-based freshwater HAB surveillance that can be used in local HAB management plans. A formative needs assessment, using semi-structured key informant interviews and qualitative data analysis methods, will be conducted to understand important content and design components for the document. Iterative feedback will be sought through the co-creation process, and a final document will be produced as a deliverable to this grant. Communities across the state and beyond have disparate access to clean freshwater services, especially as urban development and effects from climate change increase water pollution. By providing guidance on drone-based methods, communities can better anticipate, characterize, and respond to HABs and prevent and reduce algal toxin exposures. This innovative method will increase monitoring power for bloom management and allows for more timely public health HAB notification and risk communication. Generation of an adaptable drone-based sampling and photographic protocol will remove a significant barrier for under-resourced local agencies to better manage their freshwater HABs.

References

1. Hudnell, H. K. (2010). The state of U.S. freshwater harmful algal blooms assessments, policy and legislation. *Toxicon*, *55*(5), 1024–1034. https://doi.org/10.1016/j.toxicon.2009.07.021.
2. Griffith, A. W., & Gobler, C. J. (2020). Harmful algal blooms: A climate change co-stressor in marine and freshwater ecosystems. *Harmful Algae*, *91*, 101590. https://doi.org/10.1016/j.hal.2019.03.008.
3. Drobac, D., Tokodi, N., Simeunović, J., Baltić, V., Stanić, D., & Svirčev, Z. (2013). Human exposure to cyanotoxins and their effects on health. *Archives of Industrial Hygiene and Toxicology*, *64*(2), 305–316. https://doi.org/10.2478/10004-1254-64-2013-2320.
4. Hilborn, E. D., Roberts, V. A., Backer, L., Deconno, E., Egan, J. S., Hyde, J. B., Nicholas, D. C., Wiegert, E. J., Billing, L. M., Diorio, M., Mohr, M. C., Hardy, J. F., Wade, T. J., Yoder, J. S., Hlavsa, M. C., & Centers for Disease Control and Prevention (CDC). (2014). *Algal bloom-associated disease outbreaks among users of freshwater lakes--United States, 2009-2010*. MMWR. Morbidity and mortality weekly report. Retrieved January 3, 2023, from https://www.ncbi.nlm.nih.gov/pmc/articles/PMC5779332/.
5. Rolim, S. B., Veettil, B. K., Vieiro, A. P., Kessler, A. B., & Gonzatti, C. (2023). Remote sensing for mapping algal blooms in Freshwater Lakes: A Review. *Environmental Science and Pollution Research*, *30*(8), 19602–19616. https://doi.org/10.1007/s11356-023-25230-2.
6. Benson, J., Hanlon, R., Seifried, T., Baloh, P., Powers, C., Grothe, H., & Schmale, D. (2019). Microorganisms collected from the surface of freshwater lakes using a drone water sampling system (Dowse). *Water*, *11*(1), 157. https://doi.org/10.3390/w11010157.
7. Hanlon, R., Jacquemin, S. J., Birbeck, J. A., Westrick, J. A., Harb, C., Gruszewski, H., Ault, A. P., Scott, D., Foroutan, H., Ross, S. D., González-Rocha, J., Powers, C., Pratt, L., Looney, H., Baker, G., & Schmale, D. G. (2022). Drone-based water sampling and characterization of three freshwater harmful algal blooms in the United States. *Frontiers in Remote Sensing*, *3*. https://doi.org/10.3389/frsen.2022.949052.

POPULATION HEALTH INITIATIVE
UNIVERSITY of WASHINGTON

Tier 1 Project Evaluation Plan

The primary measure of success for Aim 1 will be the demonstration that using drone-based data collection, including water sampling and photographic evidence, is feasible and more effective than traditional manual collection to understand the spatial and temporal distribution of blooms. Our samples will capture an association between toxin concentrations and water quality parameters with visible algal accumulations across Echo Lake during the study period to better inform future risk management. Microcystin concentrations above state guidance values, for example, may be linked to elevated nutrient levels but no visible surface algae. To ensure the validity of our sampling results, a Model Quality Assurance Project Plan (QAPP) will be developed and implemented for all stages of the sampling methodology and logistics, lab work, and decontamination procedures. The QAPP will also include aseptic techniques, statistical data analysis, and protocols for documentation and data management. Use of field blanks, replicates, standard solutions, and properly calibrated equipment will also be ensured for precision of results. Photographic quality control will include appropriate documentation of metadata (date/time/GPS coordinates), camera type and settings, and programs used for original image archival and post-processing. For Aim 2, our primary measure of success will be a completed, co-designed drone-based data collection protocol. Our secondary measure of success will be completed and analyzed key informant interviews from at least 50% of management agencies in jurisdictional areas experiencing significant HAB activity, as reported by Washington Departments of Ecology and Health. The results of this pilot study will provide City of Shoreline freshwater managers a greater understanding of their freshwater HABs and an innovative protocol for their management. Preliminary data gained from this proposed work will generate new hypotheses for future studies. Providing evidence to demonstrate feasibility with drone-based data collection at local lakes will inspire future researchers to use drones for additional freshwater research applications. For example, future investigators may assess different water contaminants, pursue more geographically remote areas, or employ remote sensing technology. **Additionally, this study kickstarts a new collaboration between DEOHS and Fishery Sciences on a topic that has many unanswered, practice-relevant questions and with future funding mechanisms available. We intend to build the foundation for future work through the partnerships developed through this pilot grant.**

Project Timeline and Milestones

	2023								2024	
Milestones	**May**	**Jun**	**Jul**	**Aug**	**Sep**	**Oct**	**Nov**	**Dec**	**Jan**	**Feb**
Acquire FAA Part 107 Remote Pilot certification and begin drone operation training with RAPID staff and microbio lab training										
Conduct Aim 1 field work and laboratory analysis; key stakeholder interviews and iterative feedback										
Data analysis and results; methodologies writeup										
Finalize data analysis and discussion writeup										
Disseminate guidance document deliverable										

Biographies

Joey Teresi is a current masters student with a BA in geology and environmental studies and four years of experience in the environmental consulting industry. He is passionate about community-based environmental public health research.

Dr. Busch Isaksen is an associate teaching professor with over 25+ years of environmental public health experience working in public, private, and academic settings. She is co-founder of the Collaborative on Extreme Event Resilience, a lab focused on climate-resilient communities through public health policy and practice.

Dr. Meschke is a professor with DEOHS and an environmental and occupational health microbiologist, specializing in the fate, transport, detection, and control of pathogens in environmental media (air, water, food, and surfaces).

Dr. Holtgrieve is an associate professor with the School of Aquatic and Fishery Sciences and an aquatic ecosystem ecologist and fisheries scientist with over 20 years of experience in scientific research and education. Dr. Holtgrieve's expertise in nutrient cycling and ecological processes that control primary production in lakes are particularly relevant to this proposal.

POPULATION HEALTH INITIATIVE
UNIVERSITY of WASHINGTON

Tier 1 Project Budget & Justification

	Requested from Initiative	Funding Match
Salaries	PHI Tier 1 $25,000 USD	DEOHS $5,000 USD
Faculty		
Staff		
Student	11,869	
Benefits	2,536	
Supplies and Materials	2,127	3,000
Equipment		
Tuition	8,468	
Other		2,000
Total Direct Costs	25,000	5,000

The confirmation from DEOHS to provide $5,000 USD in matching funds is enclosed at the end of this application as an e-mail PDF. In addition, a letter of support from the RAPID is enclosed at the end of this application.

PERSONNEL

Tania Busch Isaksen (Principal Investigator): Effort as needed for the year, not requesting salary support. Dr. Busch Isaksen will oversee the development of the study, stakeholder engagement facilitation, supervision of graduate research assistant, analysis of data, and preparation of the protocol document.

Scott Meschke (Co-Investigator): Effort as needed for the year, not requesting salary support. Dr. Meschke will provide support for sampling design, logistics considerations, and microbiological laboratory analysis methods, including use of ELISA kits and algal cell count microscopy methods.

Gordon Holtgrieve (Co-Investigator): Effort as needed for the year, not requesting salary support. Dr. Holtgrieve will provide support for sampling design and logistics, water quality parameter sample collection (e.g., nutrients, chlorophyll) and analysis, and guidance on observed eutrophic lake conditions.

Joey Teresi (Graduate Student Assistant): About 1.50 academic months and about 0.58 summer months (or about 100 summer hours) for the year**.** The graduate student assistant will be primarily responsible for the development of the drone-based data collection protocol, drone operation and field sampling, water sample lab and photo analysis, and data analysis.

FRINGE

The following University of Washington HHS-negotiated fringe benefits rates have been applied: 24.1% for faculty members, 21.3% for academic graduate student assistants, and 21.5% for hourly student assistants.

OTHER DIRECT COSTS

Supplies & Materials:

a) Estimated costs for ELISA toxin analysis sampling kits is $5,127. Kits will be used for 6 to 8 sampling events, including 20 samples per event at about $35 per sample (5 transect samples plus 3 replicates per sample to capture variability). Toxin analysis will allow characterization of HAB distribution and comparison with other environmental conditions.

b) Estimated cost for Sedgewick Rafter is $50, a microscopy technique tool for counting algal cell counts. The Sedgewick Rafter will quantify cyanobacteria density and growth to elucidate the microbial community structure and dominant groups.

Tuition: Estimated $8,468 tuition fees for 1 quarter of Academic Graduate Student Assistant per university policy.

Equipment Rental: Estimated $1,400 rental fees (based on NSF suggested rate of $135.62/day) for DJI Phantom 4 Pro+ RTK drone for 10 days. This 10-day rental will be used for 2-4 testing days and 6-8 sampling event days.

3D Printing Costs: Estimated $375 for 3D printing the sampling apparatus component. The printed apparatus will allow sampling containers to be attached to the drone housing via a tether and carabiner clip to facilitate water sample collection.

FAA Part 107 Remote Pilot Certification Exam Fee: This certification exam will cost $175, and obtaining the certificate will strengthen the researcher's aviation-related knowledge and allow them to operate a drone for the purposes of this study.

Joey Teresi <jteresi@uw.edu>

Fwd: Tier 1 matching request

Tania M. Busch Isaksen <tania@uw.edu> Mon, Apr 10, 2023 at 10:08 AM
To: Joey Teresi <jteresi@uw.edu>

This email needs to be attached at the end of your proposal.
Tania

---------- Forwarded message ---------
From: **Taylor Hendricksen** <taylorjh@uw.edu>
Date: Mon, Apr 10, 2023 at 10:07 AM
Subject: RE: Tier 1 matching request
To: Tania M Busch Isaksen <tania@uw.edu>

Dear Tania,

This e-mail serves as confirmation, on behalf of DEOHS Chair Mike Yost and Assistant Chair for Research Chris Simpson, that DEOHS will provide $5000 in matching funds should your PHI Pilot Research Grant, “Drone use to Enhance Local Monitoring of Freshwater Harmful Algal Blooms in Washington State: A Pilot Feasibility Study”, be awarded. Best of luck with the proposal!

Take care,

Taylor

Taylor Hendricksen

Assistant Administrator

Department of Environmental & Occupational Health Sciences

taylorjh@uw.edu | 206.543.2883

Hans Rosling Center for Population Health

3980 15th Avenue NE, Box 351618 Seattle, WA 98195

ENVIRONMENTAL & OCCUPATIONAL HEALTH SCIENCES
UNIVERSITY of WASHINGTON | SCHOOL OF PUBLIC HEALTH

From: Tania M. Busch Isaksen <tania@uw.edu>
Sent: Sunday, April 9, 2023 3:03 PM
To: Taylor Hendricksen <taylorjh@uw.edu>
Subject: Tier 1 matching request

Hi Taylor

We are submitting a Tier 1 this week and are requesting a match.

Attached is a very rough draft of that grant.

Title:

Drone use to Enhance Local Monitoring of Freshwater Harmful Algal Blooms in Washington State: A Pilot Feasibility Study

Please let me know if you have any questions

Thank you!

Tania

--

Tania M. Busch Isaksen, PhD, MPH (she/her)
Associate Teaching Professor, Dept. Enviro. and Occ. Health Sciences

Co-Director, Collaborative on Extreme Event Resilience (CEER)

Director of Education and Training, Center for Health and the Global Environment (CHanGE)

DEOHS Undergraduate Program Coordinator

DEOHS MPH Practicum Program Director

QERM Graduate Faculty

Hans Rosling Center for Population Health,

Box 351618, 3980 15th Avenue NE,

University of Washington, Seattle, WA 98195

Office:255-b

tania@uw.edu

http://deohs.washington.edu/faculty/Busch_Tania

"You must become the change you wish to see in the world." ~Mahatma Gandhi

--
Tania M. Busch Isaksen, PhD, MPH (she/her)
Associate Teaching Professor, Dept. Enviro. and Occ. Health Sciences
Co-Director, Collaborative on Extreme Event Resilience (CEER)
Director of Education and Training, Center for Health and the Global Environment (CHanGE)
DEOHS Undergraduate Program Coordinator
DEOHS MPH Practicum Program Director
QERM Graduate Faculty

Hans Rosling Center for Population Health,

Box 351618, 3980 15th Avenue NE,

University of Washington, Seattle, WA 98195
Office:255-b
tania@uw.edu
http://deohs.washington.edu/faculty/Busch_Tania

"You must become the change you wish to see in the world." ~Mahatma Gandhi

4/13/2023

University of Washington
Population Health Tier 1 Grant Program

Dear Review Panel,

If the proposal submitted by Dr. Tania Busch Isaksen, et al. researching the role of climate change on Harmful Algal Bloom occurrence and severity is selected for funding by the Tier 1 grant program, it is my intent to collaborate and/or commit resources to this project.

Sincerely,

Jeffrey Berman, PhD
Operations Director
Professor, Structural Engineering
Civil & Environmental Engineering
University of Washington
(206) 616-3530
jwberman@uw.edu

Appendix B. PHI Final Report

POPULATION HEALTH INITIATIVE
UNIVERSITY of WASHINGTON

Project Title (Updated): Environmental Public Health Surveillance of Freshwater Harmful Algal Blooms in Washington State Using Drone Technology

Project Investigators: Joey Teresi, Dr. Tania Busch Isaksen (PI), Dr. Scott Meschke, Dr. Gordon Holtgrieve

Summary of Project:

Our primary project goal was to assess the ability of remotely piloted drones to detect harmful algal blooms (HABs) in a smaller-scale freshwater lake. To accomplish this goal, our primary objective was to use two different drone platforms equipped with high-resolution cameras to capture aerial imagery of Echo Lake in Shoreline, King County, Washington over the peak bloom season. Color band manipulation of the drone imagery was leveraged to estimate levels of chlorophyll a—the photosynthetic pigment found in all algae and cyanobacteria—as a proxy for phytoplankton biomass at the lake surface. Higher chlorophyll a concentrations are typically associated with higher amounts of phytoplankton biomass and act as an indicator for a potential bloom. Using linear regression, we tested ten vegetation indices against lake water samples collected for chlorophyll a validation. Our primary measure of success was to generate statistically significant correlations from the linear regression models to understand this application's predictive value and overall feasibility.

Our secondary project goal was to document the needs of local agencies managing HABs to inform the creation of a drone-based data collection protocol. To this end, our secondary objectives were to: identify protocol user needs through informal key informant interviews with public health and water resource management agencies that routinely deal with HAB monitoring and response activities; and to create a drone-based protocol document. The resulting guidance document highlights the challenges associated with drone-based monitoring methods and provides insights for a program's successful implementation, including optimal environmental conditions and drone flight parameters. Our secondary measure of success was to collaborate with local and state agencies for iterative feedback on its completion and to disseminate this deliverable to applicable agencies.

Between July and October 2023, a total of 26 unique drone flights were conducted, with 28 water samples collected and analyzed in duplicate over seven sampling events. The best estimates of chlorophyll a variation were provided by the Color Index of Vegetation Extraction (CIVE) index ($R^2 = 0.45$, $p < 0.001$). The CIVE index has been applied in previous remote sensing studies to approximate algal biomass in small inland lakes and allows a reasonable estimation of lake chlorophyll levels using a relatively inexpensive, user-friendly, and time-efficient drone monitoring tool. By increasing the frequency of flights, these drone platforms can supplement HAB forecasting tools and represent an improvement over limited shoreline visual inspections. These findings suggest remote sensing capabilities will help freshwater resource managers better anticipate the development of HABs and more rapidly communicate this environmental public health risk. In addition, we have engaged with representatives from the Washington State Departments of Health and Ecology, King County, Snohomish County, and the City of Shoreline to understand their HAB monitoring needs and limitations on drone use. We documented information on the logistics, costs, training, and optimal flight operation conditions (i.e., weather conditions, flight altitude) for successful implementation. For instance, a balance between image resolution and camera field of view affecting image stitching, determined

by flight altitude, must be considered when imaging lakes. To this end, we have generated a guidance document for local practitioners.

Budget:
Total funds for this project comprised $30,000 ($25,000 from the PHI Tier I Pilot Research Grant and $5,000 matched by DEOHS). To date, all funds have been spent, including for student salary/tuition/benefits (totaling $24,562.80) as well as lab and field supplies/equipment (e.g., drone equipment rentals, fluorescence probe) and vehicle mileage (totaling $5,437.32).

Next Steps:

The results of this study will be presented at the 2024 Washington State Environmental Health Association (WSEHA) Annual Education Conference (AEC) in Yakima, WA and the 2024 National Environmental Health Association (NEHA) AEC in Pittsburg, PA. This study will also be submitted for publication into an academic journal suited to a public practitioner audience. In addition, a guidance document deliverable for this drone application will be sent to local public health and water resource management agencies interested in conducting similar remote sensing work.

While the current graduate student for this project will not continue this work into the future, the principal investigator may continue follow-on funding for an upscaled project employing drone surveillance for lake monitoring. Future projects may expand on this work by analyzing concentrations of chlorophyll a or phycocyanin (the pigment specific to all cyanobacteria) using drones outfitted with multispectral or hyperspectral sensors, collecting additional water samples, analyzing additional lakes of varying biological productivity, or by employing different vegetation indices to approximate phytoplankton biomass. Collaboration with principal investigators specializing in remote sensing applications would be appropriate to scale up this work for follow-on funded projects.

Appendix C. Narrative Literature Review

Freshwater Harmful Algal Blooms and Human Health Risks: A Narrative Literature Review

Joseph Teresi

Department of Environmental and Occupational Health Sciences (DEOHS)

School of Public Health

University of Washington

Table of Contents

Abstract

We conducted a narrative literature review on freshwater harmful algal blooms (HABs) to better understand the risks they pose to human health. We synthesized 20 articles published across 14 academic journals that discuss freshwater cyanobacteria issues across the globe. A total of 15 review articles and 5 experimental studies were included. After using key search terms, an aggregate 643 search results were filtered, with final articles being chosen after primary and secondary review. The final 20 articles were implemented into a risk assessment framework (i.e., Hazard Identification, Dose-Response Assessment, Exposure Assessment, Risk Characterization) as well as Risk Management and Control. The articles provided toxicological, pharmacological, ecological, and epidemiologic information; case studies; and experiments aimed at better understanding the impacts of cyanobacteria and cyanotoxins on animal and human health. Major findings included recommendations for future research directions into the less understood cyanotoxins, exploration with new monitoring tools and technologies, improved public education and outreach, and a need for community-based interventions and interdisciplinary collaboration.

Introduction

Harmful algal blooms (HABs) pose a significant public health threat to the world's freshwater supply and have been estimated to cost the United States up to 4.6 billion dollars annually (Hudnell, 2010). Freshwater HABs are mainly caused by photosynthetic microorganisms called cyanobacteria, or "blue-green algae," that accumulate in excessive amounts and impair freshwater ecosystem services, including potable drinking water, recreation, and subsistence-based and sport fishing (Hudnell, 2010; Hou et al., 2022). In recent decades, freshwater HABs have increased in frequency and severity as a result of excessive nutrient pollution combined with a warming planet (Griffith & Gobler, 2020). Furthermore, in Washington State, freshwater HABs are a growing public health concern to residents, pets, livestock, and aquatic animals since blooms can produce harmful biotoxins that may result in dermatologic, gastrointestinal, respiratory, or neurologic symptoms (Drobac et al., 2013; Hilborn et al., 2014). Despite the recognition of this environmental hazard and its public health urgency, freshwater HABs are not well understood and characterization of their occurrence, development, and toxicity is needed.

Notable freshwater bodies like Lake Winnipeg, Canada; Lake Erie, USA; Lake Victoria, Kenya; and Lake Taihu, China are regularly impacted by cyanobacteria blooms (Lad et al., 2022), in addition to numerous smaller scale lakes. Significant freshwater HAB incidents causing human morbidity and mortality have been documented across the globe. For example, an outbreak in Palm Island, Australia in 1979 resulted in the hospitalization of adults and children for symptoms including malaise, anorexia, vomiting, headache, bloody diarrhea, dehydration, kidney disease, and liver failure (Lad et al., 2022). This event was tied to the toxin cylindrospermopsin contaminating the local water reservoir. Another outbreak in Caruaru, Brazil in 1996 occurred at a hemodialysis center where microcystins and cylindrospermopsins present in the dialysate water were responsible for headaches, blurred vision, eye pain, nausea, vomiting, and acute liver failure (Lad et al., 2022). In 2014, a historically large HAB event in Lake Eerie led to a temporary tap water ban and state of emergency for over 450,000 residents in Toledo, Ohio, given contamination from microcystins in their drinking water supply (Lad et al., 2022).

The United States Environmental Protection Agency (USEPA) lists cyanobacteria and cyanotoxins on their Contaminant Candidate List, which includes recognized drinking water contaminants that are not currently regulated, and provides drinking water health advisory

benchmarks (USEPA, 2022). In addition, the USEPA provides recreational standards and swimming advisories for certain cyanotoxins (USEPA, 2019). Although guidelines for these biological hazards are not federally enforced, states are continuing to take steps to protect both their drinking and recreational water sources. A general risk assessment for cyanotoxins is needed to better understand their potential to cause human illness.

Methods

We conducted a narrative literature review to understand the current state of knowledge on freshwater HABs regarding the risks they pose to human health. This review is intended for environmental public health practitioners and freshwater resource managers to gain insights on freshwater HAB biological risks to human wellbeing. A secondary goal is to identify knowledge gaps and critical research needs expressed in the current studies on this hazard. The review will follow general guidelines and frameworks adapted from the manuscript by Ferrari (2015).

The research objectives for this review are to synthesize recent literature that explored current and emerging hazards posed by cyanobacteria, the exposure pathways and routes associated with them, dose-response relationships with known toxin metabolites, general risk characterizations in recreational settings, and risk management strategies for lake toxic blooms. We generated key search terms to identify literature reviewed in the University of Washington Health Sciences Library, Web of Science, and PubMed online databases. Search terms were refined over iterative article searches with final search terms categorized as "General Search Terms" and search terms specific to each component of the risk assessment framework (i.e., Hazard Identification, Dose-Response Assessment, Exposure Assessment, Risk Characterization) as well as Risk Management and Control. See Table 1 for a summary of search terms used.

Table 1. General and Specific Search Terms Used

General Search Terms	Hazard ID	Dose-Response Assessment	Exposure Assessment	Risk Characterization	Risk Management
freshwater harmful algal bloom	human health	dose-response	exposure assessment	risk characterization	risk management
freshwater HAB	health hazard	toxicology	health exposure	risk communication	risk control
toxic cyanobacteria	cyanotoxin	bioassay	exposure route		
eutrophication	biotoxin	assay	dermal contact		
freshwater lake			oral ingestion		
recreation			oral route		
surveillance			inhalation		
monitoring			aerosol		
state of knowledge			sentinel		

Inclusion/Exclusion Criteria

Primary (title) and secondary (abstract) review of articles filtered article selection to no more than 20 articles that were fully reviewed, summarized, and synthesized into each component of the risk assessment framework. Selected articles included those written in English, published from 2013 to 2023, and which explored the human health effects of freshwater HABs through empirical research (e.g., systematic literature reviews, epidemiologic studies, toxicological experiments). Articles were excluded if they did not pertain to freshwater HABs or cyanotoxins, solely explored cyanotoxin hazards in drinking water rather than recreational water, focused on ecological impacts with little mention of human health, or became too technical to relay to a non-expert audience (local agency personnel). Saturation was determined when redundant information was identified for each risk assessment component; in other words, the researcher was confident of saturation when new information was no longer identified.

Results

A total of 20 articles published across 14 academic journals were reviewed for this narrative literature review. Eight articles were identified from PubMed, seven articles from Web of Science, and five articles from the University of Washington Health Sciences Library. Using the search terms presented in Table 1, an aggregate 643 search results were filtered, with final articles being chosen using primary and secondary review. From these articles, human health risks from freshwater HABs were reported across the world. A total of 15 review articles and five experimental studies were included. See Table 2 below for a summary of the reviewed academic articles and the primary study methods presented by the article. These articles are discussed below following the risk assessment framework and for Risk Management and Control.

Table 2. Summary of Academic Articles Reviewed

Count	Citation	Methods	Count	Citation	Methods
1	Almuhtaram et al. (2021)	Review	11	Lad et al. (2022)	Review
2	Backer et al. (2015)	Review	12	Nielsen & Jiang (2020)	Review
3	Catherine et al. (2013)	Review	13	Olson et al. (2020)	Experiment
4	Chernoff et al. (2021)	Experiment	14	Rangel et al. (2014)	Experiment
5	Christensen & Khan (2020)	Review	15	Roegner et al. (2020)	Experiment
6	Drobac et al. (2013)	Review	16	Trainer and Hardy (2015)	Review
7	Hilborn et al. (2014)	Review	17	Trevino-Garrison et al. (2015)	Review
8	Hilborn & Beasley (2015)	Review	18	Weirich & Miller (2014)	Review
9	Hu et al. (2020)	Experiment	19	Wiśniewska et al. (2019)	Review
10	Ibelings et al. (2014)	Review	20	Yang et al. (2019)	Review

Hazard Identification

Algae are classified under the kingdom *Protista* and include several major groups, including dinoflagellates (marine plankton) and photosynthetic bacteria (e.g., cyanobacteria) (Lad et al., 2022). While most algae are considered beneficial as primary producers of natural ecosystems, suitable conditions like nutrient enrichment and warmer temperatures promote a proliferation of algal growth, resulting in a major biological hazard (Lad et al., 2022). Eutrophication—an over-enrichment of nutrients in an aquatic system, particularly with nitrogen and phosphorous compounds—is the primary driver of algal growth. Harmful algal blooms (HABs) in freshwater systems are typically composed of cyanobacteria, true bacteria often referred to as "blue-green algae." Cyanobacteria may glide on the surface of a water body, float planktonically throughout the water column, or be attached to the bottom substrate—termed benthic cyanobacteria.

Furthermore, a number of cyanobacteria genera can produce harmful secondary metabolites called cyanotoxins, which are classified into three principal groups: dermatoxins, hepatotoxins, and neurotoxins (Christensen & Khan, 2020). These toxins can express themselves in multiple ways: intracellular toxins (endotoxins) typically remain inside cyanobacteria cells until they are released either naturally or upon cell death (lysis); the combined particulate (intracellular) and dissolved (extracellular) phases make up the total toxins present (Christensen & Khan, 2020). A comprehensive database developed by the USEPA called CyanoMetDB contains chemical information on secondary metabolites produced by cyanobacteria

(https://comptox.epa.gov/dashboard/chemical-lists/CYANOMETDB). This online database was facilitated by researchers to advance understanding and future research with the many chemical compounds different cyanobacteria produce (Jones et al., 2021).

The explanation for why cyanobacteria produce cyanotoxins is not forthcoming but there are many biological rationales. Cyanobacteria may express toxins as a defense mechanism against other photosynthetic organisms; as an offensive strategy to inhibit other organisms' growth in order to outcompete them; or as a way to maintain their own homeostasis, photosynthesis, or growth rates (Christensen & Khan, 2020). Moreover, the specific ecological role of cyanotoxins is still misunderstood since it is insufficiently studied. Cyanobacteria as primary producers can form the base of the food chain for ecosystems but can otherwise cause catastrophic ecological changes when they form scummy mats, block out sunlight, deplete available oxygen in the water, or produce toxins (Christensen & Khan, 2020). Besides degrading aesthetic qualities to water bodies, the combination of intracellular and extracellular toxins in drinking and recreational waters are important to measure for public health implications.

Microcystins are the most commonly studied cyanotoxins in the academic literature and their toxicological mechanism of action is well defined, primarily targeting the liver. Mouse assay studies have indicated that when this hepatotoxin enters the body, it is transported to the liver by organic anion transporting polypeptides (OATPs) and promotes cellular toxicity by the inhibition of protein phosphatases like PP1 and PP2A; this results in hyperphosphorylation, leading to cell breakdown and lysis, and metabolic formation of reactive oxygen species (ROS), which leads to oxidative stress, apoptosis, and DNA damage (Chernoff et al., 2021; Lad et al., 2022). It is important to note that the dosage and resultant response of these toxins can be difficult to infer from animal populations to human populations. Nevertheless, the International Agency for Research on Cancer (IARC) has classified the specific microcystin variant Microcystin-LR (MC-LR) as a Group 2B peptide, a possible human carcinogen (Drobac et al., 2013; Lad et al., 2022).

Cylindrospermopsins are the second most studied freshwater cyanotoxin though much less is known about its different variants; they primarily target the liver and kidney but can also negatively impact the thymus, heart, spleen, lungs, and eyes (Yang et al., 2021). As a result of its multi-organ toxicity and prevalence in the environment, cylindrospermopsins present a significant hazard to public health. Cylindrospermopsins inhibit protein synthesis, disrupt cytochrome P450, induce oxidative stress and DNA damage, bind to estrogen receptors, and impact acetylcholinesterase activity (Yang et al., 2021). Cylindrospermopsins are globally distributed and have contributed to a number of outbreak events. Yang et al. (2021) provides an extensive table detailing notable cylindrospermopsin occurrences in the world. For cylindrospermopsins, temperature, light intensity, and nutrients are major factors controlling their growth; they are able to fix nitrogen out of the atmosphere and convert it into ammonium as a competitive advantage over other phytoplankton; and they can contaminate drinking water and food sources like fish, shellfish, vegetables, and algal supplements (Yang et al., 2021).

The neurotoxins anatoxin and saxitoxin are not as well characterized as microcystins and cylindrospermopsins but nevertheless pose serious threats to public health in recreational bodies. Christensen & Khan (2020) present a systematic literature review focused on the occurrence of anatoxin-a and saxitoxin. There are at least 41 known anatoxin-a producing species and at least 15 known saxitoxin-producing species of cyanobacteria (Christensen & Khan, 2020). The complex toxicological mechanisms of each class of compounds are further described. Anatoxins tend to mimic the neurotransmitter acetylcholine and bind to acetylcholine receptors at synapses

between nerves and muscles, but they are not degraded by acetylcholinesterase, causing continuous muscle stimulation and fatigue; as a result, exposure to this toxin causes respiratory failure and brain hypoxia (Christensen & Khan, 2020). Furthermore, whereas anatoxins cause over-stimulation of the nervous system, saxitoxins cause under-stimulation of nerves and muscles. Christensen & Khan (2020) summarize saxitoxins' mode of action as a sodium channel blocker in the nervous system, which suppresses nerve impulses and leads to respiratory paralysis and death. Although saxitoxins can be found in freshwater mussels and snails, the most researched saxitoxin is the paralytic shellfish toxin (PST), which is often found in marine waters (Christensen & Khan, 2020).

Dose-Response Assessment

Cyanotoxins are secondary metabolic byproducts of cyanobacteria and include the neurotoxic anatoxins and saxitoxins and the hepatotoxic cylindrospermopsins and microcystins, with microcystins being the most frequently identified globally (Chernoff et al., 2021). Microcystins are chemically composed of a unique chain of amino acids with over 240 structural variants known and named after unique amino acid variants attached to the overall structure; the most common have been found to be microcystin-LA (MC-LA), MC-LR, MC-LY, MC-RR, and MC-YR (Chernoff et al., 2021). In order to quantify what amounts of these toxins are harmful to the human body, Chernoff et al. (2021) assessed their pathogenic effects via oral administration to mice. Building off of previous animal toxin exposure studies, the researchers administered various doses of these microcystin variants to laboratory mice in order to record the No Observed Adverse Effect Level (NOAEL), the highest dose at which an adverse health effect was not observed, and the Low Observed Adverse Effect Level (LOAEL), the lowest dose at which an adverse health effect was observed. Below the NOAEL, no toxic effects occur and above the LOAEL, toxic effects occur. Exposure outcomes were then measured and compared, including morbidity, physiological changes, and indicators of liver toxicity (Chernoff et al., 2021). The investigators ultimately found that MC-LA was the most toxic congener studied, that the relative toxicities of these variants are significantly different from each other, and that there are congener-specific differences in toxicological mechanisms of action (Chernoff et al., 2021). In addition, toxicity in lakes is most likely due to the combination of the multiple toxins present rather than by one potent toxin alone.

Lad et al. (2022) summarized the human health effects of microcystins to several major organ systems, with a particular focus on pre-existing health conditions. While microcystins are known to cause liver damage, their chronic effects on individuals with pre-existing liver conditions is less understood. In this review article, the researchers summarized a previous experimental study they conducted involving genetically modified mice and the effects of MC-LR toxicity. Mice models were genetically manipulated to be predisposed to liver disease and compared to healthy mice. Chronic, low-dose oral exposure to MC-LR at concentrations lower than acceptable limits resulted in significantly lower survival rates and increased liver injury for the mice with pre-existing liver issues over the controls (Lad et al., 2022). The researchers also found that healthy mice excreted almost 60 times more microcystin in their urine compared to the unhealthy mice, a significant difference attributed to differential metabolism between these mice (Lad et al., 2022). These results highlight how pre-existing health conditions may exacerbate adverse health outcomes after low-dose toxin exposures.

Regarding gut health, microcystins can similarly compromise organ systems of healthy mice and especially for mice with pre-existing gastrointestinal (GI) tract conditions like colitis or

or inflammatory bowel disease (IBS). Orally ingested cyanotoxins are first absorbed in the GI tract, where, studies have shown, has the highest bioaccumulation of these toxins; consequently, intestinal apoptosis (cell death), inflammation, and formation of ROS can result (Lad et al., 2022). In addition, chronic exposure to cyanotoxins in drinking water have been associated with higher human cancer rates. Epidemiologic investigations comparing drinking water with elevated microcystins, as from rivers and lakes, with treated water sources showed that the former had significantly higher colorectal cancer rates for a population in China (Lad et al., 2022).

This study highlighted several important directions for future research, including studying the effects of cyanotoxins on vulnerable populations with co-morbidities such as liver, gastrointestinal, or lung disease, as well as the health effects of chronic exposures through low-dose oral, inhalational, and dermal routes (Lad et al., 2022).

The World Health Organization (WHO) has established exposure limit guidelines for the specific congener MC-LR, based on experimental studies on mice. One of these experiments established a NOAEL of 40 micrograms per kilogram (µg/kg) of body weight per day and a LOAEL of 200 µg/kg of body weight per day for mouse liver toxicity to MC-LR (Lad et al., 2022). The WHO performed calculations correcting for interspecies variation to establish a drinking water permissible exposure limit of 1 microgram per liter (µg/L) based on these studies (Lad et al., 2022). The WHO also established a recreational exposure limit of 10 µg/L for MC-LR (Farrer et al., 2015). It is important to realize that these experimental mouse assays often involve intraperitoneal injection of cyanotoxins, which is an efficient way to determine the lethal dose required to cause mortality in 50% of subjects (LD50) but does not account for the fact that humans are often exposed through the oral route (Christensen & Khan, 2020). Additional research is needed to formulate permissible exposure levels for other specific variants of a single toxin as well as other types of toxins. Furthermore, the USEPA has established their own cyanotoxin guidelines for drinking water and recreational water, which were similarly calculated through toxicological and epidemiological studies. See Table 3 below for a summary of USEPA's guidelines.

This review has also identified dose-response values for the other common cyanotoxins discussed. The median LD50 of cylindrospermopsin in mice after a single intraperitoneal injection is 2.1 milligrams per kilogram (mg/kg) over 24 hours and 0.2 mg/kg after 5 to 6 days (Yang et al., 2021). In addition, Christensen & Khan (2020) describe dose-response relationships for anatoxin-a and saxitoxin, for different exposure routes. According to mouse toxicology studies they synthesized, the LD50 of anatoxin-a via intraperitoneal injection is 200 to 250 µg/kg body weight, and the LD50 of saxitoxin via intraperitoneal injection is 5.5 to 10 µg/kg body weight. The researchers are quick to point out that lethal oral doses of these same toxins are higher than the intraperitoneal doses. Additional doses synthesized from past studies were also compiled. For instance, the oral LD50 for mice was found to be greater than 5,000 µg/kg body weight for anatoxin-a, according to several studies (Christensen & Khan, 2020). Cyanotoxicity studies are more prevalent for mice than for other mammals, but Christensen & Khan (2020) cite an oral toxic dose for saxitoxins in humans ranging from 7 to 15 µg/kg.

Table 3. USEPA Drinking Water and Recreational Water Guideline Values for Cyanotoxins		
Drinking Water Health Advisory Levels (10-day[1]) for Common Cyanotoxins[2]		
Cyanotoxin	**Bottle-fed infants and pre-school children (<6 years old)**	**School-age children and adults (≥6 years old)**
Cylindrospermopsins	0.7 µg/L	3.0 µg/L
Microcystins	0.3 µg/L	1.6 µg/L
Anatoxins	Unavailable[3]	Unavailable
Saxitoxins	Unavailable	Unavailable
Recommended Recreational AWQC/SA[4]		
Cylindrospermopsins	15 µg/L	
Microcystins	8 µg/L	
Anatoxins	Unavailable[5]	
Saxitoxins	Unavailable	
µg/L = micrograms per liter		
AWQC/SA = Ambient Water Quality Criteria or Swimming Advisories; the recommended duration and frequency of these guidelines depend on their application as AWQC/SA		
[1]HAs describe contaminant concentrations of drinking water at which adverse health effects are not anticipated to occur over a 10-day exposure duration.		
[2]USEPA (2022)		
[3]USEPA does not currently report drinking water health advisories for Anaxotins or Saxitoxins due to limited toxicological data. Different states have adopted provisional advisory levels.		
[4]USEPA (2019); p.17		
[5]Guideline values not currently available. Different states have adopted provisional advisory levels.		

Exposure Assessment

The major exposure routes for cyanobacteria include chronic and accidental oral ingestion, dermal contact, and aerosol inhalation, while minor exposure routes include ingestion of crops irrigated with contaminated water, contaminated fish, or unregulated cyanobacterial dietary supplements, as well as the intravenous/injection route (Drobac et al., 2013). Studies reviewing these major routes and various pathways are discussed below.

Ingestion

Accidental oral ingestion of cyanotoxins from drinking water sources is a primary concern in localities plagued by freshwater HABs. Drinking water treatment facilities strive to monitor and, if present, treat contamination before water arrives at the public's tap. However, this level of regulation is absent from recreational water bodies. It is generally expected that scummy or filmy water will be avoided by the public, but cyanotoxins can be present in turbid as well as clearer waters and children and animals may still consume the water. Investigation of the effects of cyanobacteria metabolites via the oral route is appropriate.

Rangel et al. (2014) built upon earlier toxicological studies of mice exposed to cyanobacteria by measuring the toxicities of *Pseudanabaena galeata* and *Geitlerinema splendidum*, two toxic species of cyanobacteria found in reservoirs surrounding the highly urbanized city of Sao Paulo, Brazil. The researchers wanted to see if oral ingestion of these strains' acetic acid extracts presented toxicity similar to intraperitoneal injections to mice. Rangel et al. (2014) found that both strains were incredibly toxic to the mice. Early symptomology in the mice indicated eyebrow ptosis, straub tail, dyspnea, paralysis, and pain, with later necropsy and histopathology revealing liver hemorrhage, necrosis, and hyperemia, as well as kidney and lung issues (Rangel et al., 2014). The researchers confirmed that oral administration of these potent toxin-producing cyanobacteria resulted in similar morbidity and mortality as observed with injected strains in the mouse subjects. This study has wider implications for the toxin-producing genera and species lurking in water bodies used for public consumption, particularly in areas of the world without sufficient treatment technologies or surveillance efforts.

While developed countries have better infrastructure to protect their drinking water sources and accidental ingestion of cyanotoxins in recreational waters is less common, it is nevertheless important to realize that other regions must rely on the water sources they live closest to, despite the level of water treatment available. Roegner et al. (2020) investigated the impacts of freshwater HABs for nearshore fishing communities on Lake Victoria, Kenya. An increase in agricultural, industrial, and wastewater inputs to water bodies in the region, fueled by a growing human population, has resulted in widespread toxic algal blooms, according to the 2020 study. The researchers collected water quality and microbiological samples as well as interviewed local communities regarding their water usage. The study's investigators found that members of the community routinely washed clothes, bathed, cooked with, and drank from green "soup pea" water surfaces at the lake shores, resulting in gastrointestinal effects, skin irritation, and unpleasant odor and taste compounds (Roegner et al., 2020). Moreover, they identified unhealthy levels of microcystins from these water sources across multiple seasons and found that women and children—those most likely to collect the water for household use—were at higher risk of exposure to cyanotoxins (Roegner et al., 2020). Ingestion of potentially toxic water is a constant threat for communities that rely on the lake for drinking water and subsistence-based fishing. While the study focused on common water uses and the risk of ingestion of lake water, less investigation was given to ingestion of water-contaminated food. The researchers indicated that children regularly ate small, sundried fishes that have been documented to contain high levels of microcystins in their tissues and that small plots of vegetables and domesticated animals all use the same water sources (Roegner et al., 2020). It is clear that ingestion of microcystin-laden water can be identified from a myriad number of exposure pathways for these local fisher communities.

In addition, since these communities are located farther from urban centers with drinking water treatment facilities, raw water is directly used or otherwise treated at the home. The study reported boiling, chlorination, and use of a cloth filter as commonly used to clean the water; however, these practices may actually cause more harm than good. The concentration of microcystins in the water may increase due to their resistance to boiling and evaporation of the rest of the water, inadequate local chlorination products, oxidation processes, and cellular lysis—breakdown of the cyanobacterial cells and release of the intracellular toxins (Roegner et al., 2020). Based on these treatment issues, communities reliant on HAB-impacted water bodies have little recourse to filter their water without significant investment in treatment technologies. Future research must address the complex and intersecting environmental health issues of

subsistence communities in tropical regions. Roegner et al. (2020) states that baseline human health data or risk assessment related to freshwater HABs in subsistence communities is incredibly scarce, particularly in warmer, more humid regions where HABs persist for longer periods.

Dermal Contact

Guidelines for cyanotoxins are based on oral ingestion as the primary exposure route, which is appropriate to address concerns for drinking water exposure. However, the effects of dermal absorption or penetration of cyanotoxins is less understood. A wide symptomology has been reported after dermal contact: dermatitis ("swimmer's itch"), skin desquamation (shedding) and rashes, asthma, pneumonia, dry sporadic cough with vomiting and other gastro-intestinal symptoms, hay fever, conjunctivitis, ear and eye irritation, allergic reactions, severe headache, myalgia, vertigo, and mouth blistering (Drobac et al., 2013).

Nielsen & Jiang (2020) conducted a review on recreational dermal exposure to cyanotoxins and the effectiveness of human skin as a barrier to penetration. These investigators identified limited dermal exposure toxicological studies for recreational exposures but found general consensus that cyanotoxins cause mild to moderate skin irritation and possible allergic reactions. Epidemiological studies on cyanotoxin outbreaks are usually the most reliable source of human morbidity data and reported symptoms are often more severe beyond skin irritation (Nielsen & Jiang, 2020). After reviewing numerous case studies, the authors concluded that oral ingestion alone is difficult to attribute to all exhibited symptoms given the approximate volumes of water ingested relative to body size. Instead, they argue that long exposure times in the water across a large skin surface area, including mucous membrane and eye exposure, can help explain some more severe health outcomes. More specifically, one tragic instance in 2002 involved a teenager in Wisconsin who had reportedly been swimming with four other teenagers and was the only one to report accidental oral ingestion of water contaminated by Anatoxin-a. Since this toxin is readily absorbed into the GI tract, animal toxicological studies have shown rapid onset of mortality, but the teenager passed away 48 hours after exposure, suggesting longer absorption time from the skin to the bloodstream. In addition, the four other teenagers that did not report accidental ingestion suffered from GI illness, respiratory distress, fever, and mouth blisters (Nielsen & Jiang, 2020). Although interspecies variation and simple erroneous recollections may explain these observations, it is important to consider that ingestion alone may not account for all symptomology, especially when cuts and abrasions during recreational swimming occur and allow penetration through broken skin. As a final note, the 2002 event in Wisconsin reportedly occurred at a scum-covered golf course pond, and there are similar scenarios that have been recorded (Weirich & Miller, 2014).

Furthermore, the ability of different cyanotoxins to permeate the skin has been explored. Nielsen & Jiang (2020) discuss how research on transdermal drugs (e.g., nicotine) and their ability to permeate the skin to deliver an effective dose can be used to better understand dermal absorption of cyanotoxins. According to this study, skin permeability can be measured as a function of two variables. The first is the partition coefficient (P) between octanol and water (reported as log P) of a compound, with low log P meaning more hydrophilic (water-loving) and high log P meaning more lipophilic (fat-loving); biphasic substances (soluble in both water and lipids) more easily penetrate the skin. The second is the molecular weight (measured in Daltons, a unit of mass), where smaller molecules can more easily get through the skin (Nielsen & Jiang,

2020). Most cyanotoxins have the ability to penetrate either in-tact skin, broken skin, or mucous membranes. Anatoxin-a is the most likely to passively diffuse through the skin given its log P value is within an ideal range for skin absorption and its small molecular weight; microcystin, cylindrospermopsin, and saxitoxin, on the other hand, are less likely given either their larger masses or suboptimal log P values (Nielsen & Jiang, 2020). The researchers suggested that future studies should assess toxin effects to human 3D tissue models and study the role of the skin microbiome on interacting with cyanotoxins.

Aerosol Inhalation

While physical contact and oral ingestion of lake water during recreational activities are anticipated exposures, particularly for younger children and pets, less is known about the dangers of aerosol exposure. Wiśniewska et al. (2019) conducted a review on current knowledge surrounding cyanobacteria aerosol emission mechanisms, size and spatial distribution, collection methods, and impacts to human health. Mechanical transfer of freshwater HAB metabolic products from the water body into the atmosphere occurs through the bursting of air bubbles on the water surface and through wave action (Wiśniewska et al., 2019). According to these researchers, a number of meteorological factors control the dispersion, transport, and deposition of these particles, including wind speed and direction, temperature and humidity, solar irradiance, and rainfall. Air mass advection is also a key factor. It is important to note that once aerosolized, cyanobacteria are exposed to harmful factors like desiccation and ultraviolet radiation, which can impact their viability in the air (Wiśniewska et al., 2019).

Moreover, airborne freshwater picocyanobacteria (the smallest size fraction of cyanobacteria) have been measured in the field (approximately 1.6×10^5 cells/m^3) as well as the laboratory (approximately 3.6×10^5 cells/m^3), indicating that large amounts of microalgae can travel from its source (Wiśniewska et al., 2019). Picocyanobacteria cells are generally in the micron size range. Wiśniewska et al. (2019) reported that airborne microalgae have been detected in studies worldwide, including in the northern and southern latitudes and even Antarctica. In addition, higher concentrations of cyanobacteria in water will result in higher concentrations of biological particles measured in lake spray aerosols (Wiśniewska et al., 2019).

There are no standard methodologies for sampling airborne cyanobacteria and most methods are modeled after air sampling methods for bacteria and fungi (Wiśniewska et al., 2019). One of the most commonly used bioaerosol samplers is a type of inertial impactor. A multistage cascade impactor can collect bioaerosol particles of certain sizes since particles tend to impact an agar medium due to their inertia. As ambient air is drawn into the device, larger particles are collected onto Petri dishes within the initial stages of the impactor and smaller particles are collected in subsequent cascades as the air speed is increased. Since high-volume air flow can be detrimental to cyanobacteria, these devices tend to use lower air flow rates (30 L/min) and can collect cyanobacteria from below 1.1 micrometers (μm) in size to 7 μm (Wiśniewska et al., 2019). After collection, microalgae are cultivated on an enrichment medium and analyzed either by traditional microscopy using taxonomic keys or with molecular methods, as with DNA or RNA sequencing (Wiśniewska et al., 2019).

For public health practitioners, the primary concerns of airborne toxic cyanobacteria are their presence, concentration, and size ranges in the atmosphere. Microalgae size fractions tend to fall between 0.3 μm and 15 μm in diameter and consequently have the ability to travel far distances from their source (Wiśniewska et al., 2019). Dispersion of these small-sized particles

can present serious risks to the areas they deposit. A 1990 case study in a Chicago apartment building traced a localized diarrhea outbreak to cyanobacteria toxins that were present in an open water supply storage tank (Percival & Williams, 2014). It was found that airborne cyanobacteria in dust particles had entered the open tank, grew, and generated toxins that were released throughout the building's plumbing system. Furthermore, Wiśniewska et al. (2019) cited a study that measured aerosolized cyanobacteria with diameters less than 3.3 μm, an important size fraction that can penetrate the lower respiratory tract. Inhalation of microcystins can have toxic effects at lower doses as well, including acute conditions and chronic effects like gastroenteritis, non-alcoholic liver disease, and amyotrophic lateral sclerosis (Wiśniewska et al., 2019). Furthermore, Lad et al. (2022) stated that aerosols can travel over 30 kilometers from their source and that cyanotoxins have caused granulocytic inflammation in the pulmonary tissue of the lungs of rodents. Airborne and persistent cyanotoxins pose serious risks farther from their point of origin and additional work is needed to understand this route of exposure.

In order to better understand the transfer of cyanobacteria from water to air, Olson et al. (2020) collected water samples from a Michigan lake with elevated microcystin levels and were able to quantify eight variants of this toxin in both the water and laboratory-generated aerosol particles, using Enzyme-Linked Immunosorbent Assay (ELISA) and Liquid Chromatography-Mass Spectrometry (LC-MS/MS). Of the eight microcystin congeners analyzed in the water samples, seven were detected in the aerosols; moreover, these aerosol particles were less than 2.5 μm, a particle size with important implications for human health (Olson et al, 2020). The researchers found that amounts of different congeners varied between the water and aerosol phases, in that the hydrophobic (water-repelling) variant microcystin-LR was more prevalent in aerosolized particles than the hydrophilic (water-attracting) congener microcystin-RR. The explanatory mechanism for this differentiation is that hydrophobic compounds tend to adhere to the air-water interface on bubbles passing through the water column until they burst at the water surface and enter into the atmosphere. Olson et al. (2020) concluded that additional studies are needed to quantify these toxic compounds since aerosol phase concentrations are distinct from water phase concentrations and different congeners exhibit varying toxicities.

Hu et al. (2020) expanded the understanding of health effects to aerosol exposure by performing an experimental study on fruit flies (*Drosophila melanogaster*). Due to their short life span and rich genetic diversity, fruit flies make ideal model organisms to test exposure outcomes and have been used to study human diseases like Huntington's and Parkinson's (Hu et al., 2020). The researchers collected two water samples from separate lakes in Florida and analyzed their toxin concentrations in water as well as after being generated into aerosols in a controlled setting. A third sample of a monospecific culture of *Microcystis aeruginosa* with a known concentration was also procured from a separate laboratory. After early life stage exposure to the three aerosolized samples, acute and chronic health outcomes for the fruit flies were measured. Locomotor, neuromuscular, longevity, and synapse function were measured at various life stages of the fruit flies using a negative geotaxis behavior assay, which shows an age-dependent decline (Hu et al., 2020). The negative geotaxis assay relies on the natural tendency of flies to move against gravity when disturbed and is used to study conditions that promote neurodegeneration (Ali et al., 2011). Results indicated that early age exposure led to severe long-term impacts on health and longevity among all age groups of fruit flies; in addition, the researchers found strong acute responses in young groups and old males as well as brain degeneration in females exposed in early or late life stages (Hu et al., 2020). This study

confirmed short and long-term health impacts to fruit flies from exposure to aerosolized concentrations of cyanotoxins, with age of exposure being an important factor.

These review articles and experimental studies show that aerosolized cyanobacteria is a budding area of research and additional work is needed to understand inhalational risks to the public both in, near, and even far away from impacted water bodies.

Risk Characterization

Cyanobacteria pose a mounting risk to freshwater recreators across the country. A number of academic articles were identified summarizing freshwater HAB events for both human and animal morbidity and mortality. Backer et al. (2015) summarized data collected between 2007 to 2011 for 11 states that received federal funding to report freshwater HAB-related health incidents. Data were submitted to the Harmful Algal Bloom-related Illness Surveillance System (HABISS) and included a total of 4,534 events, with 458 cases of suspected and confirmed human bloom-associated illnesses and 175 animal morbidity and mortality events (Backer et al., 2015). This review article provides detailed statistics on human and animal exposure events and is among the first nationwide comprehensive reports on freshwater HABs to do so. For the state of Kansas, which did not receive funding from HABISS, Trevino-Garrison et al. (2015) reported 38 freshwater HAB-impacted water bodies across the state in 2011 and 34 related reports of human and animal health events, including five dog deaths and two human hospitalizations. According to the 2015 publication, symptoms from the human cases included eye and upper respiratory tract irritation, rash, and gastrointestinal distress, and median time from exposure to symptom onset was 24 hours (ranging from 3 to 48 hours). Impacts appeared to result from elevated levels of microcystin, which is produced by multiple species of cyanobacteria in the following genera: *Microcystis*, *Planktothrix*, *Anabaena* and *Oscillatoria* (Trevino-Garrison et al., 2015). The 2011 epidemiologic data recorded by the Kansas Department of Health and Environment is invaluable in helping future disease specialists predict risk for the state's recreational lakes.

Following this theme, Hilborn et al. (2014) summarized human health data voluntarily reported by New York, Ohio, and Washington State from 2009-2010. Information was provided to the Centers for Disease Control and Prevention (CDC). In the 2014 study, 11 freshwater HAB-related disease outbreaks were summarized, including 61 human illnesses, two hospitalizations, and no known deaths reported. Exposure routes for cyanobacteria included dermal contact, oral ingestion, and aerosol inhalation that resulted in a wide array of symptomology, including skin irritation, rash, swelling, and sores; ear and eye irritation; fever; headache; and gastrointestinal, respiratory, and neurologic distress (Hilborn et al., 2014). Furthermore, the report found that these outbreaks occurred in warmer months (June, July, and August), the time between exposure and onset of symptoms may be rapid, and that children may be at higher risk based on more frequent exposure to recreational water and a greater likelihood of ingestion (Hilborn et al., 2014). Moreover, the smaller size and body weight, risky behaviors, and developmental stage for children, teens, and younger adults constitute high risk factors and necessitate improved education and prevention efforts (Weirich & Miller, 2014).

While the Hilborn et al. (2014) study primarily focused on human impacts, suspected HAB-related illnesses and deaths of dogs, fish, and birds were reported in some of the outbreak events. Similar to a canary in the coal mine, it is important to note that animal sickness or death near a water body acts as a sentinel event warning humans of potential exposure risks. This is

especially true for benthic cyanobacteria, which has received less attention than planktonic blooms since they tend to be hidden at the bottom of freshwater bodies until they break apart, rise to the surface, and contribute to animal poisonings (Catherine et al., 2013).

Moreover, the Hilborn et al. (2014) study illuminated the challenges posed by recording HAB-related disease outbreaks. Exposure events may be anecdotal in nature and a water sample confirming the presence of cyanotoxins may or may not have been collected. Exposure may have occurred through one or multiple routes, affected individuals may experience multiple different symptoms, they may or may not seek medical care, and medical professionals may misdiagnose patients (Hilborn et al., 2014). In addition, local outbreak detection will be variable, or even nonexistent, and comprehensive reporting is often not possible. Based on these reasons, as well as the incomplete toxicological dose-response relationships discussed earlier, characterizing risk to freshwater cyanotoxins remains a challenge in environmental public health. Improved monitoring and reporting systems must be in place to gain a fuller picture of this biohazard. The 2014 study reiterates this need for improved risk characterization of freshwater HABs. Prior to this work, only three freshwater HAB-associated outbreaks were reported to the CDC between 1978 and 2008 (Hilborn et al., 2014). Without detailed environmental, epidemiological, and clinical information from freshwater HAB events, estimating the probability of human health risks is incredibly difficult. The study authors concluded that improvements in the surveillance and characterization of blooms and related human disease outbreak events are needed for proper detection and control (Hilborn et al., 2014).

One solution to an improved surveillance strategy was gleamed from Hilborn & Beasley (2015), which found that reports of human and animal illnesses and deaths associated with freshwater HABs were often investigated and reported separately, a missed opportunity to communicate animal sentinel events to the public as an early warning. The researchers performed a systematic literature review and identified 18 reports of 29 or more freshwater HAB events where animal illnesses and deaths served as a potential warning for human health risks. Among 15 of the 18 reports describing 25 or more events, freshwater HAB-related animal illness or death clearly preceded any reports of human illness and, among 11 of the 18 reports describing 15 or more events, freshwater HAB-related animal illness or death was recognized and action was taken to warn the public about the risk of exposure (Hilborn & Beasley, 2015). The study authors highlighted the necessity and efficacy of using the concept of One Health. One Health describes the interdependence of humans, animals, plants, microbes, and ecosystems and strives toward the collaboration of professionals in the wildlife, veterinary, medical, water management, laboratory, and public health fields (Hilborn & Beasley, 2015). This study builds a strong case that freshwater HABs are a multi-stakeholder problem requiring effective interagency communication to connect the dots between animal sentinel events and possible human exposures.

Currently, the CDC reports bloom events through their One Health Harmful Algal Bloom System (OHHABS). OHHABS is an online reporting system where information on HABs, including human and animal illness, is voluntarily reported by state public health and related agencies (CDC, 2021). OHHABs provides annual reports on the impacts of HABs across the country, offering public health practitioners an understanding of the spatial and temporal trends associated with HAB morbidity and mortality. Based on the 2021 Summary Report—the most recently available report—16 states reported a total of 368 HAB events, including 117 human illnesses and at least 2,715 animal illnesses (CDC, 2023). Although the information on OHHABS reveals general trends from voluntarily reported data nationwide, local environmental public

health professionals may benefit from using this database as a model for individual freshwater bodies. As Hilborn & Beasley (2015) already alluded to, an interdisciplinary effort between public health departments, clinicians, lake stewards, and others to characterize the occurrence and severity of blooms can lead to better risk prediction and communication for local lakes prone to eutrophication.

Risk Management and Control

Now that the human health risks of freshwater cyanobacteria have been discussed, it is prudent to answer the question, "What can we do about it?" This section will explore the current state of knowledge on detection, control, and management of cyanobacteria and their expressed metabolites. A focus is placed on recreational management rather than drinking water treatment control strategies.

Almuhtaram et al. (2021) provides a comprehensive review on HAB early warning systems and how to assess and respond to progressive levels of risk for a water body. The study authors propose a three-tier system with tools for detecting biological events in the first tier, tools to confirm the presence of cyanobacteria in the second tier, and tools to verify cyanobacteria metabolites (toxins and taste and odor compounds) and the genes that encode for them in the third tier (Almuhtaram et al., 2021). First tier monitoring tools are generally inexpensive and include visual assessment; measurement of adenosine triphosphate (ATP), general water quality parameters, and chlorophyll-a; and remote sensing and the use of drones. If there is a deviation in baseline biological activity, second tier tools—microscopic enumeration, automated cell imaging, measurement of phycocyanin, drone and satellite remote sensing, use of machine learning models, and the use of next generation sequencing and biosensors—are employed. Finally, third tier tools quantify cyanobacteria byproducts and include ELISA, qPCR, and other advanced laboratory analytical techniques (Almuhtaram et al., 2021). The authors argue that no single tool can provide the full picture of cyanobacteria risk but when used in combination can provide an improved risk assessment and subsequent management actions. A summary table detailing the freshwater HAB monitoring tools with respect to their costs, turnaround time, measurement accuracy, and possible interferences is also provided (Almuhtaram et al., 2021).

A successful management program not only accurately monitors for cyanobacteria and their metabolites but also provides actionable steps to reduce the risk. Ibelings et al. (2014) compares regulatory frameworks and management plans adopted by 17 different countries across the world. The review found that most countries have adopted the WHO provisional guideline value of 1 μg/L MC-LR for drinking water, but regulations for the inhalational or dermal routes, contaminated fish and foodstuffs, and elusive benthic cyanobacteria were less consistent. Furthermore, responses to recreational exposures often involved a tiered management plan with progressive alert levels. These plans followed the WHO's Water Safety Plan concept, a "catchment-to-consumer" model that incorporates multiple stakeholders to manage water resources and combats freshwater HABs at their source. For instance, irrigation practices at the catchment scale can reduce phosphorus loading, temporary lake closures or "no fishing" orders respond to elevated phosphorus levels at the waterbody scale, and drinking water treatment for confirmed cyanobacteria blooms and compounds are conducted at the consumer scale (Ibelings et al., 2014). These measures generally follow the hierarchy of controls in environmental public health practice. Addressing the broader scale issues of climate change, eutrophication,

agricultural fertilizer use, urbanization and stormwater runoff, and pollution are central to the WHO's Water Safety Plan.

A large number of countries from the Ibelings et al. (2014) study used a tiered alert system where cyanobacteria or cyanotoxin levels dictated congruent advisories or additional testing. Advisories often included "do no swim" or "do not fish" warnings. Likewise, Washington State created a Freshwater Algae Control Program in 2005 to provide funding for cyanotoxin testing from lakes across the state, as well as adopted a tiered management plan for lakes experiencing freshwater HABs (Trainer and Hardy, 2015). In less developed countries, management decisions include abstaining from washing or bathing in affected water bodies, avoiding herding of cattle into lakes, and advisories on water treatment (e.g., chlorine use and boiling practices) (Roegner et al., 2020). These practices are often the last line of defense so future management plans need to become more proactive rather than reactive. Moreover, the USEPA provides an overview for a number of waterbody treatments for cyanobacteria blooms. This includes various physical controls (aeration, mechanical mixing, use of ultrasound technology, etc.) and chemical controls (algaecides, coagulation/flocculation, alum treatment, etc.) provided on the agency website (USEPA, 2023). In addition to the USEPA's strategies for source water protection of drinking water, measures aimed at maintaining non-potable recreational lakes are critical to manage cyanobacteria risks to human health.

Discussion

After reviewing these articles, a number of findings become clear. There is a large amount of toxicological and ecological information available on cyanobacteria and their most common toxins—microcystin, cylindrospermopsin, anatoxin-a, and saxitoxin (Chernoff et al., 2021; Christensen & Khan, 2020; Drobac et al., 2013; Lad et al., 2022; Weirich & Miller, 2014; Yang et al., 2019). However, the studies' authors made clear that microcystin is by far the most well studied cyanotoxin and that a number of variants for both microcystins and the other common cyanotoxins are less understood, particularly with their health impacts. The situation is made more complicated since some genera and species of cyanobacteria can produce one or more toxins. These combinations of metabolites add to the net toxicity of blooms that develop in freshwater bodies. Catherine et al. (2013) argues that benthic cyanobacteria are an emerging concern to public health and recommend future work in studying new monitoring tools, ecological growth factors and interactions, variables that regulate toxin production, and improved mathematical models for benthic algae risk prediction. Additionally, improvements in understanding the physical, chemical, and toxicological characteristics of the neurotoxins and their global distributions; exact dose-responses for the common cyanotoxins; investigations with pre-existing conditions and the chronic effects of cyanotoxins rather than just acute exposures; and establishing more robust public education measures were among the most prominent opportunities for future work.

The experimental and review articles surrounding exposure factors were ripe with original experiments and case studies to help elucidate the impacts of cyanobacteria on mammalian systems. These articles (Hu et al., 2020; Olson et al., 2020; Nielsen & Jian, 2020; Rangel et al., 2014; Roegner et al., 2020; Wiśniewska et al., 2019) recommended considerations for improved chemical and pharmacological characterization of cyanotoxins, further inquiries into the aerosol and dermal routes of exposure over the well-established oral route, better quantification of the level of exposure to cyanotoxins from foodstuffs, and, once again, improved public outreach and education efforts. Furthermore, by investigating the freshwater HAB issue along Lake Victoria, Kenya, Roegner et al. (2020) offers a lucid point that local drivers of

nutrient input and triggers for toxin production are critical to understand in order to conserve endangered water resources. Community-based interventions focused on sustainability are essential in regions without the infrastructure and resources to combat climate change-induced eutrophication and waterborne illness (Roegner et al., 2020).

Backer et al. (2015), Hilborn et al. (2014), and Trevino-Garrison et al. (2015) provided reviews of on-the-ground epidemiologic data summarizing health exposures to both animals and humans in the past few decades. These studies showed that systematic data collection systems at the local to national level are essential to holistically understand the animal and human health risks of freshwater cyanobacteria. Despite reporting variability among locations, the voluntary nature of reporting, administrative issues, limited funding and resources, underreporting, and incomplete records, this information is invaluable to public health and epidemiologic scientists to understand the extent of health risks. These articles highlighted the continued need for these types of reviews and for continued evidence-based prevention and control strategies. Moreover, Hilborn & Beasley (2015) add that a One Health approach provides an efficient means of managing cyanobacteria risk through a collaborative mission across disciplines and professions, taking animal cases into account to better communicate human health risks.

Finally, a number of articles tackled the issue of management and control (Almuhtaram et al., 2021; Ibelings et al., 2014; Trainer and Hardy, 2015). Management plans for a host of countries were summarized, including top-down measures of government regulation, to bottom-up measures of volunteer monitoring programs. Almuhtaram et al. (2021) provides a useful summary of the early warning tools and technologies available to lake stewards today and provides an efficient tiered strategy to quantify the level of risk from cyanobacteria and its metabolites. A comprehensive effort to understand cyanobacteria risk will include volunteer efforts, interagency collaboration, state of the art monitoring technologies, laboratory analysis and result interpretation, and evidence-based controls. Iterative refinements of these tools and exploration of new technologies will help the global fight against freshwater HABs.

Concluding Remarks

Freshwater cyanobacteria present a complex and growing challenge to public health practitioners across the globe. This narrative literature review synthesized 20 articles published across 14 academic journals that discuss freshwater cyanobacteria issues across the globe. There is a wide breadth of knowledge published on this environmental health hazard; nevertheless, more research is needed to understand freshwater HABs as a natural phenomenon that threatens our shared water resources and human health. This narrative review serves as a stepping stone to understand the current knowledge and management surrounding cyanobacteria as well as future directions in research and practice that must be undertaken for successful management and control.

References

Ali, Y. O., Escala, W., Ruan, K., & Zhai, R. G. (2011). Assaying locomotor, learning, and memory deficits in *drosophila*models of neurodegeneration. *Journal of Visualized Experiments*, (49). https://doi.org/10.3791/2504.

Almuhtaram, H., Kibuye, F. A., Ajjampur, S., Glover, C. M., Hofmann, R., Gaget, V., Owen, C., Wert, E. C., & Zamyadi, A. (2021). State of knowledge on early warning tools for cyanobacteria detection. *Ecological Indicators*, *133*, 108442. https://doi.org/10.1016/j.ecolind.2021.108442.

Backer, L. C., Manassaram-Baptiste, D., LePrell, R., & Bolton, B. (2015). Cyanobacteria and Algae Blooms: Review of Health and Environmental Data from the Harmful Algal Bloom-Related Illness Surveillance System (HABISS) 2007–2011. *Toxins*, *7*(4), Article 4. https://doi.org/10.3390/toxins7041048.

CDC. (2021, September 30). *One Health Harmful Algal Bloom System (OHHABS)*. Harmful Algal Bloom (HAB)-Associated Illness. https://www.cdc.gov/habs/ohhabs.html.

CDC. (2023, July 11). *Summary Report – One Health Harmful Algal Bloom System (OHHABS), United States, 2021*. Harmful Algal Bloom (HAB)-Associated Illness. https://www.cdc.gov/habs/data/2021-ohhabs-data-summary.html.

Catherine, Q., Susanna, W., Isidora, E.-S., Mark, H., Aurélie, V., & Jean-François, H. (2013). A review of current knowledge on toxic benthic freshwater cyanobacteria – Ecology, toxin production and risk management. *Water Research*, *47*(15), 5464–5479. https://doi.org/10.1016/j.watres.2013.06.042.

Chernoff, N., Hill, D., Lang, J., Schmid, J., Farthing, A., & Huang, H. (2021). Dose–Response Study of Microcystin Congeners MCLA, MCLR, MCLY, MCRR, and MCYR Administered Orally to Mice. *Toxins*, *13*(2), Article 2. https://doi.org/10.3390/toxins13020086.

Christensen, V. G., & Khan, E. (2020). Freshwater neurotoxins and concerns for human, animal, and ecosystem health: A review of anatoxin-a and saxitoxin. *Science of The Total Environment*, *736*, 139515. https://doi.org/10.1016/j.scitotenv.2020.139515.

Drobac, D., Tokodi, N., Simeunović, J., Baltić, V., Stanić, D., & Svirčev, Z. (2013). Human exposure to cyanotoxins and their effects on health. *Archives of Industrial Hygiene and Toxicology*, *64*(2), 305–316. https://doi.org/10.2478/10004-1254-64-2013-2320.

Farrer, D., Counter, M., Hillwig, R., & Cude, C. (2015). Health-Based Cyanotoxin Guideline Values Allow for Cyanotoxin-Based Monitoring and Efficient Public Health Response to Cyanobacterial Blooms. *Toxins*, *7*(2), 457–477. https://doi.org/10.3390/toxins7020457.

Ferrari, R. (2015). Writing narrative style literature reviews. *Medical Writing*, *24*(4), 230–235. https://doi.org/10.1179/2047480615Z.000000000329.

Griffith, A. W., & Gobler, C. J. (2020). Harmful algal blooms: A climate change co-stressor in marine and freshwater ecosystems. *Harmful Algae*, *91*, 101590. https://doi.org/10.1016/j.hal.2019.03.008.

Hilborn, E. D., Roberts, V. A., Backer, L., Deconno, E., Egan, J. S., Hyde, J. B., Nicholas, D. C., Wiegert, E. J., Billing, L. M., Diorio, M., Mohr, M. C., Hardy, J. F., Wade, T. J., Yoder, J. S., Hlavsa, M. C., & Centers for Disease Control and Prevention (CDC). (2014). *Algal bloom-associated disease outbreaks among users of freshwater lakes--United States, 2009-2010*. MMWR. Morbidity and mortality weekly report. Retrieved January 3, 2023, from https://www.ncbi.nlm.nih.gov/pmc/articles/PMC5779332/.

Hilborn, E. D., & Beasley, V. R. (2015). One Health and Cyanobacteria in Freshwater Systems: Animal Illnesses and Deaths Are Sentinel Events for Human Health Risks. *Toxins*, *7*(4), Article 4. https://doi.org/10.3390/toxins7041374.

Hou, X., Feng, L., Dai, Y., Hu, C., Gibson, L., Tang, J., Lee, Z., Wang, Y., Cai, X., Liu, J., Zheng, Y., & Zheng, C. (2022). Global mapping reveals increase in lacustrine algal blooms over the past decade. *Nature Geoscience*, *15*(2), 130–134. https://doi.org/10.1038/s41561-021-00887-x.

Hu, J., Liu, J., Zhu, Y., Diaz-Perez, Z., Sheridan, M., Royer, H., Leibensperger, R., Maizel, D., Brand, L., Popendorf, K. J., Gaston, C. J., & Zhai, R. G. (2020). Exposure to aerosolized algal toxins in South Florida increases short- and long-term health risk in drosophila model of aging. *Toxins*, *12*(12), 787. https://doi.org/10.3390/toxins12120787.

Hudnell, H. K. (2010). The state of U.S. freshwater harmful algal blooms assessments, policy and legislation. *Toxicon*, *55*(5), 1024–1034. https://doi.org/10.1016/j.toxicon.2009.07.021.

Ibelings, B. W., Backer, L. C., Kardinaal, W. E. A., & Chorus, I. (2014). Current approaches to cyanotoxin risk assessment and risk management around the globe. *Harmful Algae*, *40*, 63–74. https://doi.org/10.1016/j.hal.2014.10.002.

Jones, M. R., Pinto, E., Torres, M. A., Dörr, F., Mazur-Marzec, H., Szubert, K., Tartaglione, L., Dell'Aversano, C., Miles, C. O., Beach, D. G., McCarron, P., Sivonen, K., Fewer, D. P., Jokela, J., & Janssen, E. M.-L. (2021). CyanoMetDB, a comprehensive public database of secondary metabolites from cyanobacteria. *Water Research*, *196*, 117017. https://doi.org/10.1016/j.watres.2021.117017.

Lad, A., Breidenbach, J. D., Su, R. C., Murray, J., Kuang, R., Mascarenhas, A., Najjar, J., Patel, S., Hegde, P., Youssef, M., Breuler, J., Kleinhenz, A. L., Ault, A. P., Westrick, J. A., Modyanov, N. N., Kennedy, D. J., & Haller, S. T. (2022). As We Drink and Breathe: Adverse Health Effects of Microcystins and Other Harmful Algal Bloom Toxins in the Liver, Gut, Lungs and Beyond. *Life*, *12*(3), Article 3. https://doi.org/10.3390/life12030418.

Nielsen, M. C., & Jiang, S. C. (2020). Can cyanotoxins penetrate human skin during water recreation to cause negative health effects? *Harmful Algae*, *98*, 101872. https://doi.org/10.1016/j.hal.2020.101872.

Olson, N. E., Cooke, M. E., Shi, J. H., Birbeck, J. A., Westrick, J. A., & Ault, A. P. (2020). Harmful algal bloom toxins in aerosol generated from Inland Lake Water. *Environmental Science & Technology*, *54*(8), 4769–4780. https://doi.org/10.1021/acs.est.9b07727.

Percival, S. L., & Williams, D. W. (2014). Chapter Five—Cyanobacteria. In S. L. Percival, M. V. Yates, D. W. Williams, R. M. Chalmers, & N. F. Gray. *Microbiology of Waterborne Diseases (Second Edition)*, 79–88. https://doi.org/10.1016/B978-0-12-415846-7.00005-6.

Rangel, M., Martins, J. C. G., Garcia, A. N., Conserva, G. A. A., Costa-Neves, A., Sant'Anna, C. L., & De Carvalho, L. R. (2014). Analysis of the Toxicity and Histopathology Induced by the Oral Administration of Pseudanabaena galeata and Geitlerinema splendidum (Cyanobacteria) Extracts to Mice. *Marine Drugs*, *12*(1), Article 1. https://doi.org/10.3390/md12010508.

Roegner, A., Sitoki, L., Weirich, C., Corman, J., Owage, D., Umami, M., Odada, E., Miruka, J., Ogari, Z., Smith, W., Rejmankova, E., & Miller, T. R. (2020). Harmful Algal Blooms Threaten the Health of Peri-Urban Fisher Communities: A case study in Kisumu Bay,

Lake Victoria, Kenya. *Exposure and Health*, *12*(4), 835–848. https://doi.org/10.1007/s12403-019-00342-8.

Trainer, V. L., & Hardy, F. J. (2015). Integrative Monitoring of Marine and Freshwater Harmful Algae in Washington State for Public Health Protection. *Toxins*, *7*(4), Article 4. https://doi.org/10.3390/toxins7041206.

Trevino-Garrison, I., DeMent, J., Ahmed, F. S., Haines-Lieber, P., Langer, T., Ménager, H., Neff, J., Van der Merwe, D., & Carney, E. (2015). Human Illnesses and Animal Deaths Associated with Freshwater Harmful Algal Blooms—Kansas. *Toxins*, *7*(2), Article 2. https://doi.org/10.3390/toxins7020353.

USEPA. (2019). *Recommended Human Health Recreational Ambient Water Quality Criteria or Swimming Advisories for Microcystins and Cylindrospermopsin*. Retrieved May 29, 2023, from https://www.epa.gov/sites/default/files/2019-05/documents/hh-rec-criteria-habs-document-2019.pdf.

USEPA. (2022). *EPA Drinking Water Health Advisories for Cyanotoxins*. Retrieved May 17, 2023, from https://www.epa.gov/cyanohabs/epa-drinking-water-health-advisories-cyanotoxins.

USEPA. (2023). *Control Measures for Cyanobacterial HABs in Surface Water*. Retrieved June 25, 2023, from https://www.epa.gov/cyanohabs/control-measures-cyanobacterial-habs-surface-water.

Weirich, C. A., & Miller, T. R. (2014). Freshwater Harmful Algal Blooms: Toxins and Children's Health. *Current Problems in Pediatric and Adolescent Health Care*, *44*(1), 2–24. https://doi.org/10.1016/j.cppeds.2013.10.007.

Wiśniewska, K., Lewandowska, A. U., & Śliwińska-Wilczewska, S. (2019). The importance of cyanobacteria and microalgae present in aerosols to human health and the Environment – Review Study. *Environment International*, *131*, 104964. https://doi.org/10.1016/j.envint.2019.104964.

Yang, Y., Yu, G., Chen, Y., Jia, N., & Li, R. (2021). Four decades of progress in cylindrospermopsin research: The ins and outs of a potent cyanotoxin. *Journal of Hazardous Materials*, *406*, 124653. https://doi.org/10.1016/j.jhazmat.2020.124653.

Appendix D. Detailed Laboratory Materials and Methods

Detailed Laboratory Materials and Methods

Environmental Sample Equipment Checklists

Field Checklist:

- nitrile gloves
- high-visibility vest
- hip waders
- wristwatch
- pre-labelled, 1 L opaque Nalgene bottles
- 1 L clear Nalgene bottle with DI or distilled water
- cooler containing ice
- second empty cooler
- clipboard/paperwork and sample labels/sharpie
- GPS tool (Emlid Reach RS2+ Multi-band RTK GNSS receiver with centimeter precision)
- trash bag
- paper towels

Lab Checklist:

Filtration Step:

- Nalgene autoclave bin
- vacuum pump with pressure gauge (flow rate below 6 inches mercury, or 20 kilopascals)
- sampling manifold
- filter funnel with magnetic base (x10)
- GF/F filters, Whatman (47-mm, pore size of 0.7 µm)
- 2 L volumetric flask with side arm
- 250 mL graduated cylinder
- Saturated magnesium carbonate ($MgCO_3$) solution (1 gram powdered MgCO3 diluted in 100 mL distilled water)
- plastic tubing from vacuum pump source with pressure gauge to Vacu-guard inline filter
- plastic tubing from Vacu-guard inline filter to flask side arm
- plastic tubing with plunger from manifold side nozzle to flask top
- metal forceps/tweezers
- metal scissors
- plastic Petri dishes
- aluminum foil
- sharpie and marking tape
- paper towels and lab tissues
- polyethylene squirt bottles and DI tap water
- paperwork to record sample volumes/times/notes

Extraction Step:

- aq. acetone solution [90% High Performance Liquid Chromatography (HPLC) Grade acetone/10% distilled, deionized water)

- waste aq. acetone bottles
- safety goggles
- 50 mL plastic conical tubes
- 15 mL screw cap plastic centrifuge tubes
- test tube racks (x2 for 15 mL centrifuge tubes and x1 for 50 mL conical tubes)
- metal forceps/tweezers
- metal scissors
- metal spatula and glass rod
- plastic funnels
- volumetric pipettes (serological pipettes and pipette tips)
- aluminum foil
- polyethylene squirt bottles and DI tap water
- paper towels and lab tissues
- small cooler with ice
- timer
- Beckman Coulter Avanti J-20 XP centrifuge, including balancing and weighing calibration materials
- paperwork to record sample processing times

Instrument Analysis Step:

- SPECTRAmax^{TM} PLUS microplate spectrophotometer, including SoftMax Pro microplate reader control and analysis software (Molecular Devices Corporation, 1997)
- glass cells/cuvettes for spectrophotometer – x16 cells
- aq. 90% acetone solution
- aq. acetone waste container
- 1-20 µL, and 10-200 µL, and 100-1000 µL serological pipettes and tips
- red biowaste container
- aluminum foil
- test tube rack for cuvettes and 15 mL centrifuge tubes
- small cooler
- sample labelling tape and indelible marker
- Stock Standard Solution in -20°C freezer
- 15 mL centrifuge tubes for mixing SSS-diluted standards (pre-wrapped and pre-labelled)
- paperwork to record sample and dilution results
- 0.1 M Hydrochloric acid
- Labelled glass container with warning labels
- timer

Stock Standard Solution (SSS) Preparation Step:

- SPECTRAmax^{TM} PLUS microplate spectrophotometer, including SoftMax Pro microplate reader control and data analysis software
- 90%/10% aq. acetone solution
- waste acetone container (with funnel)
- SSS (chilled at -20°C, pre-labelled, pre-wrapped in aluminum foil)
- serological pipettes and corresponding pipette tips
- red biowaste container

- labels/sharpie/notebook
- glass cells/cuvettes with lids
- 15 mL conical tubes (pre-labelled, pre-wrapped in aluminum foil)
- test tube rack for cuvettes and for conical tubes
- small cooler

Environmental Sample Lab Procedures

Procedure – Field Sampling:

- Complete all required paperwork and sample labelling prior to work
- Place coolers and equipment near work area
- Don hip waders, high-visibility vest, and nitrile gloves
- Record GPS coordinates of sample locations
- Prime the pre-labelled 1 L opaque sample containers by rinsing in lake water 3 times
- Collect samples by slowly submerging the bottle upside down/nose-down to a depth of 0.5 meters, inverting it slightly, and allowing it to fill slowly
- Seal container and immediately place on ice in cooler (keep at temperature of 4°C)
- Repeat process for all samples and exchange disposable gloves
- Transfer field blank with distilled water from 1 L clear Nalgene bottle into 1 L opaque sampling container and place in cooler with the other sample bottles
- Doff equipment and clean up area
- At lab, transfer the sample containers from the cooler into the 4°C fridge
- Decon equipment and clean up area

Procedure – Filtration Step:

- Perform all work in dim light and avoid heat when handling samples
- Assemble vacuum pump and apparatus/manifold (connect all tubing lines from vacuum pump source with pressure gauge to regulator disc, from regulator disc to side arm of 2 L flask, and from manifold to top of flask; ensure secure connections and that pump flow is cut off to the manifest (No Flow horizontal position)
- Position the filter funnels with magnetic bases onto the manifold
- Remove filter funnel and use a dedicated forceps/tweezers to center a clean GF/F filter onto the magnetic base (textured/gritted side up); ensure the filter funnel is secure and position the graduated marks facing you
- Turn on vacuum pump and check pressure gauge; vacuum filtration should not exceed 6 in. Hg (20 kPa)
- Retrieve one sample container from fridge at a time and gently but thoroughly invert container to homogenize; process samples so that field blank is processed first and then lab blank is processed last
- Over the sink, rinse the 250 mL graduated cylinder with sample water from the chilled sampling container (priming it 3 times)
- Transfer sample water into the graduated cylinder and measure volume to the bottom of the meniscus; measure in 100 mL increments
- Pour sample water into the filter funnel and carefully open valve on apparatus for vacuum; watch the level of water filter through and slow the pressure by turning the

valve when the water is close to being expended; turn off completely before water is completely filtered and do not suck filter dry with vacuum
- Add additional 100 mL until filter is sufficiently strained; do not overload the filter
- As applicable, add 2 mL of $MgCO_3$ buffering solution just before the filtering process is completed
- Once completely filtered shut off valve and pump
- Remove filter funnel and use forceps/tweezers to remove filter from the magnetic base
- Use the scissors to cut the outer circumference of the filter (the non-filtered portion) to aid with extraction) and discard this portion
- Using tweezers, fold filter in half (with sample inside) and place onto pre-labelled, clean Petri dish; dab the outside of each side of the filter with lab tissue to remove excess water
- Cover container with pre-labelled tin foil and store in the freezer at -20°C until extraction
- Use different filter funnels and Petri dishes for each sample – no need to decon the funnels or bases/manifold/tubing/flask; decon metal implements and graduated cylinder between samples
- Turn off vacuum pump, decon and clean up area

Procedure – Extraction Step:
- Retrieve Petri dish with frozen filter from -20°C freezer
- Remove filter with clean tweezers and use scissors to cut it into pieces to facilitate extraction step
- Let pieces fall into the new, pre-labelled 50 mL conical tube on test tube rack
- Push filter down to bottom using a metal spatula or glass rod
- Use a volumetric pipette to add 4 mL of aqueous acetone solution into the 50 mL conical tube to create a slurry
- Place grinding tube into a small cooler with ice to ensure maceration does not overheat the sample
- Grind filter slurry manually using metal spatula for 5 minutes using timer
- Once it appears sufficiently macerated, transfer the 4 mL + slurry from 50 mL conical tube into a clean, prelabelled, pre-tinfoil wrapped 15 mL centrifuge plastic tube
- Using a volumetric pipet, rinse the metal spatula/glass rod and the 50 mL conical tube with 6 mL of the aqueous acetone solution; add the rinseate to the centrifuge tube containing the filter slurry; add to get to approximately 10 mL for final extraction volume
- Cap the centrifuge tube and shake it vigorously. Place it in the 4°C fridge in a test tube rack before proceeding to the next filter extraction
- Decon all equipment between samples
- Proceed to next Petri dish with preserved filter and repeat the steps above
- Samples should be allowed to steep for a minimum of 2 h but not to exceed 24 h; tubes should be shaken at least once, preferably two to three times, during the steeping period to allow the extraction solution to have maximum contact with the filter slurry
- Decon and clean up area
- After steeping is complete, centrifuge all the samples for 15 min at 675 G (700 G on instrument) or for 5 min at 1000 G
- Centrifuge Instructions:
    - Use gloves at all times when using the centrifuge
    - Complete logbook entry per use

    - Turn on to let warm up
    - Set settings:
        - Match rotor name on screen to what's written on rotor
        - Set the RCF (gravity) to 700 G
        - Set time [15 min at 675 G (700 G) or 5 min at 1000 G]
        - Set temperature to 20°C
    - Use foot pedal to open lid and check to make sure rotor is correct and secured
    - Balance buckets by using scale; double check that buckets are the same weight; insert 15 mL centrifuge test tubes and place lids onto buckets when weighing; add or remove water using spray bottle
    - Make sure clamps on buckets are tightened and secure; push on lower sides to make sure they don't pop out
    - Once balanced, place buckets directly and vertically into centrifuge and secure
    - Close lid, press Enter, and then Press Start; do not leave area while the centrifuge is running
    - When finished, remove test tubes from the buckets and place in test tube rack (avoid mixing/vibrations to leave supernatant separated)
    - When finished, turn off the instrument and leave lid open to vent out after use

Procedure – Instrument Analysis Step:

- Turn on spectrophotometer so it can warm up and auto-calibrate
- Log into desktop computer and open SoftMax Pro software
- Pipette 2 mL supernatant of extracted sample from 15 mL centrifuge tube into the glass spectrophotometer cell/cuvette ; repeat for all samples
- Handle all cuvettes with gloves and only touch the frosted sides
- Transfer all cuvettes in test tube rack within the smaller cooler between rooms
- Pipette 2 mL of 90% acetone reference solution into a clean cuvette and use to zero the instrument at the selected wavelengths
- Enter in desired wavelengths to measure into the program (750, 664, 647, and 630 nm) and select "REF" to analyze reference solution
- Once reference is entered, insert glass cell into the instrument and press "READ"; collect and average 3 readings for instrument reproducibility
- Make sure to appropriately position the cell into the instrument (frosted side perpendicular to where the light passes through) and analyze all samples
- Record values and output from program and save project data to desktop
- Use Excel calculation spreadsheet to convert optical density (OD) readings to µg/L chlorophyll a
- After acquiring uncorrected sample results, repeat the analysis process with acid-corrected extractions; perform this step by adding 0.06 mL (60 µL) of 0.1 N HCl to the 2 mL cuvette to obtain an acid concentration of 0.003 N, pipette mix for 90 seconds (avoid aerating the sample), and then re-run; complete acid correction calculations in Excel
    - The acid correction step is implemented to correct for pheopigments, non-photosynthetic degradation products of the chlorophyll pigments (notably pheopigment-a)
- Decon glass cuvettes, dispose all equipment, and clean up area when finished
- Turn off spectrophotometer and log out of desktop computer

Procedure – SSS Preparation Step:

- Calculate dilutions needed to create a standard/calibration curve for chlorophyll a; generally 1:25, 1:50, 1:100, 1:200, and 1:500 dilutions
- Transfer appropriate amounts needed of SSS and aq. acetone into the centrifuge tubes
- Pipette mix the solutions to homogenize by pressing down on the pipette (before submerging) and (while submerged) release and press the plunger back and forth without pressing all the way down (to not introduce air bubbles)
- Once the dilutions are well mixed, transfer 2 mL to a glass cuvette; each dilution will be analyzed in triplicate, with a total of 15 cuvettes used for the 5 dilutions
- Enter in a reference cuvette of aq. acetone and read in the prepared dilutions into the spectrophotometer; calculate these values in Excel to get final results
- Repeat steps above for acid-corrected dilutions using similar methodology described above
- Decon all equipment and dump dilutions into designated waste container

Appendix E. Site Health and Safety Plan

FIELDWORK SAFETY PLAN – TEMPLATE #2			
Field Site Location:	*Northeast portion of Echo Lake (19901 Ashworth Avenue N., Shoreline, WA 98133)*		
Activity Description:	*Field reconnaissance at Echo Lake (aerial photo acquisition using a drone platform and surface water sampling for masters thesis work).*		
Plan Created for:	*Dr. Tania M. Busch Isaksen*	**Date of revision:**	*07/14/2023*
Date(s) of Travel:	*Planned biweekly sampling events on Mondays (07/24, 08/07, 08/21, 09/04, 09/18, 10/02), onsite 7am-12pm and return to campus*		

Site Information		
Location	*Latitude:* ***47.77292001281817 (from Google Maps)***	*Longitude:* ***-122.34131688195039 (from Google Maps)***
Site Information	*An approximately 12-acre freshwater recreational lake in the City of Shoreline, King County, Washington. A residential complex, single-family residences, and a public access park adjoin the perimeter of the lake. Aurora Avenue North/U.S. Route 99 is located to the west and the surrounding area is highly urbanized.*	
Travel to Site	*Travel in personal vehicle.*	
Site Access	*Echo Lake Park has a public parking lot located on the northeast portion of the lake. Access to the lake is found at the park and along the bike path adjoining the lake.*	
Environmental Hazards	*Weather (summer heat, rain), Biological hazards (mosquitos, poison ivy), Ergonomic hazards (lifting heavy equipment)*	
Security	*Low risk for harassment or violence at the public park. Researcher will be alert and attentive to all park inhabitants. See "Personal Safety & Security" section for more details on communications plan.*	
No Go Criteria	*Heavy rains and wind, excessive heat (temperatures > 100°F), wildfire smoke at an unhealthy level (AQI > 100).*	
Expected Weather	*Researcher will check the forecast prior to each field visit and dress appropriately for typical summer weather. Inclement weather will interfere with drone operations.*	

Drinking Water Availability	☐ Plumbed water available ☐ Water cooler with ice provided ☒ Bottled water provided ☐ Natural source and treatment methods (e.g. filtration, boiling, chemical disinfection):
Access to Shade/Shelter	If forecast exceeds 80°, shade must be provided by natural or artificial means for rest breaks. ☒ Building structures ☒ Trees ☐ Temporary Canopy/Tarp ☒ Vehicle with A/C ☐ Other:
High Heat Procedures	*The following high heat procedures will be followed when the temperature is at or above 80 degrees Fahrenheit:* *1) A mandatory cool down rest period in the shade or an air-conditioned personal vehicle for the following temperature conditions:* • *10 minute rest period/2 hours at or above 90°F* • *15 minute rest period/1 hour at or above 100°F* • *Note that the researcher will not be onsite if the temperature is expected to exceed 100°F* *2) Self-observation for signs and symptoms of heat-related illness by means of:* • *Regular (hourly) communication by cellular phone with advisor (see detailed communications plan in "Personal Safety & Security" section). The researcher will contact advisor if signs or symptoms of heat-related illness manifest.* • *911 will be contacted if the researcher experiences extreme signs or symptoms of heat-related illness.* *In addition, the researcher will check all forecasts to anticipate air temperatures before heading to the field. The researcher will don appropriate clothing (breathable shirt, sunglasses, hat), bring plenty of drinking water, and work in the shade when feasible. In addition, the most strenuous tasks will be performed in the early to mid-morning hours (7am-11am).* *☐ Direct supervision ☐ Buddy system ☒ Reliable cell or radio contact ☐ Other:*
Emergency Services and Contact Information	

Local Contact	*Stefan Grozev, Senior Surface Water Program Specialist, Public Works | City of Shoreline, sgrozev@shorelinewa.gov* **Lodging location:** *N/A*	**University Contact** Not on trip. Provide a copy of this plan.	*Dr. Tania Busch Isaksen, Associate Teaching Professor, DEOHS, UW, tania@uw.edu* **Frequency of check ins:** *Update at end of field work day and weekly meetings*
Emergency Medical Services (EMS)	*Contact 911 in an emergency situation*		
Nearest Emergency Department (ED)	***Nearest Hospital**: UW Medical Center - Northwest | Seattle Hospital 1560 N 115th St, Seattle, WA 98133* ***Phone**: (206) 668-1558* *Evacuation Plan: If possible, gather all equipment and head to NE parking lot to travel to hospital in personal vehicle; estimated travel time is 10–18 min (6.8 miles)* *See attached Google Map directions*		
Cell Phone Coverage	***Primary Number:*** **omitted** ***Coverage:*** *good* ***Nearest location with coverage:*** *N/A*	***Satellite phone/ device*** *N/A*	***Device carried?*** ☒*yes* ☐*no* ***Type/number:*** *Cell phone/* **omitted**
Nearby Facilities	*A restroom is located onsite adjacent to the park.*		
Side Trips	*N/A*		
Participant Information			
Field Team/ Participants	Is anyone working alone? ☒ Yes ☐ No If yes, develop a communications plan with strict check-in procedures; if cell coverage is unreliable, carry a satellite communication device or personal locator beacon (see "Personal Safety & Security" section for detailed communications plan) Primary Field Team Leader: *Joey Teresi* Secondary Field Team Leader: *N/A* ☒ Field Team/Participant list is attached as training documentation ☐ Other attachment: e.g. course roster		
Physical Demands	- *Carry up to 20 pounds of equipment* - *Use of hip waders to sample from the lake surface*		

Mental Demands	- *Time-sensitive work requires pre-planning and efficiency* - *Possible engagement with curious members of the public*
First Aid Training & Supplies	*Joey Teresi – CPR/AED/First Aid Certified (Provider: CPR Seattle – expires 02/2024)* Location and description of group medical/first aid kit: *A standard first aid kit is available in the trunk of the researcher's personal vehicle*.
Immunizations or Medical Evaluation	*N/A*
Equipment and Activities – Consult with EH&S for specific training and requirements.	
Research Activities	*Field reconnaissance at Echo Lake (aerial photo acquisition using a drone platform and surface water sampling for masters thesis work).*
Field Transportation	*Personal vehicle*
Research Tools	*DJI Phantom 4 Drone with RTK base station (Certified FAA Part 107 Remote Pilot and training through the UW RAPID facility)*
Chemicals and Hazardous Materials	*N/A*
Other Research Hazards	*Drone use – presence of tall trees, powerlines, other people, etc. as well as weather hazards during flight operation.* *Entering water body from beach area to collect water samples.*
Personal Protective Equipment	*Required: nitrile gloves, hip waders* *Recommended: long pants, hat, sunglasses, insect repellant, sunscreen*
Additional Considerations	
Insurance	*UW RAPID facility's insurance for equipment*
International Activities	*N/A*

Personal Safety & Security (communicati-ons plan)	*A communications plan will be implemented since the researcher anticipates conducting field work alone. The researcher will perform the following procedures:* *1) Check in with advisor via cellular phone when arriving onsite.* *2) Practice situational awareness at all times and use common sense when potential security issues arise.* *3) Contact advisor via cellular phone when feeling unsafe from individuals at the park or when showing signs of heat-related illness. If able, the researcher will gather all equipment before entering their personal vehicle to isolate themselves from the potential danger or security risk. 911 will be contacted if researcher deems it is appropriate to do so.* *4) Check in with advisor via cellular phone when leaving site each day.* *As part of this communications plan, the researcher will contact the city government official if security issues arise.*
Campus Contacts	
UWPD	*(206) 543-0507*
Campus Health Services	*Hall Health Center: 206-685-1011*
EH&S	*(206) 543-7262*
UW Travel Emergency Assistance	Risk Services, Office of Global Affairs – UW Global Emergency Line
Report Injuries	Online Accident Reporting System (OARS)

First Aid Reference – Signs & Symptoms of Illness *(examples for heat illnesses included)*		
Signs & Symptoms	**Treatment**	**Response Action:**

HEAT EXHAUSTION • *Dizziness, headache* • *Rapid heart rate* • *Pale, cool, clammy or flushed skin* • *Nausea and/or vomiting* • *Fatigue, thirst, muscle cramps*	1. *Stop all exertion.* 2. *Move to a cool shaded place.* 3. *Hydrate with cool water.*	*Heat exhaustion is the most common type of heat illness. Initiate treatment. If no improvement, call 911 and seek medical help. Do not return to work in the sun. Heat exhaustion can progress to heat stroke.*
HEAT STROKE • *Disoriented, irritable, combative, unconscious* • *Hallucinations, seizures, poor balance* • *Rapid heart rate* • *Hot, dry and red skin* • *Fever, body temperature above 104 °F*	1. *Move (gently) to a cooler spot in shade.* 2. *Loosen clothing and spray clothes and exposed skin with water and fan.* 3. *Cool by placing ice or cold packs along neck, chest, armpits and groin (Do not place ice directly on skin)*	***Call 911 or seek medical help immediately.*** ***Heat stroke is a life threatening medical emergency. A victim can die within minutes if not properly treated. Efforts to reduce body temperature must begin immediately!***

Include any additional resources: route/location maps, photos of general terrain and areas requiring extra caution, etc. – SEE HOSPITAL DIRECTIONS ATTACHED

Signature of PI/Supervisor:

I acknowledge this safety plan has been prepared for field work under my supervision.

Name	Signature	Date	Phone Number
Tania Busch Isaksen	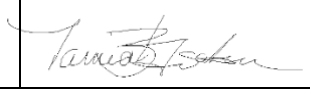	**7/1/23**	**omitted**

Field Team/Participant Roster - Training Documentation

I verify that I have read this Field Safety Plan, understand its contents, and agree to comply with its requirements.

Name/Phone Number	Signature	Date	Emergency Contact/Phone Number
Joey Teresi/ omitted		07-24-23	Tania Busch Isaksen/ omitted
Joey Teresi/ omitted		08-07-23	Tania Busch Isaksen/ omitted
Joey Teresi/ omitted		08-21-23	Tania Busch Isaksen/ omitted
Joey Teresi/ omitted		09-02-23	Tania Busch Isaksen/ omitted
Joey Teresi/ omitted		09-11-23	Tania Busch Isaksen/ omitted
Joey Teresi/ omitted	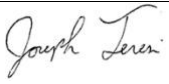	10-07-23	Tania Busch Isaksen/ omitted
Joey Teresi/ omitted		10-23-23	Tania Busch Isaksen/ omitted

19901 Ashworth Ave N, Shoreline, WA 98133 to UW Medical Center - Northwest | Seattle Hospital, 1560 N 115th St, Seattle, WA 98133

Drive 6.8 miles, 10–18 min

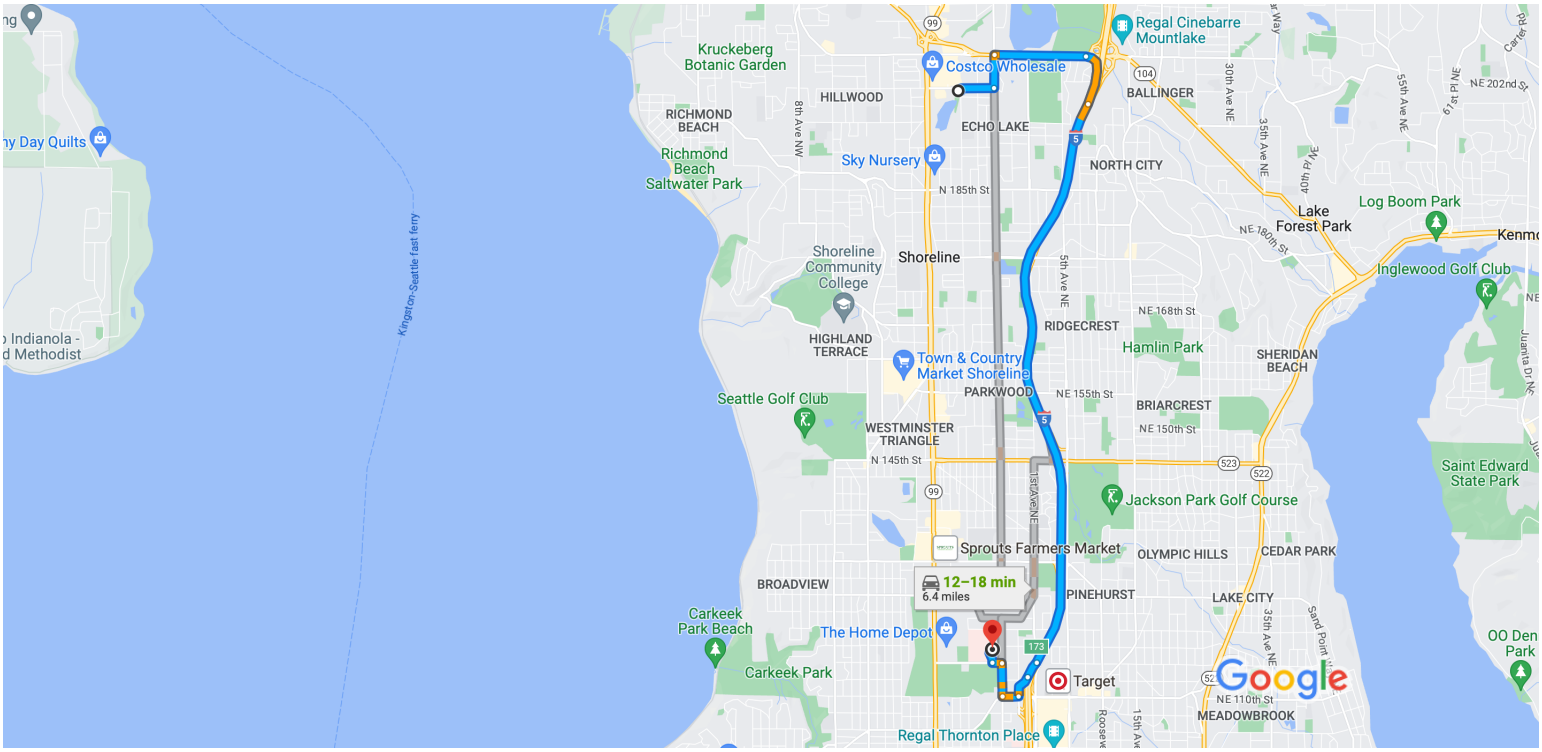

19901 Ashworth Ave N
Shoreline, WA 98133

Get on I-5 S from WA-104 E/NE 205th St/Lake Ballinger Way

4 min (1.6 mi)

1. Head north on Ashworth Ave N toward N 200th St

105 ft

2. Turn right at the 1st cross street onto N 200th St

0.2 mi

3. Turn left onto Meridian Ave N

0.3 mi

4. Turn right onto WA-104 E/NE 205th St/Lake Ballinger Way

0.7 mi

5. Use the right lane to merge onto I-5 S via the ramp to Seattle

0.4 mi

Follow I-5 S to N Northgate Way in Seattle. Take exit 173 from I-5 S

5 min (4.7 mi)

6. Merge onto I-5 S

4.4 mi

7. Take exit 173 for Northgate Way toward 1st Ave NE

0.1 mi

8. Keep right, follow signs for Northgate Way W

0.2 mi

Continue on N Northgate Way to your destination

3 min (0.5 mi)

9. Turn right onto N Northgate Way

0.1 mi

10. Turn right onto Meridian Ave N

0.3 mi

11. Turn left onto N 115th St

367 ft

12. Turn right

423 ft

13. Turn right

Destination will be on the right

115 ft

UW Medical Center - Northwest | Seattle Hospital

1560 N 115th St, Seattle, WA 98133

Appendix F. Data Analysis R Code

Teresi Masters Thesis - R Markdown Data Analysis Code

Joey Teresi

2024-04-22

R Markdown Document Setup

```
## Load packages
library(tidyverse)   ## for ggplot2, dplyr, etc.
library(tinytex)     ## for TexLive Helper Functions, Compile LaTeX Documents
library(knitr)       ## for knitting nice PDF files
library(sandwich)    ## for Robust Covariance Matrix Estimators
library(kableExtra)  ## for Construct Complex Table with 'kable' and Pipe Syntax
library(lattice)     ## for Trellis Graphics for R
library(rigr)        ## for Regression, Inference, and General Data Analysis Tools in R
library(formatR)     ## for formatting R source code
library(psych)       ## for descriptive statistics
library(ggplot2)     ## for creating and editing plots
library(ggpubr)      ## for creating and editing plots

## Use opts_chunk$set() to set global knit options for this document.
knitr::opts_chunk$set(echo=FALSE, message=FALSE, warnings=TRUE, fig.align='center',
                      tidy=TRUE, tidy.opts=list(width.cutoff=50, ncol=20))

## Clear all of the objects from your workspace to start with a clean environment
rm(list=ls())
```

Read in the thesis datasets, described below:

"Teresi_data1.csv" ('dat1') = All Chlorophyll-a duplicate and averaged results (for descriptive analysis)

"Teresi_data2.csv" ('dat2') = Extract Chlorophyll-a and Absorbance Results of Dilutions (for calibration curves)

"Teresi_data3.csv" ('dat3') = Average Chlorophyll-a results and RGB Vegetation Index values (for inferential analysis)

"Teresi_data4.csv" ('dat4') = Average Chlorophyll-a results and Multispectral Vegetation Index values (for inferential analysis)

```
## Create variables that read in the thesis
## datasets
```

```r
dat1 <- read.csv("Teresi_data1.csv", header = T)
dat2 <- read.csv("Teresi_data2.csv", header = T)
dat3 <- read.csv("Teresi_data3.csv", header = T)
dat4 <- read.csv("Teresi_data4.csv", header = T)
```

Descriptive Statistics Analysis

This section will use 'dat1' to generate desccriptive statistics tables and boxplots for the chlorophyll a results.

```
## Overview the entire 'dat1' dataset using the
## descrip() and summary() functions to yield
## descriptive statistics
descrip(dat1)
```

```
##            N     Msng  Mean      Std Dev    Min       25%       Mdn
##      ID:      28     0   14.50     8.226     1.000     7.750     14.50
##     Loc:      28     0   2.500     1.139     1.000     1.750     2.500
## ChlaAvg:      28     0   26.26     19.95     6.190     11.05     22.70
##             75%       Max
##      ID:     21.25     28.00
##     Loc:     3.250     4.000
## ChlaAvg:     34.59     82.28
```

```
summary(dat1)
```

```
##       ID                 Loc               ChlaAvg
##  Length:28          Length:28          Min.   : 6.19
##  Class :character   Class :character   1st Qu.:11.05
##  Mode  :character   Mode  :character   Median :22.70
##                                        Mean   :26.26
##                                        3rd Qu.:34.59
##                                        Max.   :82.28
```

```
## Create a variable ('bw1') that generates a
## boxplot for all the averaged chlorophyll a
## values. Boxplots are useful to visualize the
## central tendency, distribution, and outliers
## present in the data (i.e., locality, spread,
## and skewness).
bw1 <- boxplot(dat1$ChlaAvg, data = dat1, main = "Boxplot of All Chlorophyll a Results",
    ylab = "Chlorophyll a (ug/L)", xlab = "", col = 3)
```

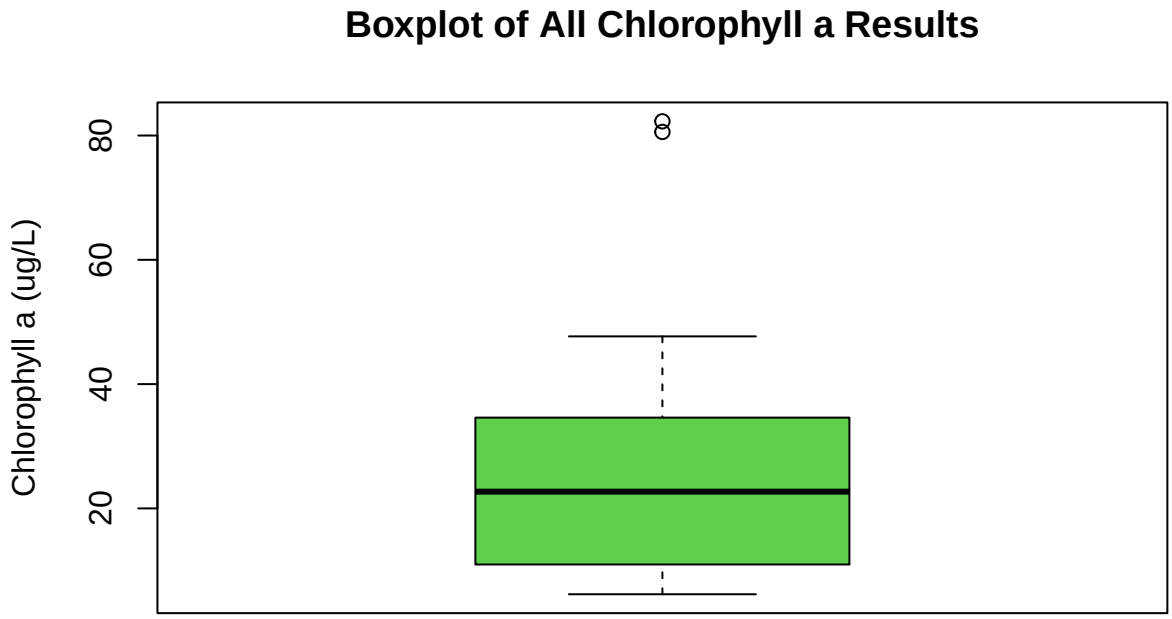


```
## Create variables that recode the averaged
## chlorophyll a values into the four sampling
## locations (Beach, North Dock, West Docks -
## North, and West Docks - South).
Beach <- subset(dat1, Loc == "Beach")
NDock <- subset(dat1, Loc == "NDock")
WDocksN <- subset(dat1, Loc == "WDocksN")
WDocksS <- subset(dat1, Loc == "WDocksS")

## Summarize the stratified data. Note each
## location has a sample size of 7.
summary(Beach)
```

```
##       ID                 Loc                ChlaAvg
##  Length:7           Length:7           Min.   : 7.22
##  Class :character   Class :character   1st Qu.:10.46
##  Mode  :character   Mode  :character   Median :19.13
##                                        Mean   :30.88
##                                        3rd Qu.:44.17
##                                        Max.   :80.58
```

```
summary(NDock)
```

```
##       ID                 Loc                ChlaAvg
```

```
##  Length:7           Length:7           Min.   : 8.15
##  Class :character   Class :character   1st Qu.:13.46
##  Mode  :character   Mode  :character   Median :22.27
##                                        Mean   :31.26
##                                        3rd Qu.:39.59
##                                        Max.   :82.28
```

```
summary(WDocksN)
```

```
##       ID                 Loc                ChlaAvg
##  Length:7           Length:7           Min.   : 6.19
##  Class :character   Class :character   1st Qu.:14.40
##  Mode  :character   Mode  :character   Median :23.12
##                                        Mean   :21.70
##                                        3rd Qu.:29.57
##                                        Max.   :34.65
```

```
summary(WDocksS)
```

```
##       ID                 Loc                ChlaAvg
##  Length:7           Length:7           Min.   : 6.450
##  Class :character   Class :character   1st Qu.: 9.645
##  Mode  :character   Mode  :character   Median :24.180
##                                        Mean   :21.207
##                                        3rd Qu.:30.945
##                                        Max.   :36.640
```

```
descrip(dat1$ChlaAvg, strata = dat1$Loc)
```

```
##                                N     Msng  Mean      Std Dev    Min
## dat1$ChlaAvg:  All               28     0   26.26     19.95     6.190
## dat1$ChlaAvg:    Str  Beach       7     0   30.88     27.02     7.220
## dat1$ChlaAvg:    Str  NDock       7     0   31.26     26.00     8.150
## dat1$ChlaAvg:    Str  WDocksN     7     0   21.70     10.84     6.190
## dat1$ChlaAvg:    Str  WDocksS     7     0   21.21     12.61     6.450
##                                 25%       Mdn       75%       Max
## dat1$ChlaAvg:  All               11.05     22.70     34.59     82.28
## dat1$ChlaAvg:    Str  Beach      10.45     19.13     44.17     80.58
## dat1$ChlaAvg:    Str  NDock      13.46     22.27     39.59     82.28
## dat1$ChlaAvg:    Str  WDocksN    14.40     23.12     29.56     34.65
## dat1$ChlaAvg:    Str  WDocksS    9.645     24.18     30.94     36.64
```

```
## Create boxplots for all the averaged
## chlorophyll a values stratified by sample
## location. Create a variable ('label1')
## containing a list of the labels to be used for
## the plot's x-axis.
label1 <- c("Beach", "North Dock", "West Docks - N",
    "West Docks - S")
bw2 <- boxplot(dat1$ChlaAvg ~ dat1$Loc, data = dat1,
    main = "Boxplots of All Chlorophyll a Results By Sample Location",
    ylab = "Chlorophyll a (ug/L)", xlab = "Sample Location",
    names = label1, col = c(2, 3, 4, 5))
```

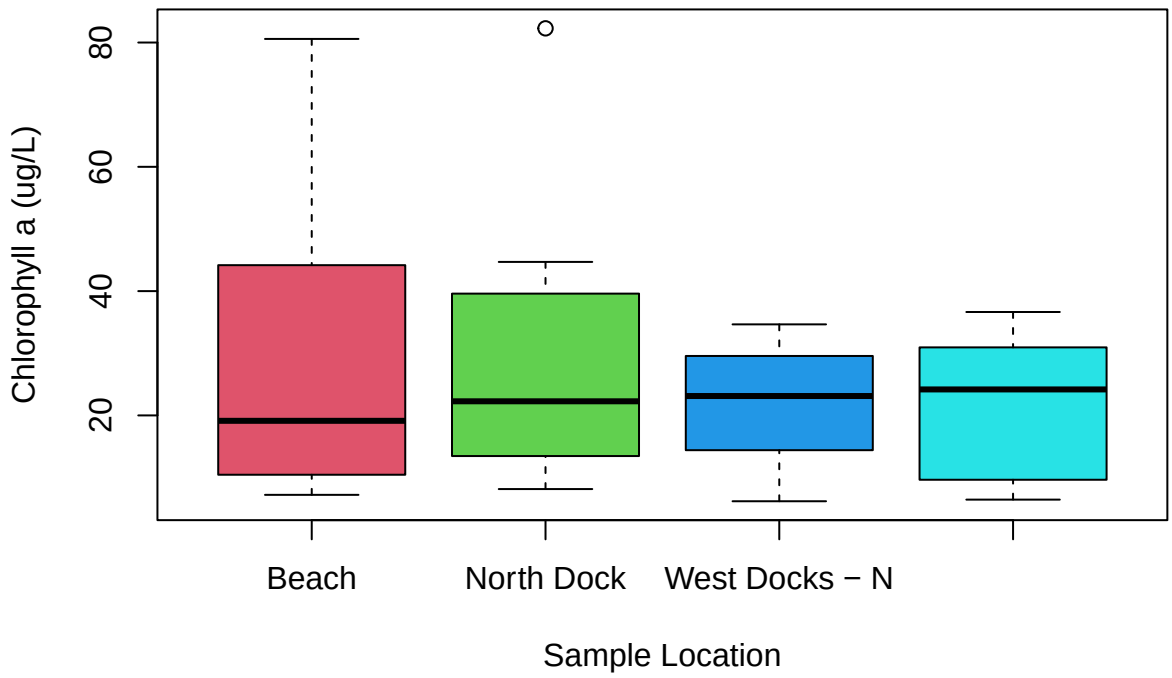


```
## Create seven variables that recode the dataset
## to be stratified by sampling event.
FirstEvent <- dat1[1:4, ]
SecondEvent <- dat1[5:8, ]
ThirdEvent <- dat1[9:12, ]
FourthEvent <- dat1[13:16, ]
FifthEvent <- dat1[17:20, ]
SixthEvent <- dat1[21:24, ]
SeventhEvent <- dat1[25:28, ]

## Generate descriptive statistics summaries for
## these variables.
summary(FirstEvent)
```

```
##       ID                 Loc                ChlaAvg
##  Length:4           Length:4           Min.   :19.13
##  Class :character   Class :character   1st Qu.:21.48
##  Mode  :character   Mode  :character   Median :22.70
##                                        Mean   :22.18
##                                        3rd Qu.:23.39
##                                        Max.   :24.18
```

```
summary(SecondEvent)
```

```
##       ID                 Loc                ChlaAvg
```

```
##  Length:4           Length:4           Min.   :34.65
##  Class :character   Class :character   1st Qu.:36.14
##  Mode  :character   Mode  :character   Median :38.66
##                                        Mean   :39.16
##                                        3rd Qu.:41.68
##                                        Max.   :44.70
```

```
summary(ThirdEvent)
```

```
##       ID                 Loc                ChlaAvg
##  Length:4           Length:4           Min.   :6.190
##  Class :character   Class :character   1st Qu.:6.385
##  Mode  :character   Mode  :character   Median :6.835
##                                        Mean   :7.003
##                                        3rd Qu.:7.452
##                                        Max.   :8.150
```

```
summary(FourthEvent)
```

```
##       ID                 Loc                ChlaAvg
##  Length:4           Length:4           Min.   :11.12
##  Class :character   Class :character   1st Qu.:11.44
##  Mode  :character   Mode  :character   Median :13.81
##                                        Mean   :13.96
##                                        3rd Qu.:16.34
##                                        Max.   :17.08
```

```
summary(FifthEvent)
```

```
##       ID                 Loc                ChlaAvg
##  Length:4           Length:4           Min.   : 7.75
##  Class :character   Class :character   1st Qu.: 9.28
##  Mode  :character   Mode  :character   Median :10.31
##                                        Mean   :10.03
##                                        3rd Qu.:11.05
##                                        Max.   :11.73
```

```
summary(SixthEvent)
```

```
##       ID                 Loc                ChlaAvg
##  Length:4           Length:4           Min.   :24.56
##  Class :character   Class :character   1st Qu.:26.66
##  Mode  :character   Mode  :character   Median :53.97
##                                        Mean   :53.70
##                                        3rd Qu.:81.00
##                                        Max.   :82.28
```

```
summary(SeventhEvent)
```

```
##       ID                 Loc               ChlaAvg
##  Length:4           Length:4           Min.   :34.49
##  Class :character   Class :character   1st Qu.:34.52
##  Mode  :character   Mode  :character   Median :34.55
##                                        Mean   :37.82
##                                        3rd Qu.:37.85
##                                        Max.   :47.68
```

```
descrip(FirstEvent)
```

```
##            N     Msng  Mean      Std Dev    Min       25%       Mdn
##      ID:       4     0   2.500     1.291     1.000     1.750     2.500
##     Loc:       4     0   2.500     1.291     1.000     1.750     2.500
## ChlaAvg:       4     0   22.18     2.175     19.13     21.48     22.70
##             75%       Max
##      ID:     3.250     4.000
##     Loc:     3.250     4.000
## ChlaAvg:     23.38     24.18
```

```
descrip(SecondEvent)
```

```
##            N     Msng  Mean      Std Dev    Min       25%       Mdn
##      ID:       4     0   2.500     1.291     1.000     1.750     2.500
##     Loc:       4     0   2.500     1.291     1.000     1.750     2.500
## ChlaAvg:       4     0   39.16     4.460     34.65     36.14     38.66
##             75%       Max
##      ID:     3.250     4.000
##     Loc:     3.250     4.000
## ChlaAvg:     41.68     44.70
```

```
descrip(ThirdEvent)
```

```
##            N     Msng  Mean      Std Dev    Min       25%       Mdn
##      ID:       4     0   2.500     1.291     1.000     1.750     2.500
##     Loc:       4     0   2.500     1.291     1.000     1.750     2.500
## ChlaAvg:       4     0   7.003     0.8812    6.190     6.385     6.835
##             75%       Max
##      ID:     3.250     4.000
##     Loc:     3.250     4.000
## ChlaAvg:     7.453     8.150
```

```
descrip(FourthEvent)
```

```
##            N     Msng  Mean      Std Dev    Min       25%       Mdn
##      ID:       4     0   2.500     1.291     1.000     1.750     2.500
##     Loc:       4     0   2.500     1.291     1.000     1.750     2.500
## ChlaAvg:       4     0   13.96     3.066     11.12     11.43     13.81
##             75%       Max
##      ID:     3.250     4.000
##     Loc:     3.250     4.000
## ChlaAvg:     16.34     17.08
```

```
descrip(FifthEvent)
```

```
##            N     Msng  Mean      Std Dev    Min       25%       Mdn
##      ID:       4     0   2.500     1.291     1.000     1.750     2.500
##     Loc:       4     0   2.500     1.291     1.000     1.750     2.500
## ChlaAvg:       4     0   10.03     1.711     7.750     9.280     10.31
##             75%       Max
##      ID:     3.250     4.000
##     Loc:     3.250     4.000
## ChlaAvg:     11.05     11.73
```

```
descrip(SixthEvent)
```

```
##            N     Msng  Mean      Std Dev    Min       25%       Mdn
##      ID:       4     0   2.500     1.291     1.000     1.750     2.500
##     Loc:       4     0   2.500     1.291     1.000     1.750     2.500
## ChlaAvg:       4     0   53.70     32.05     24.56     26.66     53.97
##             75%       Max
##      ID:     3.250     4.000
##     Loc:     3.250     4.000
## ChlaAvg:     81.00     82.28
```

```
descrip(SeventhEvent)
```

```
##            N     Msng  Mean      Std Dev    Min       25%       Mdn
##      ID:       4     0   2.500     1.291     1.000     1.750     2.500
##     Loc:       4     0   2.500     1.291     1.000     1.750     2.500
## ChlaAvg:       4     0   37.82     6.575     34.49     34.52     34.55
##             75%       Max
##      ID:     3.250     4.000
##     Loc:     3.250     4.000
## ChlaAvg:     37.85     47.68
```

```
## Create a new variable ('ChlaByEvent') that
## uses the data.frame() function to subset the
## averaged chlorophyll a values for each
## sampling event.
ChlaByEvent <- data.frame(FirstEvent$ChlaAvg, SecondEvent$ChlaAvg,
    ThirdEvent$ChlaAvg, FourthEvent$ChlaAvg, FifthEvent$ChlaAvg,
    SixthEvent$ChlaAvg, SeventhEvent$ChlaAvg)

## Create boxplots for all the averaged
## chlorophyll a values stratified by sample
## event. Create a variable ('label2') containing
## a list of the labels to be used for the plot's
## x-axis.
label2 <- c("1st", "2nd", "3rd", "4th", "5th", "6th",
    "7th")
bw3 <- boxplot(ChlaByEvent, data = dat1, main = "Boxplots of Chlorophyll a Results By Sample Event",
    ylab = "Chlorophyll a (ug/L)", xlab = "Sample Event",
    names = label2, col = c(2, 7, 8, 5, 6, 3, 4))
```

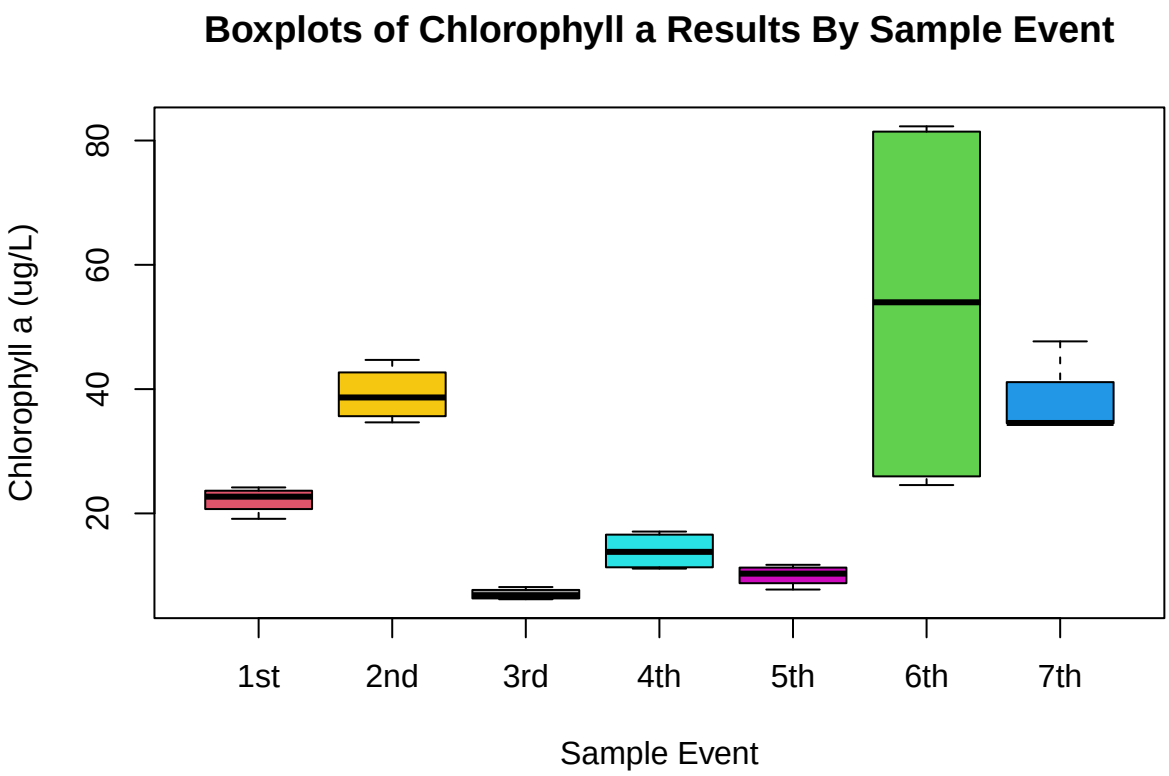
Boxplots of Chlorophyll a Results By Sample Event
Chlorophyll a (ug/L)
20
40
60
80
1st
2nd
3rd
4th
5th
6th
7th
Sample Event

Calibration Curve Scatter Plot Analysis

This section will use 'dat2' to generate scatter plots for the positive control analyses, with each sample event's respective calibration curve all in one plot.

The overall purpose of this code chunk is to use a function sourced online to compute the various regression models' equation coefficients and R^2 value and convert them into a string data type for later use to display on a plot. This operation is iteratively applied to each sample event's data, and regression/correlation plots are created and saved to a single figure.

Code Source Citation for the equation used:

Ramnath. (2011, September 26). Answer to: "Add regression line equation and R^2 on graph." Edited by MrFlick. (2019, July 2). Meta Stack Exchange. https://stackoverflow.com/questions/7549694/add-regression-line-equation-and-r2-on-graph/7549819#7549819.

```
## Create a variable ('lm_eqn' for linear model
## equation) that creates a function that takes 1
## argument ('df' for dataframe). Within the
## equation, create a variable ('m' for model)
## that creates the linear regression model
## between Abs664Avg (x) and ChlaExAvg (y) from
## the 'dat2' dataset, taking 'df' as the data
## argument. Create a variable ('eq' for
## equation) that uses the substitute() argument
## to specify the linear regression equation's
## slope (a), y intercept (b), and R^2 value (r2)
## and their specific formatting (italics font, 5
## decimal places). The as.character() argument
## converts these calculated values into text.
## Note: the lm_robust() function was not used
## since we are not interested in calculating
## robust standard error for these models
## (impacts the confidence intervals on the
## figures).
lm_eqn <- function(df) {
    m <- lm(Abs664Avg ~ ChlaExAvg, df)
    eq <- substitute(italic(y) == a + b %.% italic(x) *
        "," ~ ~italic(r)^2 ~ "=" ~ r2, list(a = format(unname(coef(m)[1]),
        digits = 4), b = format(unname(coef(m)[2]),
        digits = 4), r2 = format(summary(m)$r.squared,
        digits = 4)))
    as.character(as.expression(eq))
}

## Create a variable ('dat2_labeled') that will
## ultimately parse the 'dat2' dataset. The pipe
## operator '%>%' takes the output of a function
## and passes it into another function as an
## argument, allowing a sequence of steps to
## occur. The group_by() function converts the
## 'dat2' table into a grouped table where
## operations are performed by the 'Event'
```

```
## column. The grouped table then becomes nested,
## which creates a list-column of data frames,
## meaning one row is created for each group
## (1st, 2nd, etc.) and is defined by the
## non-nested columns (ID, ChlaAvg ,etc.). The
## mutate() function creates new columns of the
## existing variables, which is specified by a
## label. The map() function returns a list,
## where the 'data' variable is created by
## default by the nest() function and the
## previous function ('lm_eqn') is applied to all
## Events (calculating their regression
## coefficients and R^2 value and converting them
## to text). The select() function selects the
## Event column and new label. The label is then
## unnested (converts from a dataframe back to
## rows and columns) and is ungrouped since the
## calculations were completed. The final
## variable yields a table with a regression
## equation and R^2 value for each sample event.
dat2_labeled <- dat2 %>%
    group_by(Event) %>%
    nest() %>%
    mutate(Label = map(data, lm_eqn)) %>%
    select(Event, Label) %>%
    unnest(Label) %>%
    ungroup()

## Create a variable ('gdat2') that will create
## the customized plots for all the sample
## events. The ggplot() function takes the
## arguments: data source and the plot aesthetics
## (ChlaExAvg as x and Abs664Abg as y). Elements
## are added to the plot using the '+' operator.
## The geom_point() function creates a
## scatterplot and has arguments that set the
## color of the points to match the dataset's
## 'Type' column (S for sample or D for dilution)
## and alpha sets the transparency. The
## scale_color_manual() function creates a
## discrete scale specifying the labels and
## colors for the points. The geom_smooth()
## function creates the default lowess smoother
## (regression line), which accepts the lm
## character vector and lm formula arguments,
## along with the line's color, width, and
## transparency. It also displays the confidence
## interval by default. The geom_text() function
## facilitates plot labelling by specifying the
## 'dat2_labeled' variable created, mapping to
## create the labels at (x,y) coordinates on the
## plot (specified by axis values), and allowing
## adjustments for label size and nudging the
```

```
## label down the y-axis slightly. The parse
## argument is needed to parse the substitute()
## function above. The facet_wrap() function
## specifies how many columns to display and
## stratified by sample event. The labs()
## function labels the title and axes, the
## theme() function adjusts the alignment of the
## plot title, and the theme_bw() function sets
## the style of the overall plot background and
## gridlines.
gdat2 <- ggplot(dat2, aes(x = ChlaExAvg, y = Abs664Avg)) +
    geom_point(aes(color = Type), alpha = 0.6) + scale_color_manual(labels = c("Dilution",
    "Sample"), values = c("forestgreen", "black")) +
    geom_smooth(method = "lm", formula = "y ~ x", color = "black",
        linewidth = 0.5, alpha = 0.6) + geom_text(data = dat2_labeled,
    mapping = aes(x = 1500, y = 0.29), label = dat2_labeled$Label,
    parse = TRUE, size = 2.5, nudge_y = -0.05) + facet_wrap("~ Event",
    ncol = 2) + labs(title = "Chlorophyll-a Calibration Curve by Sample Event Number",
    x = "Extract Chlorophyll a Concentration (µg/L)",
    y = "Absorbance at 664 nanometers") + theme(plot.title = element_text(hjust = 0.5)) +
    theme_bw()

## Use the ggsave() function to save a .png file
## to view the output plots
ggsave("Figure 4. Chlorophyll-a Calibration Curve by Event Number.png",
    gdat2, width = 7)

## Call variable to output figure
gdat2
```

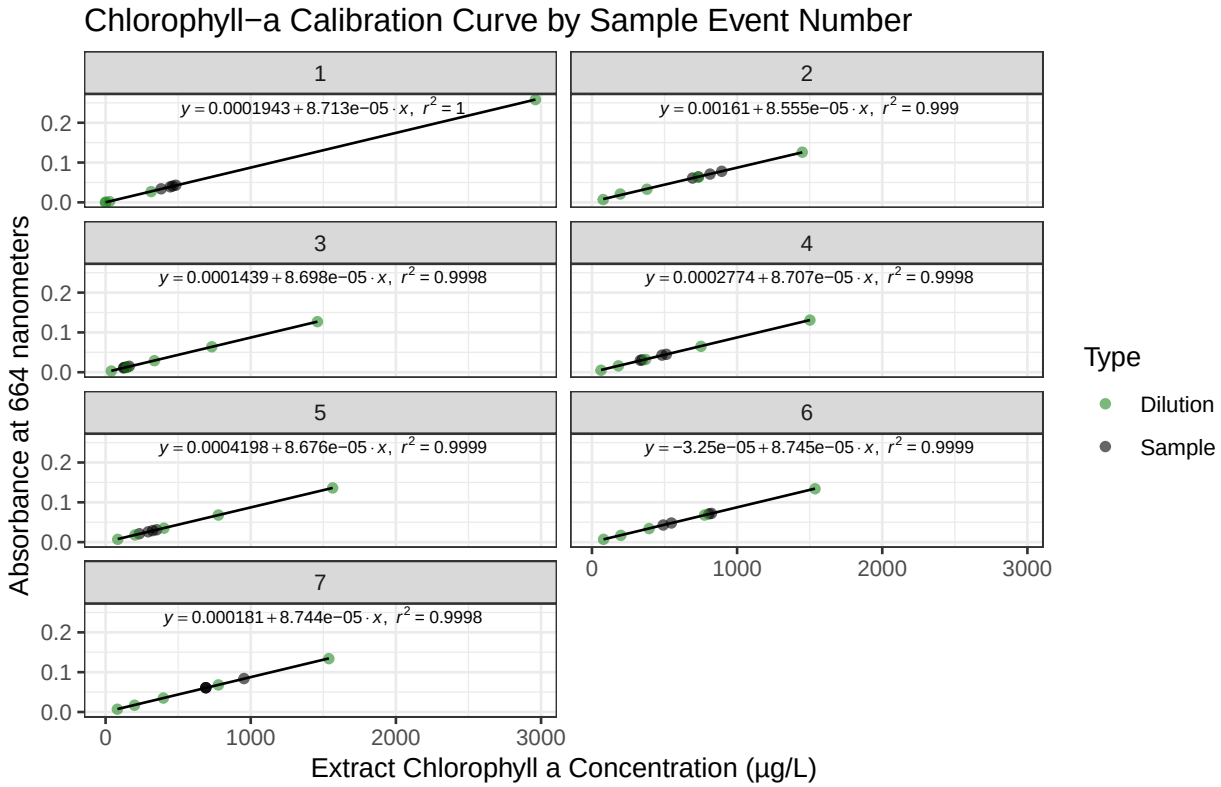
Chlorophyll−a Calibration Curve by Sample Event Number
1
y = 0.0001943 + 8.713e−05 · x, r² = 1
2
y = 0.00161 + 8.555e−05 · x, r² = 0.999
3
y = 0.0001439 + 8.698e−05 · x, r² = 0.9998
4
y = 0.0002774 + 8.707e−05 · x, r² = 0.9998
5
y = 0.0004198 + 8.676e−05 · x, r² = 0.9999
6
y = −3.25e−05 + 8.745e−05 · x, r² = 0.9999
7
y = 0.000181 + 8.744e−05 · x, r² = 0.9998
Absorbance at 664 nanometers
0.0
0.1
0.2
0
1000
2000
3000
Extract Chlorophyll a Concentration (µg/L)
Type
Dilution
Sample

This section will use 'dat2' to generate scatter plots for each individual calibration curve.

```
## For each sample event, create a scatterplot
## with a fitted regression line for the standard
## stock solution serial dilutions, including the
## chlorophyll a extract concentrations (in ug/L)
## and absorbance values measured at 664
## nanometers (the absorption peak for
## chlorophyll a).  Note: error bars showing
## standard deviation are not shown graphically
## since they are very small.

## First create variables to subset the data from
## 'dat2' so that each sample event can be
## analyzed independently.
FirstEventALL <- dat2[1:9, ]
SecondEventALL <- dat2[10:18, ]
ThirdEventALL <- dat2[19:27, ]
FourthEventALL <- dat2[28:36, ]
FifthEventALL <- dat2[37:45, ]
SixthEventALL <- dat2[46:54, ]
SeventhEventALL <- dat2[55:63, ]

## Use the plot() function to create a
## scatterplot for the first sampling event and
## add a fitted regression line to the model.
## Note: the 'pch' argument changes the symbology
## of the plotted points; the 'col' argument
## changes the color of the plotted points or the
## regression line.
plot(FirstEventALL$ChlaExAvg, FirstEventALL$Abs664Avg,
    main = "First Sampling Event Chlorophyll-a Calibration Curve",
    xlab = "Extract Chlorophyll a Concentration (µg/L)",
    ylab = "Absorbance at 664 nanometers", pch = 19) +
    abline(lm(FirstEventALL$Abs664Avg ~ FirstEventALL$ChlaExAvg),
        col = "blue")
```

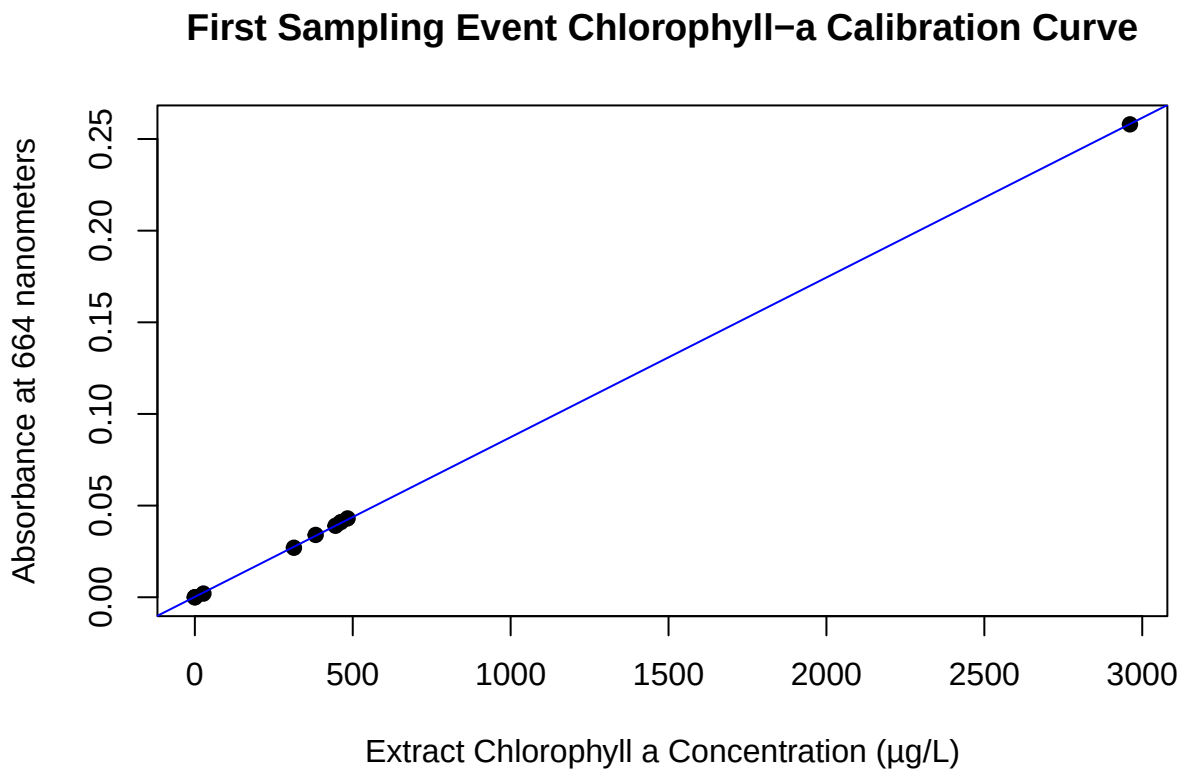


```
## integer(0)
```

```
## Create a scatterplot for the second sampling
## event and add a fitted regression line to the
## model.
plot(SecondEventALL$ChlaExAvg, SecondEventALL$Abs664Avg,
    main = "Second Sampling Event Chlorophyll-a Calibration Curve",
    xlab = "Extract Chlorophyll a Concentration (µg/L)",
    ylab = "Absorbance at 664 nanometers", pch = 19) +
    abline(lm(SecondEventALL$Abs664Avg ~ SecondEventALL$ChlaExAvg),
        col = "blue")
```

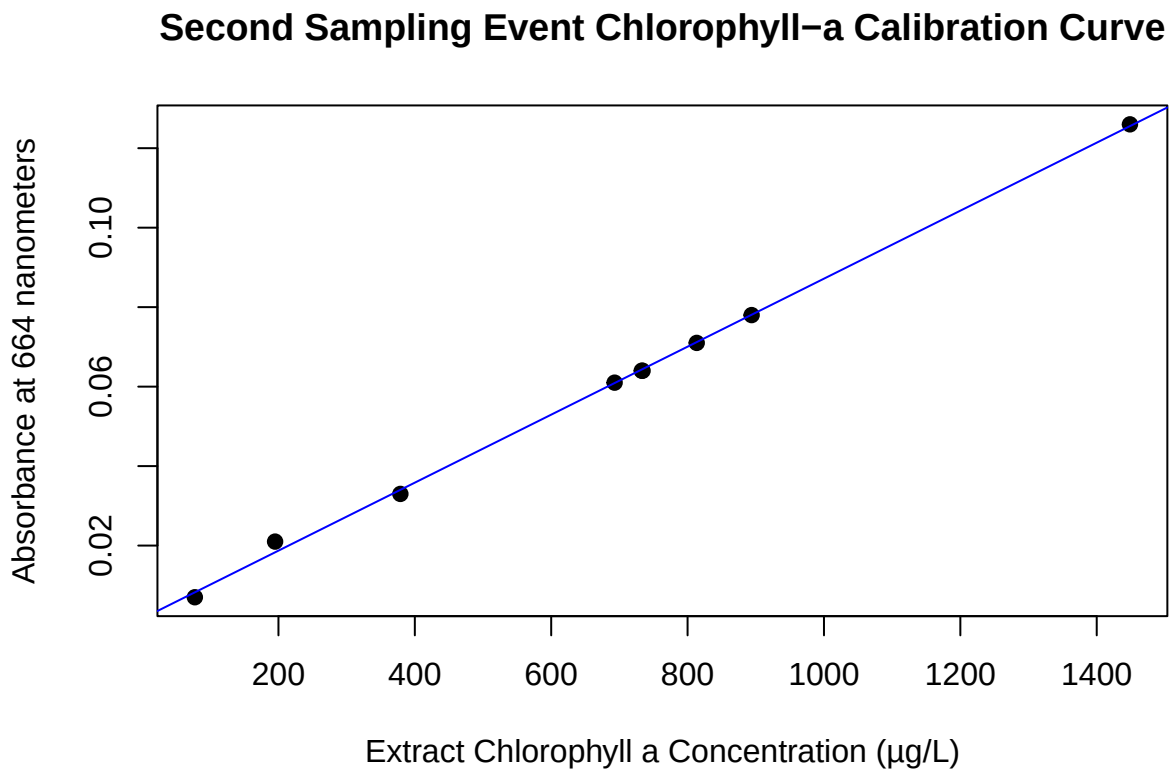


```
## integer(0)
```

```
## Create a scatterplot for the third sampling
## event and add a fitted regression line to the
## model.
plot(ThirdEventALL$ChlaExAvg, ThirdEventALL$Abs664Avg,
    main = "Third Sampling Event Chlorophyll-a Calibration Curve",
    xlab = "Extract Chlorophyll a Concentration (µg/L)",
    ylab = "Absorbance at 664 nanometers", pch = 19) +
    abline(lm(ThirdEventALL$Abs664Avg ~ ThirdEventALL$ChlaExAvg),
        col = "blue")
```

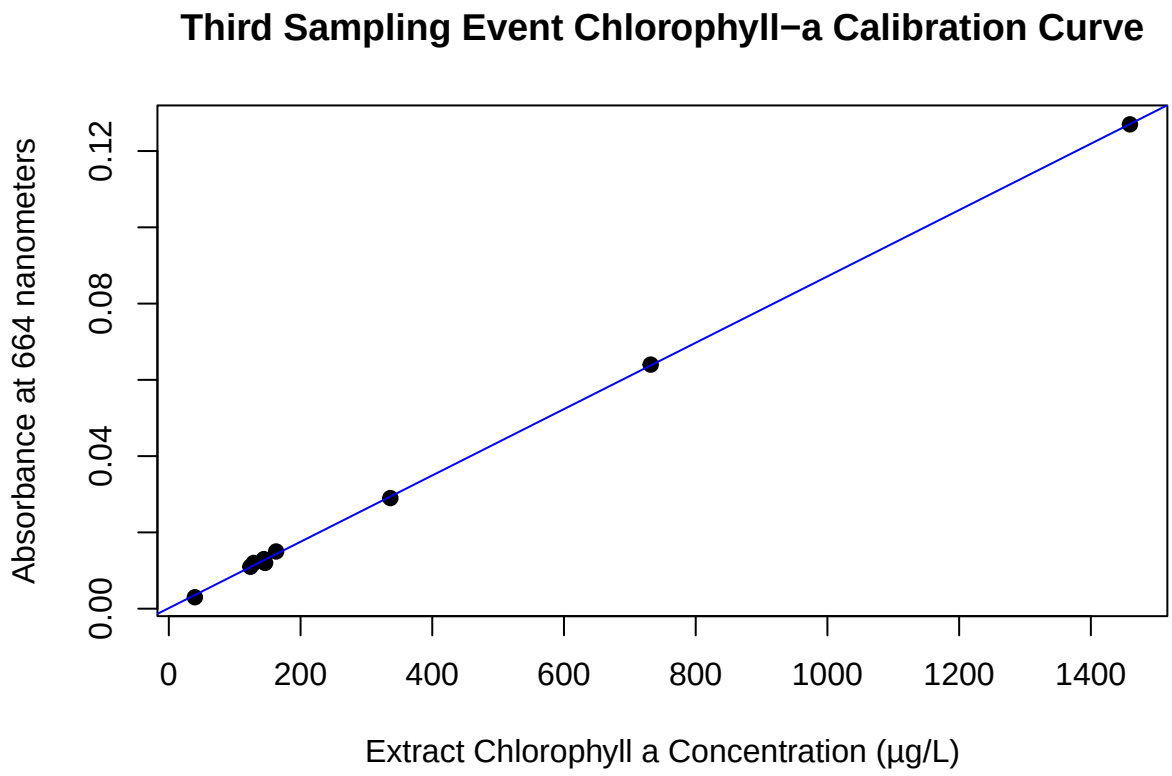


```
## integer(0)
```

```
## Create a scatterplot for the fourth sampling
## event and add a fitted regression line to the
## model.
plot(FourthEventALL$ChlaExAvg, FourthEventALL$Abs664Avg,
    main = "Fourth Sampling Event Chlorophyll-a Calibration Curve",
    xlab = "Extract Chlorophyll a Concentration (µg/L)",
    ylab = "Absorbance at 664 nanometers", pch = 19) +
    abline(lm(FourthEventALL$Abs664Avg ~ FourthEventALL$ChlaExAvg),
        col = "blue")
```

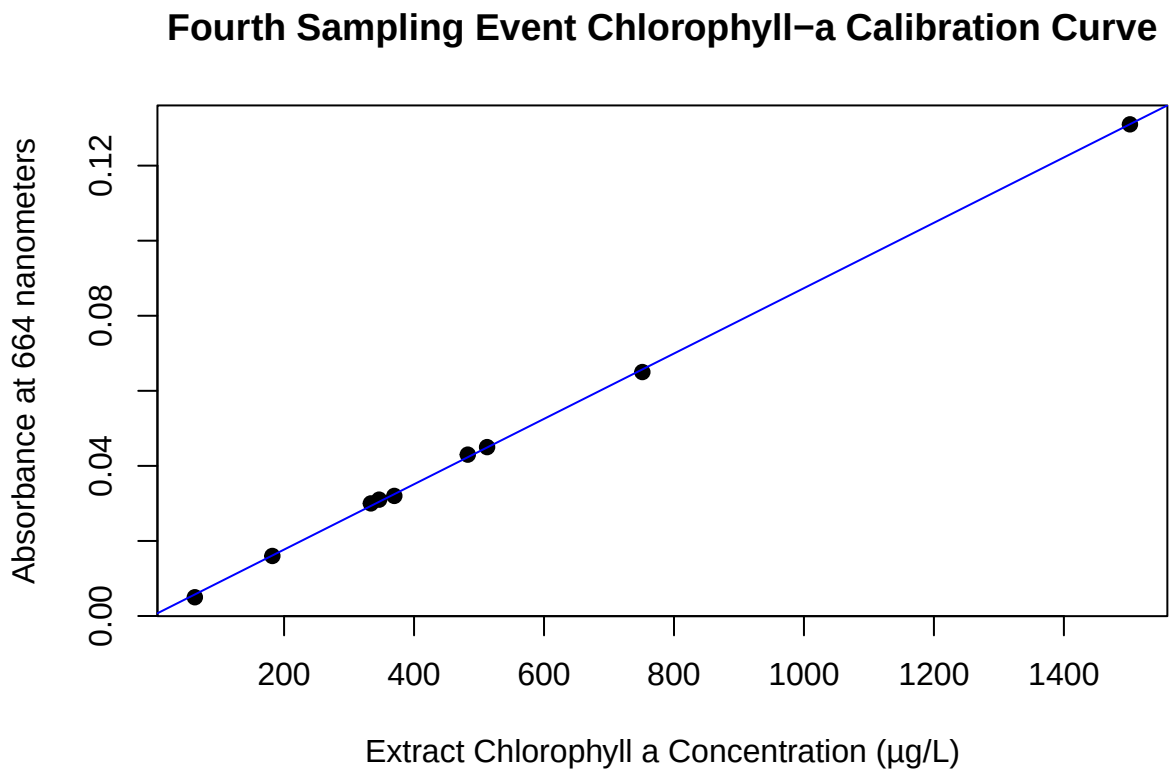


```
## integer(0)
```

```
## Create a scatterplot for the fifth sampling
## event and add a fitted regression line to the
## model.
plot(FifthEventALL$ChlaExAvg, FifthEventALL$Abs664Avg,
    main = "Fifth Sampling Event Chlorophyll-a Calibration Curve",
    xlab = "Extract Chlorophyll a Concentration (µg/L)",
    ylab = "Absorbance at 664 nanometers", pch = 19) +
    abline(lm(FifthEventALL$Abs664Avg ~ FifthEventALL$ChlaExAvg),
        col = "blue")
```

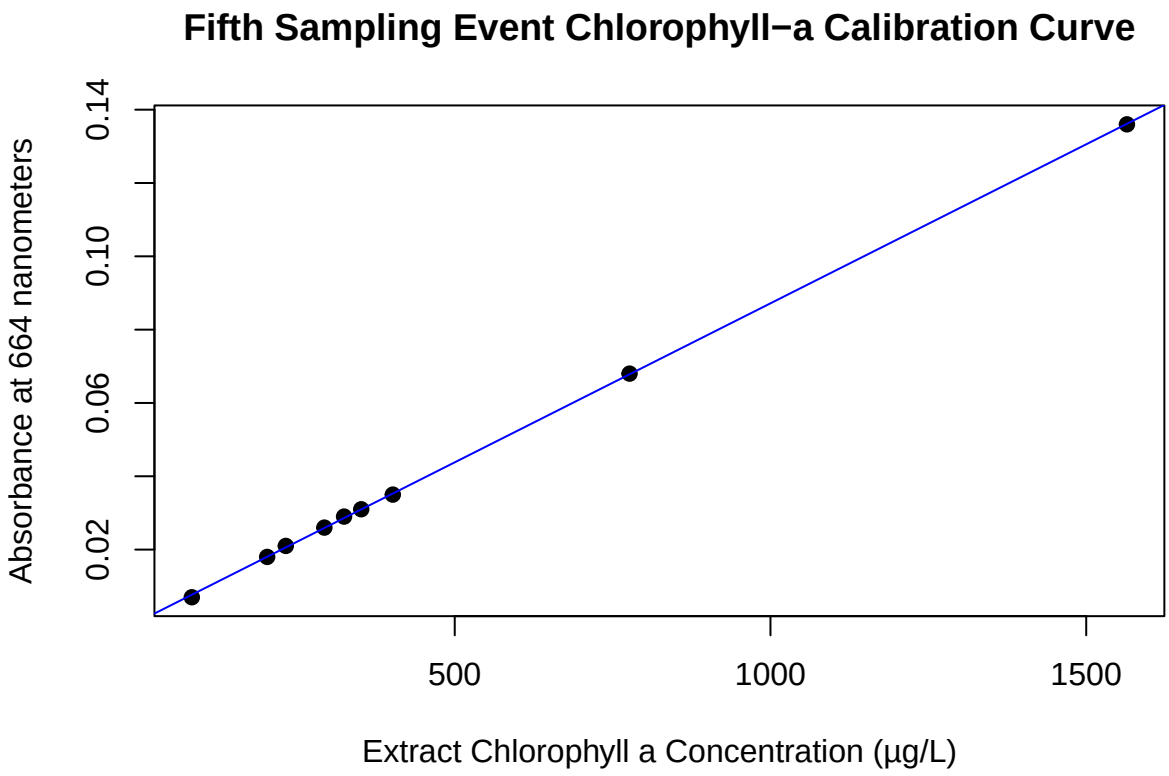


```
## integer(0)
```

```
## Create a scatterplot for the sixth sampling
## event and add a fitted regression line to the
## model.
plot(SixthEventALL$ChlaExAvg, SixthEventALL$Abs664Avg,
    main = "Sixth Sampling Event Chlorophyll-a Calibration Curve",
    xlab = "Extract Chlorophyll a Concentration (µg/L)",
    ylab = "Absorbance at 664 nanometers", pch = 19) +
    abline(lm(SixthEventALL$Abs664Avg ~ SixthEventALL$ChlaExAvg),
        col = "blue")
```

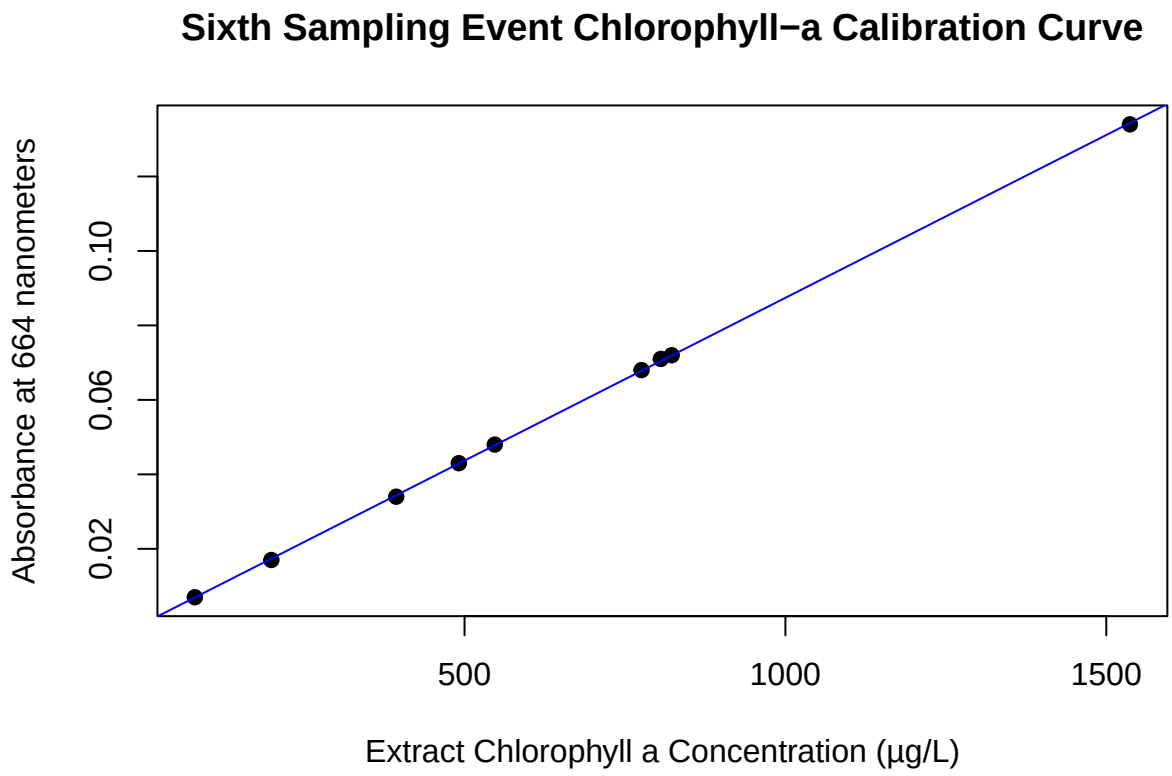


```
## integer(0)
```

```
## Create a scatterplot for the seventh sampling
## event and add a fitted regression line to the
## model.
plot(SeventhEventALL$ChlaExAvg, SeventhEventALL$Abs664Avg,
    main = "Seventh Sampling Event Chlorophyll-a Calibration Curve",
    xlab = "Extract Chlorophyll a Concentration (µg/L)",
    ylab = "Absorbance at 664 nanometers", pch = 19) +
    abline(lm(SeventhEventALL$Abs664Avg ~ SeventhEventALL$ChlaExAvg),
        col = "blue")
```

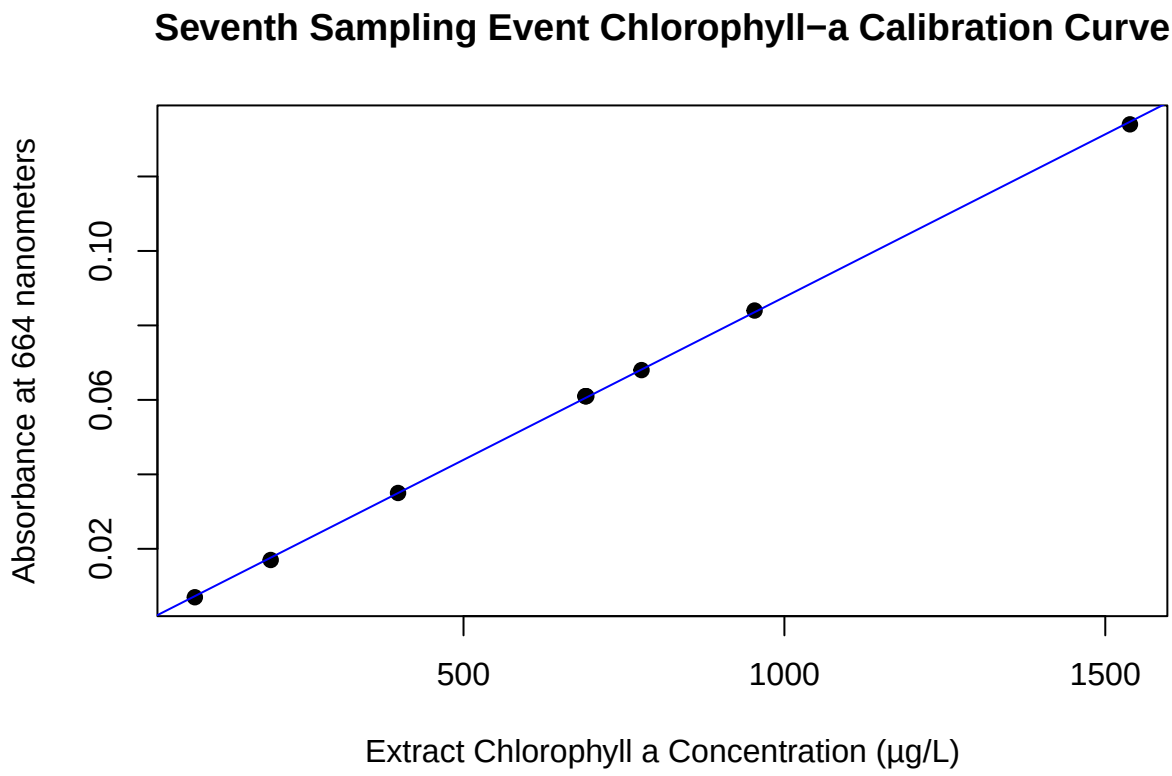
Seventh Sampling Event Chlorophyll−a Calibration Curve
Absorbance at 664 nanometers
0.02
0.06
0.10
500
1000
1500
Extract Chlorophyll a Concentration (µg/L)

```
## integer(0)
```

Inferential Statistics Analysis - RGB Imagery

This section will use 'dat3' to generate simple linear regression models and R^2 values for the RGB imagery, for all sample events. Plots were created for each flight altitude by vegetation index.

```
## Reshape 'dat3' for use with ggplot(). Create
## variable 'dat3_long' and pipe 'dat3' into the
## pivot_longer() function. This function
## 'lengthens' the data, increasing the number of
## rows and decreasing the number of columns. The
## columns are specified to match the vegetation
## index columns (starting at the beginning and
## seeing whether they have the uppercase
## lettering. The names_to argument creates new
## columns specified by the index type (e.g.,
## CIVE, EXG, etc.) and flight elevation (e.g.,
## 60m, 90m, 120m). The names_pattern argument
## stores vegetation index values from the
## dataset into 'veg_index,' as specified by the
## indexes and elevations. The mutate() function
## specifies the different flight altitute
## factors and assigns them labels.
dat3_long <- dat3 %>%
    pivot_longer(cols = matches("^(?:CIVE|EXG|KIVU|NGRDI|VDVI)"),
        names_to = c("index_type", "elevation"), names_pattern = "([A-Z]*)([\\d]+m)",
        values_to = "veg_index") %>%
    mutate(elevation = factor(elevation, levels = c("60m",
        "90m", "120m"), labels = c("60m", "90m", "120m")))

## Create the 'plotsdat3' variable with similar
## code to the calibration curves. This creates a
## list of 5 plots, each containing 3 elevations.
## The pull() function pulls the plot out of the
## df argument.
plotsdat3 <- dat3_long %>%
    group_by(index_type) %>%
    nest() %>%
    mutate(plot = map(data, ~ggplot(.x, aes(x = veg_index,
        y = Chla)) + geom_point() + facet_wrap("~ elevation",
        ncol = 3))) %>%
    pull(plot)

## Repeat code that calculates the regression
## equations and R^2 values
lm_eqn2 <- function(df) {
    m <- lm(Chla ~ veg_index, df)

    eq <- substitute(italic(y) == a + b %.% italic(x) *
        "," ~ ~italic(r)^2 ~ "=" ~ r2, list(a = format(unname(coef(m)[1]),
        digits = 4), b = format(unname(coef(m)[2]),
        digits = 4), r2 = format(summary(m)$r.squared,
        digits = 4)))
```

```
    as.character(as.expression(eq))
}

## Repeat code that labels the regression
## equations and R^2 values
dat3_labeled <- dat3_long %>%
    group_by(index_type, elevation) %>%
    nest() %>%
    mutate(Label = map(data, lm_eqn2)) %>%
    select(index_type, elevation, Label) %>%
    unnest(Label) %>%
    ungroup()

## Create a list of indices ('index_types'
## variable) and a variable that creates a
## function applied to those index types
## ('plots2_list'). An in-line function is
## created taking .x and .y as input and outpout
## arguments. The ggplot() function is used with
## similar arguments as discussed and
## incorporates these variables (including the
## function). This will create plots by index
## type, where each plot has three facets, one
## for each elevation. Use return() function to
## return the output plots out of this variable
## ('gdat3') since the in-line function is not
## global.
index_types <- c("CIVE", "EXG", "KIVU", "NGRDI", "VDVI")
plots2_list <- lapply(index_types, function(x) {
    .x <- dat3_long %>%
        filter(index_type == x)
    .y <- dat3_labeled %>%
        filter(index_type == x)
    gdat3 <- ggplot(.x, aes(x = veg_index, y = Chla)) +
        geom_point() + geom_smooth(method = "lm", formula = "y ~ x",
        color = "black", linewidth = 0.5, alpha = 0.6) +
        geom_text(data = .y, mapping = aes(x = mean(c(max(.x$veg_index,
            na.rm = TRUE), min(.x$veg_index, na.rm = TRUE)),
            na.rm = TRUE), y = max(.x$Chla, na.rm = TRUE) *
            1.1, label = Label), parse = TRUE, size = 2.5,
            nudge_y = -0.05) + facet_wrap("elevation",
        ncol = 3, scales = "free_x") + labs(title = paste(x,
        "Vegetation Index Regression Analysis"), x = "Index Spectral Value",
        y = "Chlorophyll a Concentration (µg/L)") +
        theme(plot.title = element_text(hjust = 0.5)) +
        theme_bw()
    ggsave(paste(x, "Vegetation Index and Elevation Plots.png"))
    return(gdat3)
})
plots2_list
```

```
## [[1]]
```

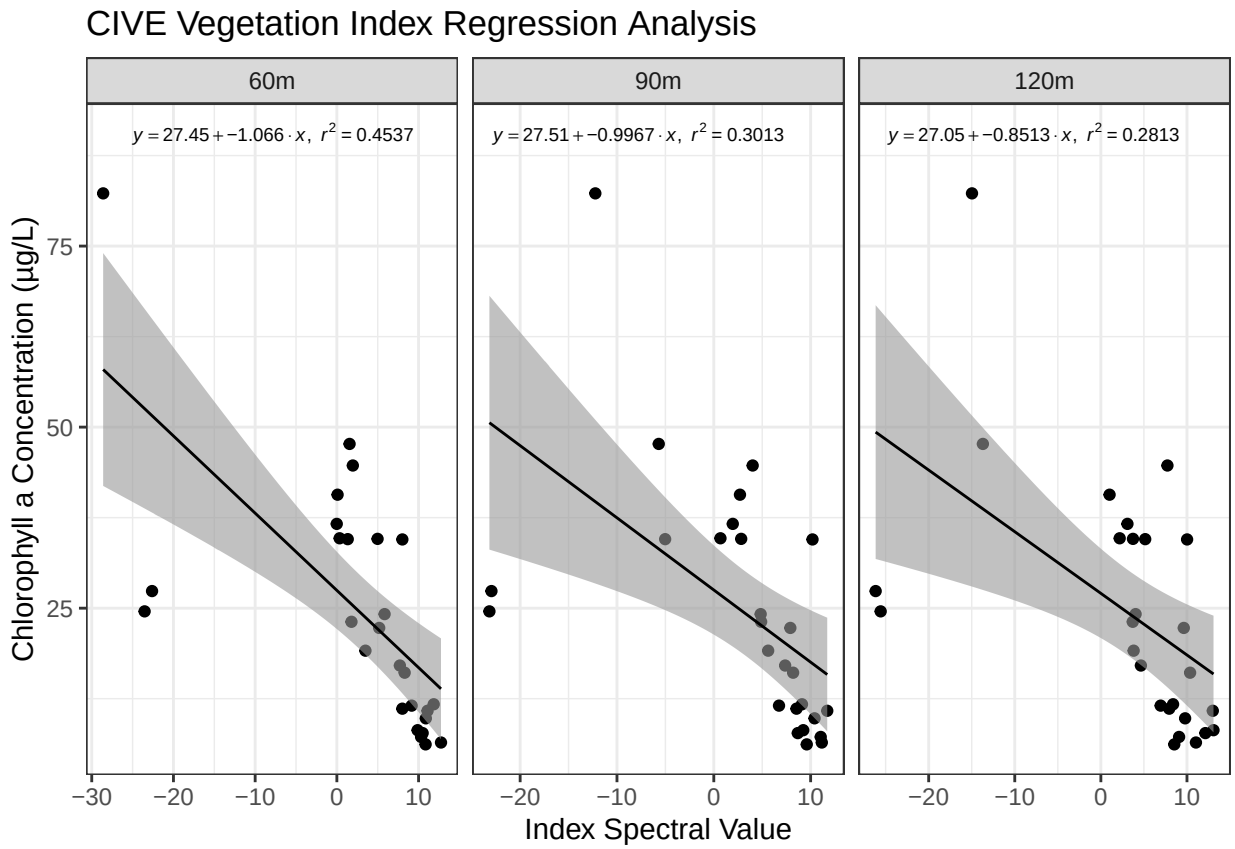
CIVE Vegetation Index Regression Analysis
60m
90m
120m
y = 27.45 + −1.066 · x, r² = 0.4537
y = 27.51 + −0.9967 · x, r² = 0.3013
y = 27.05 + −0.8513 · x, r² = 0.2813
Chlorophyll a Concentration (µg/L)
75
50
25
−30
−20
−10
0
10
Index Spectral Value

```
##
## [[2]]
```

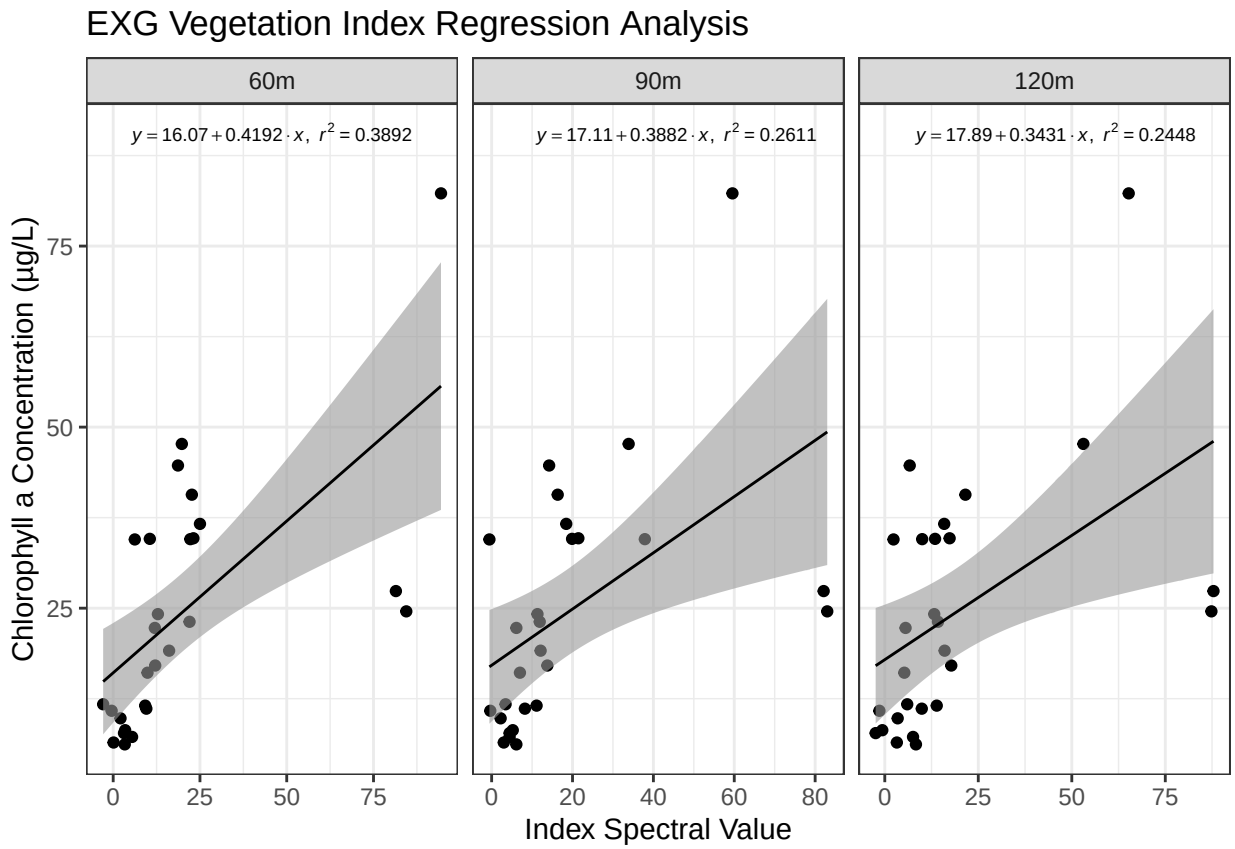
EXG Vegetation Index Regression Analysis
60m
90m
120m
y = 16.07 + 0.4192 · x, r² = 0.3892
y = 17.11 + 0.3882 · x, r² = 0.2611
y = 17.89 + 0.3431 · x, r² = 0.2448
Chlorophyll a Concentration (µg/L)
75
50
25
0
25
50
75
0
20
40
60
80
0
25
50
75
Index Spectral Value

```
##
## [[3]]
```

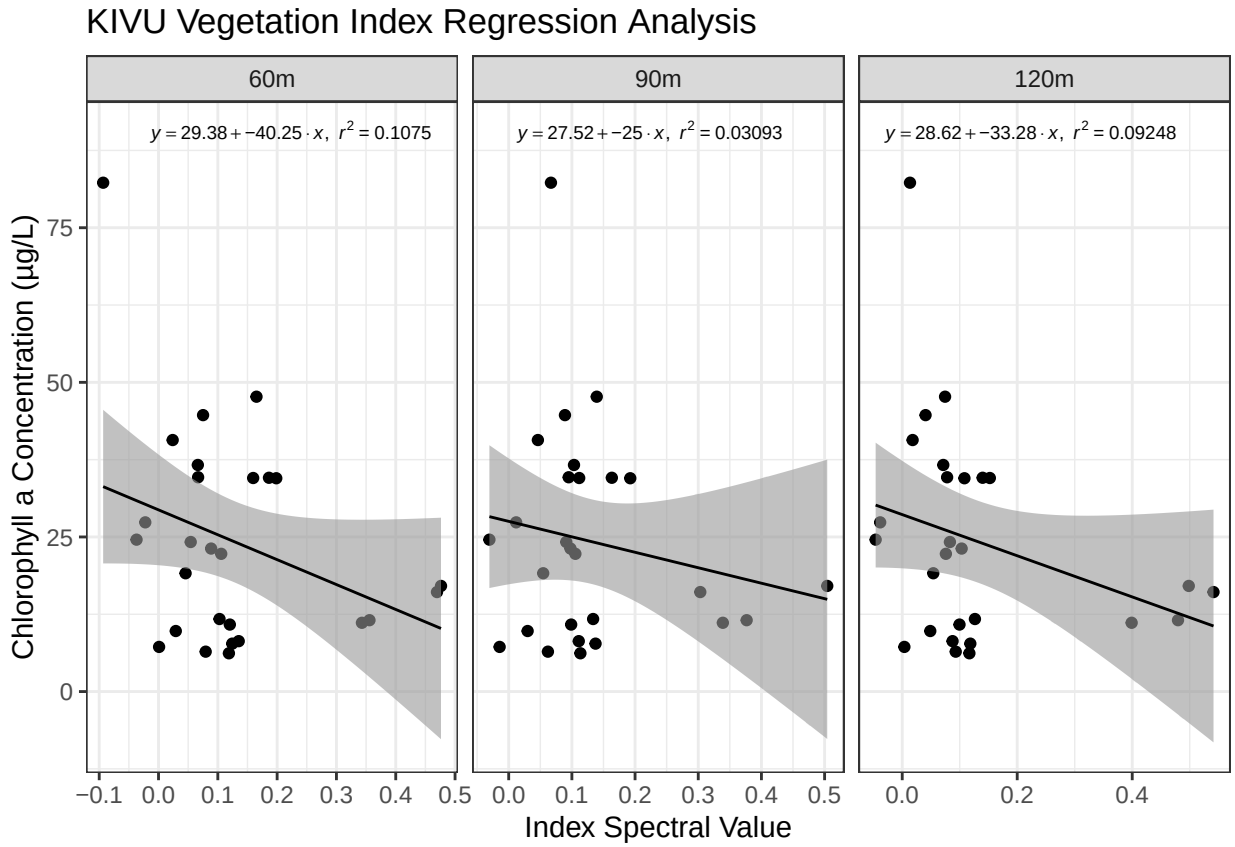
KIVU Vegetation Index Regression Analysis
60m
90m
120m
y = 29.38 + −40.25 · x, r² = 0.1075
y = 27.52 + −25 · x, r² = 0.03093
y = 28.62 + −33.28 · x, r² = 0.09248
Chlorophyll a Concentration (µg/L)
0
25
50
75
−0.1 0.0 0.1 0.2 0.3 0.4 0.5
0.0 0.1 0.2 0.3 0.4 0.5
0.0 0.2 0.4
Index Spectral Value

```
##
## [[4]]
```

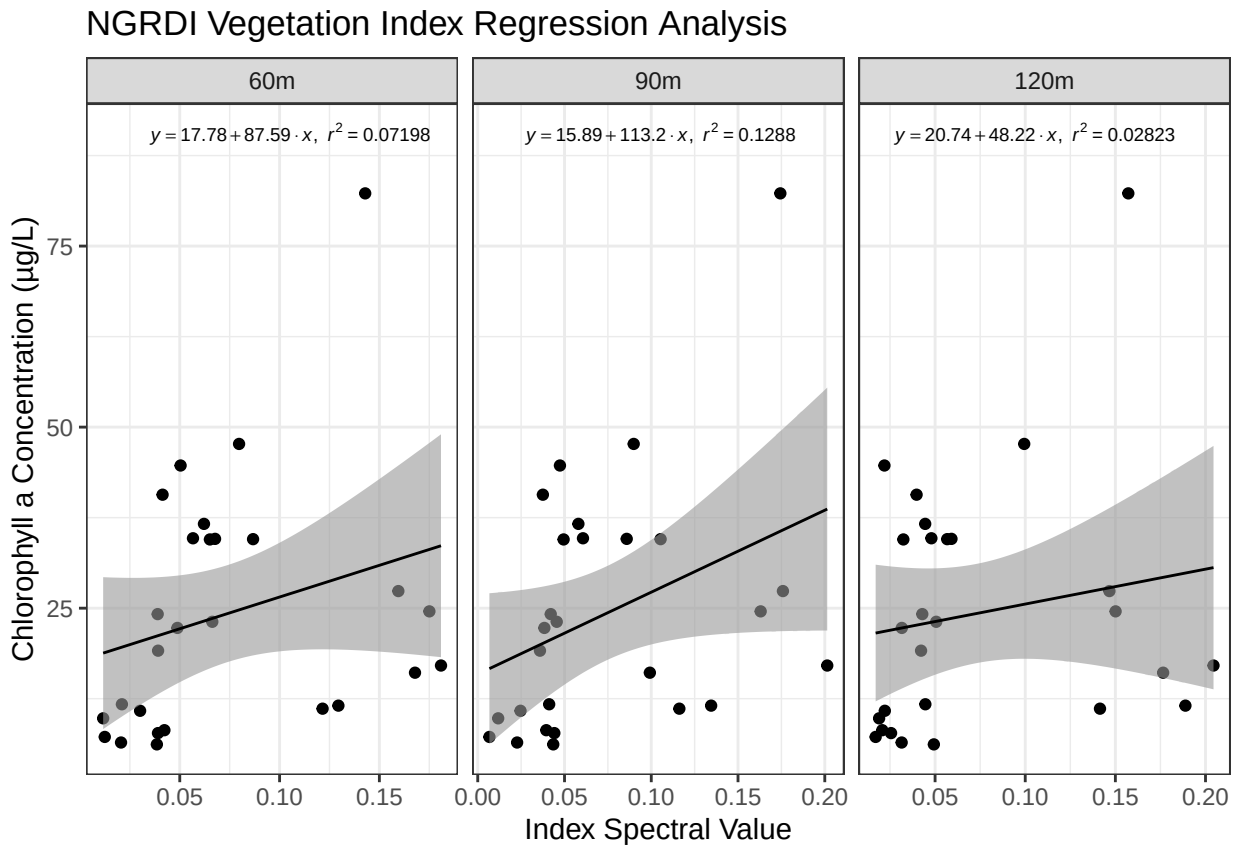
NGRDI Vegetation Index Regression Analysis
60m
90m
120m
$y = 17.78 + 87.59 \cdot x,\ r^2 = 0.07198$
$y = 15.89 + 113.2 \cdot x,\ r^2 = 0.1288$
$y = 20.74 + 48.22 \cdot x,\ r^2 = 0.02823$
Chlorophyll a Concentration (µg/L)
75
50
25
0.05
0.10
0.15
0.00
0.05
0.10
0.15
0.20
0.05
0.10
0.15
0.20
Index Spectral Value

```
##
## [[5]]
```

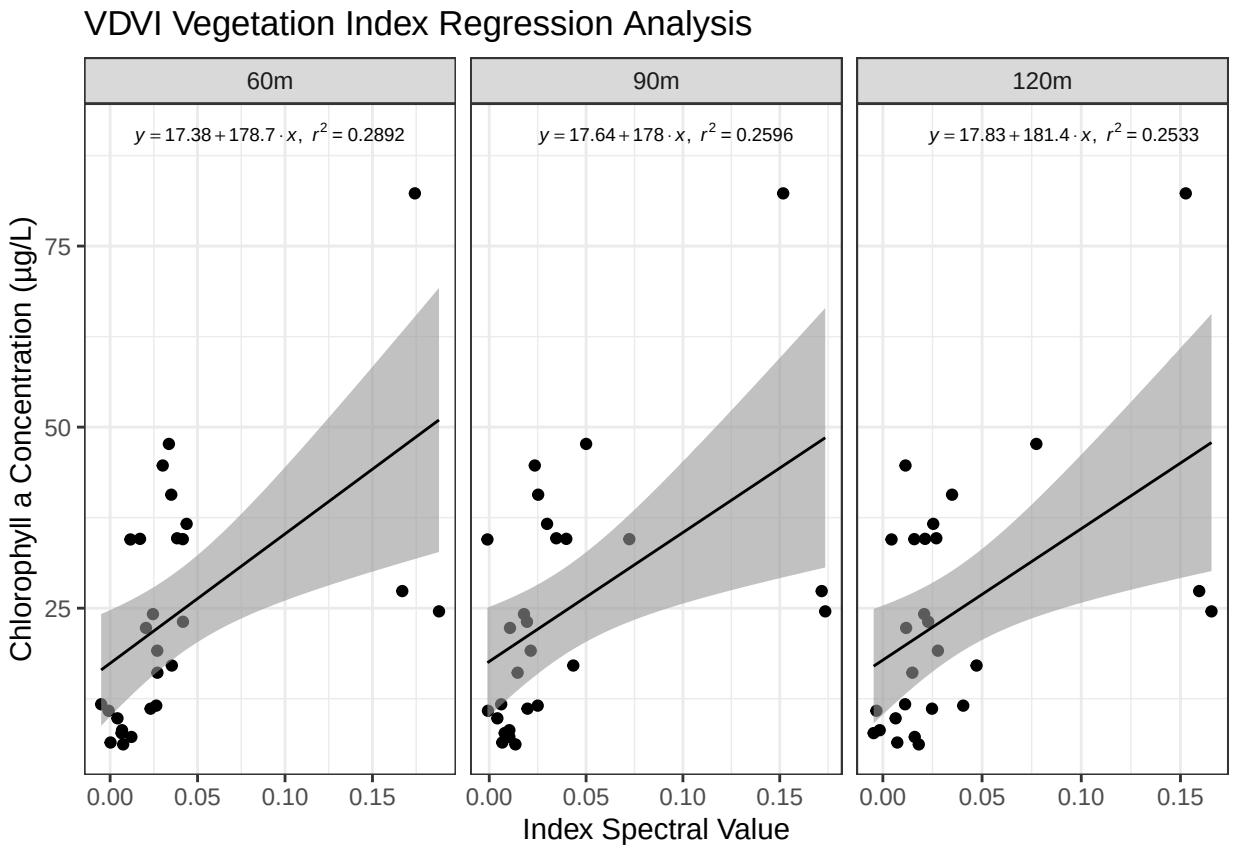
VDVI Vegetation Index Regression Analysis
60m
90m
120m
$y = 17.38 + 178.7 \cdot x,\ r^2 = 0.2892$
$y = 17.64 + 178 \cdot x,\ r^2 = 0.2596$
$y = 17.83 + 181.4 \cdot x,\ r^2 = 0.2533$
Chlorophyll a Concentration (µg/L)
75
50
25
0.00
0.05
0.10
0.15
Index Spectral Value

This section will use 'dat3' to generate plots for each individual regression model for the RGB imagery.

```
## Create linear regression models comparing
## chlorophyll-a concentrations as a function of
## the RGB spectral index values, at each flight
## altitude, for all sampling events.

##### CIVE ##### Fit a simple linear regression
##### model with dependent variable 'Chla' and
##### independent variable 'CIVE60m' Call
##### variable after defining
fitCIVE60m <- regress("mean", Chla ~ CIVE60m, robustSE = FALSE,
    data = dat3)
fitCIVE60m
```

```
##
## Call:
## regress(fnctl = "mean", formula = Chla ~ CIVE60m, data = dat3,
##     robustSE = FALSE)
##
## Residuals:
##     Min      1Q  Median      3Q     Max
## -27.987  -7.599  -2.515   8.831  24.323
##
## Coefficients:
##                   Estimate  Std Err   95%L         95%H         F stat    df
## [1] Intercept      27.45     2.591     22.12        32.79         112.24 1
## [2] CIVE60m       -1.066     0.2341   -1.549       -0.5844         20.76 1
##                   Pr(>F)
## [1] Intercept    < 0.00005
## [2] CIVE60m         1e-04
##
## Residual standard error: 12.96 on 25 degrees of freedom
## Multiple R-squared:  0.4537, Adjusted R-squared:  0.4318
## F-statistic: 20.76 on 1 and 25 DF,  p-value: 0.0001177
```

```
## Create a scatterplot for 'fitCIVE60m'
plot(dat3$CIVE60m, dat3$Chla, xlab = "CIVE 60m Spectral Index Value",
    ylab = "Chlorophyll-a (µg/L)", pch = 20)
## Add a fitted regression line to the model and
## customized text to the plot
abline(lm(Chla ~ CIVE60m, data = dat3))
```

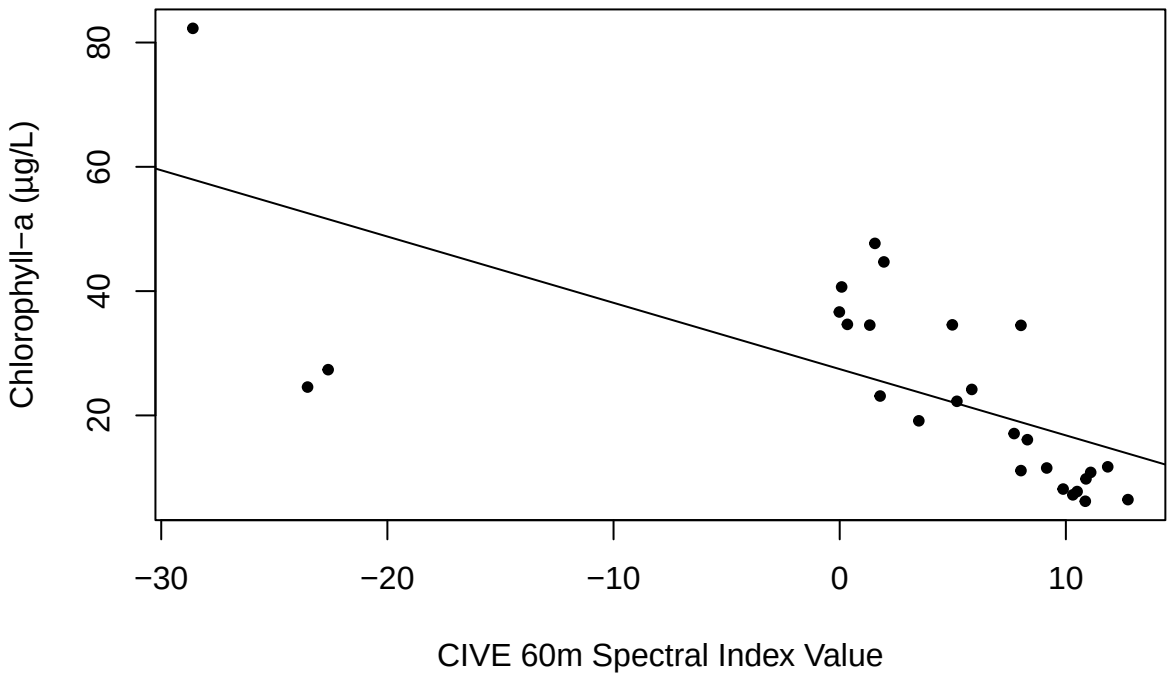


```
## Fit a simple linear regression model with
## dependent variable 'Chla' and independent
## variable 'CIVE90m' Call variable after
## defining
fitCIVE90m <- regress("mean", Chla ~ CIVE90m, robustSE = FALSE,
    data = dat3)
fitCIVE90m
```

```
##
## Call:
## regress(fnctl = "mean", formula = Chla ~ CIVE90m, data = dat3,
##     robustSE = FALSE)
##
## Residuals:
##     Min      1Q  Median      3Q     Max
## -26.050  -9.272  -3.087   8.850  42.573
##
## Coefficients:
##                  Estimate  Std Err   95%L         95%H         F stat    df
## [1] Intercept      27.51     2.990     21.35        33.67          84.63 1
## [2] CIVE90m       -0.9967    0.3036   -1.622       -0.3715         10.78 1
##                  Pr(>F)
## [1] Intercept    < 0.00005
## [2] CIVE90m         0.003
##
## Residual standard error: 14.66 on 25 degrees of freedom
```

```
## Multiple R-squared:  0.3013, Adjusted R-squared:  0.2733
## F-statistic: 10.78 on 1 and 25 DF,  p-value: 0.003028
```

```
## Create a scatterplot for 'fitCIVE90m'
plot(dat3$CIVE90m, dat3$Chla, xlab = "CIVE 90m Spectral Index Value",
    ylab = "Chlorophyll-a (µg/L)", pch = 20)
## Add a fitted regression line to the model
abline(lm(Chla ~ CIVE90m, data = dat3))
```

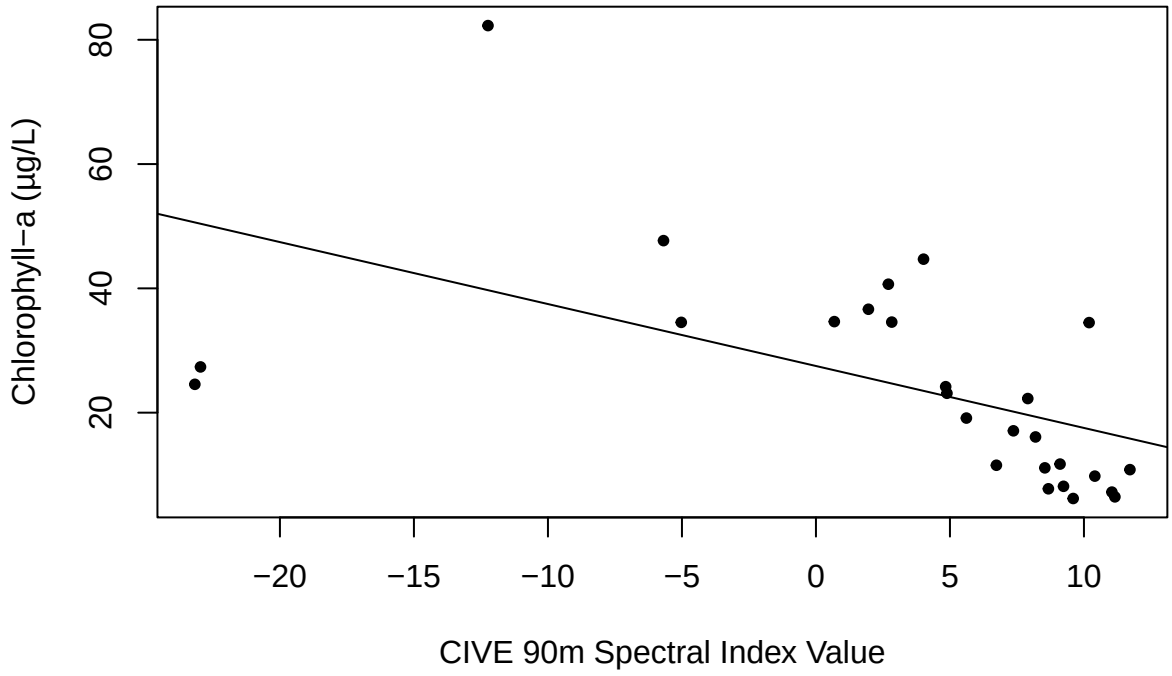


```
## Fit a simple linear regression model with
## dependent variable 'Chla' and independent
## variable 'CIVE120m' Call variable after
## defining
fitCIVE120m <- regress("mean", Chla ~ CIVE120m, robustSE = FALSE,
    data = dat3)
fitCIVE120m
```

```
##
## Call:
## regress(fnctl = "mean", formula = Chla ~ CIVE120m, data = dat3,
##     robustSE = FALSE)
##
## Residuals:
##     Min      1Q  Median      3Q     Max
## -24.260  -9.064  -4.672  10.083  42.492
```

```
##
## Coefficients:
##                  Estimate  Std Err   95%L         95%H         F stat    df
## [1] Intercept      27.05     2.997     20.87        33.22          81.43 1
## [2] CIVE120m      -0.8513    0.2721   -1.412       -0.2908          9.79 1
##                  Pr(>F)
## [1] Intercept    < 0.00005
## [2] CIVE120m       0.0044
##
## Residual standard error: 14.86 on 25 degrees of freedom
## Multiple R-squared:  0.2813, Adjusted R-squared:  0.2526
## F-statistic: 9.786 on 1 and 25 DF,  p-value: 0.004428
```

```
## Create a scatterplot for 'fitCIVE120m'
plot(dat3$CIVE120m, dat3$Chla, xlab = "CIVE 120m Spectral Index Value",
    ylab = "Chlorophyll-a (µg/L)", pch = 20)
## Add a fitted regression line to the model
abline(lm(Chla ~ CIVE120m, data = dat3))
```

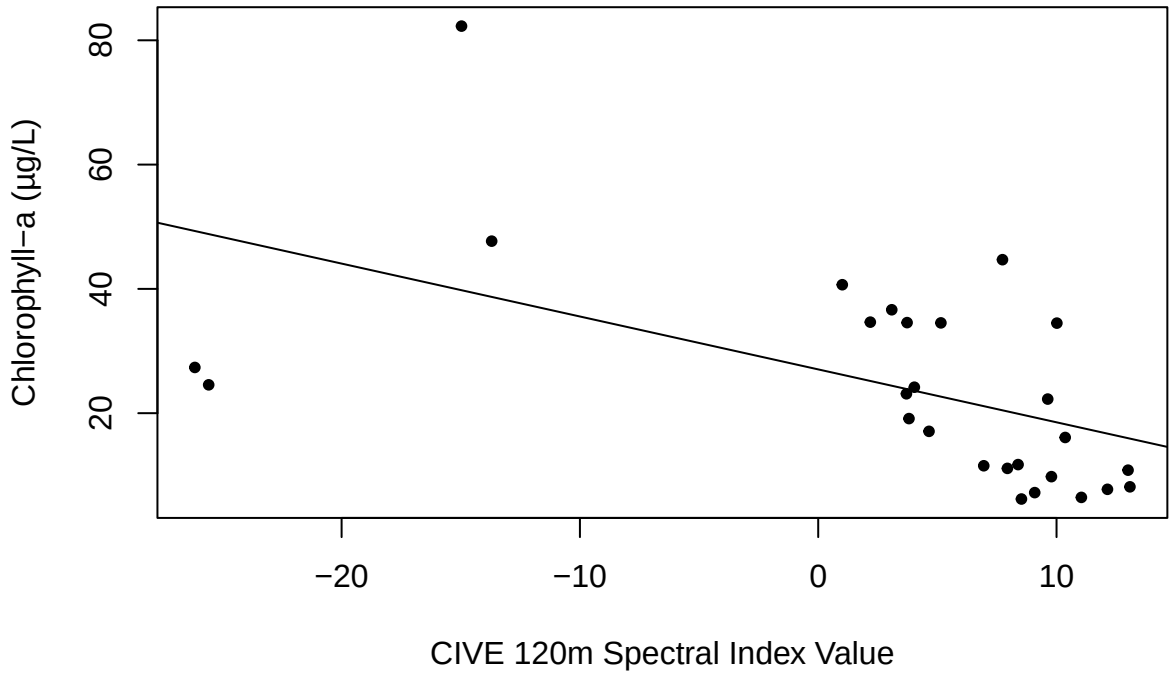


```
##### EXG ##### Fit a simple linear regression
##### model with dependent variable 'Chla' and
##### independent variable 'EXG60m' Call variable
##### after defining
fitEXG60m <- regress("mean", Chla ~ EXG60m, robustSE = FALSE,
    data = dat3)
fitEXG60m
```

```
##
## Call:
## regress(fnctl = "mean", formula = Chla ~ EXG60m, data = dat3,
##     robustSE = FALSE)
##
## Residuals:
##     Min      1Q  Median      3Q     Max
## -26.917  -9.165  -3.699   9.612  26.611
##
## Coefficients:
##                   Estimate  Std Err   95%L         95%H         F stat    df
## [1] Intercept       16.07     3.339     9.197        22.95          23.17 1
## [2] EXG60m          0.4192    0.1050    0.2029       0.6356         15.93 1
##                   Pr(>F)
## [1] Intercept       1e-04
## [2] EXG60m          5e-04
##
## Residual standard error: 13.7 on 25 degrees of freedom
## Multiple R-squared:  0.3892, Adjusted R-squared:  0.3648
## F-statistic: 15.93 on 1 and 25 DF,  p-value: 0.0005067
```

```
## Create a scatterplot for 'fitEXG60m'
plot(dat3$EXG60m, dat3$Chla, xlab = "EXG 60m Spectral Index Value",
    ylab = "Chlorophyll-a (µg/L)", pch = 20)
## Add a fitted regression line to the model
abline(lm(Chla ~ EXG60m, data = dat3))
```

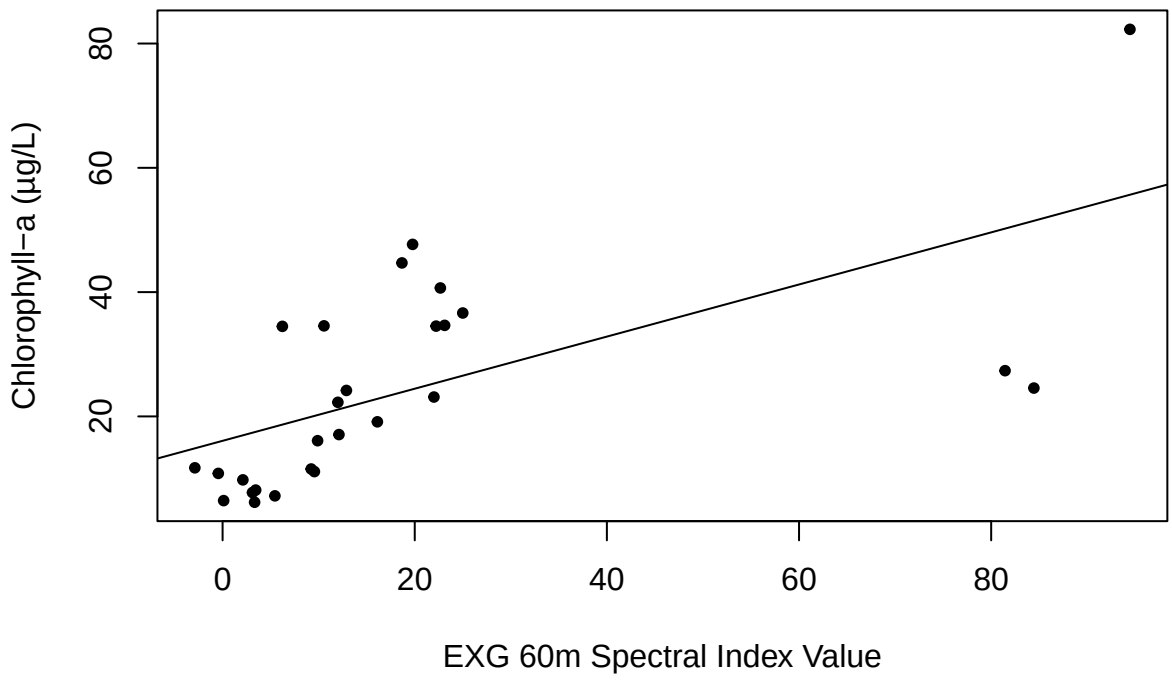

```r
## Fit a simple linear regression model with
## dependent variable 'Chla' and independent
## variable 'EXG90m' Call variable after defining
fitEXG90m <- regress("mean", Chla ~ EXG90m, robustSE = FALSE,
    data = dat3)
fitEXG90m
```

```
##
## Call:
## regress(fnctl = "mean", formula = Chla ~ EXG90m, data = dat3,
##     robustSE = FALSE)
##
## Residuals:
##     Min      1Q  Median      3Q     Max
## -24.774 -10.440  -3.742   9.473  42.047
##
## Coefficients:
##                   Estimate  Std Err   95%L         95%H         F stat    df
## [1] Intercept       17.11     3.766     9.360        24.87          20.66 1
## [2] EXG90m          0.3882    0.1306    0.1192       0.6572          8.83 1
##                   Pr(>F)
## [1] Intercept       0.0001
## [2] EXG90m          0.0065
##
## Residual standard error: 15.07 on 25 degrees of freedom
## Multiple R-squared:  0.2611, Adjusted R-squared:  0.2315
## F-statistic: 8.832 on 1 and 25 DF,  p-value: 0.006459
```

```r
## Create a scatterplot for 'fitEXG90m'
plot(dat3$EXG90m, dat3$Chla, xlab = "EXG 90m Spectral Index Value",
    ylab = "Chlorophyll-a (µg/L)", pch = 20)
## Add a fitted regression line to the model
abline(lm(Chla ~ EXG90m, data = dat3))
```

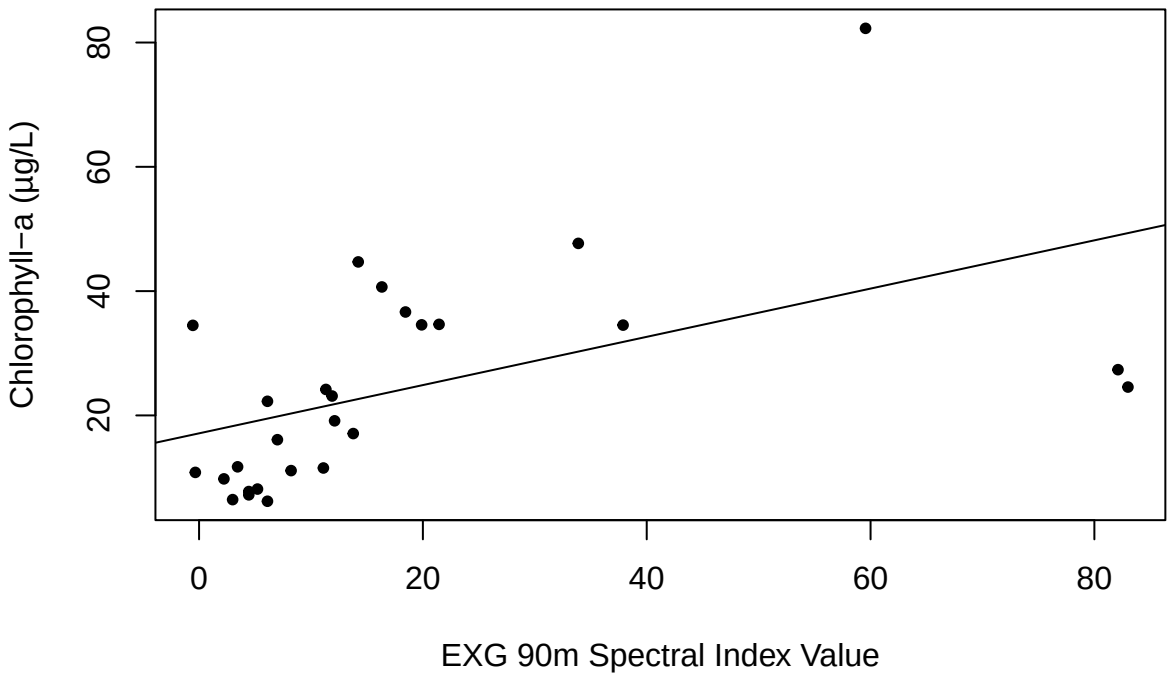


```
## Fit a simple linear regression model with
## dependent variable 'Chla' and independent
## variable 'EXG120m' Call variable after
## defining
fitEXG120m <- regress("mean", Chla ~ EXG120m, robustSE = FALSE,
    data = dat3)
fitEXG120m
```

```
##
## Call:
## regress(fnctl = "mean", formula = Chla ~ EXG120m, data = dat3,
##     robustSE = FALSE)
##
## Residuals:
##     Min      1Q  Median      3Q     Max
## -23.294  -9.837  -4.250  11.817  42.012
##
## Coefficients:
##                  Estimate  Std Err   95%L         95%H         F stat    df
## [1] Intercept      17.89     3.687     10.30        25.48          23.55 1
## [2] EXG120m        0.3431    0.1205   0.09489       0.5913          8.10 1
##                  Pr(>F)
## [1] Intercept      0.0001
## [2] EXG120m        0.0087
##
## Residual standard error: 15.24 on 25 degrees of freedom
```

```
## Multiple R-squared:  0.2448, Adjusted R-squared:  0.2146
## F-statistic: 8.105 on 1 and 25 DF,  p-value: 0.008696
```

```
## Create a scatterplot for 'fitEXG120m'
plot(dat3$EXG120m, dat3$Chla, xlab = "EXG 120m Spectral Index Value",
    ylab = "Chlorophyll-a (µg/L)", pch = 20)
## Add a fitted regression line to the model
abline(lm(Chla ~ EXG120m, data = dat3))
```

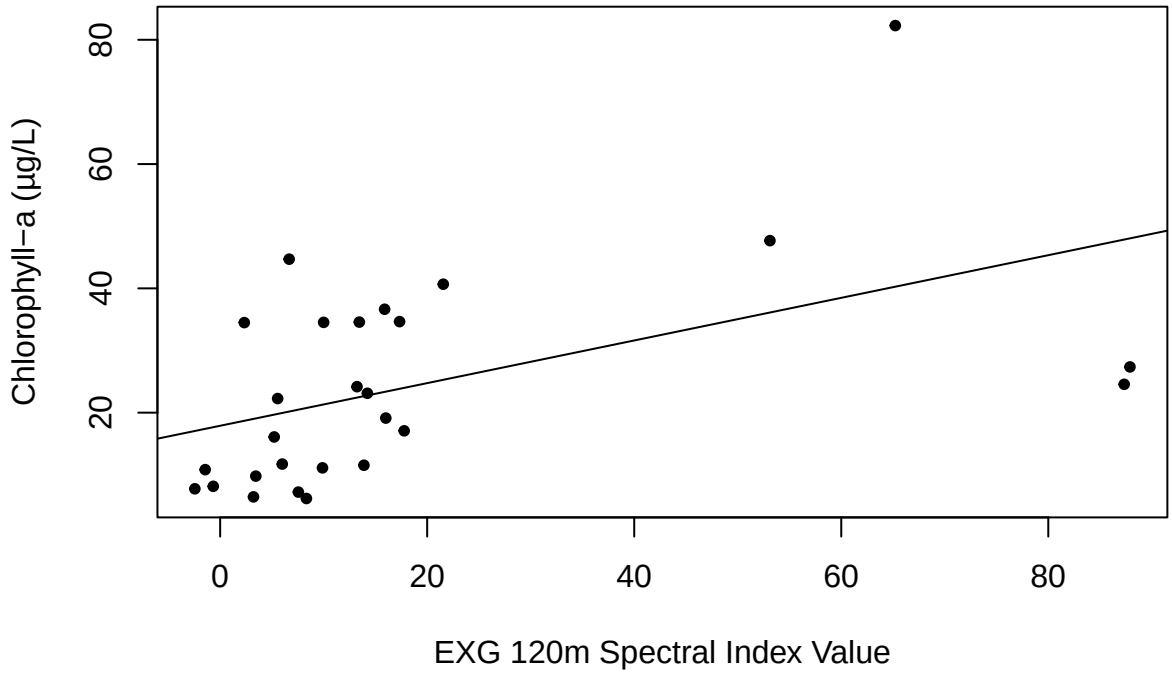


```
##### KIVU ##### Fit a simple linear regression
##### model with dependent variable 'Chla' and
##### independent variable 'KIVU60m' Call
##### variable after defining
fitKIVU60m <- regress("mean", Chla ~ KIVU60m, robustSE = FALSE,
    data = dat3)
fitKIVU60m
```

```
##
## Call:
## regress(fnctl = "mean", formula = Chla ~ KIVU60m, data = dat3,
##     robustSE = FALSE)
##
## Residuals:
##     Min      1Q  Median      3Q     Max
## -22.118 -13.607  -2.916  10.754  49.146
```

```
##
## Coefficients:
##                  Estimate  Std Err   95%L         95%H         F stat    df
## [1] Intercept      29.38     4.346     20.43        38.33          45.69 1
## [2] KIVU60m       -40.25     23.19    -88.02        7.511           3.01 1
##                  Pr(>F)
## [1] Intercept    < 0.00005
## [2] KIVU60m        0.0949
##
## Residual standard error: 16.56 on 25 degrees of freedom
## Multiple R-squared:  0.1075, Adjusted R-squared:  0.07184
## F-statistic: 3.013 on 1 and 25 DF,  p-value: 0.09493
```

```
## Create a scatterplot for 'fitKIVU60m'
plot(dat3$KIVU60m, dat3$Chla, xlab = "KIVU 60m Spectral Index Value",
    ylab = "Chlorophyll-a (µg/L)", pch = 20)
## Add a fitted regression line to the model
abline(lm(Chla ~ KIVU60m, data = dat3))
```

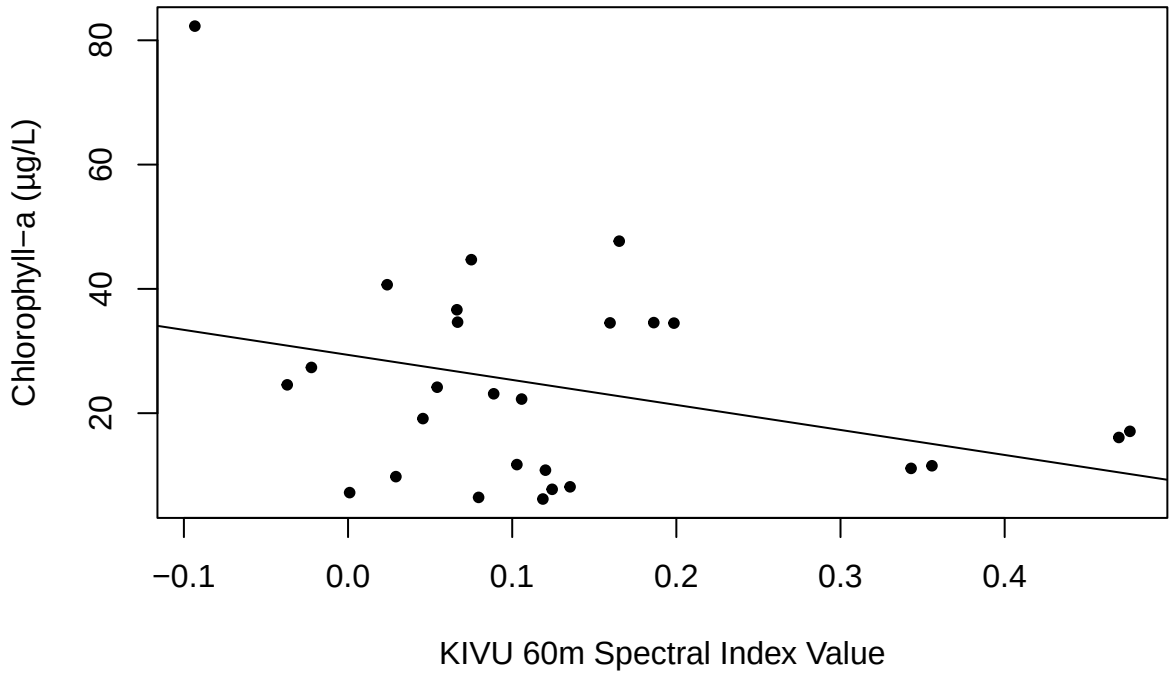


```
## Fit a simple linear regression model with
## dependent variable 'Chla' and independent
## variable 'KIVU90m' Call variable after
## defining
fitKIVU90m <- regress("mean", Chla ~ KIVU90m, robustSE = FALSE,
    data = dat3)
fitKIVU90m
```

```
##
## Call:
## regress(fnctl = "mean", formula = Chla ~ KIVU90m, data = dat3,
##     robustSE = FALSE)
##
## Residuals:
##     Min      1Q  Median      3Q     Max
## -20.662 -13.335  -2.613  10.464  56.430
##
## Coefficients:
##                   Estimate  Std Err   95%L         95%H         F stat    df
## [1] Intercept      27.52     4.944     17.34        37.70          30.99 1
## [2] KIVU90m       -25.00     27.99    -82.65        32.64           0.80 1
##                   Pr(>F)
## [1] Intercept    < 0.00005
## [2] KIVU90m        0.3802
##
## Residual standard error: 17.26 on 25 degrees of freedom
## Multiple R-squared:  0.03093,    Adjusted R-squared:  -0.007831
## F-statistic: 0.798 on 1 and 25 DF,  p-value: 0.3802
```

```
## Create a scatterplot for 'fitKIVU90m'
plot(dat3$KIVU90m, dat3$Chla, xlab = "KIVU 90m Spectral Index Value",
    ylab = "Chlorophyll-a (µg/L)", pch = 20)
## Add a fitted regression line to the model
abline(lm(Chla ~ KIVU90m, data = dat3))
```

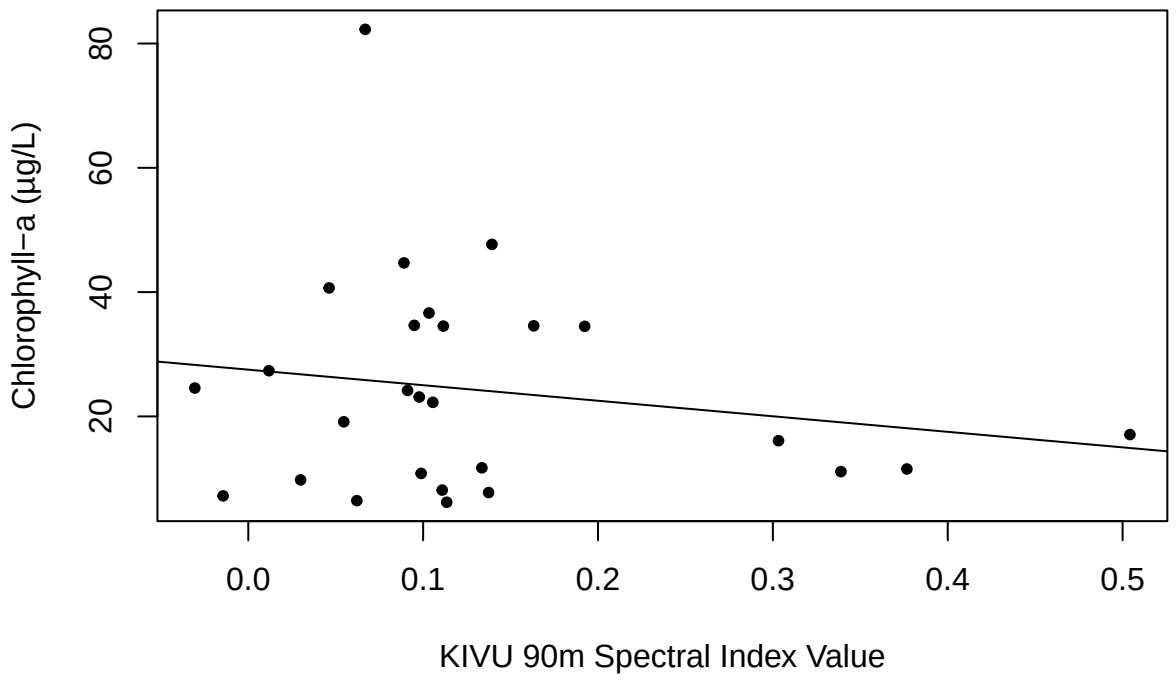

```
## Fit a simple linear regression model with
## dependent variable 'Chla' and independent
## variable 'KIVU120m' Call variable after
## defining
fitKIVU120m <- regress("mean", Chla ~ KIVU120m, robustSE = FALSE,
    data = dat3)
fitKIVU120m
```

```
##
## Call:
## regress(fnctl = "mean", formula = Chla ~ KIVU120m, data = dat3,
##     robustSE = FALSE)
##
## Residuals:
##     Min      1Q  Median      3Q     Max
## -21.271 -13.574  -2.055   9.937  54.114
##
## Coefficients:
##                   Estimate  Std Err   95%L         95%H         F stat    df
## [1] Intercept      28.62     4.220     19.92        37.31          45.97 1
## [2] KIVU120m      -33.28     20.85    -76.22        9.663           2.55 1
##                   Pr(>F)
## [1] Intercept    < 0.00005
## [2] KIVU120m       0.123
##
## Residual standard error: 16.7 on 25 degrees of freedom
## Multiple R-squared:  0.09248,    Adjusted R-squared:  0.05618
## F-statistic: 2.548 on 1 and 25 DF,  p-value: 0.123
```

```
## Create a scatterplot for 'fitKIVU120m'
plot(dat3$KIVU120m, dat3$Chla, xlab = "KIVU 120m Spectral Index Value",
    ylab = "Chlorophyll-a (µg/L)", pch = 20)
## Add a fitted regression line to the model
abline(lm(Chla ~ KIVU120m, data = dat3))
```

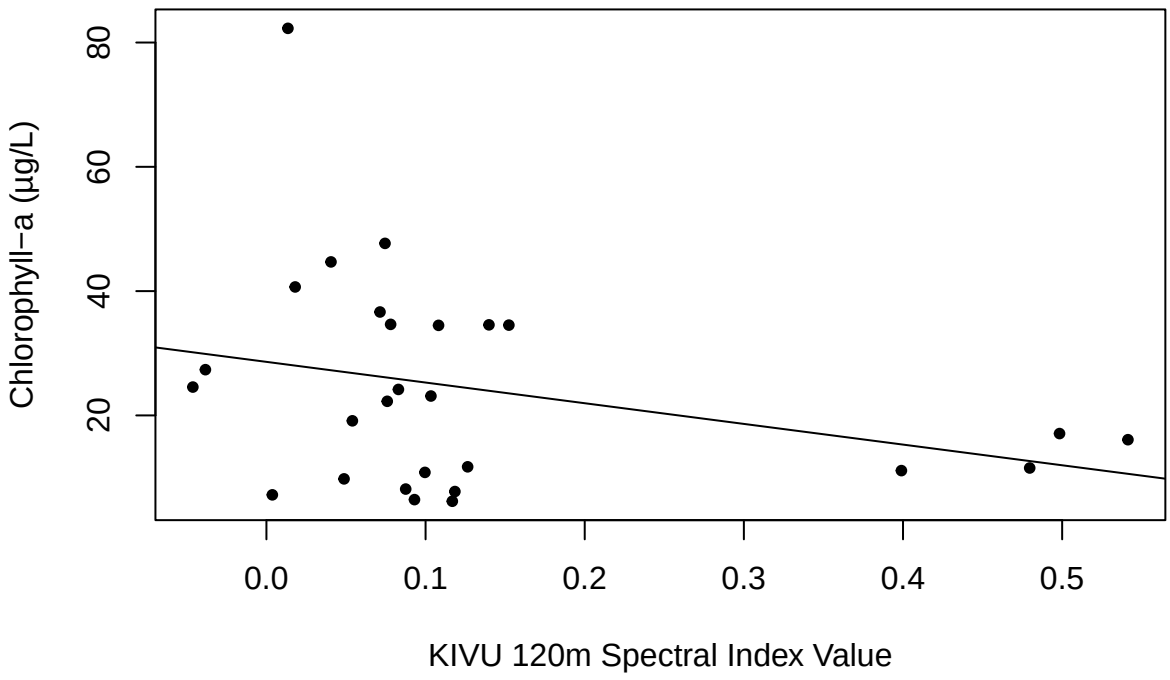


```
##### NGRDI ##### Fit a simple linear regression
##### model with dependent variable 'Chla' and
##### independent variable 'NGRDI60m' Call
##### variable after defining
fitNGRDI60m <- regress("mean", Chla ~ NGRDI60m, robustSE = FALSE,
    data = dat3)
fitNGRDI60m
```

```
##
## Call:
## regress(fnctl = "mean", formula = Chla ~ NGRDI60m, data = dat3,
##     robustSE = FALSE)
##
## Residuals:
##     Min      1Q  Median      3Q     Max
## -17.578 -13.229  -4.387  10.939  51.987
##
## Coefficients:
##                  Estimate  Std Err   95%L         95%H         F stat    df
## [1] Intercept      17.78     5.673     6.093        29.46           9.82 1
## [2] NGRDI60m       87.59     62.90    -41.95        217.1           1.94 1
##                  Pr(>F)
## [1] Intercept      0.0044
## [2] NGRDI60m       0.1760
##
## Residual standard error: 16.89 on 25 degrees of freedom
```

```
## Multiple R-squared:  0.07198,    Adjusted R-squared:  0.03486
## F-statistic: 1.939 on 1 and 25 DF,  p-value: 0.176
```

```
## Create a scatterplot for 'fitNGRDI60m'
plot(dat3$NGRDI60m, dat3$Chla, xlab = "NGRDI 60m Spectral Index Value",
    ylab = "Chlorophyll-a (µg/L)", pch = 20)
## Add a fitted regression line to the model
abline(lm(Chla ~ NGRDI60m, data = dat3))
```

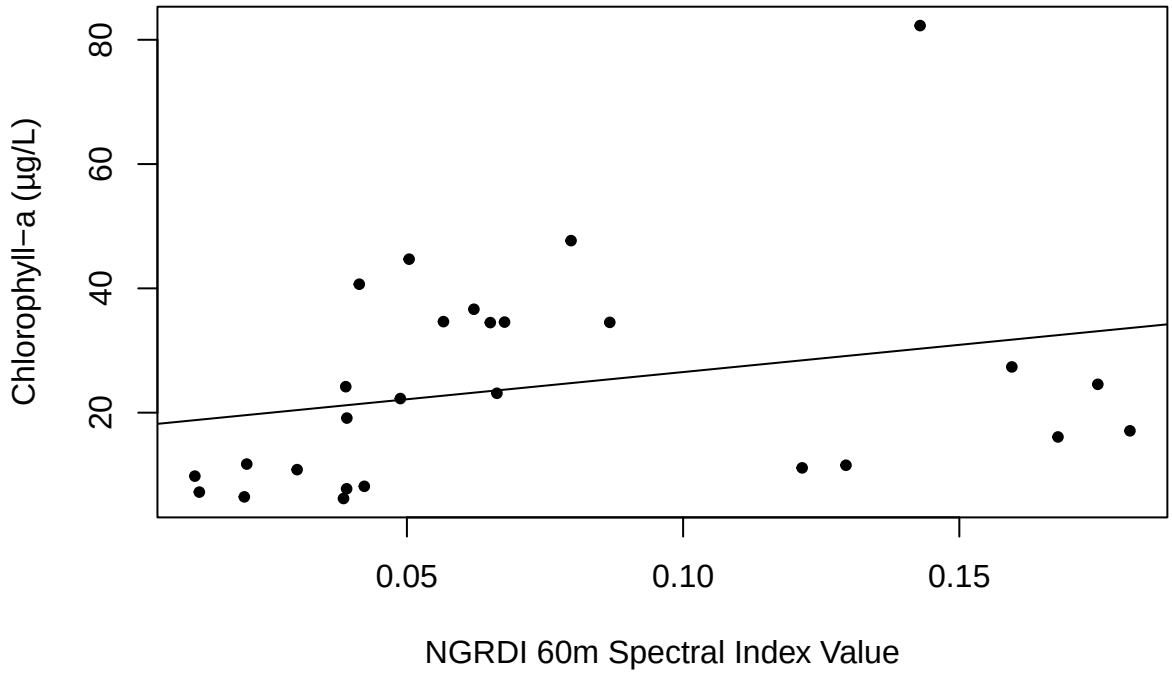


```
## Fit a simple linear regression model with
## dependent variable 'Chla' and independent
## variable 'NGRDI90m' Call variable after
## defining
fitNGRDI90m <- regress("mean", Chla ~ NGRDI90m, robustSE = FALSE,
    data = dat3)
fitNGRDI90m
```

```
##
## Call:
## regress(fnctl = "mean", formula = Chla ~ NGRDI90m, data = dat3,
##     robustSE = FALSE)
##
## Residuals:
##     Min      1Q  Median      3Q     Max
## -21.606 -11.516  -7.432  10.431  46.654
```

```
##
## Coefficients:
##                   Estimate  Std Err   95%L         95%H         F stat    df
## [1] Intercept       15.89     5.371     4.828        26.95           8.75 1
## [2] NGRDI90m        113.2     58.88    -8.086        234.4           3.69 1
##                   Pr(>F)
## [1] Intercept       0.0067
## [2] NGRDI90m        0.0660
##
## Residual standard error: 16.37 on 25 degrees of freedom
## Multiple R-squared:  0.1288, Adjusted R-squared:  0.09391
## F-statistic: 3.695 on 1 and 25 DF,  p-value: 0.06605
```

```
## Create a scatterplot for 'fitNGRDI90m'
plot(dat3$NGRDI90m, dat3$Chla, xlab = "NGRDI 90m Spectral Index Value",
    ylab = "Chlorophyll-a (µg/L)", pch = 20)
## Add a fitted regression line to the model
abline(lm(Chla ~ NGRDI90m, data = dat3))
```

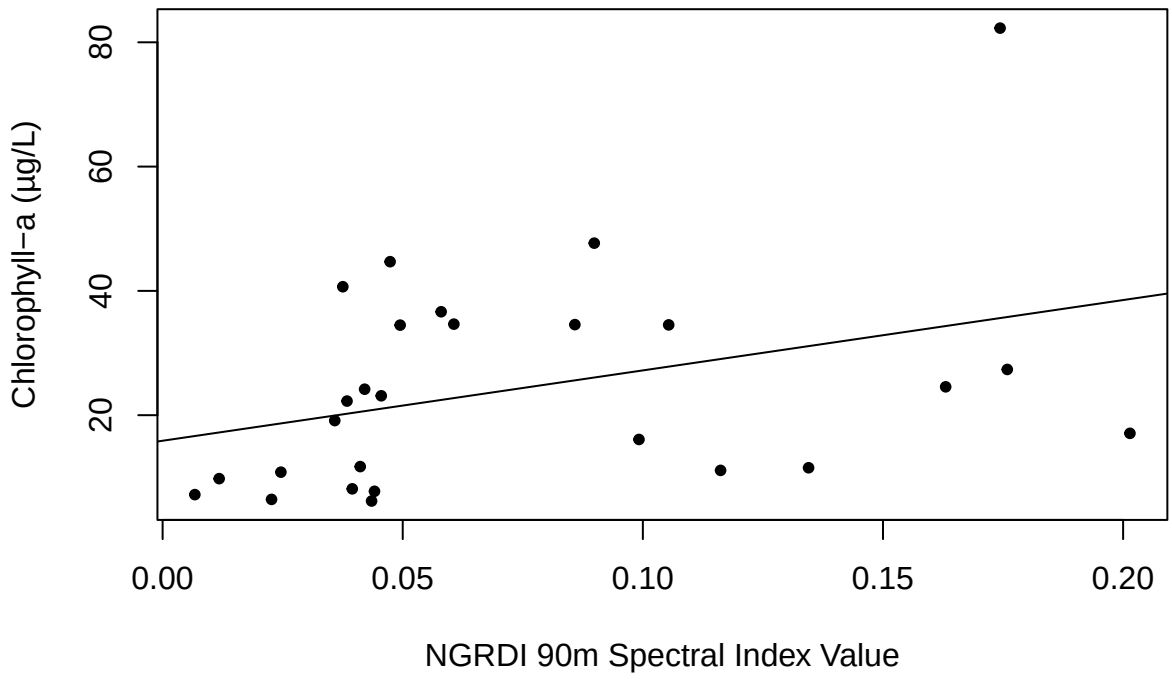


```
## Fit a simple linear regression model with
## dependent variable 'Chla' and independent
## variable 'NGRDI120m' Call variable after
## defining
fitNGRDI120m <- regress("mean", Chla ~ NGRDI120m, robustSE = FALSE,
    data = dat3)
fitNGRDI120m
```

```
##
## Call:
## regress(fnctl = "mean", formula = Chla ~ NGRDI120m, data = dat3,
##     robustSE = FALSE)
##
## Residuals:
##     Min      1Q  Median      3Q     Max
## -18.310 -13.556  -3.422  11.323  53.957
##
## Coefficients:
##                   Estimate  Std Err   95%L         95%H         F stat    df
## [1] Intercept       20.74     5.292     9.843        31.64          15.36 1
## [2] NGRDI120m       48.22     56.59    -68.32        164.8           0.73 1
##                   Pr(>F)
## [1] Intercept       0.0006
## [2] NGRDI120m       0.4022
##
## Residual standard error: 17.29 on 25 degrees of freedom
## Multiple R-squared:  0.02823,    Adjusted R-squared:  -0.01064
## F-statistic: 0.7262 on 1 and 25 DF,  p-value: 0.4022
```

```r
## Create a scatterplot for 'fitNGRDI120m'
plot(dat3$NGRDI120m, dat3$Chla, xlab = "NGRDI 120m Spectral Index Value",
    ylab = "Chlorophyll-a (µg/L)", pch = 20)
## Add a fitted regression line to the model
abline(lm(Chla ~ NGRDI120m, data = dat3))
```

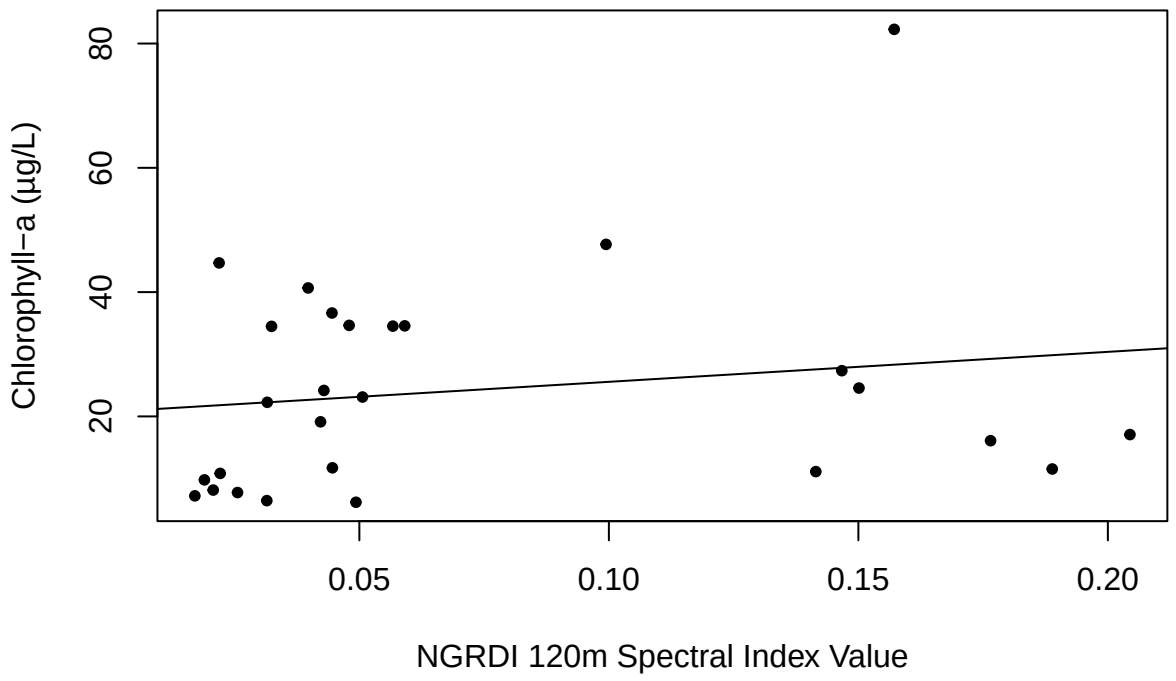

```
##### VDVI ##### Fit a simple linear regression
##### model with dependent variable 'Chla' and
##### independent variable 'VDVI60m' Call
##### variable after defining
fitVDVI60m <- regress("mean", Chla ~ VDVI60m, robustSE = FALSE,
    data = dat3)
fitVDVI60m
```

```
##
## Call:
## regress(fnctl = "mean", formula = Chla ~ VDVI60m, data = dat3,
##     robustSE = FALSE)
##
## Residuals:
##     Min      1Q  Median      3Q     Max
## -26.433 -10.505  -4.739  10.928  33.753
##
## Coefficients:
##                   Estimate  Std Err   95%L         95%H         F stat    df
## [1] Intercept       17.38     3.568     10.04        24.73          23.74 1
## [2] VDVI60m         178.7     56.04     63.32        294.2          10.17 1
##                   Pr(>F)
## [1] Intercept       0.0001
## [2] VDVI60m         0.0038
##
## Residual standard error: 14.78 on 25 degrees of freedom
## Multiple R-squared:  0.2892, Adjusted R-squared:  0.2608
## F-statistic: 10.17 on 1 and 25 DF,  p-value: 0.003814
```

```
## Create a scatterplot for 'fitVDVI60m'
plot(dat3$VDVI60m, dat3$Chla, xlab = "VDVI 60m Spectral Index Value",
    ylab = "Chlorophyll-a (µg/L)", pch = 20)
## Add a fitted regression line to the model
abline(lm(Chla ~ VDVI60m, data = dat3))
```

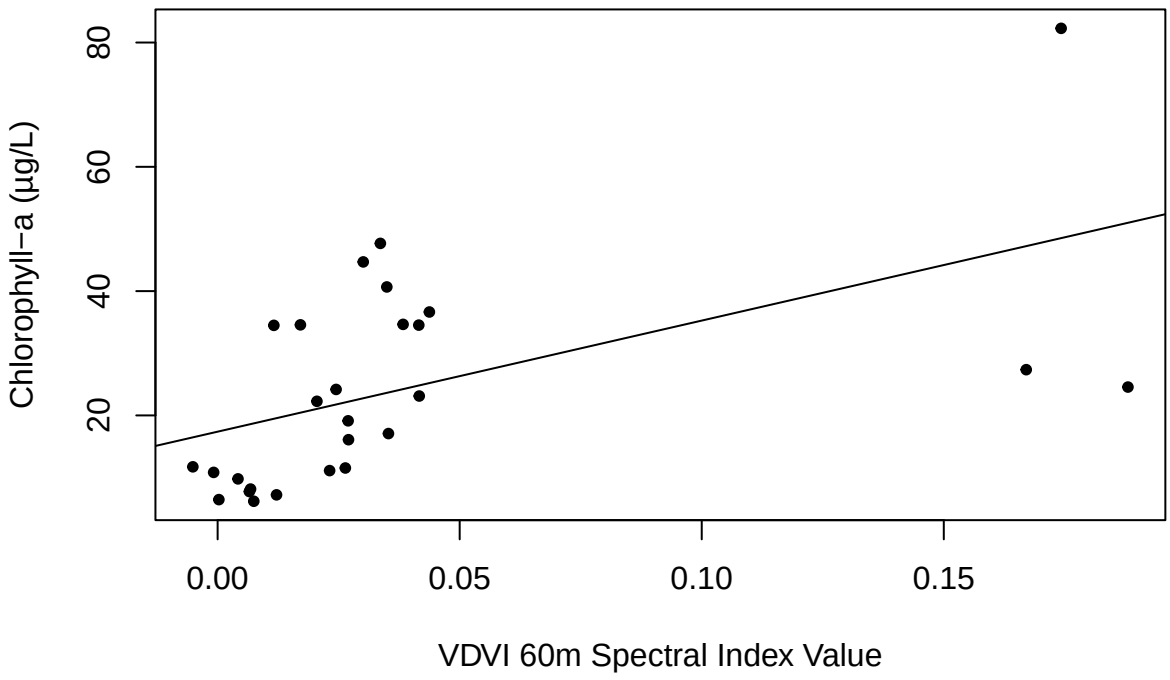


```
## Fit a simple linear regression model with
## dependent variable 'Chla' and independent
## variable 'VDVI90m' Call variable after
## defining
fitVDVI90m <- regress("mean", Chla ~ VDVI90m, robustSE = FALSE,
    data = dat3)
fitVDVI90m
```

```
##
## Call:
## regress(fnctl = "mean", formula = Chla ~ VDVI90m, data = dat3,
##     robustSE = FALSE)
##
## Residuals:
##     Min      1Q  Median      3Q     Max
## -23.971 -10.933  -4.159  10.347  37.616
##
## Coefficients:
##                  Estimate  Std Err   95%L         95%H         F stat    df
## [1] Intercept      17.64     3.662     10.10        25.19          23.21 1
## [2] VDVI90m        178.0     60.14     54.18        301.9           8.76 1
##                  Pr(>F)
## [1] Intercept      0.0001
## [2] VDVI90m        0.0066
##
## Residual standard error: 15.09 on 25 degrees of freedom
```

```
## Multiple R-squared:  0.2596, Adjusted R-squared:   0.23
## F-statistic: 8.764 on 1 and 25 DF,  p-value: 0.006639
```

```
## Create a scatterplot for 'fitVDVI90m'
plot(dat3$VDVI90m, dat3$Chla, xlab = "VDVI 90m Spectral Index Value",
    ylab = "Chlorophyll-a (µg/L)", pch = 20)
## Add a fitted regression line to the model
abline(lm(Chla ~ VDVI90m, data = dat3))
```

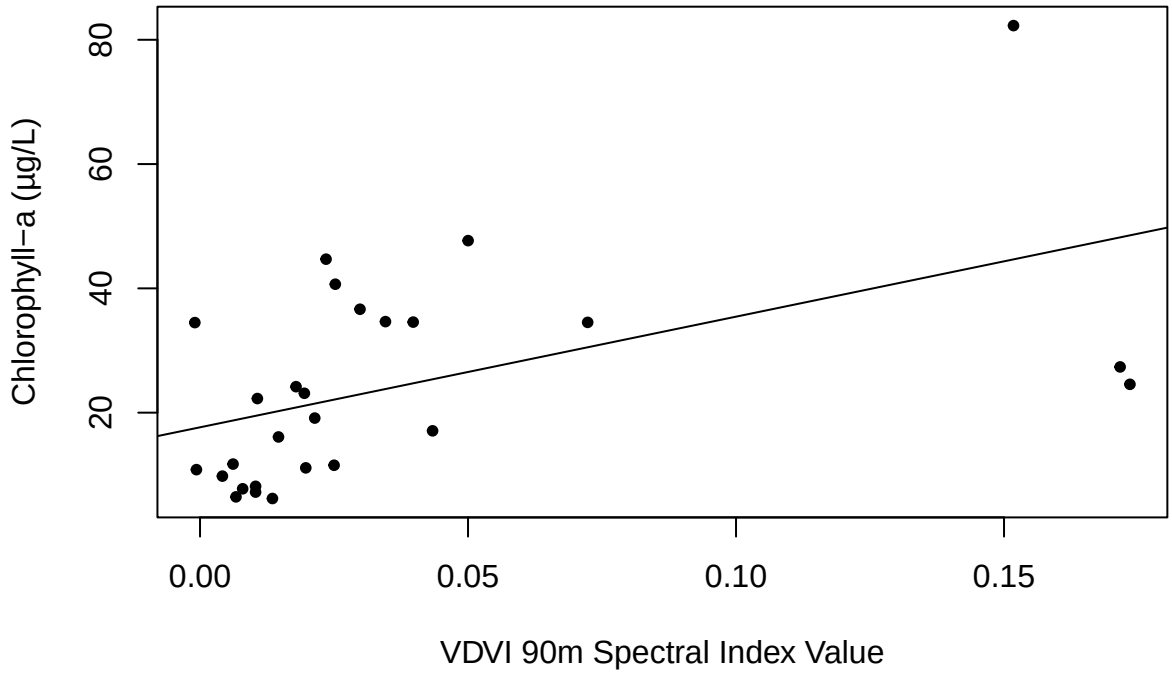


```
## Fit a simple linear regression model with
## dependent variable 'Chla' and independent
## variable 'VDVI120m' Call variable after
## defining
fitVDVI120m <- regress("mean", Chla ~ VDVI120m, robustSE = FALSE,
    data = dat3)
fitVDVI120m
```

```
##
## Call:
## regress(fnctl = "mean", formula = Chla ~ VDVI120m, data = dat3,
##     robustSE = FALSE)
##
## Residuals:
##     Min      1Q  Median      3Q     Max
## -23.313 -10.301  -4.439  13.352  36.757
```

```
##
## Coefficients:
##                   Estimate  Std Err   95%L         95%H         F stat    df
## [1] Intercept       17.83     3.655     10.31        25.36          23.81 1
## [2] VDVI120m        181.4     62.27     53.10        309.6           8.48 1
##                   Pr(>F)
## [1] Intercept       0.0001
## [2] VDVI120m        0.0074
##
## Residual standard error: 15.15 on 25 degrees of freedom
## Multiple R-squared:  0.2533, Adjusted R-squared:  0.2235
## F-statistic: 8.481 on 1 and 25 DF,  p-value: 0.007447
```

```r
## Create a scatterplot for 'fitVDVI120m'
plot(dat3$VDVI120m, dat3$Chla, xlab = "VDVI 120m Spectral Index Value",
    ylab = "Chlorophyll-a (µg/L)", pch = 20)
## Add a fitted regression line to the model
abline(lm(Chla ~ VDVI120m, data = dat3))
```

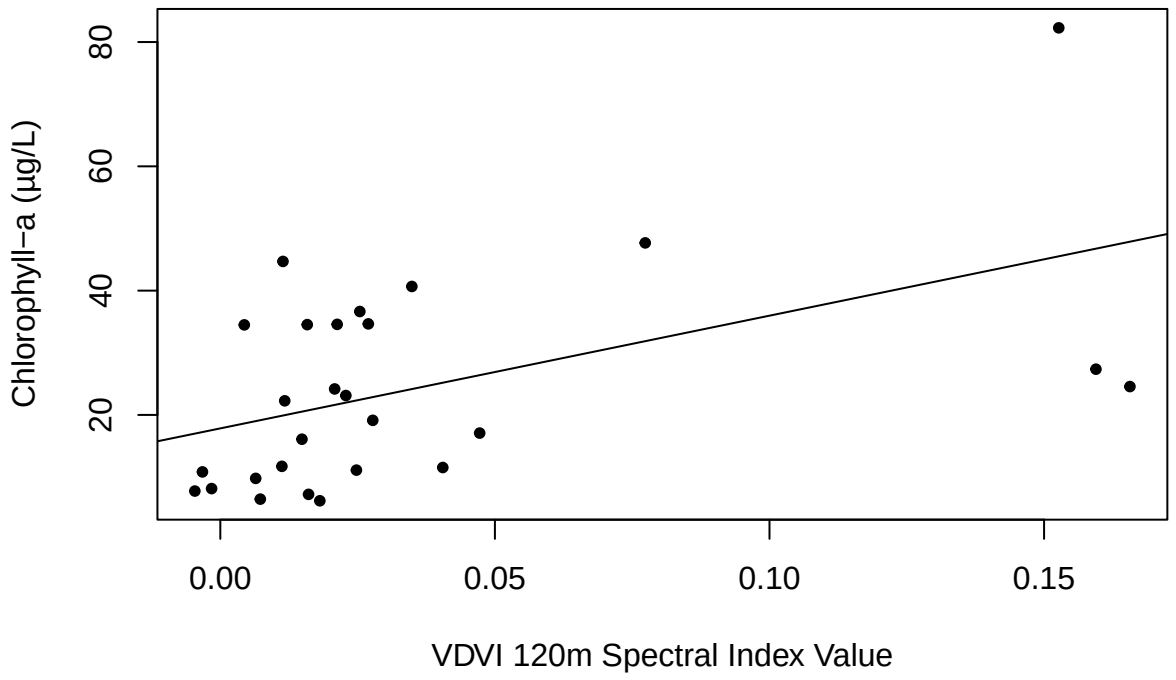

Model Checking - RGB Imagery

This section will assess the linearity, independence, normality, and equal variance assumptions for the RGB linear regression models previously generated using 'dat3.'

```
##### CIVE60m ##### Linearity and Equal Variance
##### Model Check Create variables 'resCIVE60m'
##### and 'fittedCIVE60m' to calculate residuals
##### (using the jackknife method) and fitted
##### values for 'fitCIVE60m.'
resCIVE60m <- residuals(fitCIVE60m, type = "jackknife")
fittedCIVE60m <- predict(fitCIVE60m)[, 1]

## Plot residuals vs. fitted values (residual
## plot) and customize graph
plot(resCIVE60m ~ fittedCIVE60m, xlab = "Fitted values",
    ylab = "Residuals", main = "Residual Plot CIVE 60m")
abline(h = 0, lwd = 1.5, col = "red", lty = 2)
lines(lowess(resCIVE60m ~ fittedCIVE60m), lwd = 2,
    col = "blue")
```

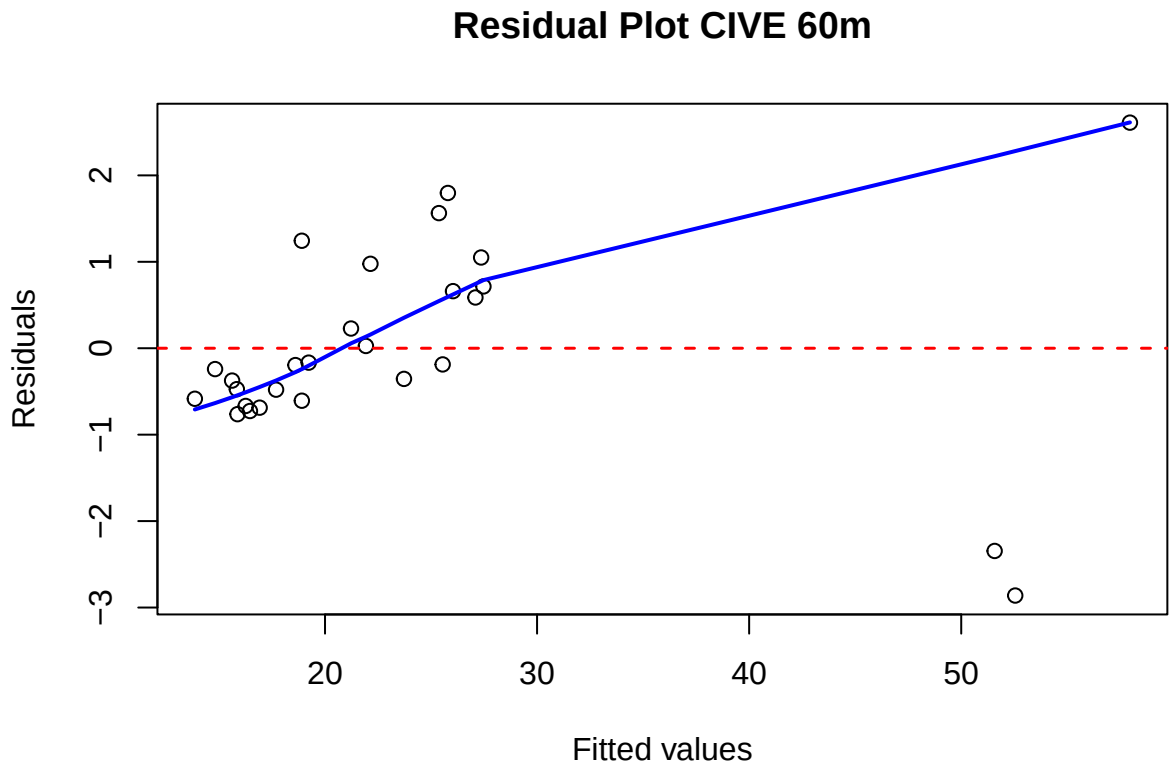


```
## Interpretation: the plot of residuals vs.
## fitted values suggests possible non-linearity
## in the conditional mean of chlorophyll a
```

```
## concentration given the mean CIVE 60m spectral
## index value. This is due to the behavior of
## the lowess line on the right side of the
## graph. It is important to note that since the
## lowess line averages over nearby points, it is
## more susceptible to the outliers on the right
## side of the plot (the curve is more dominated
## by these points). However, the residuals on
## the left side of the plot appear to be an
## unstructured horizontal band of points
## centered around 0. Based on this, evidence for
## non-linearity is somewhat equivocal; however,
## it appears that the linearity assumption has
## been violated when accounting for these
## outlier values.

## Moreover, the residual points of the graph
## appear to be placed nicely around the
## horizontal line at 0 on the left side of the
## plot but deviate on the right side of the
## plot. Based on the behavior of the outliers,
## the assumption of equal variance is also
## equivocal. Even accounting for the outliers,
## we conclude that there is evidence of
## heteroscedasticity, meaning our assumption of
## homoscedasticity or equal/constant variance
## has not been met.

## We can conclude from this residual analysis
## that our confidence interval of the mean may
## be impacted due to some limited evidence of
## nonlinearity and heteroscedasticity, based on
## the presence of outliers. This represents a
## study limitation.

#### Independence Model Check Independence is
#### based on the study design - since the water
#### samples (yielding chlorophyll a results) and
#### drone flights (yielding spectral index
#### values) were collected independently from
#### each other for each sampling event, the
#### assumption of independence has been met.
#### This does not represent a study limitation.

#### Normality Model Check Create QQ plot
qqnorm(resCIVE60m, main = "QQ Plot CIVE 60m")
qqline(resCIVE60m)
```

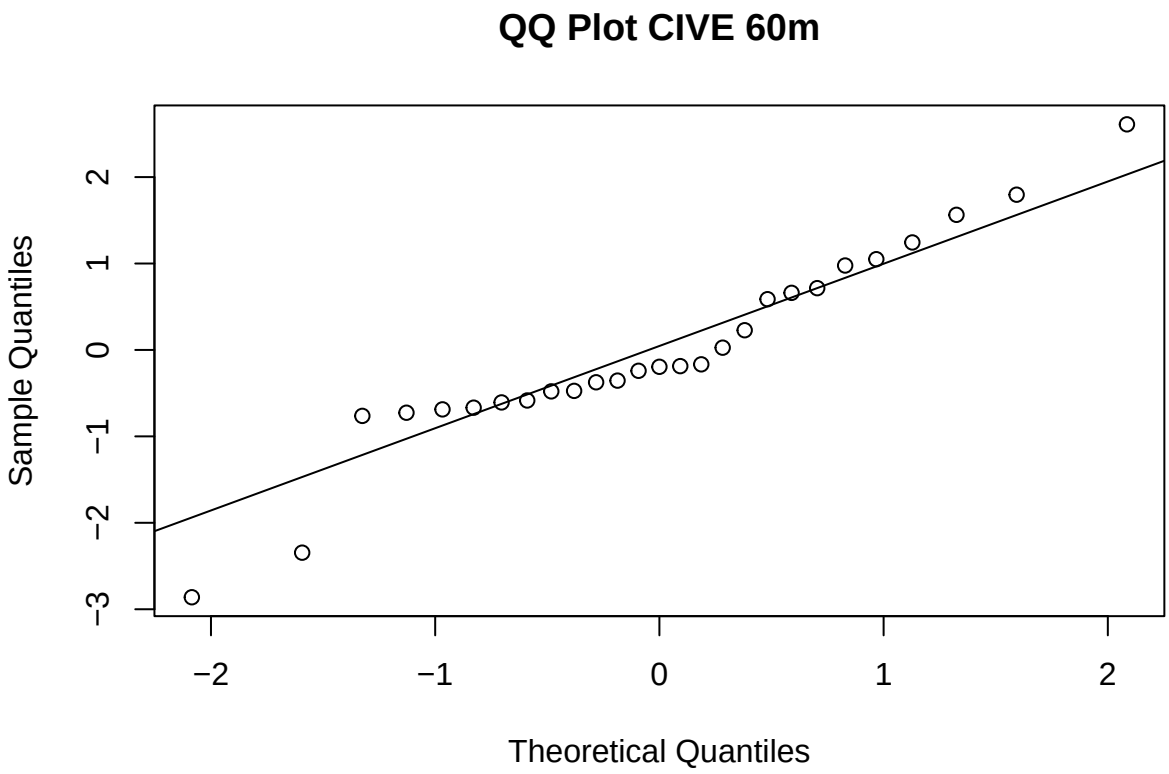


```
## Interpretation: the QQ (Quantile-Quantile)
## plot shows that the dataset values are
## normally distributed since most residual
## points lie approximately along the diagonal
## line. There are, however, several points on
## the tails that deviate from the diagonal line.
## This suggests a small deviation from
## normality, most likely as a result of the
## small sample size and presence of outlier
## points. Overall, the normality assumption is
## determined to have not been violated and this
## does not represent a study limitation.

## To summarize, model checking showed that
## assumptions for this CIVE 60m linear
## regression model have been violated for
## linearity and equal variance, but not for
## independence or normality. This is due to a
## small sample size and the presence of
## outliers. Repeat analysis with CIVE 90m and
## CIVE 120m models may show similar conclusions.
## This overall finding represents a study
## limitation.

## For the remainder of the linear regression
## models analyzed, model checking
```

```r
## interpretations are summarized in the main
## thesis document 'Discussion' section.

##### CIVE90m #####
resCIVE90m <- residuals(fitCIVE90m, type = "jackknife")
fittedCIVE90m <- predict(fitCIVE90m)[, 1]

plot(resCIVE90m ~ fittedCIVE90m, xlab = "Fitted values",
    ylab = "Residuals", main = "Residual Plot CIVE 90m")
abline(h = 0, lwd = 1.5, col = "red", lty = 2)
lines(lowess(resCIVE90m ~ fittedCIVE90m), lwd = 2,
    col = "blue")
```

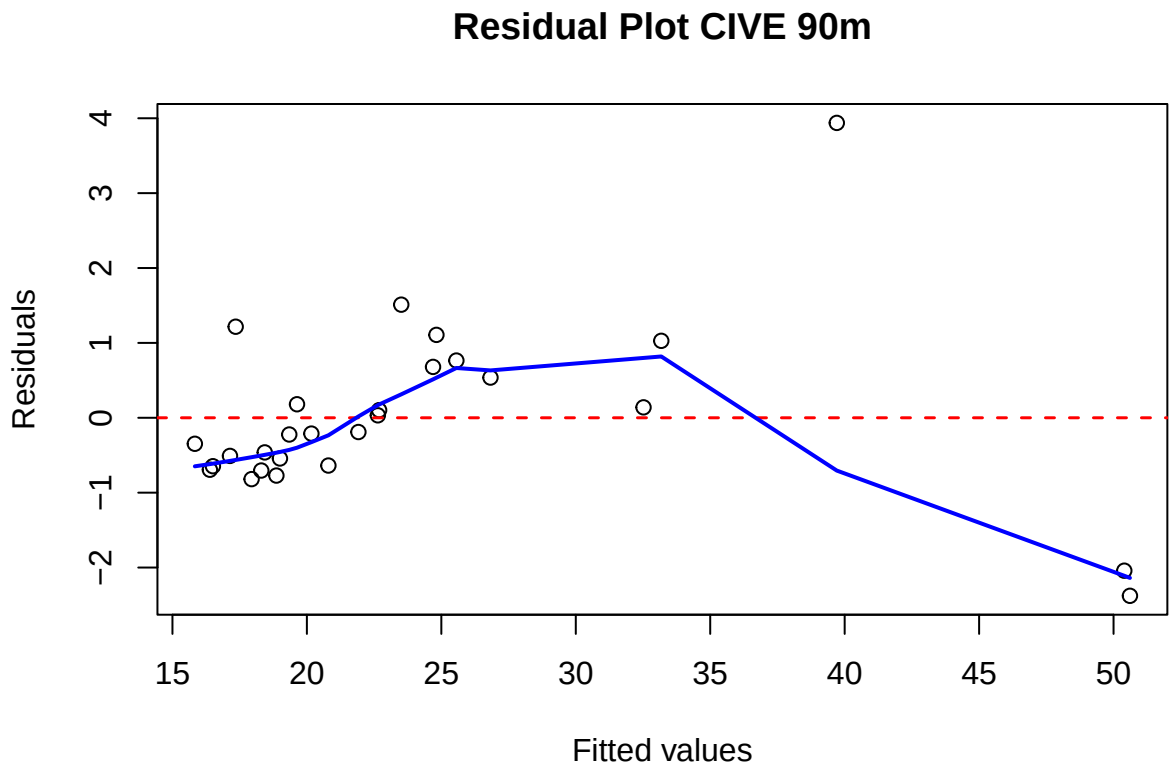


```r
qqnorm(resCIVE90m, main = "QQ Plot CIVE 90m")
qqline(resCIVE90m)
```

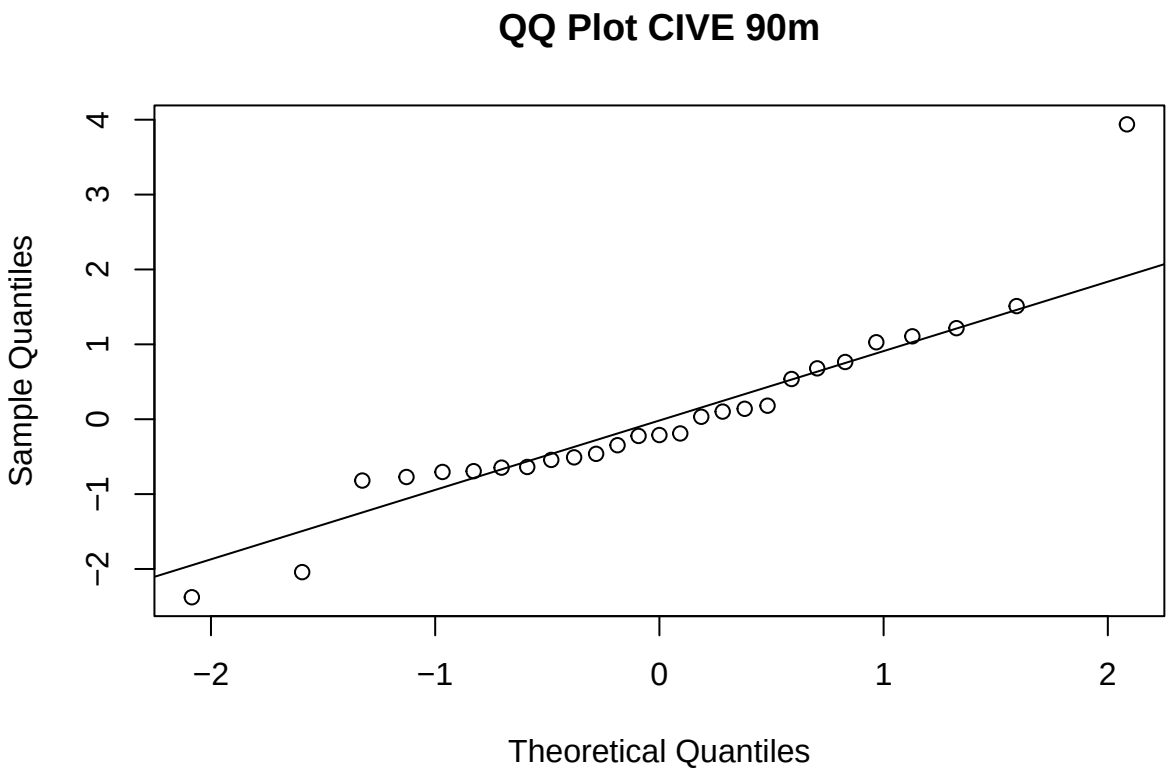


```
##### CIVE120m #####
resCIVE120m <- residuals(fitCIVE120m, type = "jackknife")
fittedCIVE120m <- predict(fitCIVE120m)[, 1]

plot(resCIVE120m ~ fittedCIVE120m, xlab = "Fitted values",
    ylab = "Residuals", main = "Residual Plot CIVE 120m")
abline(h = 0, lwd = 1.5, col = "red", lty = 2)
lines(lowess(resCIVE120m ~ fittedCIVE120m), lwd = 2,
    col = "blue")
```

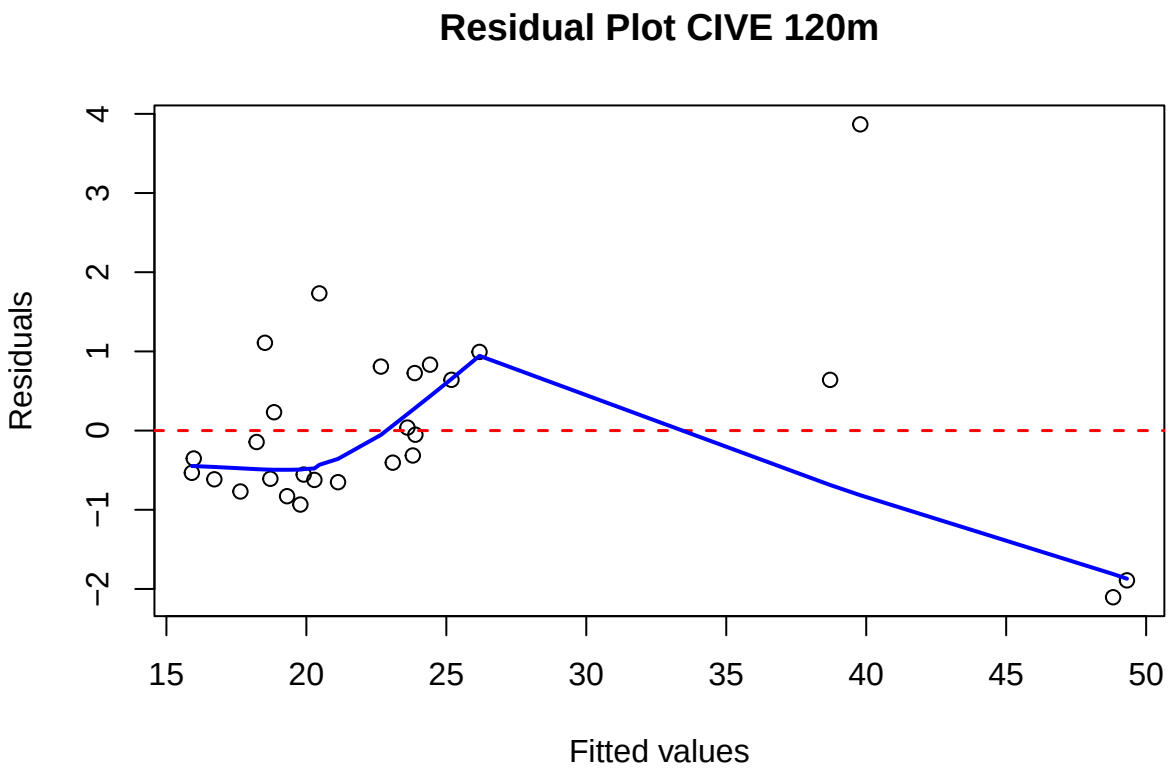


```
qqnorm(resCIVE120m, main = "QQ Plot CIVE 120m")
qqline(resCIVE120m)
```

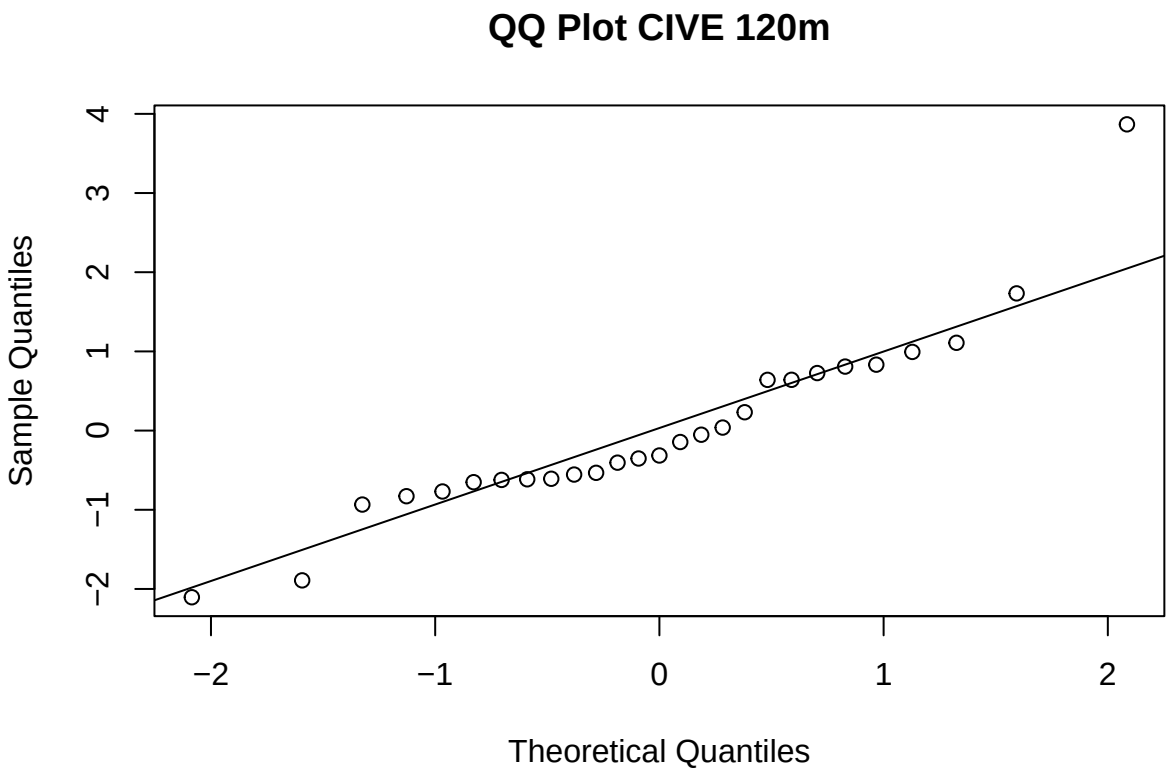


```
##### EXG60m #####
resEXG60m <- residuals(fitEXG60m, type = "jackknife")
fittedEXG60m <- predict(fitEXG60m)[, 1]

plot(resEXG60m ~ fittedEXG60m, xlab = "Fitted values",
    ylab = "Residuals", main = "Residual Plot EXG 60m")
abline(h = 0, lwd = 1.5, col = "red", lty = 2)
lines(lowess(resEXG60m ~ fittedEXG60m), lwd = 2, col = "blue")
```

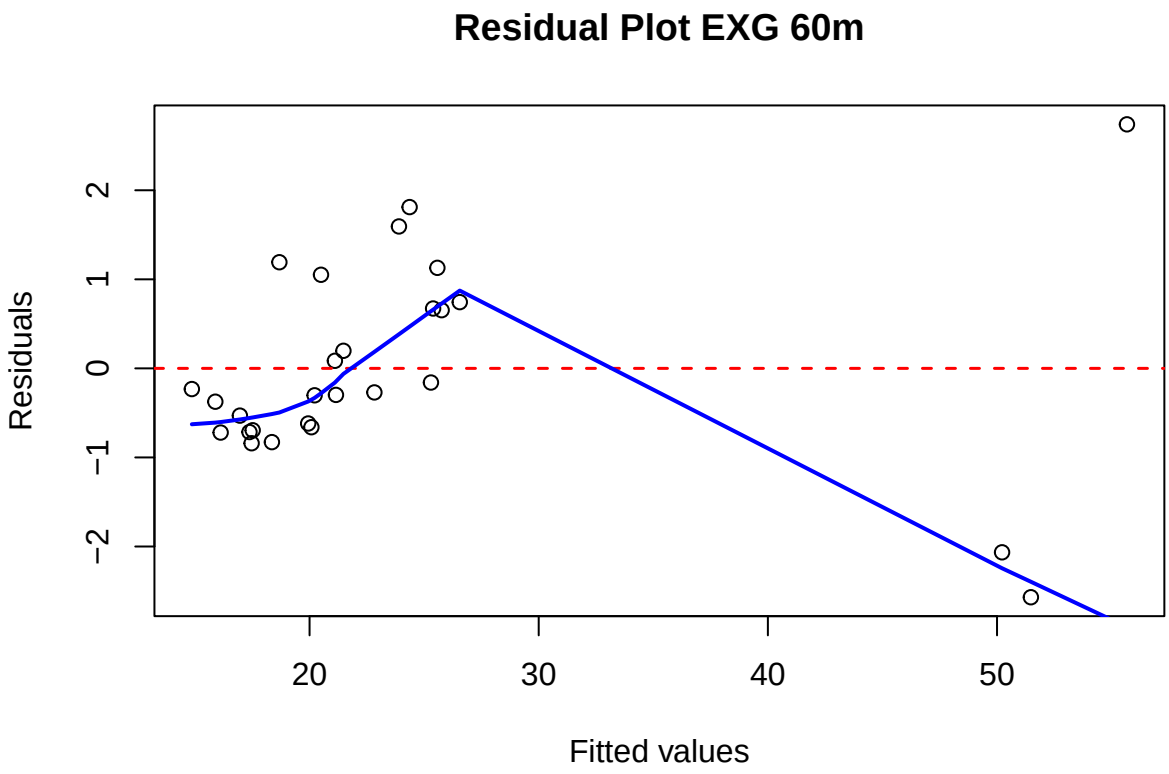


```
qqnorm(resEXG60m, main = "QQ Plot EXG 60m")
qqline(resEXG60m)
```

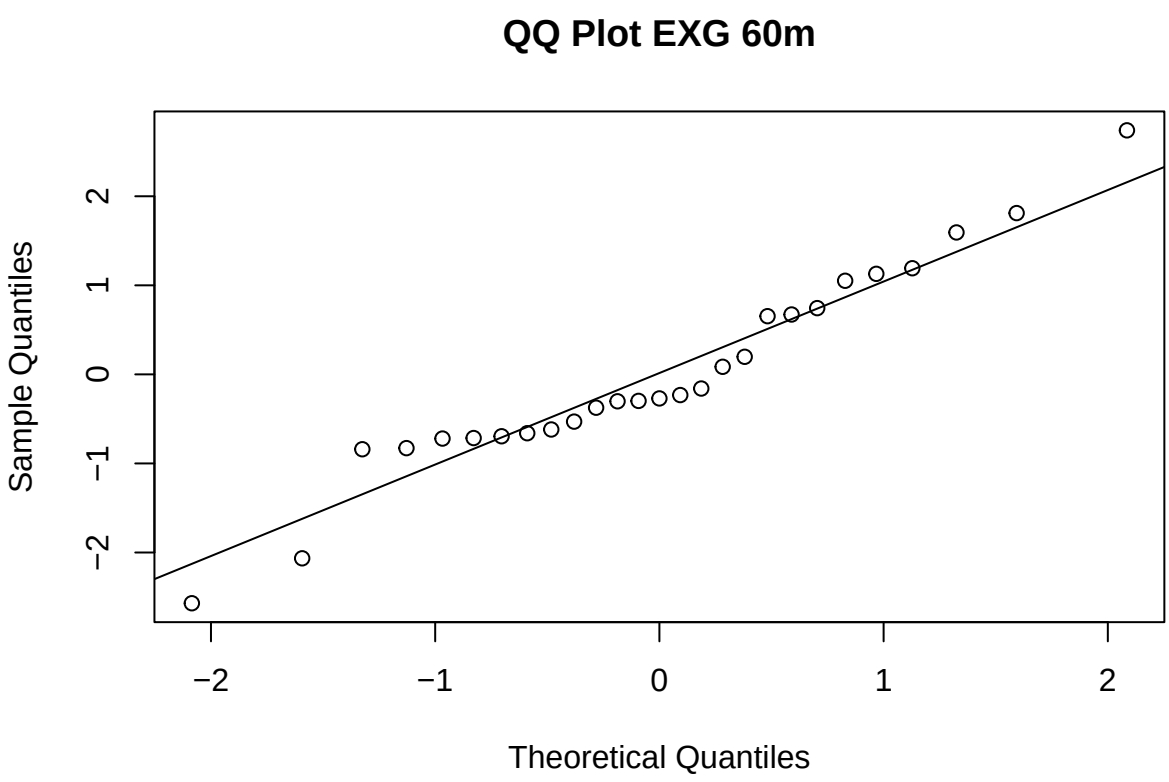


```
##### EXG90m #####
resEXG90m <- residuals(fitEXG90m, type = "jackknife")
fittedEXG90m <- predict(fitEXG90m)[, 1]

plot(resEXG90m ~ fittedEXG90m, xlab = "Fitted values",
    ylab = "Residuals", main = "Residual Plot EXG 90m")
abline(h = 0, lwd = 1.5, col = "red", lty = 2)
lines(lowess(resEXG90m ~ fittedEXG90m), lwd = 2, col = "blue")
```

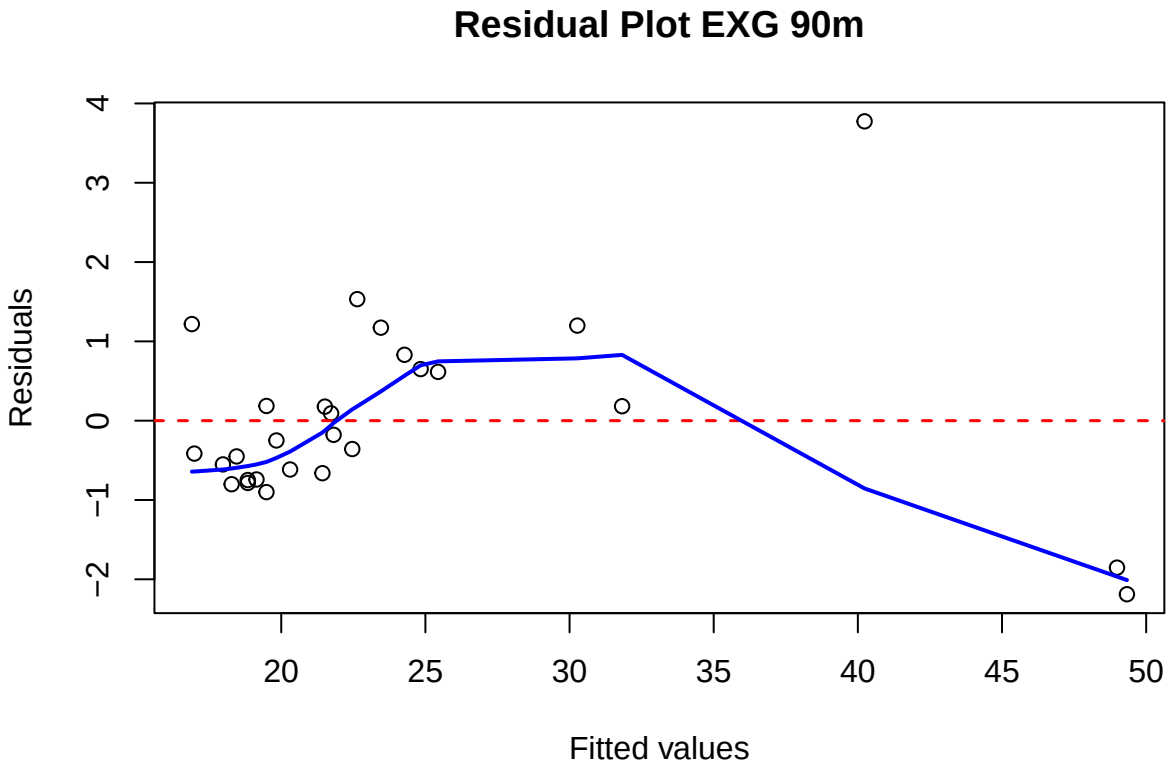


```
qqnorm(resEXG90m, main = "QQ Plot EXG 90m")
qqline(resEXG90m)
```

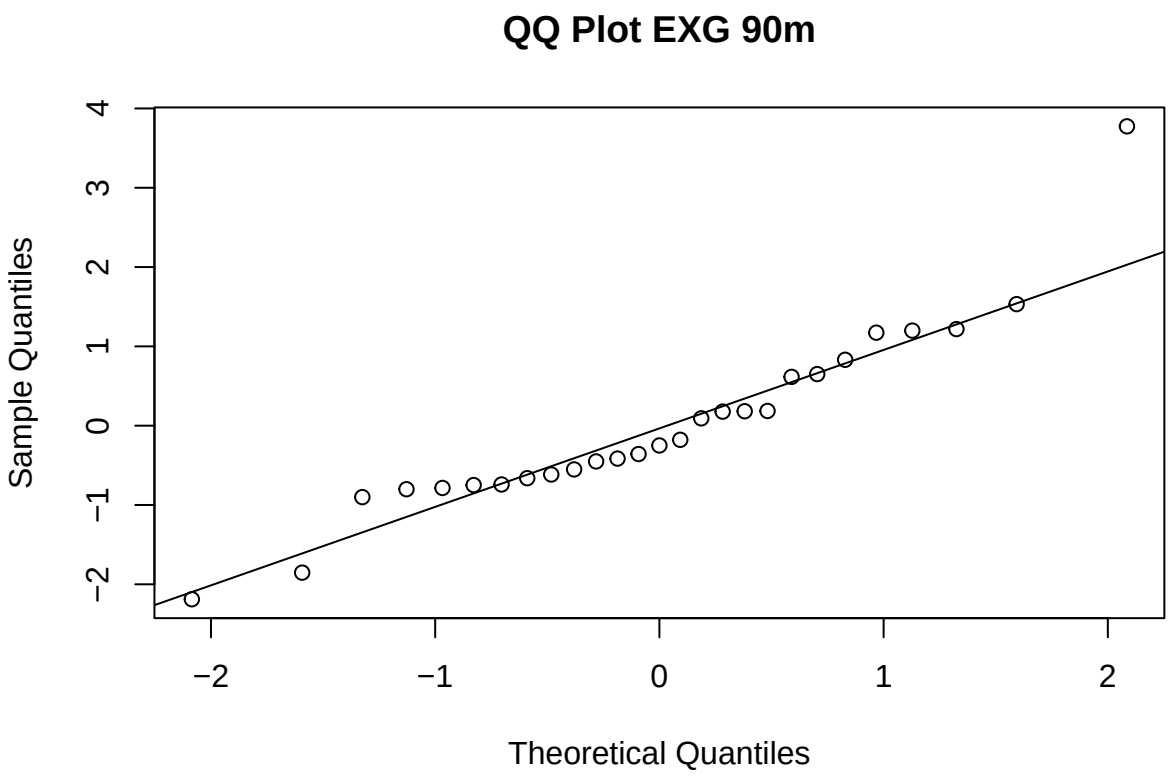


```
##### EXG120m #####
resEXG120m <- residuals(fitEXG120m, type = "jackknife")
fittedEXG120m <- predict(fitEXG120m)[, 1]

plot(resEXG120m ~ fittedEXG120m, xlab = "Fitted values",
    ylab = "Residuals", main = "Residual Plot EXG 120m")
abline(h = 0, lwd = 1.5, col = "red", lty = 2)
lines(lowess(resEXG120m ~ fittedEXG120m), lwd = 2,
    col = "blue")
```

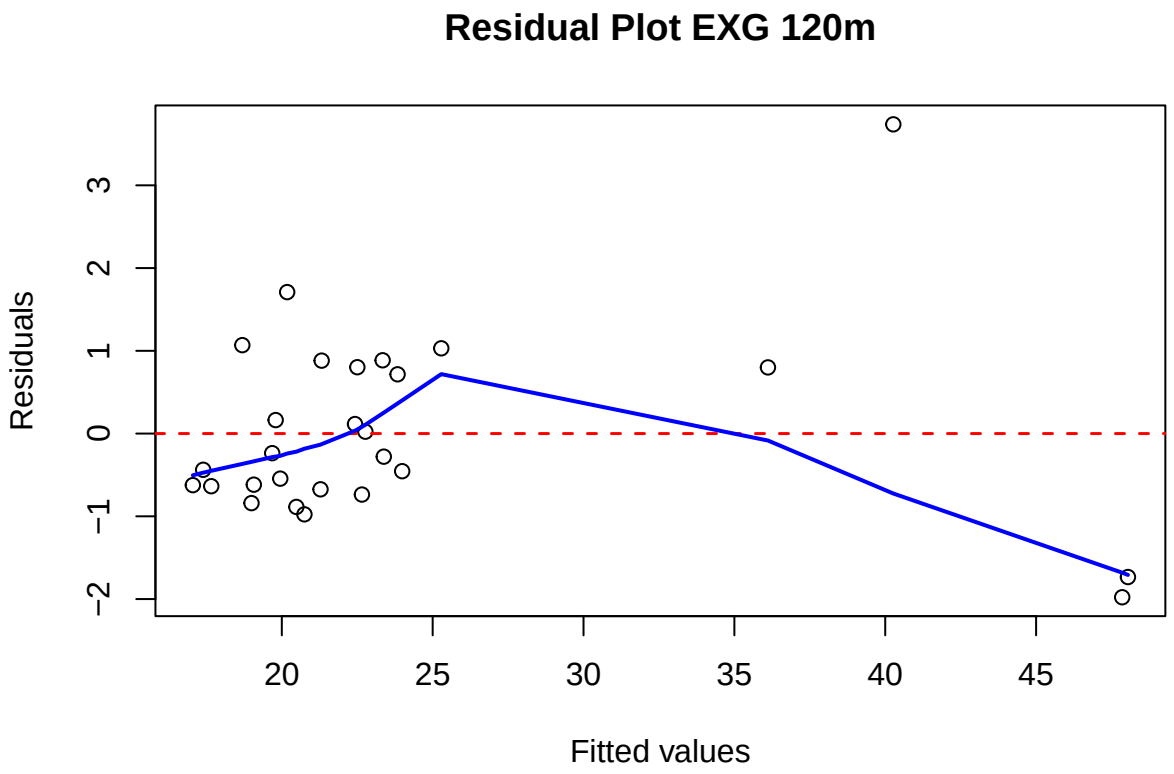


```
qqnorm(resEXG120m, main = "QQ Plot EXG 120m")
qqline(resEXG120m)
```

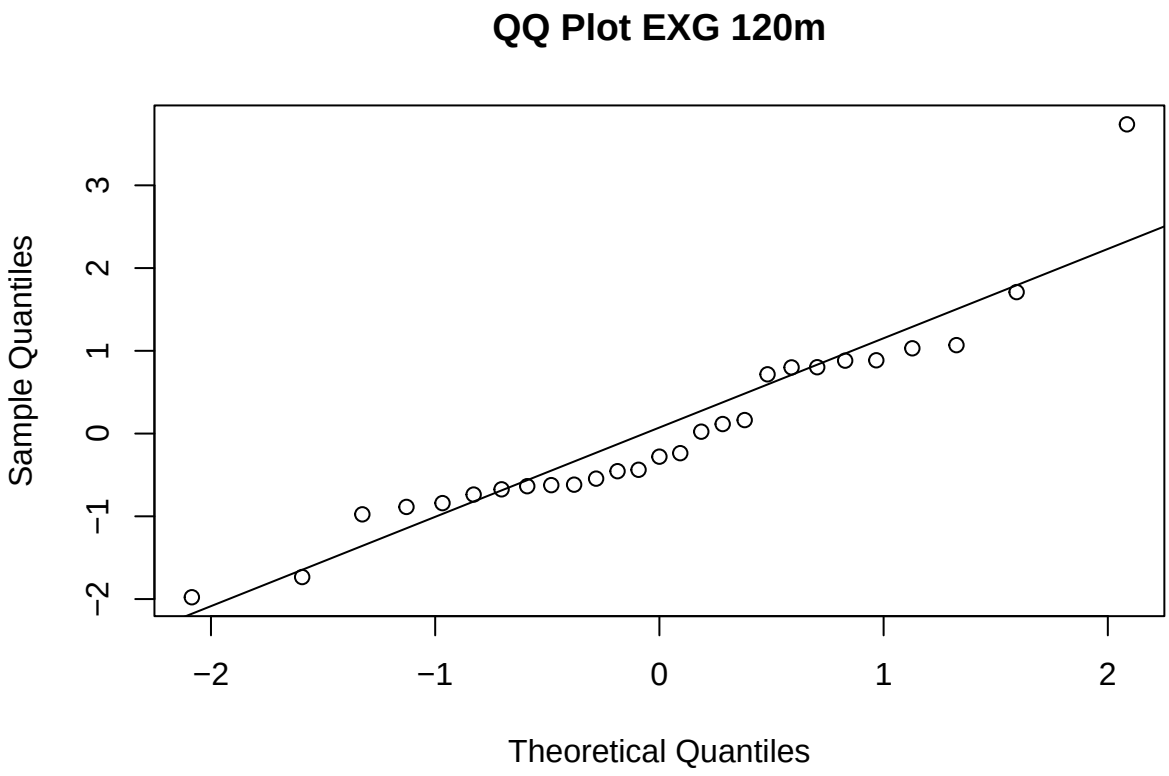


```
##### KIVU60m #####
resKIVU60m <- residuals(fitKIVU60m, type = "jackknife")
fittedKIVU60m <- predict(fitKIVU60m)[, 1]

plot(resKIVU60m ~ fittedKIVU60m, xlab = "Fitted values",
    ylab = "Residuals", main = "Residual Plot KIVU 60m")
abline(h = 0, lwd = 1.5, col = "red", lty = 2)
lines(lowess(resKIVU60m ~ fittedKIVU60m), lwd = 2,
    col = "blue")
```

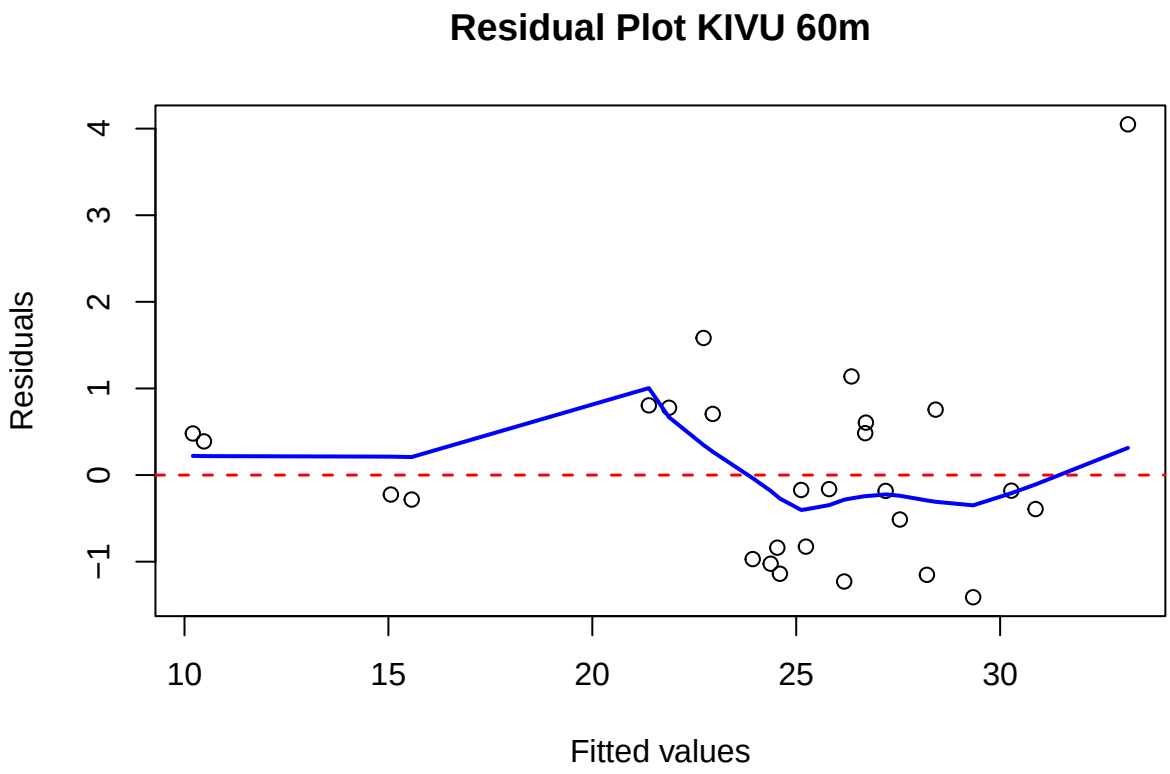


```
qqnorm(resKIVU60m, main = "QQ Plot KIVU 60m")
qqline(resKIVU60m)
```

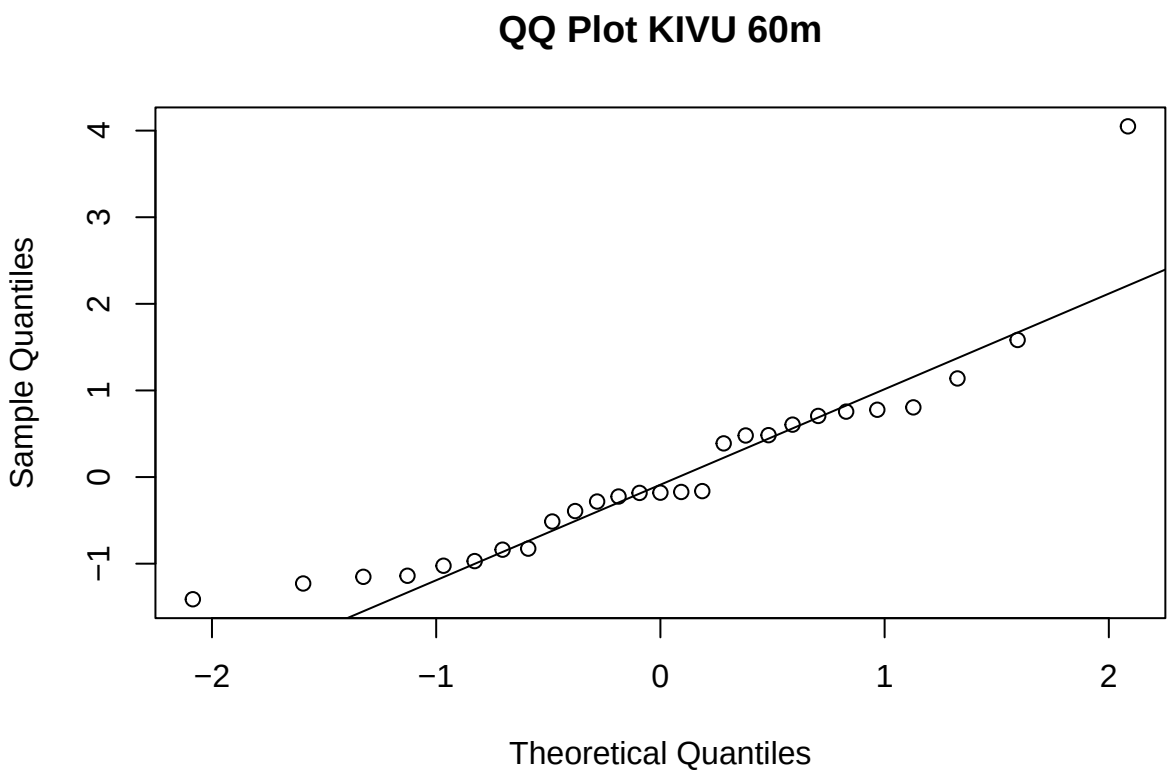


```
##### KIVU90m #####
resKIVU90m <- residuals(fitKIVU90m, type = "jackknife")
fittedKIVU90m <- predict(fitKIVU90m)[, 1]

plot(resKIVU90m ~ fittedKIVU90m, xlab = "Fitted values",
    ylab = "Residuals", main = "Residual Plot KIVU 90m")
abline(h = 0, lwd = 1.5, col = "red", lty = 2)
lines(lowess(resKIVU90m ~ fittedKIVU90m), lwd = 2,
    col = "blue")
```

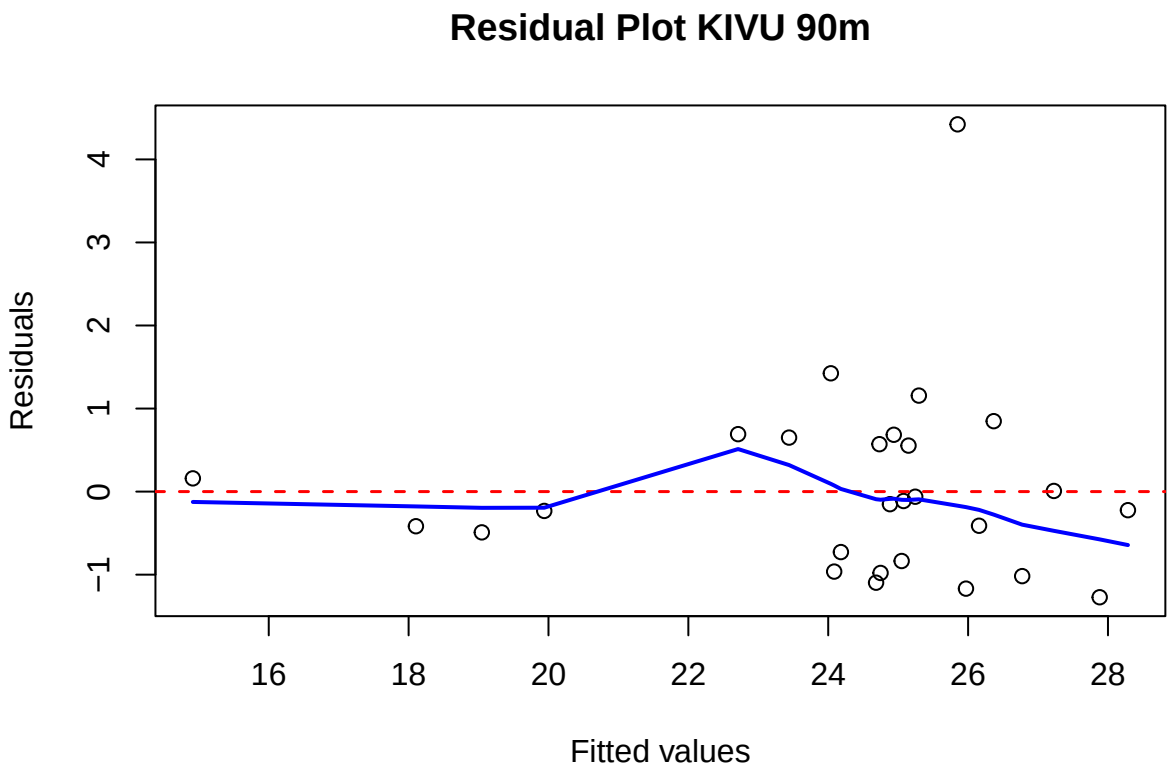


```
qqnorm(resKIVU90m, main = "QQ Plot KIVU 90m")
qqline(resKIVU90m)
```

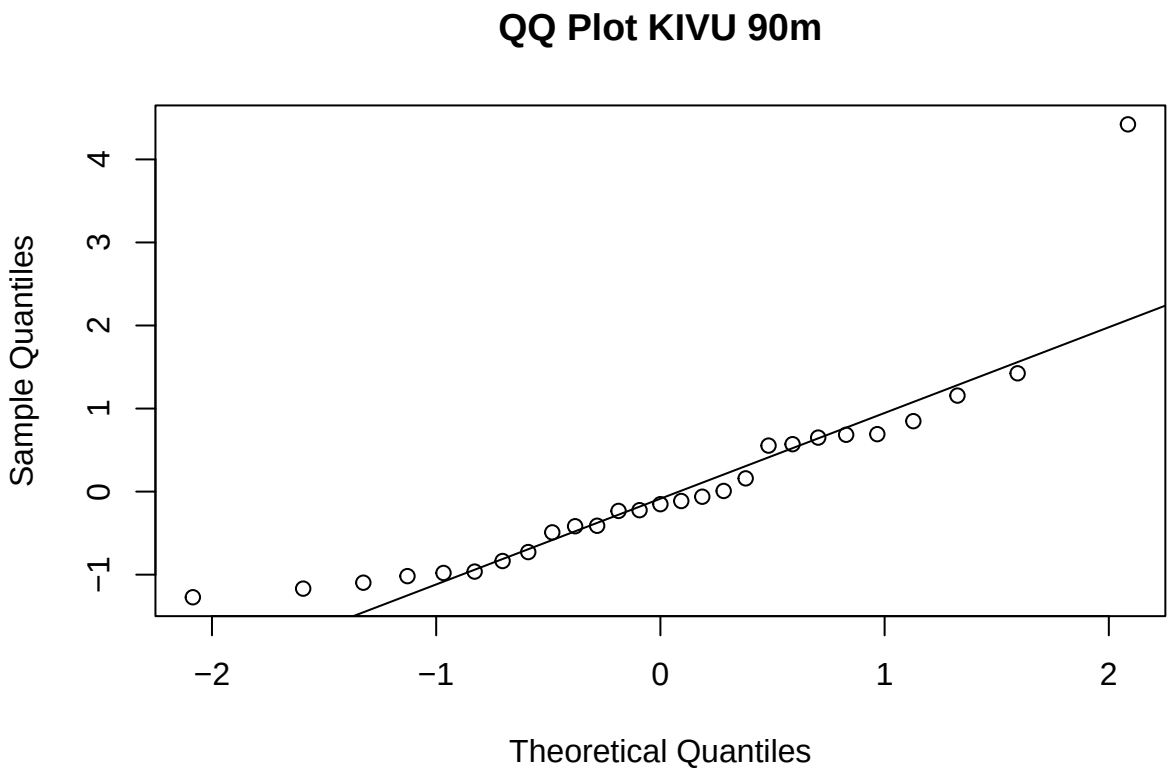


```
##### KIVU120m #####
resKIVU120m <- residuals(fitKIVU120m, type = "jackknife")
fittedKIVU120m <- predict(fitKIVU120m)[, 1]

plot(resKIVU120m ~ fittedKIVU120m, xlab = "Fitted values",
    ylab = "Residuals", main = "Residual Plot KIVU 120m")
abline(h = 0, lwd = 1.5, col = "red", lty = 2)
lines(lowess(resKIVU120m ~ fittedKIVU120m), lwd = 2,
    col = "blue")
```

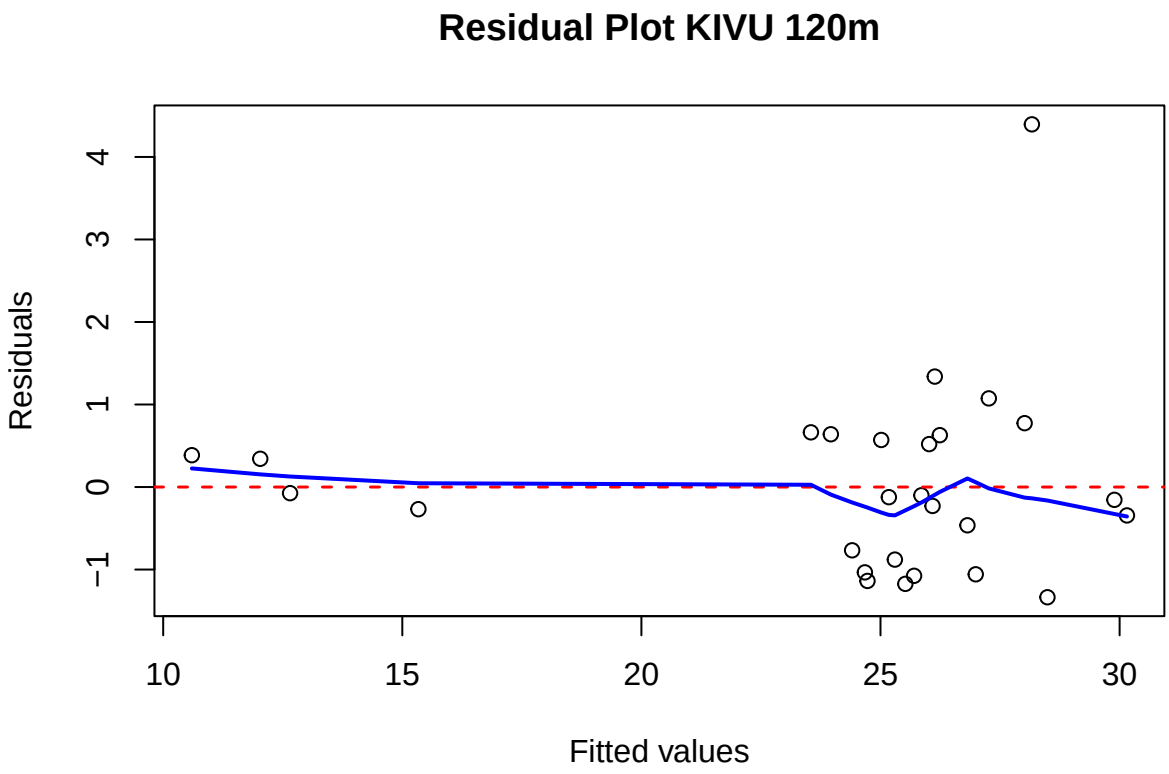


```
qqnorm(resKIVU120m, main = "QQ Plot KIVU 120m")
qqline(resKIVU120m)
```

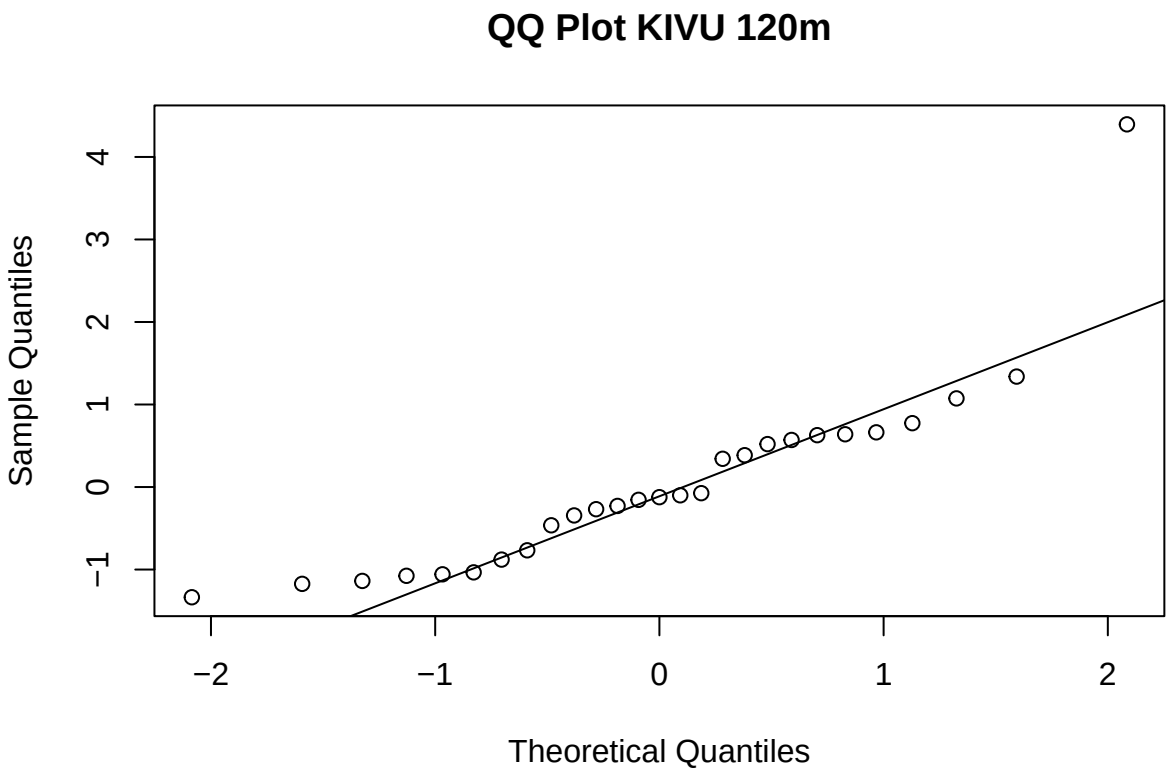


```r
##### NGRDI60m #####
resNGRDI60m <- residuals(fitNGRDI60m, type = "jackknife")
fittedNGRDI60m <- predict(fitNGRDI60m)[, 1]

plot(resNGRDI60m ~ fittedNGRDI60m, xlab = "Fitted values",
    ylab = "Residuals", main = "Residual Plot NGRDI 60m")
abline(h = 0, lwd = 1.5, col = "red", lty = 2)
lines(lowess(resNGRDI60m ~ fittedNGRDI60m), lwd = 2,
    col = "blue")
```

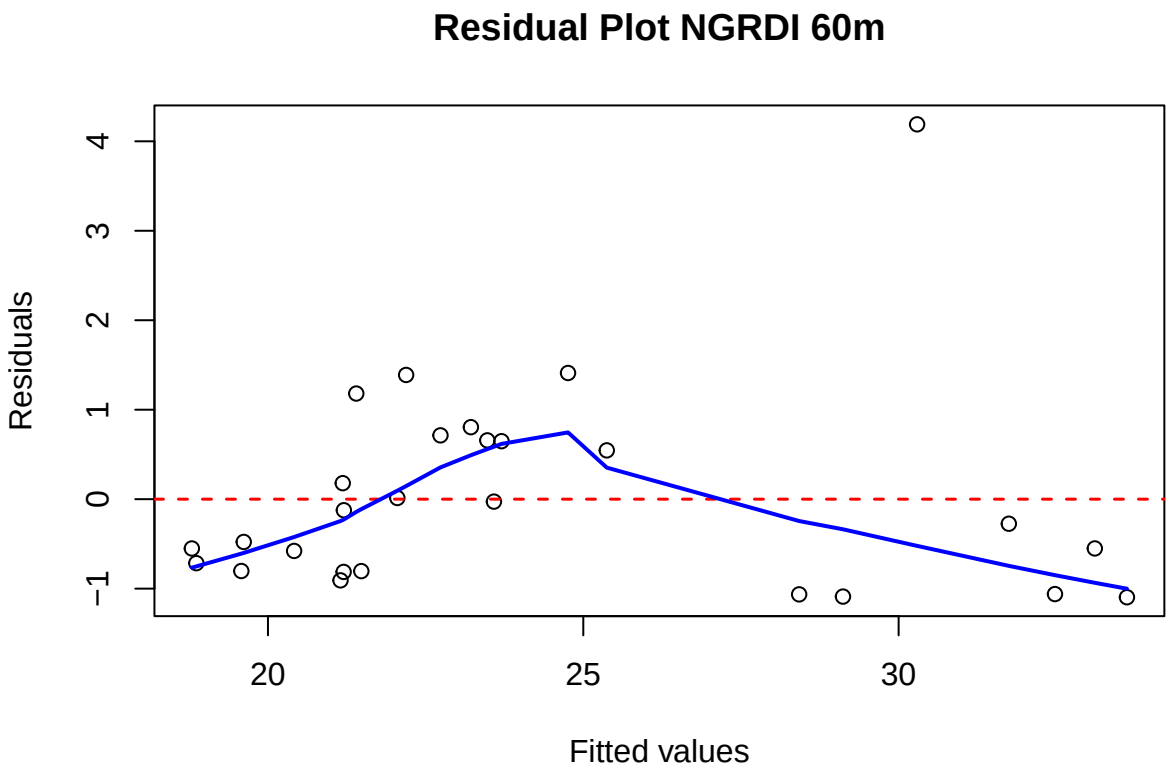


```
qqnorm(resNGRDI60m, main = "QQ Plot NGRDI 60m")
qqline(resNGRDI60m)
```

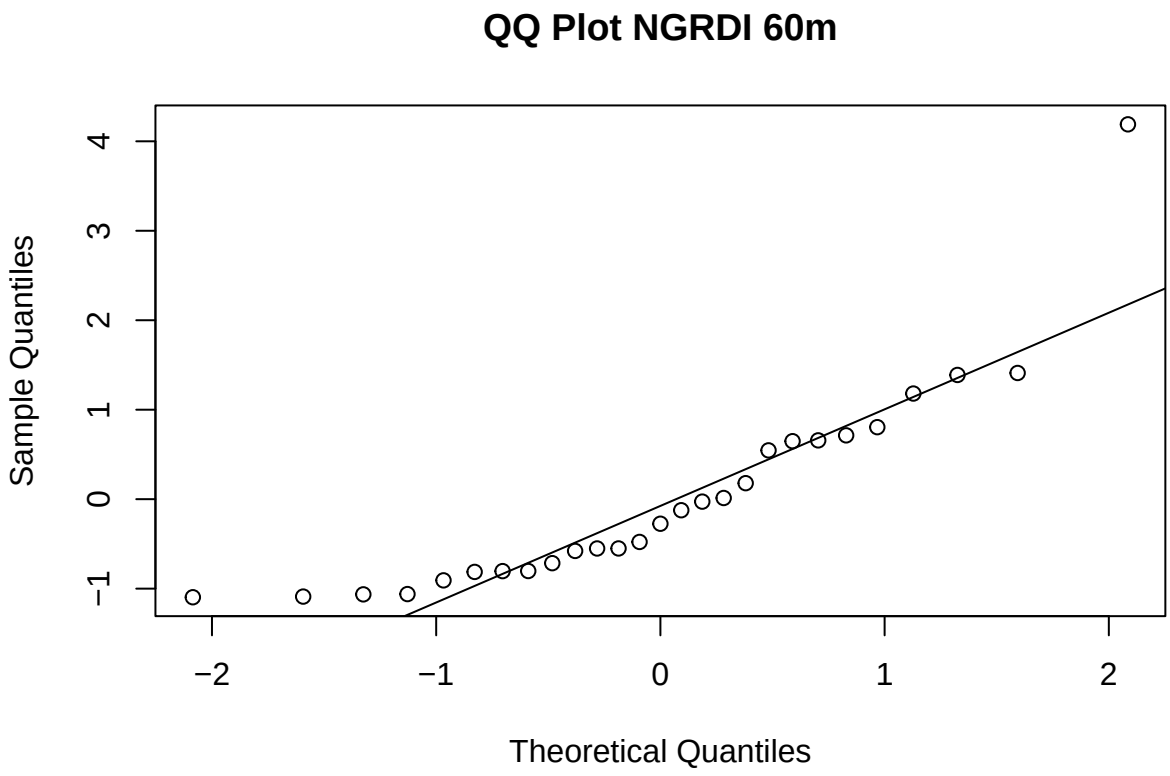


```r
##### NGRDI90m #####
resNGRDI90m <- residuals(fitNGRDI90m, type = "jackknife")
fittedNGRDI90m <- predict(fitNGRDI90m)[, 1]

plot(resNGRDI90m ~ fittedNGRDI90m, xlab = "Fitted values",
    ylab = "Residuals", main = "Residual Plot NGRDI 90m")
abline(h = 0, lwd = 1.5, col = "red", lty = 2)
lines(lowess(resNGRDI90m ~ fittedNGRDI90m), lwd = 2,
    col = "blue")
```

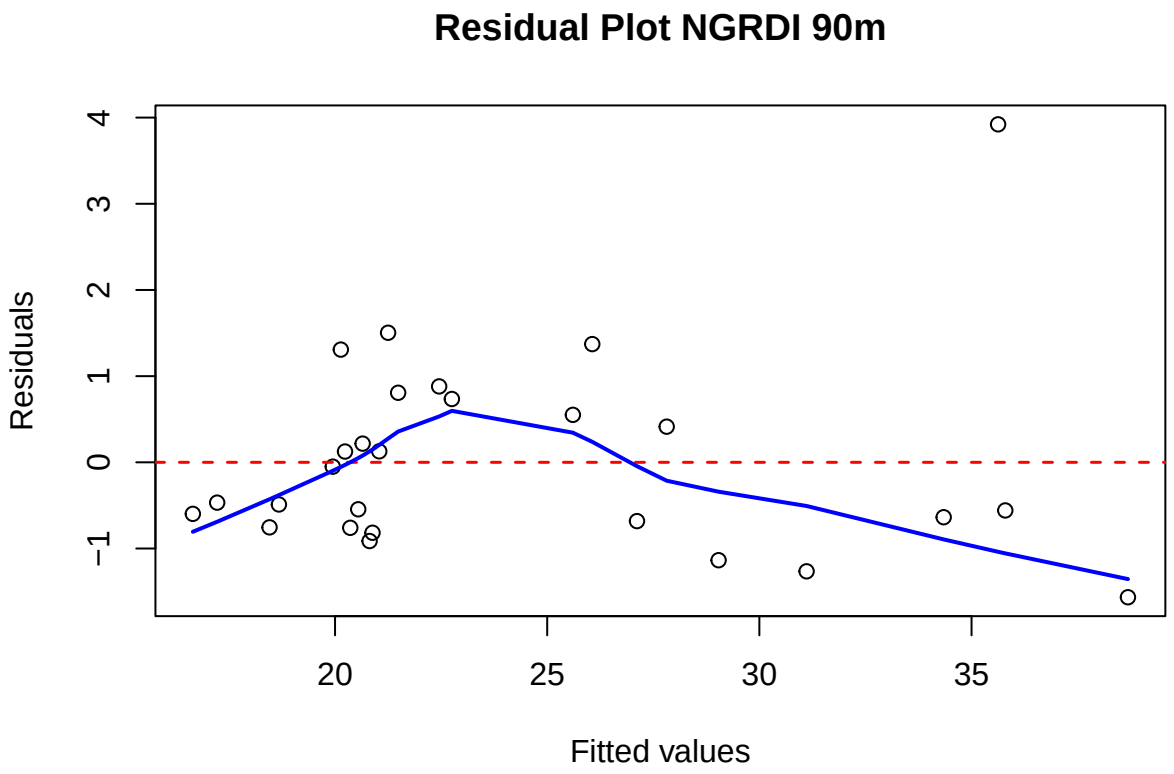


```
qqnorm(resNGRDI90m, main = "QQ Plot NGRDI 90m")
qqline(resNGRDI90m)
```

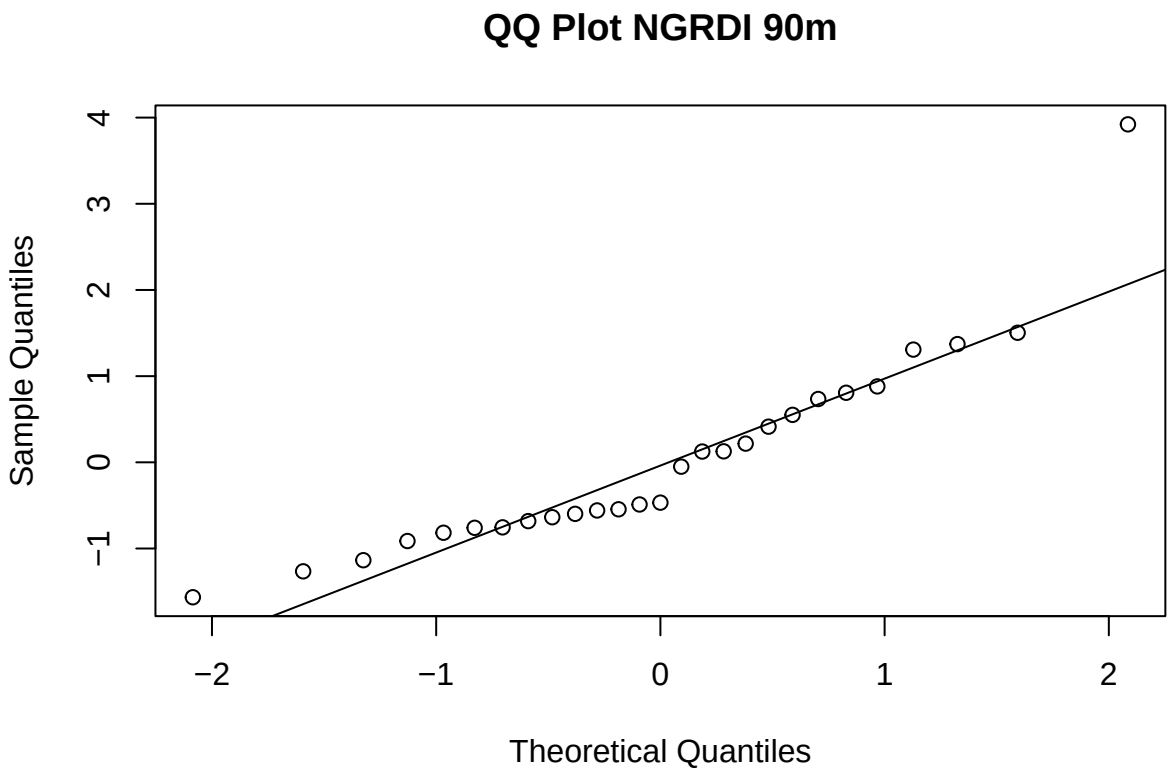


```
##### NGRDI120m #####
resNGRDI120m <- residuals(fitNGRDI120m, type = "jackknife")
fittedNGRDI120m <- predict(fitNGRDI120m)[, 1]

plot(resNGRDI120m ~ fittedNGRDI120m, xlab = "Fitted values",
    ylab = "Residuals", main = "Residual Plot NGRDI 120m")
abline(h = 0, lwd = 1.5, col = "red", lty = 2)
lines(lowess(resNGRDI120m ~ fittedNGRDI120m), lwd = 2,
    col = "blue")
```

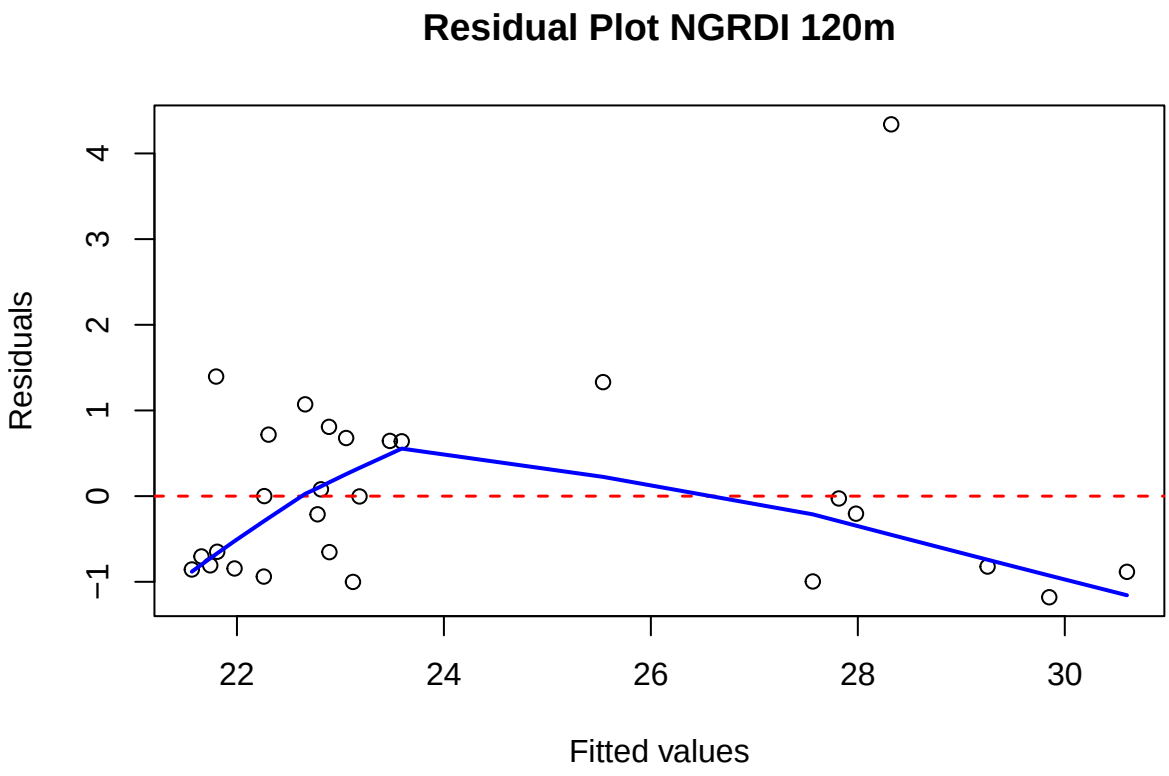


```
qqnorm(resNGRDI120m, main = "QQ Plot NGRDI 120m")
qqline(resNGRDI120m)
```

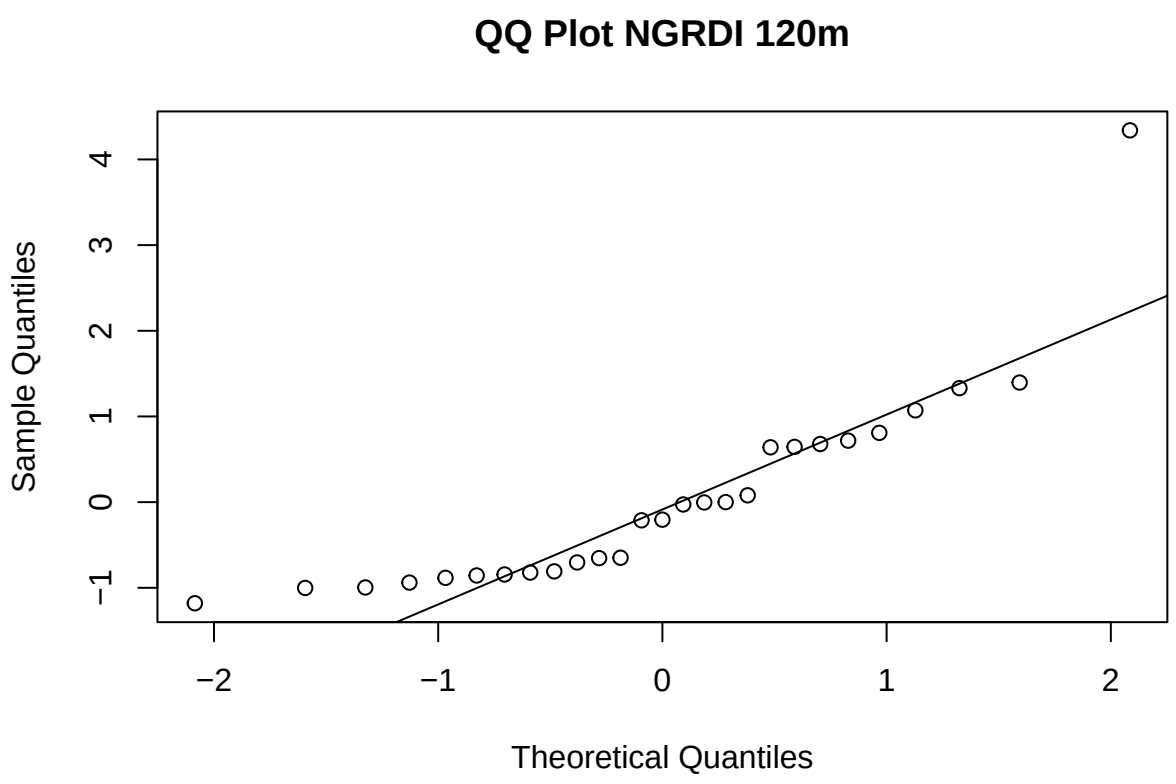


```
##### VDVI60m #####
resVDVI60m <- residuals(fitVDVI60m, type = "jackknife")
fittedVDVI60m <- predict(fitVDVI60m)[, 1]

plot(resVDVI60m ~ fittedVDVI60m, xlab = "Fitted values",
    ylab = "Residuals", main = "Residual Plot VDVI 60m")
abline(h = 0, lwd = 1.5, col = "red", lty = 2)
lines(lowess(resVDVI60m ~ fittedVDVI60m), lwd = 2,
    col = "blue")
```

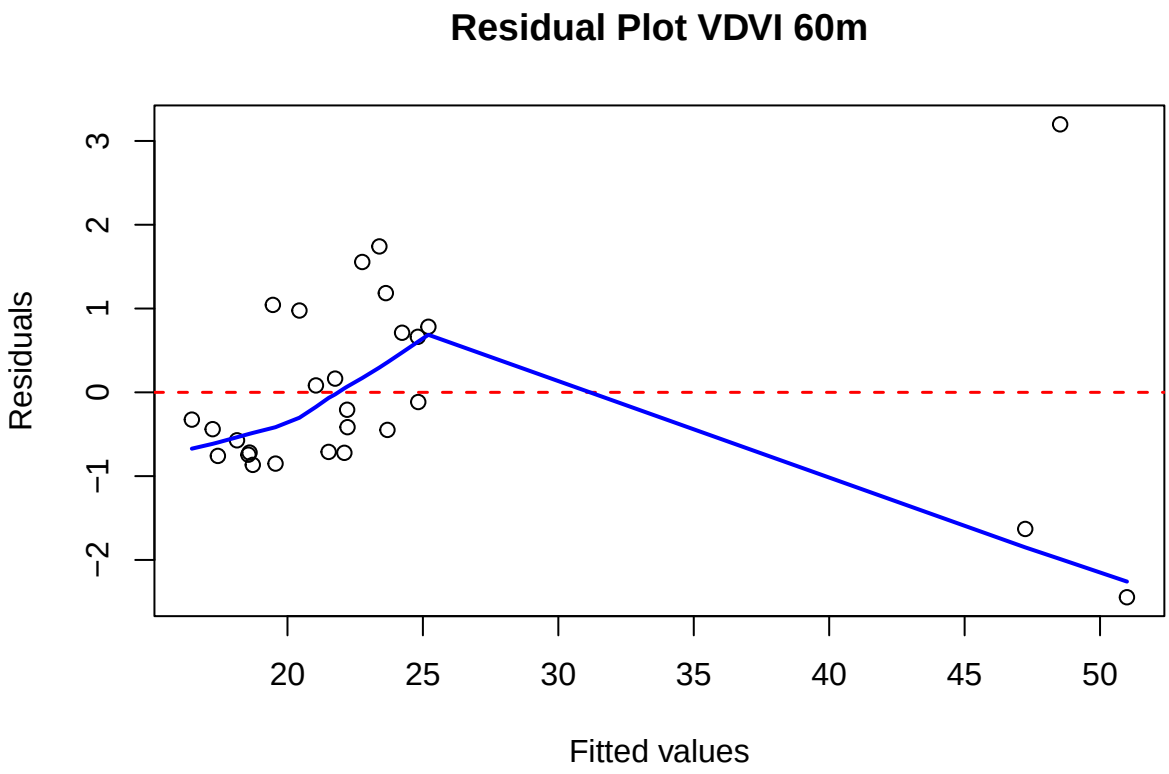


```
qqnorm(resVDVI60m, main = "QQ Plot VDVI 60m")
qqline(resVDVI60m)
```

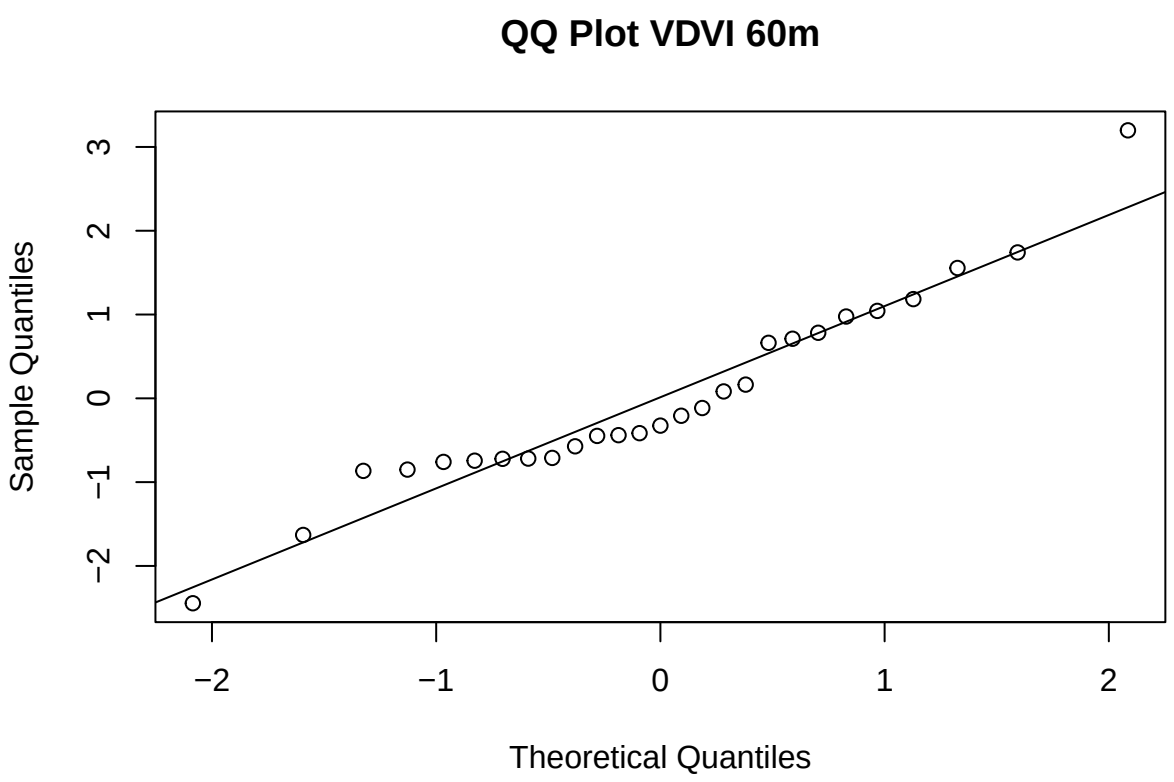


```
##### VDVI90m #####
resVDVI90m <- residuals(fitVDVI90m, type = "jackknife")
fittedVDVI90m <- predict(fitVDVI90m)[, 1]

plot(resVDVI90m ~ fittedVDVI90m, xlab = "Fitted values",
    ylab = "Residuals", main = "Residual Plot VDVI 90m")
abline(h = 0, lwd = 1.5, col = "red", lty = 2)
lines(lowess(resVDVI90m ~ fittedVDVI90m), lwd = 2,
    col = "blue")
```

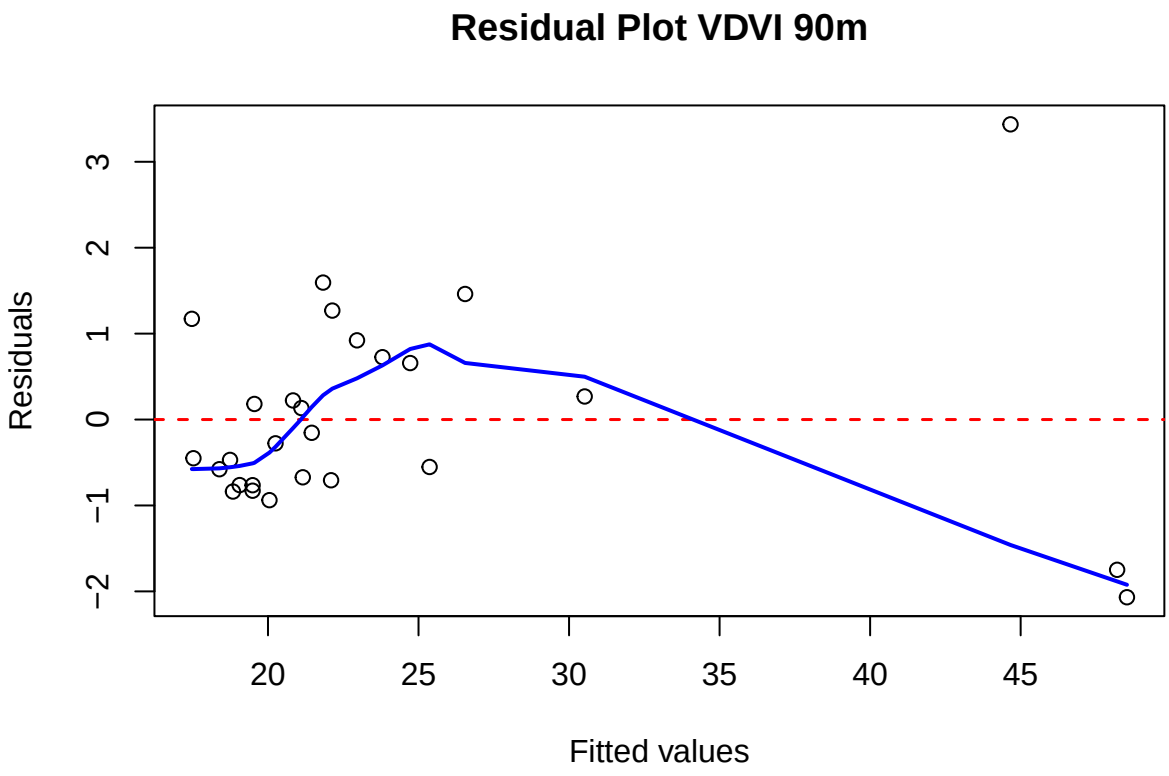


```
qqnorm(resVDVI90m, main = "QQ Plot VDVI 90m")
qqline(resVDVI90m)
```

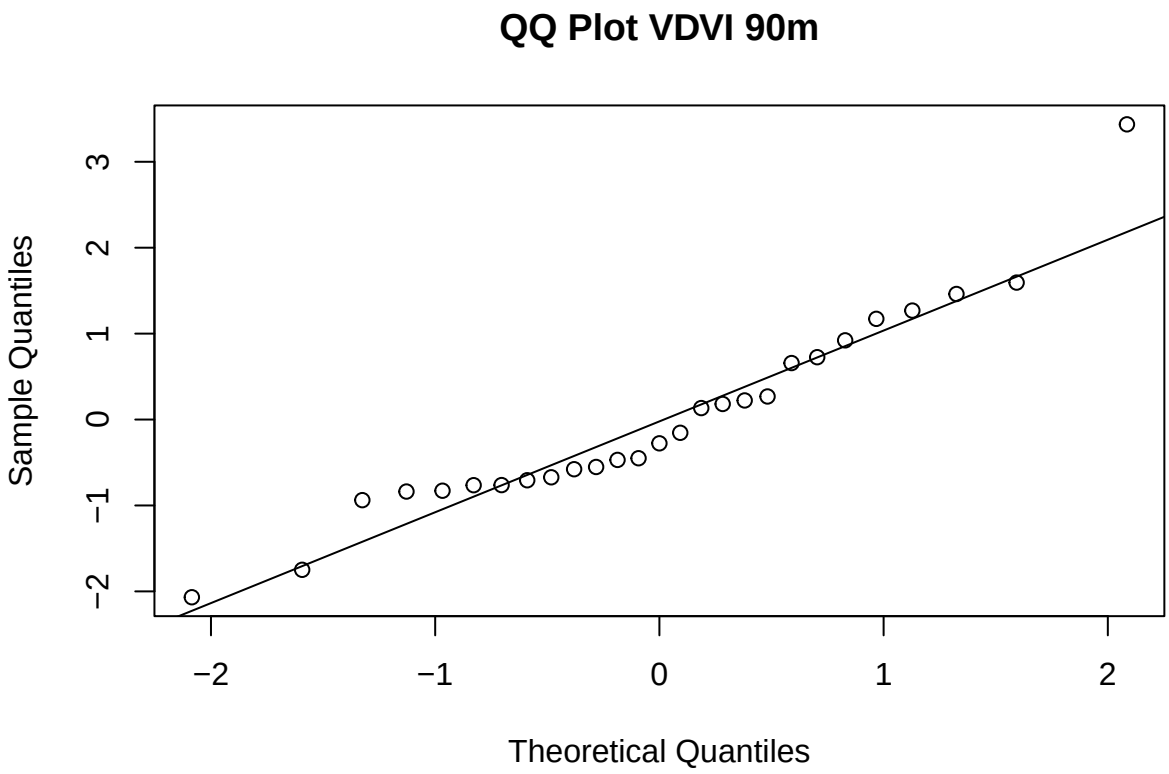


```
##### VDVI120m #####
resVDVI120m <- residuals(fitVDVI120m, type = "jackknife")
fittedVDVI120m <- predict(fitVDVI120m)[, 1]

plot(resVDVI120m ~ fittedVDVI120m, xlab = "Fitted values",
    ylab = "Residuals", main = "Residual Plot VDVI 120m")
abline(h = 0, lwd = 1.5, col = "red", lty = 2)
lines(lowess(resVDVI120m ~ fittedVDVI120m), lwd = 2,
    col = "blue")
```

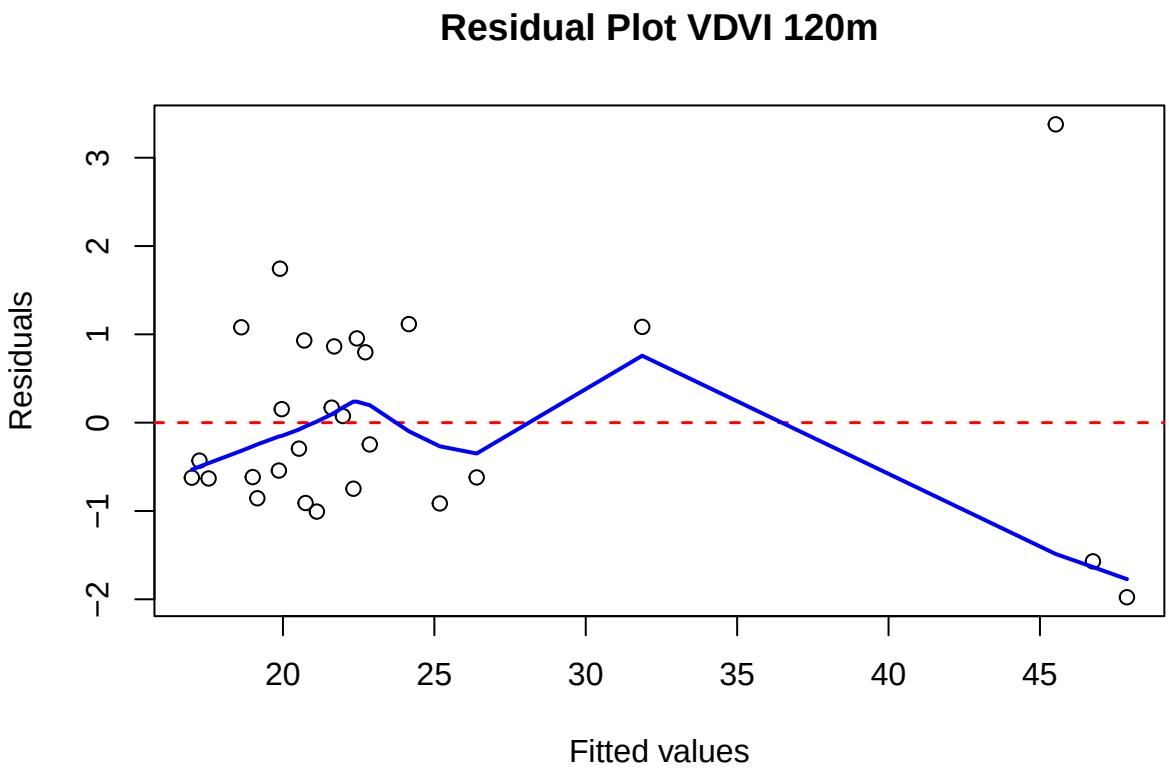


```
qqnorm(resVDVI120m, main = "QQ Plot VDVI 120m")
qqline(resVDVI120m)
```

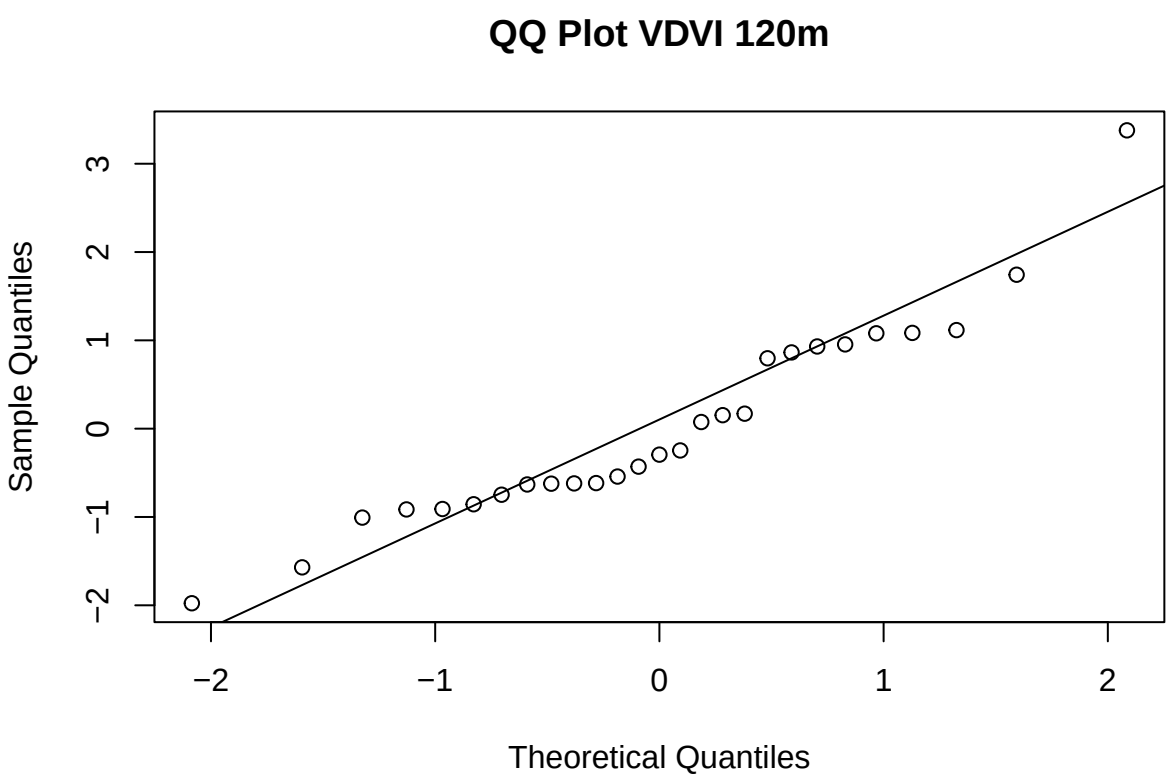
QQ Plot VDVI 120m
Sample Quantiles
Theoretical Quantiles
−2
−1
0
1
2
3

Inferential Statistics Analysis - Multispectral Imagery

This section will use 'dat4' to generate simple linear regression models and R^2 values for the multispectral imagery, for all sample events. Plots were created for each flight altitude by vegetation index.

```
## Reshape 'dat4' for use with ggplot(). Code is
## similar to RGB imagery inferential analysis.
dat4_long <- dat4 %>%
    pivot_longer(cols = matches("^(?:NDVI|BG|RVI|GNDVI|EVI)"),
        names_to = c("index_type", "elevation"), names_pattern = "([A-Z]*)([\\d]+m)",
        values_to = "veg_index") %>%
    mutate(elevation = factor(elevation, levels = c("60m",
        "90m", "120m"), labels = c("60m", "90m", "120m")))

## Repeat code that creates the 5 plots faceted
## by elevation
plotsdat4 <- dat4_long %>%
    group_by(index_type) %>%
    nest() %>%
    mutate(plot = map(data, ~ggplot(.x, aes(x = veg_index,
        y = Chla)) + geom_point() + facet_wrap("~ elevation",
        ncol = 3))) %>%
    pull(plot)

## Repeat code that calculates the regression
## equations and R^2 values
lm_eqn3 <- function(df) {
    m <- lm(Chla ~ veg_index, df)
    eq <- substitute(italic(y) == a + b %.% italic(x) *
        "," ~ ~italic(r)^2 ~ "=" ~ r2, list(a = format(unname(coef(m)[1]),
        digits = 3), b = format(unname(coef(m)[2]),
        digits = 3), r2 = format(summary(m)$r.squared,
        digits = 2)))
    as.character(as.expression(eq))
}

## Repeat code that labels the regression
## equations and R^2 values
dat4_labeled <- dat4_long %>%
    group_by(index_type, elevation) %>%
    nest() %>%
    mutate(Label = map(data, lm_eqn3)) %>%
    select(index_type, elevation, Label) %>%
    unnest(Label) %>%
    ungroup()

## Repeat code that generates the plots
index_types <- c("NDVI", "BG", "RVI", "GNDVI", "EVI")
plots2_list <- lapply(index_types, function(x) {
    .x <- dat4_long %>%
        filter(index_type == x)
    .y <- dat4_labeled %>%
```

```
        filter(index_type == x)
    gdat4 <- ggplot(.x, aes(x = veg_index, y = Chla)) +
        geom_point() + geom_smooth(method = "lm", formula = "y ~ x",
        color = "black", linewidth = 0.5, alpha = 0.6) +
        geom_text(data = .y, mapping = aes(x = median(.x$veg_index +
            0.005, na.rm = TRUE), y = max(.x$Chla,
            na.rm = TRUE) * 1.4, label = Label), parse = TRUE,
            size = 2.5, nudge_y = -0.05) + facet_wrap("elevation",
        ncol = 3, scales = "free_x") + labs(title = paste(x,
        "Vegetation Index Regression Analysis"), x = "Index Spectral Value",
        y = "Chlorophyll a Concentration (µg/L)") +
        theme(plot.title = element_text(hjust = 0.5)) +
        theme_bw()
    ggsave(paste(x, "Vegetation Index and Elevation Plots.png"))
    return(gdat4)
})
plots2_list
```

```
## [[1]]
```

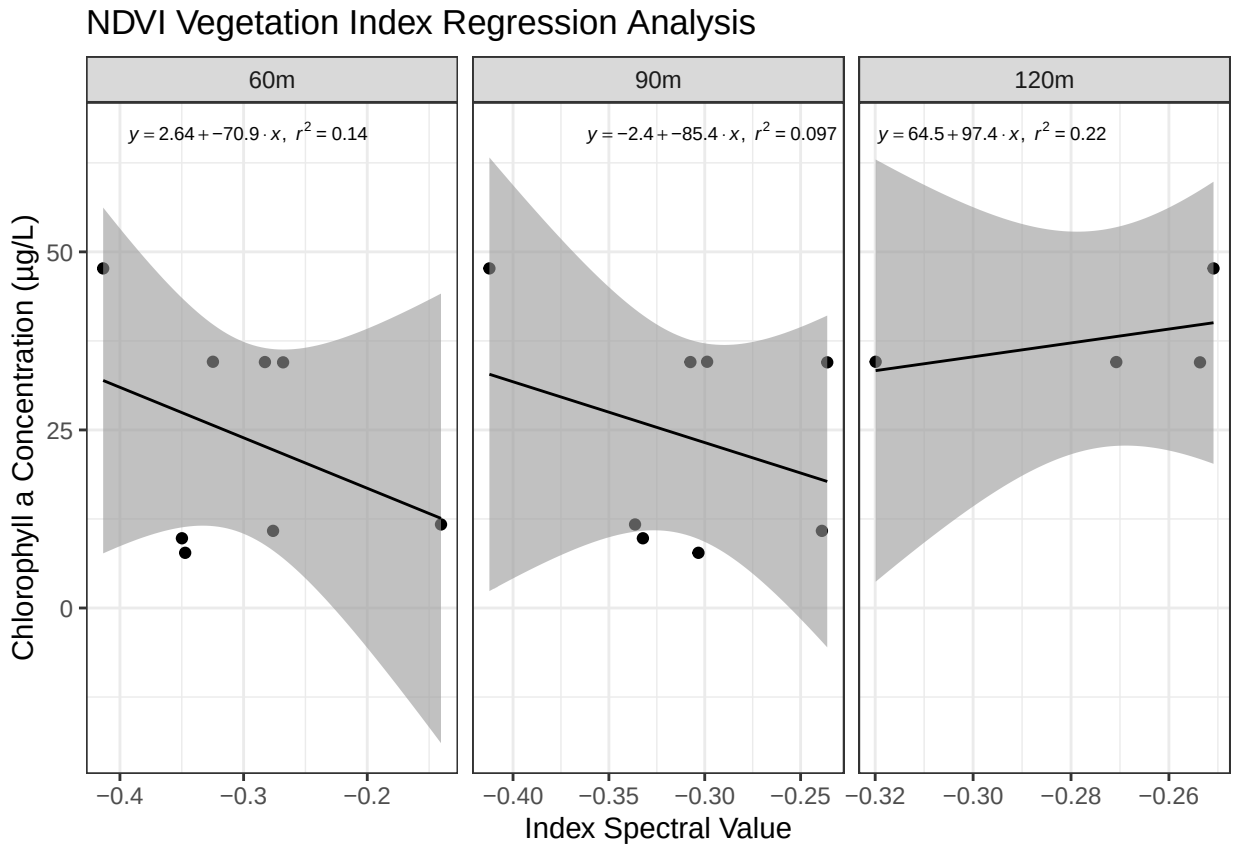


```
##
## [[2]]
```

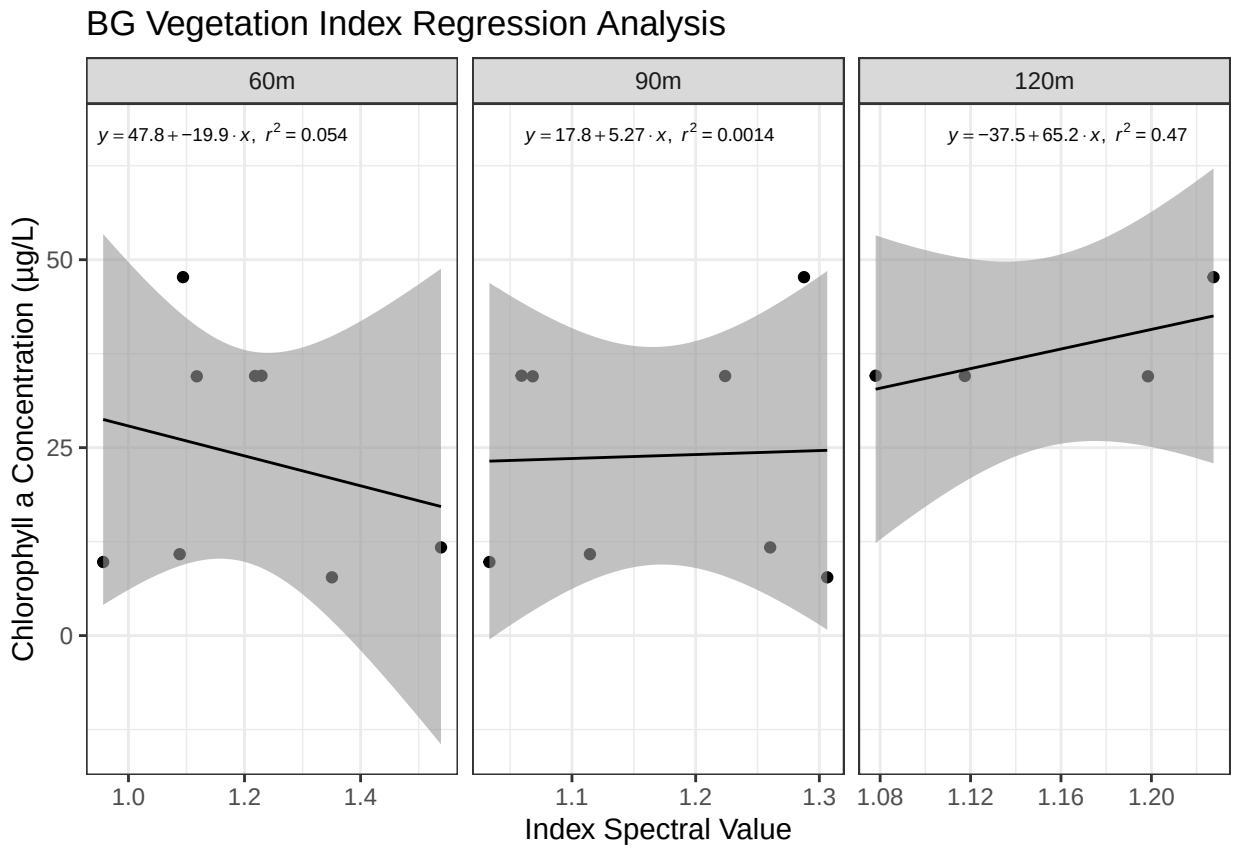
BG Vegetation Index Regression Analysis
60m
90m
120m
y = 47.8 + −19.9 · x, r² = 0.054
y = 17.8 + 5.27 · x, r² = 0.0014
y = −37.5 + 65.2 · x, r² = 0.47
Chlorophyll a Concentration (µg/L)
50
25
0
1.0
1.2
1.4
1.1
1.2
1.3
1.08
1.12
1.16
1.20
Index Spectral Value

```
##
## [[3]]
```

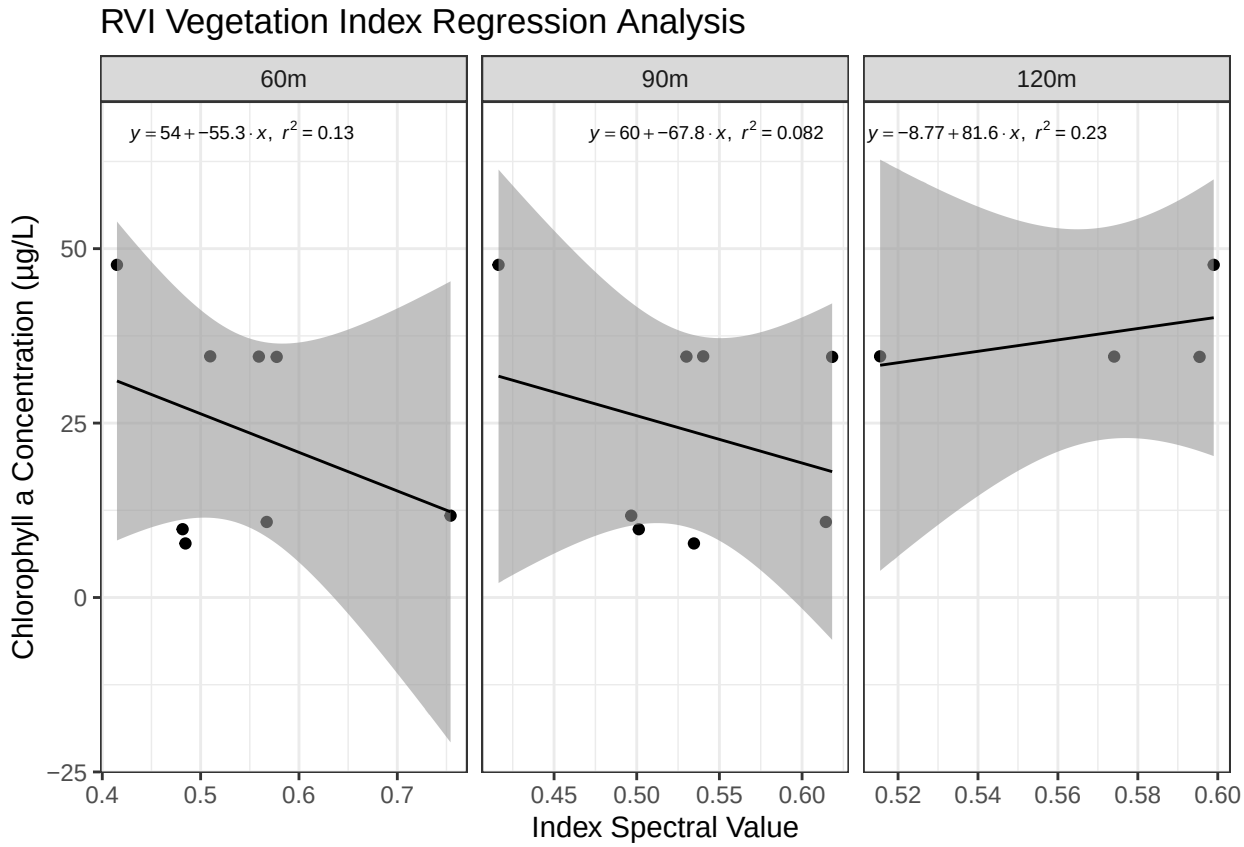
RVI Vegetation Index Regression Analysis
60m
90m
120m
y = 54 + −55.3 · x, r² = 0.13
y = 60 + −67.8 · x, r² = 0.082
y = −8.77 + 81.6 · x, r² = 0.23
Chlorophyll a Concentration (µg/L)
50
25
0
−25
0.4
0.5
0.6
0.7
0.45
0.50
0.55
0.60
0.52
0.54
0.56
0.58
0.60
Index Spectral Value

```
##
## [[4]]
```

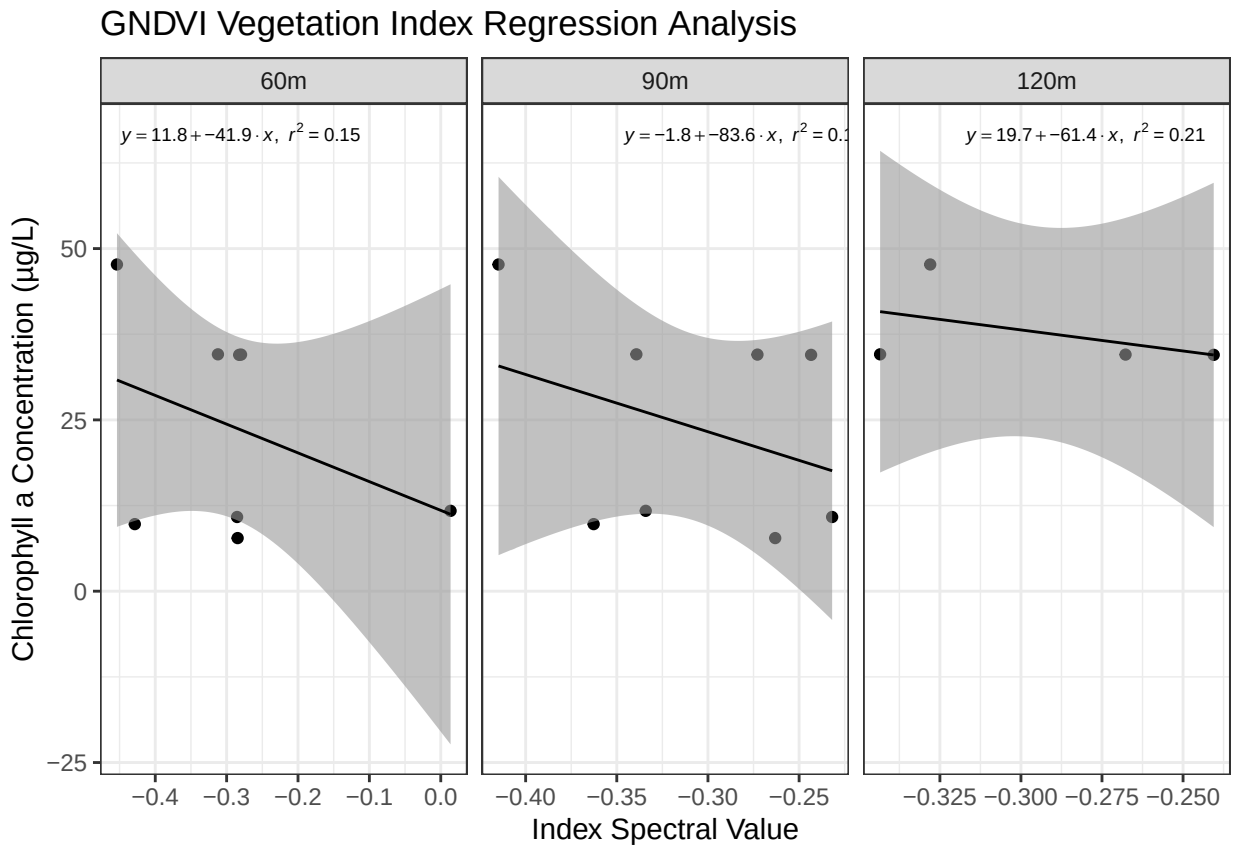
GNDVI Vegetation Index Regression Analysis
60m
90m
120m
y = 11.8 + −41.9 · x, r² = 0.15
y = −1.8 + −83.6 · x, r² = 0.1
y = 19.7 + −61.4 · x, r² = 0.21
Chlorophyll a Concentration (µg/L)
50
25
0
−25
−0.4
−0.3
−0.2
−0.1
0.0
−0.40
−0.35
−0.30
−0.25
−0.325
−0.300
−0.275
−0.250
Index Spectral Value

```
##
## [[5]]
```

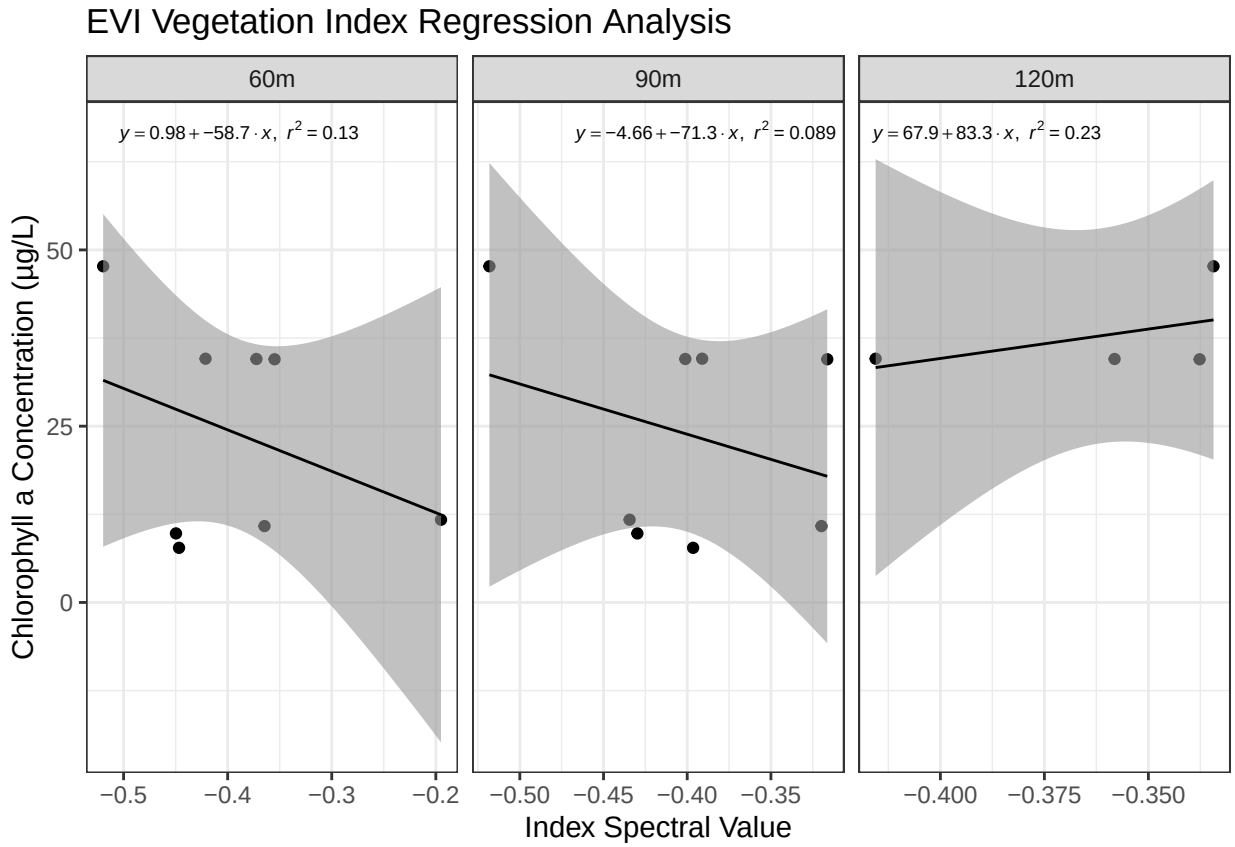
EVI Vegetation Index Regression Analysis
60m
90m
120m
y = 0.98 + −58.7 · x, r² = 0.13
y = −4.66 + −71.3 · x, r² = 0.089
y = 67.9 + 83.3 · x, r² = 0.23
Chlorophyll a Concentration (µg/L)
50
25
0
−0.5
−0.4
−0.3
−0.2
−0.50
−0.45
−0.40
−0.35
−0.400
−0.375
−0.350
Index Spectral Value

This section will use 'dat4' to generate plots for each individual regression model for the multispectral imagery.

```
## Create linear regression models comparing
## chlorophyll-a concentrations as a function of
## the multispectral index values, at each flight
## altitude, for all multispectral sampling
## events.

##### NDVI ##### Fit a simple linear regression
##### model with dependent variable 'Chla' and
##### independent variable 'NDVI60m' Call
##### variable after defining
fitNDVI60m <- regress("mean", Chla ~ NDVI60m, robustSE = FALSE,
    data = dat4)
fitNDVI60m
```

```
##
## Call:
## regress(fnctl = "mean", formula = Chla ~ NDVI60m, data = dat4,
##     robustSE = FALSE)
##
## Residuals:
##     Min      1Q  Median      3Q     Max
## -19.494 -12.943   4.031  12.106  15.737
##
## Coefficients:
##                   Estimate  Std Err   95%L         95%H         F stat    df
## [1] Intercept      2.638     22.58    -52.62        57.89           0.01 1
## [2] NDVI60m       -70.86     72.91    -249.3        107.5           0.94 1
##                   Pr(>F)
## [1] Intercept      0.9108
## [2] NDVI60m        0.3686
##
## Residual standard error: 15.57 on 6 degrees of freedom
## Multiple R-squared:  0.136,  Adjusted R-squared:  -0.007983
## F-statistic: 0.9446 on 1 and 6 DF,  p-value: 0.3686
```

```
## Create a scatterplot for 'fitNDVI60m'
plot(dat4$NDVI60m, dat4$Chla, xlab = "NDVI 60m Spectral Index Value",
    ylab = "Chlorophyll-a (µg/L)", pch = 20)
## Add a fitted regression line to the model
abline(lm(Chla ~ NDVI60m, data = dat4))
```

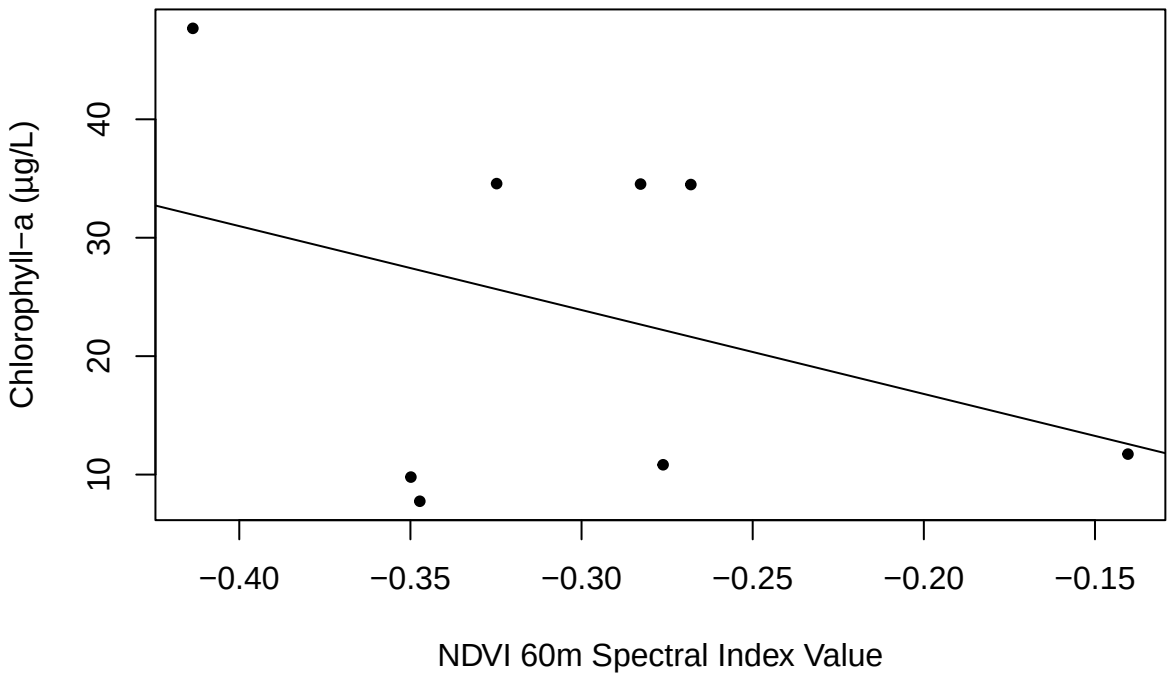


```
## Fit a simple linear regression model with
## dependent variable 'Chla' and independent
## variable 'NDVI90m' Call variable after
## defining
fitNDVI90m <- regress("mean", Chla ~ NDVI90m, robustSE = FALSE,
    data = dat4)
fitNDVI90m
```

```
##
## Call:
## regress(fnctl = "mean", formula = Chla ~ NDVI90m, data = dat4,
##     robustSE = FALSE)
##
## Residuals:
##     Min      1Q  Median      3Q     Max
## -16.188 -14.886   1.748  12.307  16.725
##
## Coefficients:
##                  Estimate  Std Err   95%L         95%H         F stat    df
## [1] Intercept     -2.397     33.31    -83.90        79.11           0.01 1
## [2] NDVI90m       -85.40     106.5    -346.1        175.3           0.64 1
##                  Pr(>F)
## [1] Intercept      0.9450
## [2] NDVI90m        0.4533
##
## Residual standard error: 15.92 on 6 degrees of freedom
```

```
## Multiple R-squared:  0.09675,    Adjusted R-squared:  -0.05379
## F-statistic: 0.6427 on 1 and 6 DF,  p-value: 0.4533
```

```
## Create a scatterplot for 'fitNDVI90m'
plot(dat4$NDVI90m, dat4$Chla, xlab = "NDVI 90m Spectral Index Value",
    ylab = "Chlorophyll-a (µg/L)", pch = 20)
## Add a fitted regression line to the model
abline(lm(Chla ~ NDVI90m, data = dat4))
```

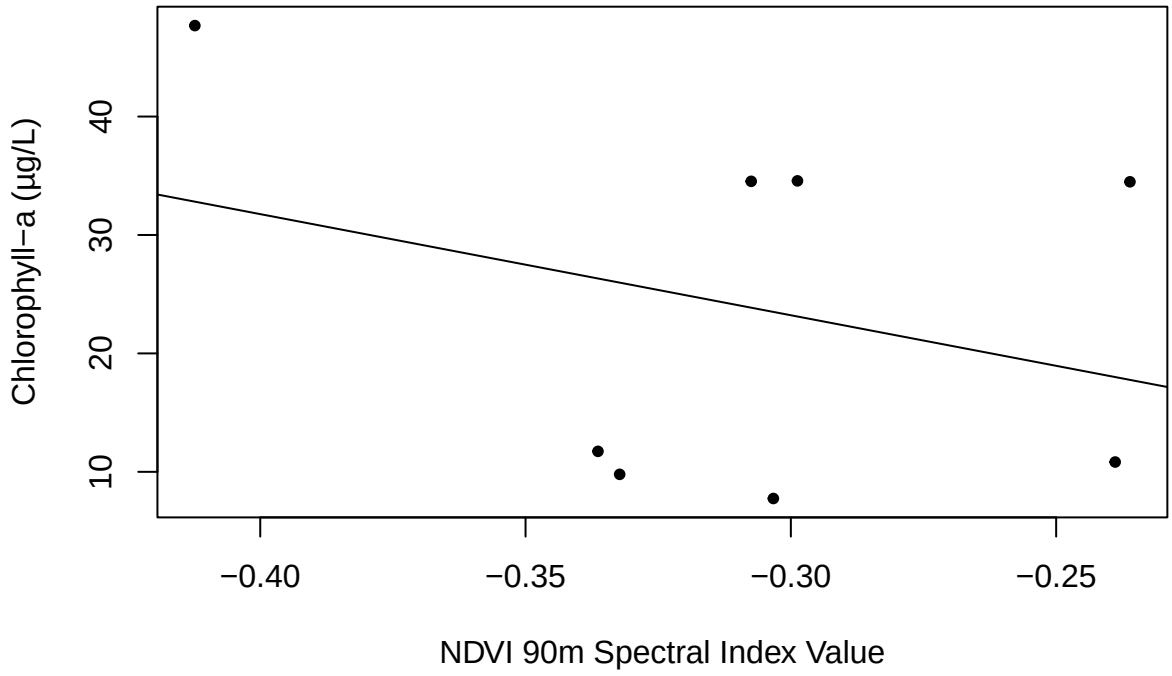


```
## Fit a simple linear regression model with
## dependent variable 'Chla' and independent
## variable 'NDVI120m' Call variable after
## defining
fitNDVI120m <- regress("mean", Chla ~ NDVI120m, robustSE = FALSE,
    data = dat4)
fitNDVI120m
```

```
## ( 4  cases deleted due to missing values)
##
##
## Call:
## regress(fnctl = "mean", formula = Chla ~ NDVI120m, data = dat4,
##     robustSE = FALSE)
##
## Residuals:
```

```
##      5      6      7      8
##  7.632 -5.290  1.243 -3.585
##
## Coefficients:
##                   Estimate  Std Err   95%L         95%H         F stat    df
## [1] Intercept      64.48     35.25    -87.21        216.2           3.35 1
## [2] NDVI120m       97.39     128.1    -453.8        648.6           0.58 1
##                   Pr(>F)
## [1] Intercept      0.2089
## [2] NDVI120m       0.5265
##
## Residual standard error: 7.093 on 2 degrees of freedom
##   (4 observations deleted due to missingness)
## Multiple R-squared:  0.2242, Adjusted R-squared:  -0.1637
## F-statistic: 0.5779 on 1 and 2 DF,  p-value: 0.5265
```

```
## Create a scatterplot for 'fitNDVI120m'
plot(dat4$NDVI120m, dat4$Chla, xlab = "NDVI 120m Spectral Index Value",
    ylab = "Chlorophyll-a (µg/L)", pch = 20)
## Add a fitted regression line to the model
abline(lm(Chla ~ NDVI120m, data = dat4))
```

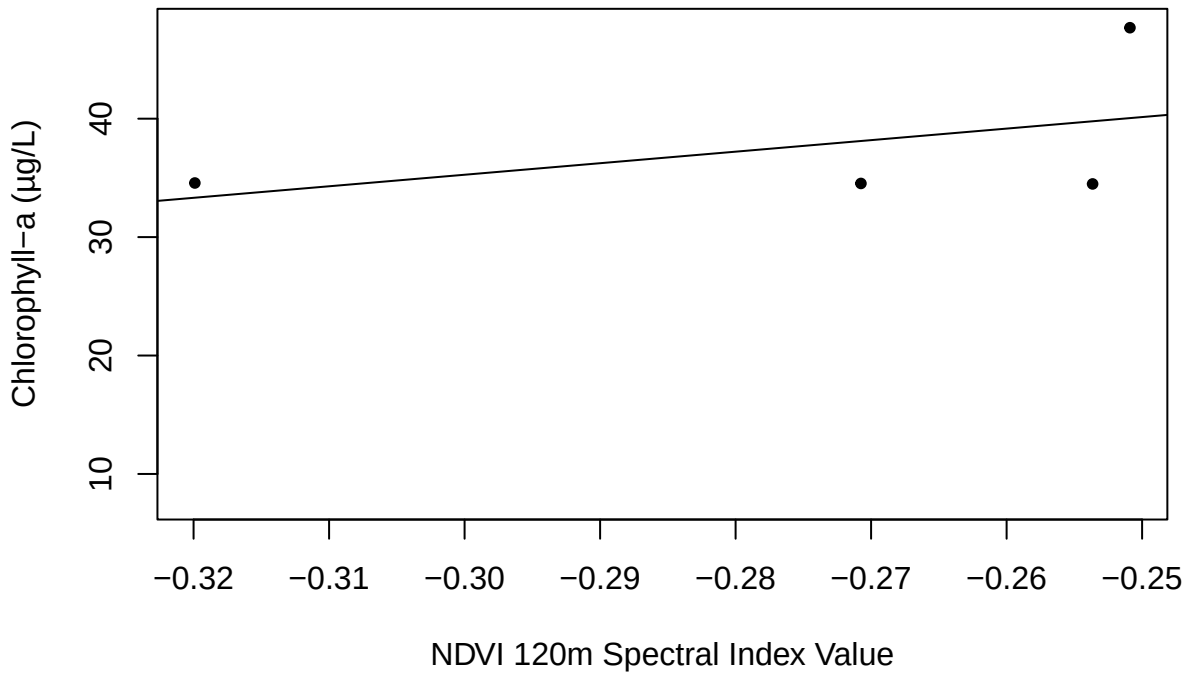


```
##### BG ##### Fit a simple linear regression
##### model with dependent variable 'Chla' and
##### independent variable 'BG60m' Call variable
```

```r
##### after defining
fitBG60m <- regress("mean", Chla ~ BG60m, robustSE = FALSE,
    data = dat4)
fitBG60m
```

```
##
## Call:
## regress(fnctl = "mean", formula = Chla ~ BG60m, data = dat4,
##     robustSE = FALSE)
##
## Residuals:
##     Min      1Q  Median      3Q     Max
## -18.960 -13.692   1.756  11.053  21.667
##
## Coefficients:
##                  Estimate  Std Err   95%L         95%H         F stat    df
## [1] Intercept      47.78     41.30    -53.27        148.8           1.34 1
## [2] BG60m         -19.90     34.10    -103.3        63.55           0.34 1
##                  Pr(>F)
## [1] Intercept      0.2913
## [2] BG60m          0.5809
##
## Residual standard error: 16.29 on 6 degrees of freedom
## Multiple R-squared:  0.05368,    Adjusted R-squared:  -0.104
## F-statistic: 0.3404 on 1 and 6 DF,  p-value: 0.5809
```

```r
## Create a scatterplot for 'fitBG60m'
plot(dat4$BG60m, dat4$Chla, xlab = "BG 60m Spectral Index Value",
    ylab = "Chlorophyll-a (µg/L)", pch = 20)
## Add a fitted regression line to the model
abline(lm(Chla ~ BG60m, data = dat4))
```

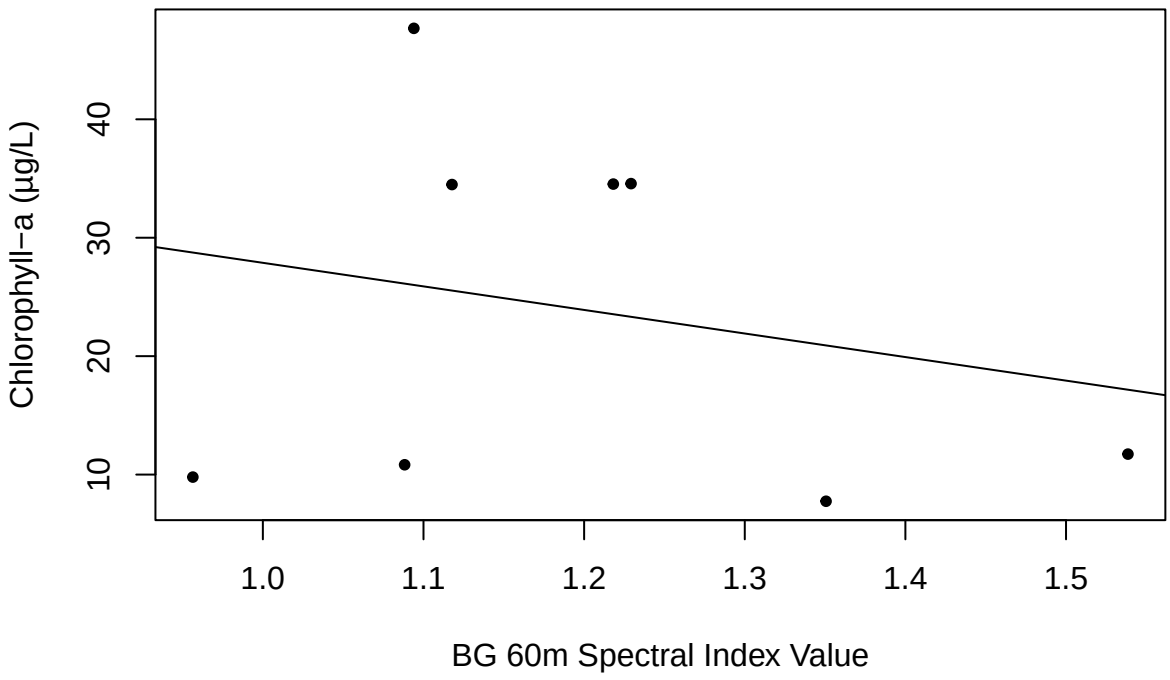


```
## Fit a simple linear regression model with
## dependent variable 'Chla' and independent
## variable 'BG90m' Call variable after defining
fitBG90m <- regress("mean", Chla ~ BG90m, robustSE = FALSE,
    data = dat4)
fitBG90m
```

```
##
## Call:
## regress(fnctl = "mean", formula = Chla ~ BG90m, data = dat4,
##     robustSE = FALSE)
##
## Residuals:
##     Min      1Q  Median      3Q     Max
## -16.894 -12.957  -1.175  11.132  23.135
##
## Coefficients:
##                  Estimate  Std Err   95%L        95%H        F stat    df
## [1] Intercept      17.76     66.28    -144.4       180.0          0.07 1
## [2] BG90m          5.266     56.47    -132.9       143.4          0.01 1
##                  Pr(>F)
## [1] Intercept      0.7977
## [2] BG90m          0.9287
##
## Residual standard error: 16.74 on 6 degrees of freedom
## Multiple R-squared:  0.001447,   Adjusted R-squared:  -0.165
```

```
## F-statistic: 0.008696 on 1 and 6 DF,  p-value: 0.9287
```

```
## Create a scatterplot for 'fitBG90m'
plot(dat4$BG90m, dat4$Chla, xlab = "BG 90m Spectral Index Value",
    ylab = "Chlorophyll-a (µg/L)", pch = 20)
## Add a fitted regression line to the model
abline(lm(Chla ~ BG90m, data = dat4))
```

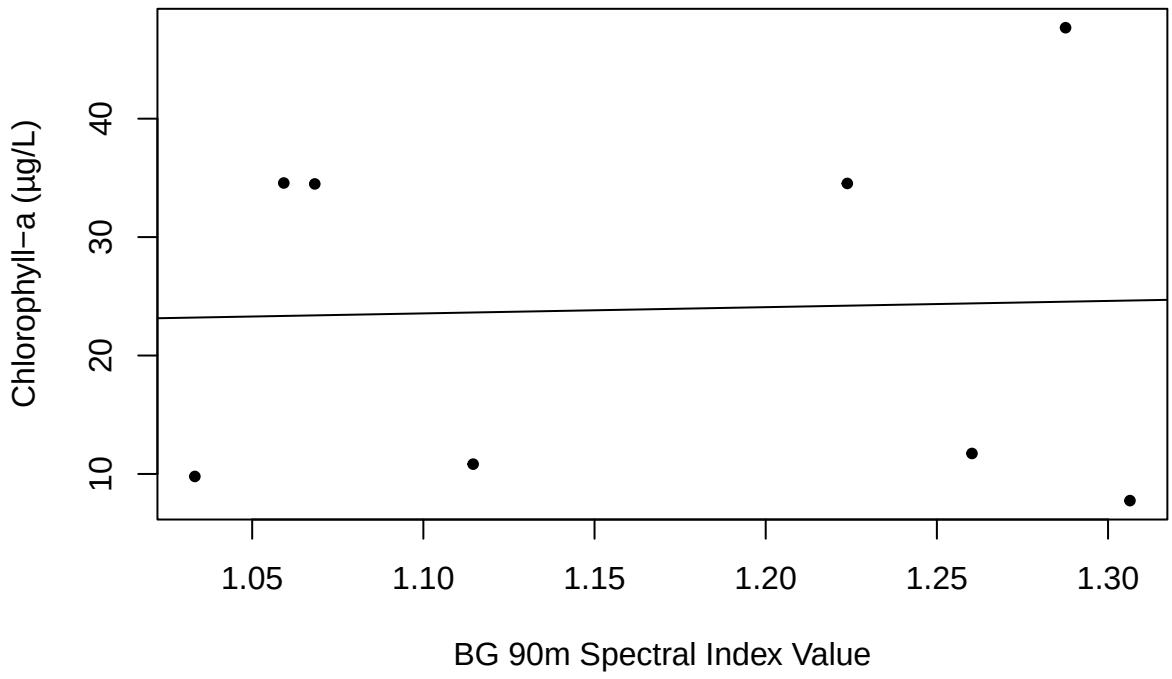


```
## Fit a simple linear regression model with
## dependent variable 'Chla' and independent
## variable 'BG120m' Call variable after defining
fitBG120m <- regress("mean", Chla ~ BG120m, robustSE = FALSE,
    data = dat4)
fitBG120m
```

```
## ( 4  cases deleted due to missing values)
##
##
## Call:
## regress(fnctl = "mean", formula = Chla ~ BG120m, data = dat4,
##     robustSE = FALSE)
##
## Residuals:
##      5      6      7      8
##  5.162 -6.137  1.793 -0.818
```

```
##
## Coefficients:
##                  Estimate  Std Err   95%L         95%H         F stat    df
## [1] Intercept     -37.48     56.15    -279.1        204.1           0.45 1
## [2] BG120m         65.17     48.53    -143.6        274.0           1.80 1
##                  Pr(>F)
## [1] Intercept      0.5732
## [2] BG120m         0.3114
##
## Residual standard error: 5.84 on 2 degrees of freedom
##   (4 observations deleted due to missingness)
## Multiple R-squared:  0.4741, Adjusted R-squared:  0.2112
## F-statistic: 1.803 on 1 and 2 DF,  p-value: 0.3114
```

```
## Create a scatterplot for 'fitBG120m'
plot(dat4$BG120m, dat4$Chla, xlab = "BG 120m Spectral Index Value",
    ylab = "Chlorophyll-a (µg/L)", pch = 20)
## Add a fitted regression line to the model
abline(lm(Chla ~ BG120m, data = dat4))
```

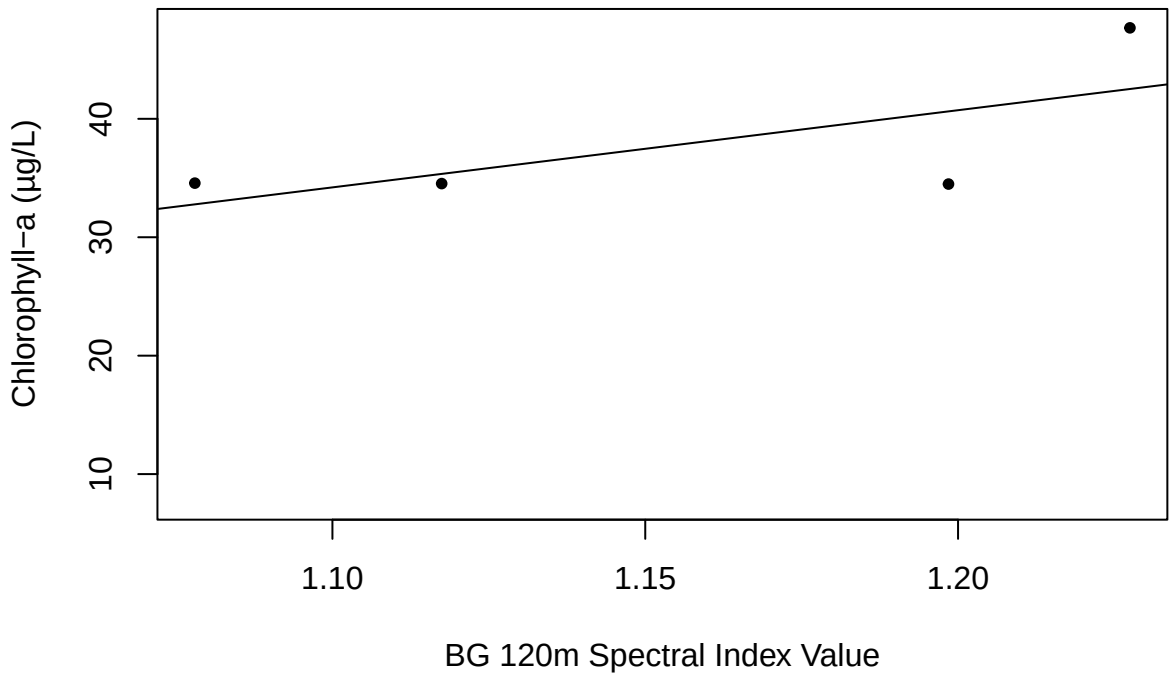


```
##### RVI ##### Fit a simple linear regression
##### model with dependent variable 'Chla' and
##### independent variable 'RVI60m' Call variable
##### after defining
fitRVI60m <- regress("mean", Chla ~ RVI60m, robustSE = FALSE,
```

```
    data = dat4)
fitRVI60m
```

```
##
## Call:
## regress(fnctl = "mean", formula = Chla ~ RVI60m, data = dat4,
##     robustSE = FALSE)
##
## Residuals:
##     Min      1Q  Median      3Q     Max
## -19.435 -13.228   4.113  11.713  16.644
##
## Coefficients:
##                   Estimate  Std Err   95%L         95%H         F stat    df
## [1] Intercept      53.98     32.30    -25.05        133.0           2.79 1
## [2] RVI60m        -55.29     58.53    -198.5        87.93           0.89 1
##                   Pr(>F)
## [1] Intercept      0.1457
## [2] RVI60m         0.3813
##
## Residual standard error: 15.63 on 6 degrees of freedom
## Multiple R-squared:  0.1295, Adjusted R-squared:  -0.01561
## F-statistic: 0.8924 on 1 and 6 DF,  p-value: 0.3813
```

```
## Create a scatterplot for 'fitRVI60m'
plot(dat4$RVI60m, dat4$Chla, xlab = "RVI 60m Spectral Index Value",
    ylab = "Chlorophyll-a (µg/L)", pch = 20)
## Add a fitted regression line to the model
abline(lm(Chla ~ RVI60m, data = dat4))
```

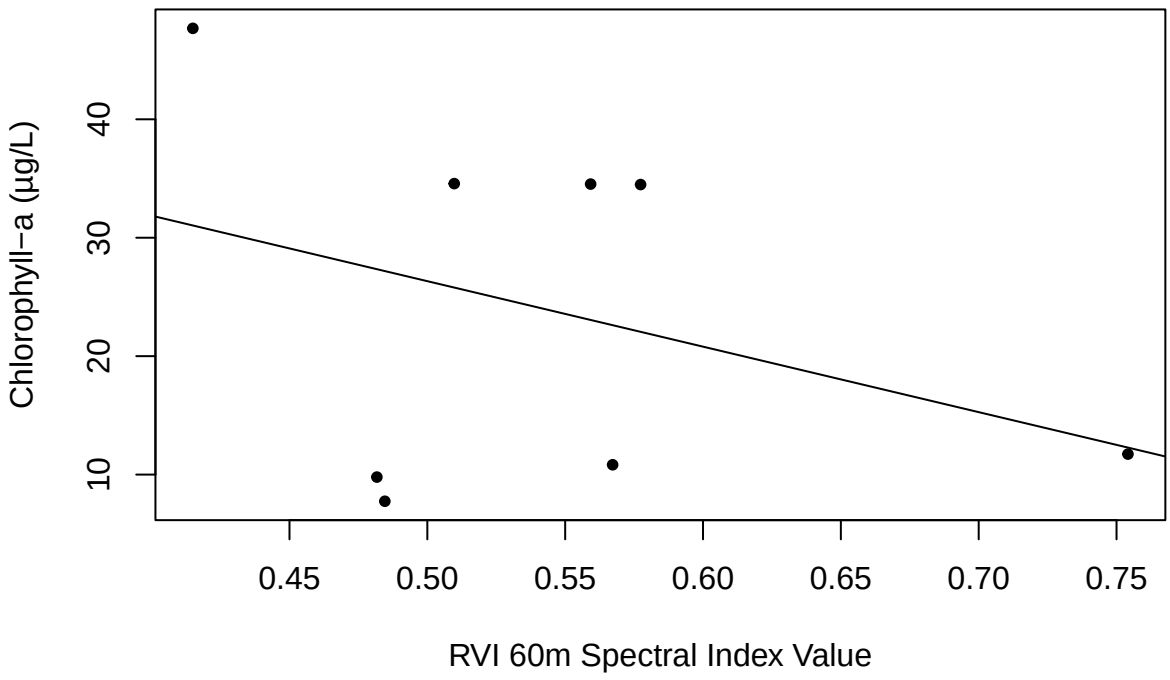


```
## Fit a simple linear regression model with
## dependent variable 'Chla' and independent
## variable 'RVI90m' Call variable after defining
fitRVI90m <- regress("mean", Chla ~ RVI90m, robustSE = FALSE,
    data = dat4)
fitRVI90m
```

```
##
## Call:
## regress(fnctl = "mean", formula = Chla ~ RVI90m, data = dat4,
##     robustSE = FALSE)
##
## Residuals:
##     Min      1Q  Median      3Q     Max
## -16.181 -14.903   1.522  12.420  16.448
##
## Coefficients:
##                  Estimate  Std Err   95%L         95%H         F stat    df
## [1] Intercept      59.96     49.71    -61.68        181.6           1.45 1
## [2] RVI90m        -67.81     92.92    -295.2        159.6           0.53 1
##                  Pr(>F)
## [1] Intercept      0.2731
## [2] RVI90m         0.4931
##
## Residual standard error: 16.05 on 6 degrees of freedom
## Multiple R-squared:  0.08151,    Adjusted R-squared:  -0.07157
```

```
## F-statistic: 0.5325 on 1 and 6 DF,  p-value: 0.4931
```

```
## Create a scatterplot for 'fitRVI90m'
plot(dat4$RVI90m, dat4$Chla, xlab = "RVI 90m Spectral Index Value",
    ylab = "Chlorophyll-a (µg/L)", pch = 20)
## Add a fitted regression line to the model
abline(lm(Chla ~ RVI90m, data = dat4))
```

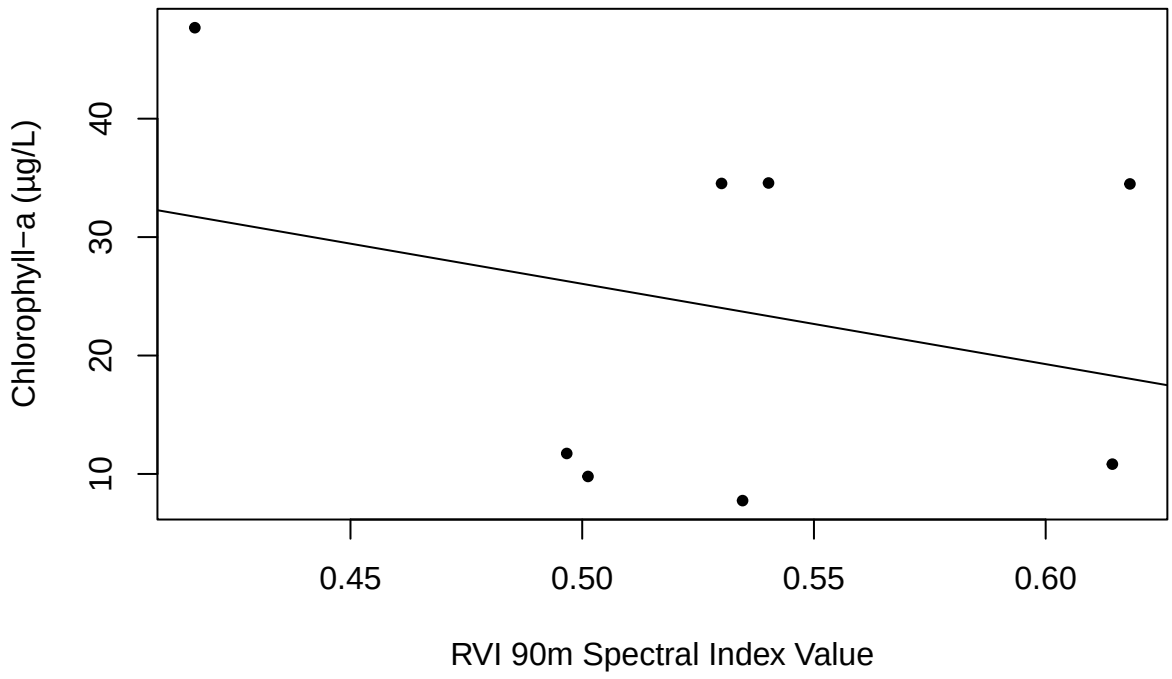


```
## Fit a simple linear regression model with
## dependent variable 'Chla' and independent
## variable 'RVI120m' Call variable after
## defining
fitRVI120m <- regress("mean", Chla ~ RVI120m, robustSE = FALSE,
    data = dat4)
fitRVI120m
```

```
## ( 4  cases deleted due to missing values)
##
##
## Call:
## regress(fnctl = "mean", formula = Chla ~ RVI120m, data = dat4,
##     robustSE = FALSE)
##
## Residuals:
##      5      6      7      8
```

```
##  7.579 -5.322  1.281 -3.538
##
## Coefficients:
##                  Estimate  Std Err   95%L         95%H         F stat    df
## [1] Intercept     -8.773     60.47    -269.0        251.4           0.02 1
## [2] RVI120m        81.59     105.7    -373.3        536.5           0.60 1
##                  Pr(>F)
## [1] Intercept       0.898
## [2] RVI120m         0.521
##
## Residual standard error: 7.069 on 2 degrees of freedom
##   (4 observations deleted due to missingness)
## Multiple R-squared:  0.2295, Adjusted R-squared:  -0.1558
## F-statistic: 0.5956 on 1 and 2 DF,  p-value: 0.521
```

```
## Create a scatterplot for 'fitRVI120m'
plot(dat4$RVI120m, dat4$Chla, xlab = "RVI 120m Spectral Index Value",
    ylab = "Chlorophyll-a (µg/L)", pch = 20)
## Add a fitted regression line to the model
abline(lm(Chla ~ RVI120m, data = dat4))
```

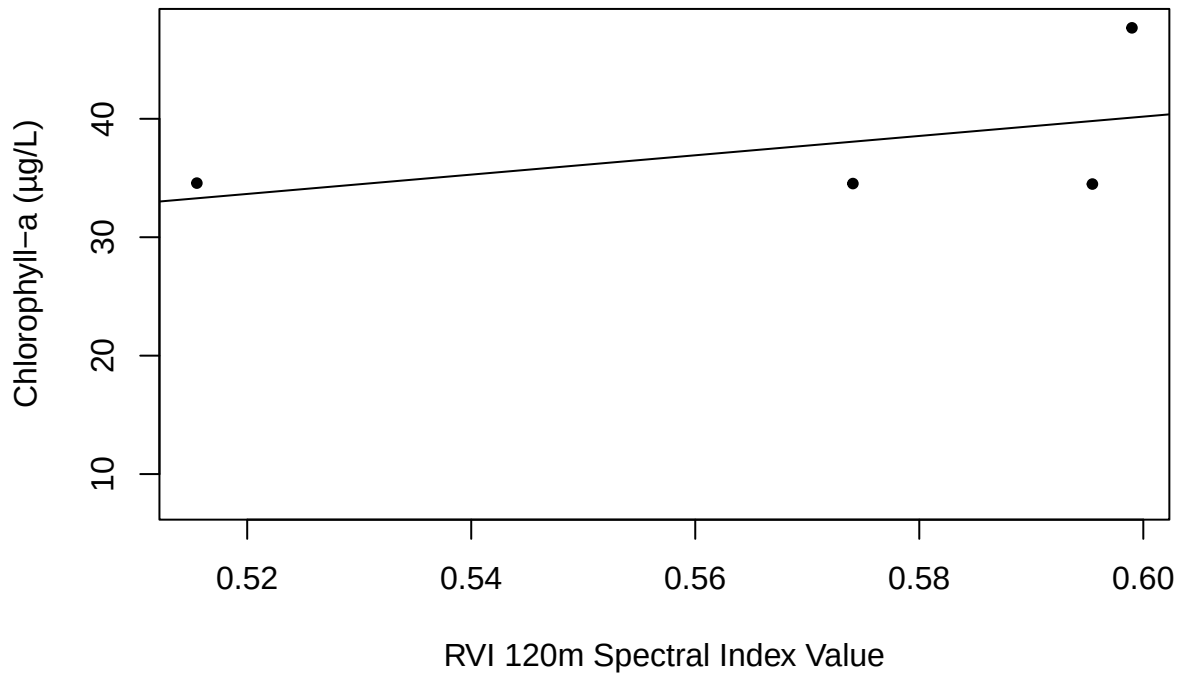


```
##### GNDVI ##### Fit a simple linear regression
##### model with dependent variable 'Chla' and
##### independent variable 'GNDVI60m' Call
##### variable after defining
```

```
fitGNDVI60m <- regress("mean", Chla ~ GNDVI60m, robustSE = FALSE,
    data = dat4)
fitGNDVI60m
```

```
##
## Call:
## regress(fnctl = "mean", formula = Chla ~ GNDVI60m, data = dat4,
##     robustSE = FALSE)
##
## Residuals:
##     Min      1Q  Median      3Q     Max
## -19.984 -13.695   5.096  10.887  16.859
##
## Coefficients:
##                   Estimate  Std Err   95%L         95%H         F stat    df
## [1] Intercept      11.80     13.20    -20.50        44.09           0.80 1
## [2] GNDVI60m      -41.94     41.54    -143.6        59.71           1.02 1
##                   Pr(>F)
## [1] Intercept      0.4059
## [2] GNDVI60m       0.3517
##
## Residual standard error: 15.49 on 6 degrees of freedom
## Multiple R-squared:  0.1452, Adjusted R-squared:  0.002725
## F-statistic: 1.019 on 1 and 6 DF,  p-value: 0.3517
```

```
## Create a scatterplot for 'fitGNDVI60m'
plot(dat4$GNDVI60m, dat4$Chla, xlab = "GNDVI 60m Spectral Index Value",
    ylab = "Chlorophyll-a (µg/L)", pch = 20)
## Add a fitted regression line to the model
abline(lm(Chla ~ GNDVI60m, data = dat4))
```

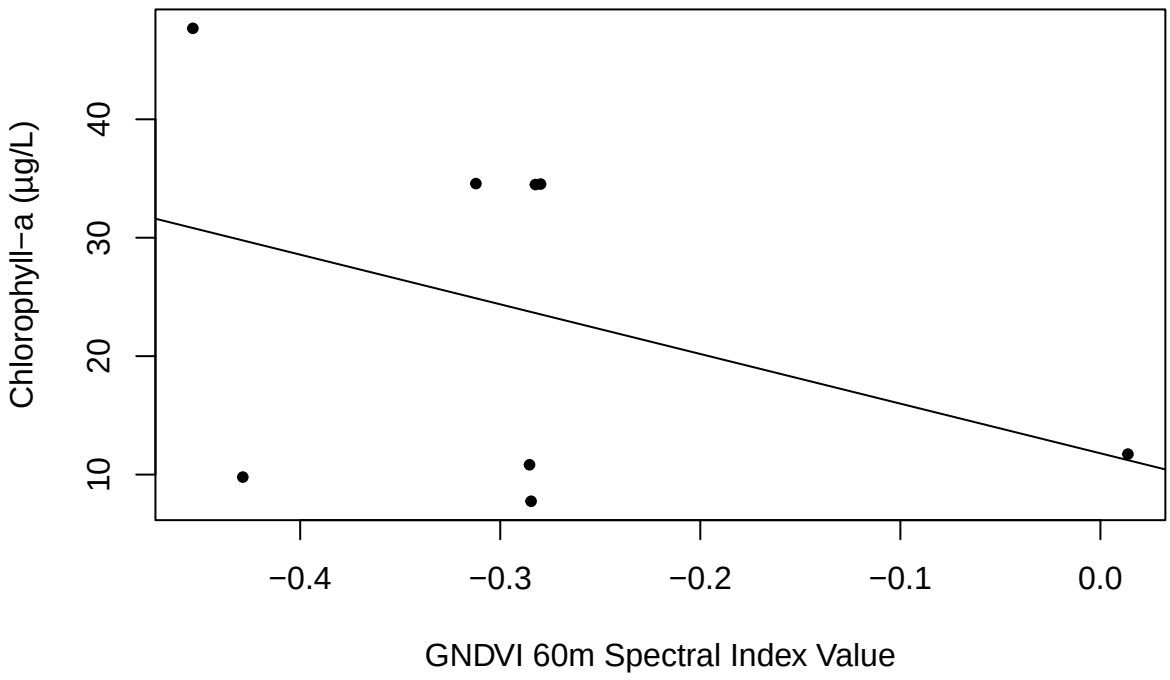


```
## Fit a simple linear regression model with
## dependent variable 'Chla' and independent
## variable 'GNDVI90m' Call variable after
## defining
fitGNDVI90m <- regress("mean", Chla ~ GNDVI90m, robustSE = FALSE,
    data = dat4)
fitGNDVI90m
```

```
##
## Call:
## regress(fnctl = "mean", formula = Chla ~ GNDVI90m, data = dat4,
##     robustSE = FALSE)
##
## Residuals:
##      Min       1Q   Median       3Q      Max
## -18.7204 -12.9275   0.6348  13.8477  15.9472
##
## Coefficients:
##                  Estimate  Std Err   95%L         95%H         F stat    df
## [1] Intercept     -1.802     28.78    -72.21        68.61           0.00 1
## [2] GNDVI90m      -83.58     91.74    -308.1        140.9           0.83 1
##                  Pr(>F)
## [1] Intercept      0.9521
## [2] GNDVI90m       0.3974
##
## Residual standard error: 15.7 on 6 degrees of freedom
```

```
## Multiple R-squared:  0.1215, Adjusted R-squared:  -0.0249
## F-statistic: 0.8299 on 1 and 6 DF,  p-value: 0.3974
```

```
## Create a scatterplot for 'fitGNDVI90m'
plot(dat4$GNDVI90m, dat4$Chla, xlab = "GNDVI 90m Spectral Index Value",
    ylab = "Chlorophyll-a (µg/L)", pch = 20)
## Add a fitted regression line to the model
abline(lm(Chla ~ GNDVI90m, data = dat4))
```

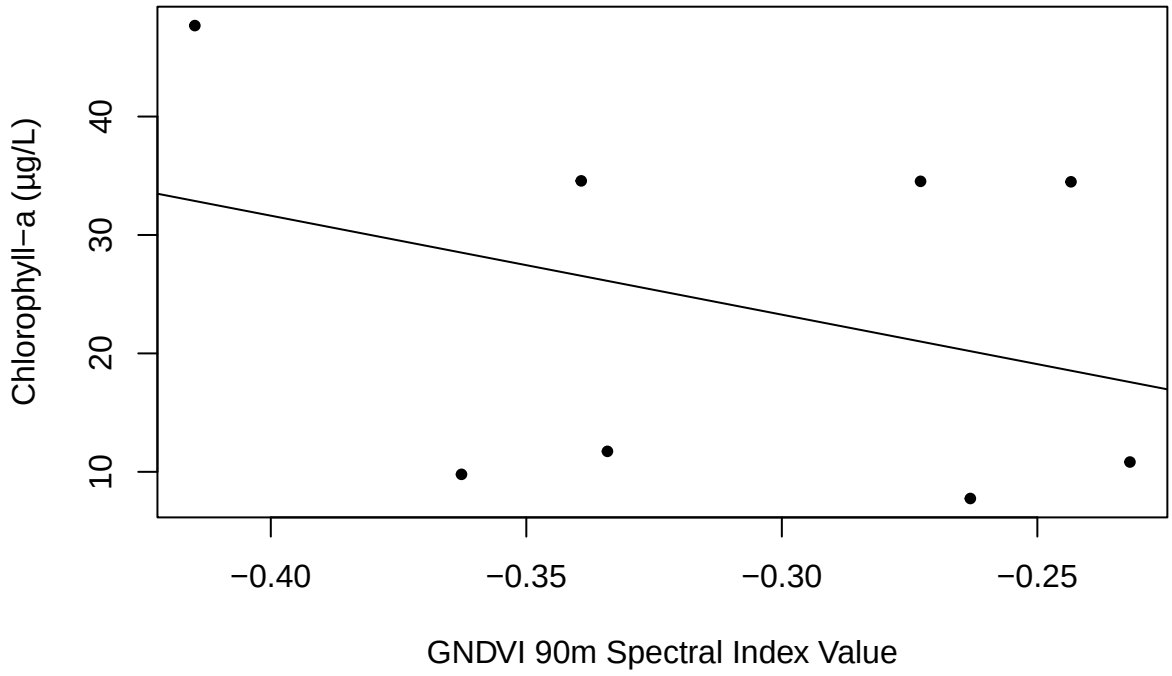


```
## Fit a simple linear regression model with
## dependent variable 'Chla' and independent
## variable 'GNDVI120m' Call variable after
## defining
fitGNDVI120m <- regress("mean", Chla ~ GNDVI120m, robustSE = FALSE,
    data = dat4)
fitGNDVI120m
```

```
## ( 4  cases deleted due to missing values)
##
##
## Call:
## regress(fnctl = "mean", formula = Chla ~ GNDVI120m, data = dat4,
##     robustSE = FALSE)
##
## Residuals:
```

```
##        5        6        7        8
##  7.83161  0.01341 -6.22789 -1.61714
##
## Coefficients:
##                  Estimate  Std Err   95%L         95%H         F stat    df
## [1] Intercept      19.70     25.26    -89.00        128.4           0.61 1
## [2] GNDVI120m     -61.43     84.79    -426.3        303.4           0.52 1
##                  Pr(>F)
## [1] Intercept      0.5171
## [2] GNDVI120m      0.5441
##
## Residual standard error: 7.167 on 2 degrees of freedom
##   (4 observations deleted due to missingness)
## Multiple R-squared:  0.2079, Adjusted R-squared:  -0.1882
## F-statistic: 0.5248 on 1 and 2 DF,  p-value: 0.5441
```

```
## Create a scatterplot for 'fitGNDVI120m'
plot(dat4$GNDVI120m, dat4$Chla, xlab = "GNDVI 120m Spectral Index Value",
    ylab = "Chlorophyll-a (µg/L)", pch = 20)
## Add a fitted regression line to the model
abline(lm(Chla ~ GNDVI120m, data = dat4))
```

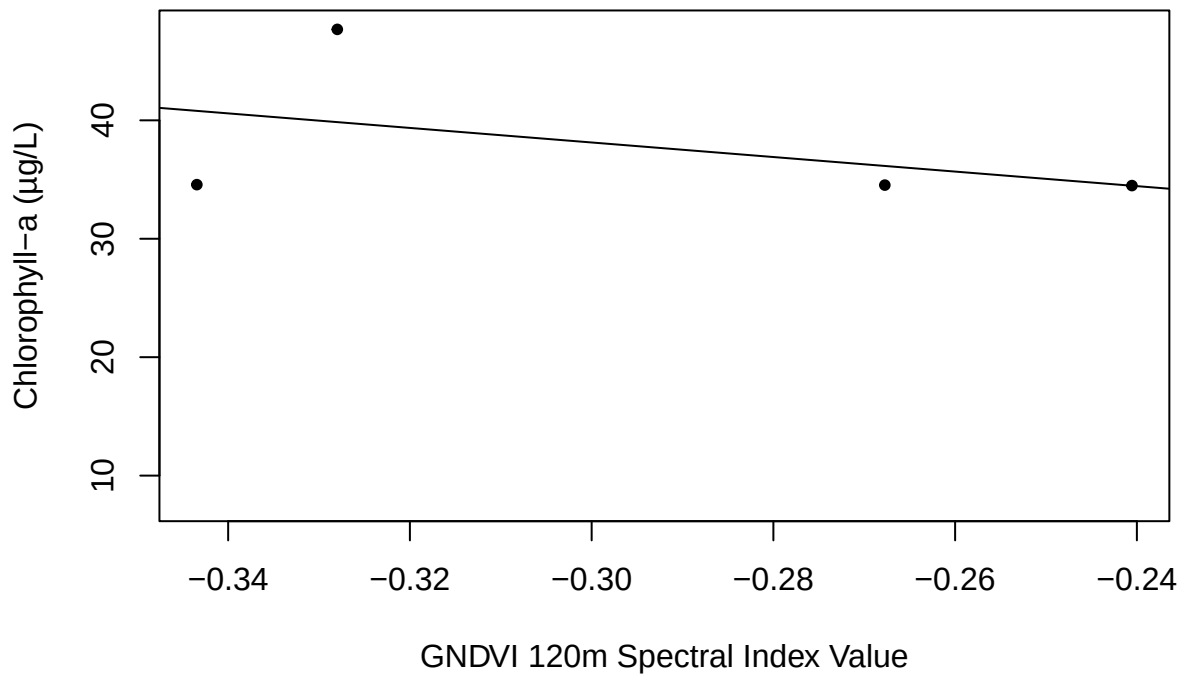


```
##### EVI2 ##### Note: 'EVI2' changed to 'EVI' in
##### 'dat4' due to issues with coding summary
##### plots Fit a simple linear regression model
```

```
##### with dependent variable 'Chla' and
##### independent variable 'EVI60m' Call variable
##### after defining
fitEVI260m <- regress("mean", Chla ~ EVI60m, robustSE = FALSE,
    data = dat4)
fitEVI260m
```

```
##
## Call:
## regress(fnctl = "mean", formula = Chla ~ EVI60m, data = dat4,
##     robustSE = FALSE)
##
## Residuals:
##     Min      1Q  Median      3Q     Max
## -19.472 -13.079   4.069  11.920  16.175
##
## Coefficients:
##                   Estimate  Std Err   95%L         95%H         F stat    df
## [1] Intercept      0.9801    24.57    -59.13        61.09           0.00 1
## [2] EVI60m        -58.74     61.30    -208.7        91.25           0.92 1
##                   Pr(>F)
## [1] Intercept      0.9695
## [2] EVI60m         0.3749
##
## Residual standard error: 15.6 on 6 degrees of freedom
## Multiple R-squared:  0.1327, Adjusted R-squared:  -0.0118
## F-statistic: 0.9184 on 1 and 6 DF,  p-value: 0.3749
```

```
## Create a scatterplot for 'fitEVI260m'
plot(dat4$EVI60m, dat4$Chla, xlab = "EVI2 60m Spectral Index Value",
    ylab = "Chlorophyll-a (µg/L)", pch = 20)
## Add a fitted regression line to the model
abline(lm(Chla ~ EVI60m, data = dat4))
```

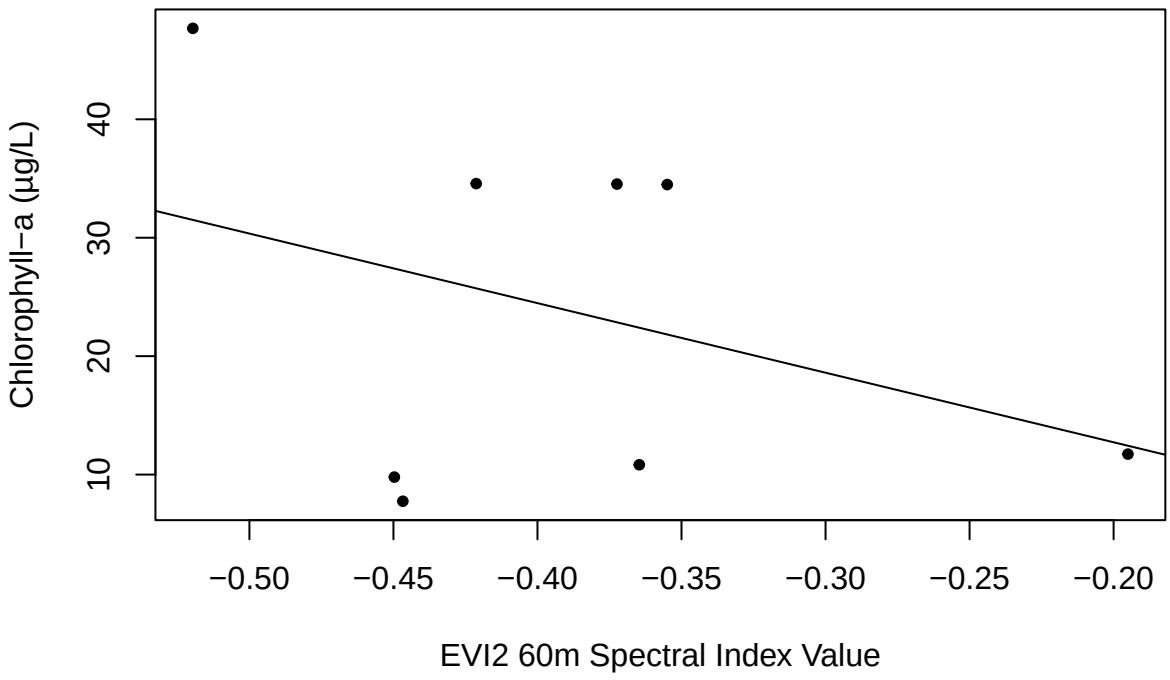


```
## Fit a simple linear regression model with
## dependent variable 'Chla' and independent
## variable 'EVI290m' Call variable after
## defining
fitEVI290m <- regress("mean", Chla ~ EVI90m, robustSE = FALSE,
    data = dat4)
fitEVI290m
```

```
##
## Call:
## regress(fnctl = "mean", formula = Chla ~ EVI90m, data = dat4,
##     robustSE = FALSE)
##
## Residuals:
##     Min      1Q  Median      3Q     Max
## -16.190 -14.900   1.641  12.361  16.598
##
## Coefficients:
##                  Estimate  Std Err   95%L         95%H         F stat    df
## [1] Intercept     -4.663     37.70    -96.92        87.60           0.02 1
## [2] EVI90m        -71.30     92.99    -298.8        156.2           0.59 1
##                  Pr(>F)
## [1] Intercept      0.9056
## [2] EVI90m         0.4723
##
## Residual standard error: 15.98 on 6 degrees of freedom
```

```
## Multiple R-squared:  0.08925,    Adjusted R-squared:  -0.06255
## F-statistic: 0.5879 on 1 and 6 DF,  p-value: 0.4723
```

```
## Create a scatterplot for 'fitEVI290m'
plot(dat4$EVI90m, dat4$Chla, xlab = "EVI2 90m Spectral Index Value",
    ylab = "Chlorophyll-a (µg/L)", pch = 20)
## Add a fitted regression line to the model
abline(lm(Chla ~ EVI90m, data = dat4))
```

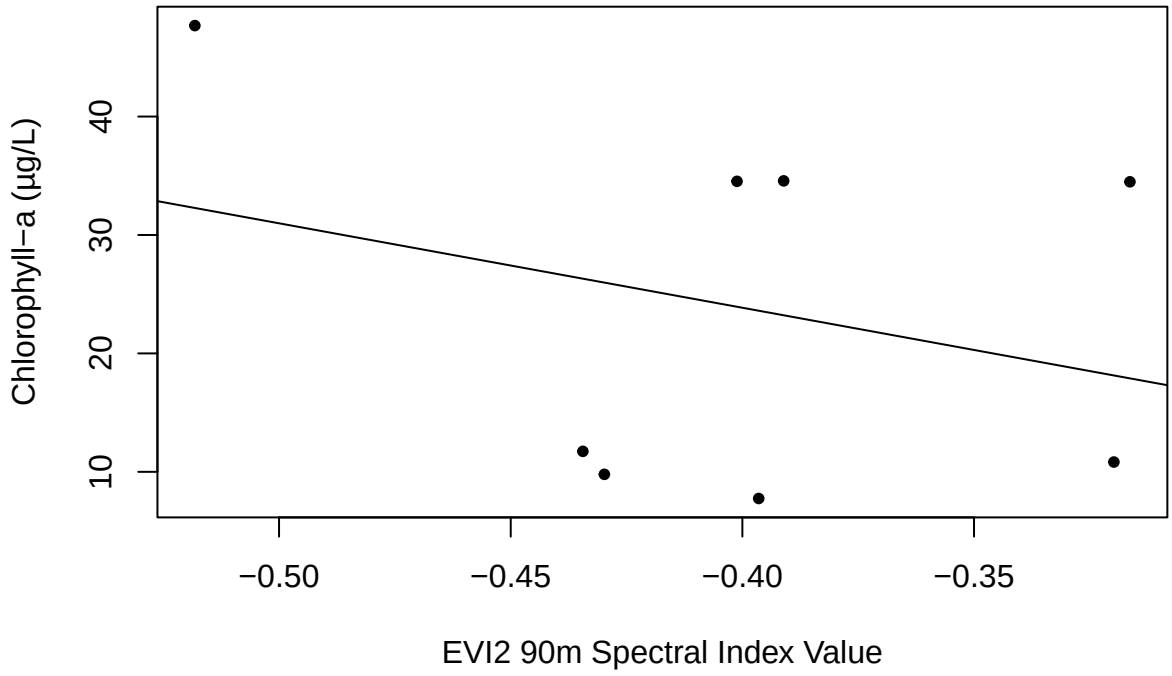


```
## Fit a simple linear regression model with
## dependent variable 'Chla' and independent
## variable 'EVI2120m' Call variable after
## defining
fitEVI2120m <- regress("mean", Chla ~ EVI120m, robustSE = FALSE,
    data = dat4)
fitEVI2120m
```

```
## ( 4  cases deleted due to missing values)
##
##
## Call:
## regress(fnctl = "mean", formula = Chla ~ EVI120m, data = dat4,
##     robustSE = FALSE)
##
## Residuals:
```

```
##      5      6      7      8
##  7.607 -5.305  1.261 -3.563
##
## Coefficients:
##                   Estimate  Std Err   95%L         95%H         F stat    df
## [1] Intercept      67.92     39.47    -101.9        237.8           2.96 1
## [2] EVI120m        83.28     108.8    -384.7        551.3           0.59 1
##                   Pr(>F)
## [1] Intercept      0.2275
## [2] EVI120m        0.5239
##
## Residual standard error: 7.082 on 2 degrees of freedom
##   (4 observations deleted due to missingness)
## Multiple R-squared:  0.2267, Adjusted R-squared:  -0.16
## F-statistic: 0.5862 on 1 and 2 DF,  p-value: 0.5239
```

```
## Create a scatterplot for 'fitEVI2120m'
plot(dat4$EVI120m, dat4$Chla, xlab = "EVI2 120m Spectral Index Value",
    ylab = "Chlorophyll-a (µg/L)", pch = 20)
## Add a fitted regression line to the model
abline(lm(Chla ~ EVI120m, data = dat4))
```

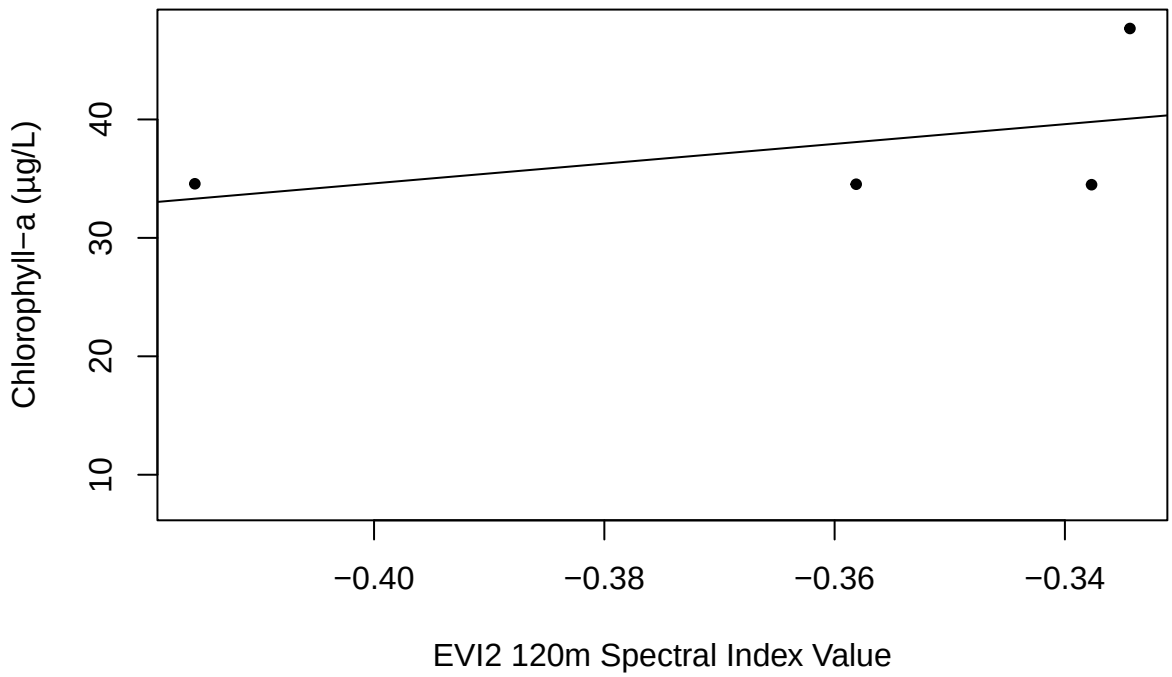

L.I.N.E. model checking was not completed for the multispectral SLR analyses because of low sample size. This represents a study limitation and is discussed further in the writeup.

End Code

Appendix G. Guidance Document Deliverable

Guidance Document Deliverable

Purpose

The purpose of this document is to provide information to water resource managers and public health practitioners on best practices using remotely piloted drones for the monitoring of harmful cyanobacterial blooms (HCBs) in small inland lakes. Considerations for certification and training, drone platforms and operation, camera sensors and settings, environmental conditions, site access and logistics, data storage and safety, costs, and other parameters will be discussed based on the findings of a pilot research project conducted by a graduate student at the University of Washington. The goal of this deliverable is to help guide future investigators when implementing drones for lake HCB surveillance work. Please note that these findings represent lessons learned from this pilot project. It is the drone operator's responsibility to maintain compliance with local, state, and federal laws as well as regulations mandated by the Federal Aviation Administration (FAA) for remotely piloted drones.

Background

The dynamics of HCBs are complex and must be monitored comprehensively—no single tool or approach is appropriate to understand their occurrence or health risk. In addition to in-situ sampling, tools like remote sensing offer a complimentary source of data to integrate with traditional surveillance methods. In Washington, the State Department of Health (DOH) and State Department of Ecology (Ecology) often work together to manage the risks of HCBs. Washington has implemented its Freshwater Algae Control Program, a passive HCB surveillance program that 1) connects state resources with Washington's 39 counties, including 35 local health jurisdictions as well as local citizen scientists, 2) provides state-mandated funding for toxicity testing in lakes, and 3) provides guidance on lake advisories and risk communication materials. The pilot project team met with representatives from Washington jurisdictions and identified the following concerns associated with current HCB monitoring programs: insufficient resources on testing and decision making for different counties, improvements needed for community engagement, a need for more rapid indicators to communicate risks to the public, a need for additional surveillance and diagnostic tools for HCBs, risks from septic systems to nearby water bodies, and increased HCB risks to drinking water sources due to climate change.

Concerns from jurisdictions specific to the use of drones as an HCB monitoring tool were also identified. Many jurisdictions do not currently use drones for environmental surveillance of HCBs due to a variety of reasons ranging from costs and technical difficulties to liability issues and a lack of standardized methods. Specifically, costs associated with drone equipment, staff training, insurance, and requiring third party consultants for operation were described. Additional concerns included logistical difficulties with drone-based sampling, place-based flight restrictions, inclement weather conditions hindering flights, challenges with determining the best time of day to avoid sun glare and water glint effects, time constraints for aerial image processing and technical difficulties with mapping water surfaces, the need for accurate ground control points, and the lack of knowledge surrounding the implementation of drones as an environmental monitoring tool for HCBs. This document aims to address the questions and concerns surrounding the use of drone technology for lake monitoring activities. For additional information, please refer to the full master's thesis associated with this work provided on the University of Washington's ResearchWorks Archive, a digital repository for scholarly work.

Certification and Training

In order to fly a drone under the FAA's Small Unmanned Aerial System (UAS) Rule (Part 107), you must obtain a Remote Pilot Certificate from the FAA. The FAA provides aviation handbooks and manuals for pilots seeking certification, including for remotely piloted drones. A number of resources—including study guides, practice tests, and informational videos—are available online as well. In addition to obtaining the initial certificate, Part 107 remote pilots must complete the Part 107 Small UAS Recurrent (ALC-677) online training course once every 24 months. This is meant to keep pilot knowledge current on aviation regulations, operating requirements, and flight safety. While the FAA does not provide training on flying drones, it is recommended to follow guidance from the drone platform's user manual and available tutorial videos. In addition, drone manufacturers such as DJI will recommend downloading mobile applications compatible with the drone platform, such as DJI Fly or DJI Go, to operate and control different aspects of the drone and its camera. Lastly, FAA requires registration of purchased drone platforms. Certification and registration are required to remain compliant with FAA regulations and standards.

Drone Platforms and Operation

For the pilot research project, the following drone platforms and GPS equipment were used: the DJI Phantom 4 Pro+ (Phantom) using a Real Time Kinematic (RTK) receiver and corresponding base station, and the DJI Matrice 210 (Matrice) using Ground Control Points (GCPs) measured with a handheld GPS unit. The drone equipment and a summary table of their specifications are shown below.

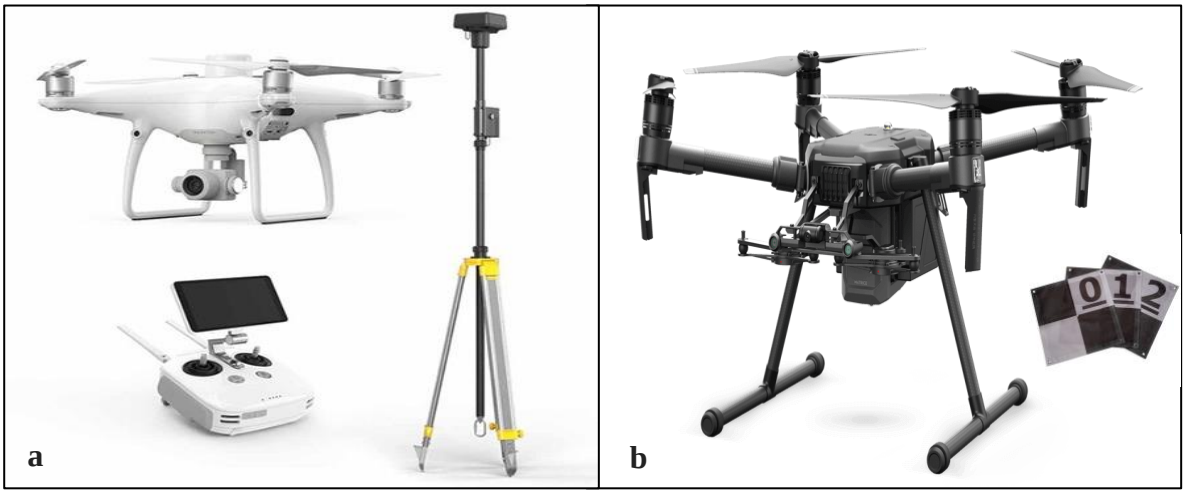

Drone platforms used for the pilot project: the DJI Phantom 4 Pro+ RTK with corresponding base station (a) and the DJI Matrice 210 with Ground Control Points (b).

Drone Platform Specifications Summary		
Parameter	**DJI Phantom 4 Pro+ RTK**	**DJI Matrice 210**
Approximate Weight with Batteries	1.391 kg	4.8 kg
Diagonal Length	350 mm	643 mm
Vertical Position Accuracy	±0.1 m	±0.5 m
Horizontal Position Accuracy	±0.1 m	±1.5 m
Max Payload Capacity	0.5 kg	1.34 kg
Max Speed	31 mph	50.3 mph
Max Wind Speed Resistance	10 m/s	12 m/s
Max Flight Time (per battery)	30 min.	34 min.
Retail Value	$6,600 USD	$12,000 USD
Notes:		
kg = kilograms		
m = meters		
mm = millimeters		
m/s = meters per second		
mph = miles per hour		
RTK = Real Time Kinematic		

Drone platform and GPS selection will depend on the project budget and project objectives. Pilots typically control the drone using a drone controller or a tablet device that has an Internet connection with access to a compatible mobile application. These interfaces allow the pilot to operate the drone and its camera, create a flight plan, and view the drone's camera view in real time. It is also important for the pilot to be familiar with battery life and connectivity indicators. A flight plan should be created for the study area of interest. Flights should be pre-programmed to follow a "lawnmower pattern" across the lake surface, flying back and forth in equally spaced flight lines; this allows optimal coverage of the study area. In addition, this process is automated, meaning manual operation of the drone during the flight is not necessary except in cases when the pilot must assume control of the drone for safety reasons. It is critical to launch the drone from a stable, unmoving surface such as a drone landing pad (similar to a helicopter pad) located on dry land. Landing the drone should be similarly completed. Before beginning operation, ensure proper calibration of the drone's GPS, verify sufficiently charged batteries for all hardware, and evaluate the strength of the wireless connection between the drone controller and the connected hardware.

The project team also experimented with flying the drones at three different altitudes, measured as meters (m) above ground level, at 60m, 90m, and 120m. Flight altitude affects the image resolution, drone speed, and number of images collected. Flights were conducted at an average speed of 9 meters per second (m/s) for the Phantom platform and between 9 to 12 m/s for the Matrice platform. Average times per flight were 14.6 minutes (60m Phantom), 10.2 minutes (90m Phantom), 8.9 minutes (120m Phantom), 38 minutes (60m Matrice), and 13 minutes (90m Matrice), along with a total flight time of 8 minutes for the 120m Matrice flight.

Camera Sensors and Settings

For the pilot research project, the following drone sensors were used: the Phantom's Red/Green/Blue (RGB) optical camera and a Micasense Altum multispectral sensor capable of measuring RGB, Near Infrared (NIR), and Red Edge (RE) wavelengths of light. The drone sensors are shown along with a specifications summary table below.

Selection of drone camera sensors will depend on the project budget and project objectives. Drone imagery can be a powerful tool to improve visual inspections of a lake surface when looking for algal scum formation. It can also be used to track chlorophyll a, the

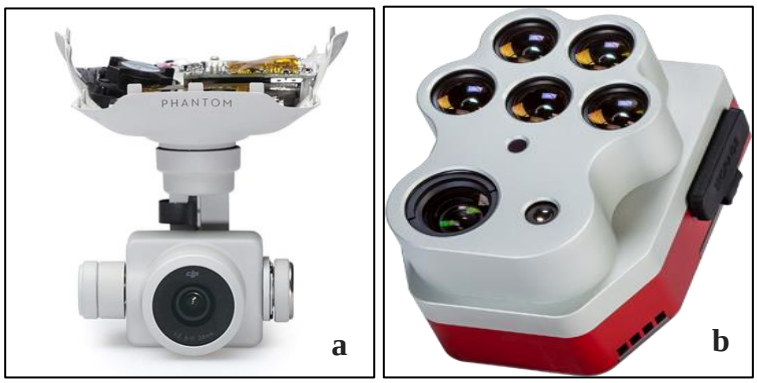

Drone sensors used for the pilot project: the Phantom's RGB optical camera (a) and a Micasense Altum multispectral sensor (b).

Drone Sensor Specifications Summary		
Parameter	**DJI Phantom 4 Pro+ RTK**	**DJI Matrice 210**
Sensor Type	1" CMOS RGB Camera	Micasense Altum Multispectral Sensor
Spatial Resolution	20 MP	2064 x 1544 pixels (3.2 MP x 5 imagers)
Focal Length	24 mm	8 mm
Field of View	84° 8.8 mm/24 mm	48° x 36.8°
Retail Value	(included with platform)	$16,000 USD
Notes:		
CMOS = Complementary Metal-Oxide-Semiconductor		
mm = millimeters		
MP = Megapixels		
RGB = Red, Green, Blue		
RTK = Real Time Kinematic		

photosynthetic pigment present in all algae and an indicator for algal biomass. More advanced sensors like the Micasense Altum can detect phycocyanin, the pigment unique to cyanobacteria. Drone imagery can either be used to inspect lake surfaces in real time or multiple photos of an entire lake can be collected for additional analysis. Pigments like chlorophyll a and phycocyanin reflect green and NIR light and this can be captured by the drone sensors. Ensure that the drone sensor is properly calibrated to ambient light conditions before use.

Considerations for different camera settings will next be discussed based on the pilot project. Flight altitude is an important consideration since it can affect the resolution of the imagery, the field of view that is visible in each image, and the number of photos collected at a lake. The intermediate flight altitude at 90m was found to be an appropriate balance between image resolution and image stitchability. Image stitchability refers to how well the collected images can be combined into a single image of the lake. However, flight altitude chosen will depend on the size of the flight plan area. It also depends on limitations at the study area. For

example, the drone must fly high enough to clear surrounding vegetation and building structures. Regarding camera settings, the drones collected imagery using a timed shooting mode (i.e., every few seconds) instead of a distance shooting mode (i.e., every few meters) for the pilot project. Although both methods are similar, timed shooting was preferred for this application. Images were collected with the camera positioned at nadir (downward-facing). Ensure there are no reflective surfaces attached to the drone (e.g., reflective tape) as this will negatively impact the photography. A photo ratio of 3:2 was used and an image overlap of 75% vertical and 75% horizontal were determined to be optimal. The white balance setting should match the ambient sky conditions (e.g., cloudy setting for overcast conditions, sunny setting for full or partial sun). The DJI platforms use a proprietary "shutter priority mode," which automatically adjusts the camera's shutter speed and ISO values using local light conditions and motion blur corrections. In addition, the drone sensors provide high resolution imagery (in the centimeter range). This is determined by the sensor's ground sampling distance (GSD), measured in centimeters per pixel (cm/pix.), and is an important consideration for this application. High resolution, clearer imagery will aid investigators in identifying surface water color changes associated with algal growth. For this pilot project, drone sensors provided a GSD between 1.7 and 5.5 cm/pix. As GSD decreases, image resolution increases.

Environmental Conditions

Weather forecasts must be checked diligently and often. For this pilot project, it was found that stitching of the aerial images was most successful when operating the drone platforms during sunny, clear skies or when the sky was overcast. For partly cloudy skies, the lake reflected too many clouds across the sky, creating a "moving terrain" that impeded image stitching as the lake surface appeared to change. Landmark features such as buoys, docks, or established vegetation are helpful as points of reference for the imagery. Rainy, foggy, hazy, or smoky conditions are not recommended for flight operation. While most drones can sustain a wide range of temperatures, their batteries are sensitive to colder weather and will drain faster. Check the drone platform user manual to make sure that air temperatures are not too extreme and plan flights accordingly. In addition, check that the humidity or dew point do not indicate excess moisture that will impact drone sensors. Drones should never be flown in the rain or with high humidity. Drones operate best when the wind speed is low or close to 0 miles per hour (mph)

whereas more intense winds at higher elevations will push the drone off track and expend the battery as it fights to maintain its programmed flight path. It is best to avoid wind speeds gusting up to 15 to 20 mph. Wind speed and direction are important factors to consider since they affect the spatial and temporal distribution of HCBs. In addition, flights should be conducted when the solar altitude—the angle between the horizon and the sun, measured in degrees (°)—is 43° or lower. This will help to avoid a sun angle that causes sun glint and water glitter effects on the lake surface, which are detrimental to the images. Solar altitude also determines the shadow length of surrounding features. Shadows blocking the reflection of certain water surfaces can make the imagery and downstream analysis unusable. Flights for this pilot project were conducted between 07:30am and 14:00pm over the project period and generally avoided sun glint effects but experienced difficulties with tree shadows during a sunny flight.

Environmental Monitoring Instruments

For the pilot project, the drone-derived imagery was compared to chlorophyll a concentrations measured in a laboratory. The project team also used a Turner Designs FluoroSense Handheld Fluorometer to measure phycocyanin levels in the lake. This portable, battery-powered probe is able to measure the fluorescence of phycocyanin in cyanobacteria cells. It has a range of detection from 0 to 199 micrograms per liter (µg/L) and a resolution of 1 µg/L. Fluorescence probes can be used to measure both chlorophyll a and phycocyanin concentrations. Future applications comparing drone imagery to chlorophyll a or phycocyanin readings can

Turner Designs FluoroSense Handheld Fluorometer, able to measure chlorophyll a or phycocyanin pigment concentrations.

leverage handheld fluorescence probes to measure ambient lake water pigment concentrations. Fluorescence probes are relatively cheaper, simpler, and faster than traditional laboratory methods and can be used to validate algal growth observed in the drone imagery.

Site Access and Logistics

Access to different lakes will vary considerably. While utilizing a public access location is convenient, it is recommended to operate the drone from an ideal vantage point on the lake to view the drone during its entire flight. A poor vantage point may result in incompliant line of sight issues. Building relationships with the local community to facilitate access to different areas of the lake (e.g., docks, backyards) is best suited to conduct aerial imagery acquisition safely and effectively. Access to parking and launch areas should be evaluated prior to field work. Notification of work to residents is also recommended to maintain communication and trust since drones can generate noise when operating in the airspaces near residential homes. Docks on the lake allow ideal access for drone flights and water sample collection.

Data Storage Considerations

The number of photos collected can range from hundreds to thousands of photos and will depend on the size of the lake being studied, flight altitude, total flight time, and other factors. It is important to ensure that the drone platform has appropriate onboard memory card storage to hold these images. For this work, the Phantom platform used a 256 Gigabyte (GB) micro SD card to store flight images. The Matrice platform's Micasense Altum camera used a 128 GB micro SD card. Photo and processing files were later stored on a 512 GB flash drive. Remember to back up flight imagery after each deployment to ensure proper data documentation and storage. Data backup for this work was facilitated using the Natural Hazards Engineering Research Infrastructure (NHERI) cloud-based data management database DesignSafe.

Photo Processing Applications

For this work, we used Pix4Dmapper (Version 4.8.4) photogrammetry software to process the drone-collected imagery and create orthomosaic imagery products. Orthomosaics compile numerous photos into a single image of the entire lake area. Pix4Dmapper licenses are available for both individual user accounts and organizations. While Pix4Dmapper is the leading

photogrammetry software for professional drone mapping, a number of open-source photogrammetry software programs are available and can be similarly used to process drone-collected imagery for downstream analysis. In addition, we used ArcGIS Pro (Version 3.1.0) for further processing of the orthomosaics to create vegetation index maps. Vegetation index maps help to highlight vegetated and unvegetated areas observed in the orthomosaics. These maps provide a more quantitative measurement of water surface areas with more or less algal growth.

Safety Considerations

Flights should be conducted at a safe location away from potential major distractions, such as heavy traffic, wildlife, or the public, if feasible. In public spaces, it is recommended to have a second staff member present to speak to the public or address potential distractions while the first staff member operates the drone. Use the drone controller's "return to home" button when potential distractions or emergencies arise so that the drone is safely and quickly returned to the launch point. It is also important to consider the heights of various structures, including trees, electrical powerlines, moving construction cranes, and nearby buildings to ensure a safe distance between them and the drone platform while in flight. In addition, wildlife hazards such as territorial birds must be avoided if possible. To maintain compliance with FAA regulations, ensure an appropriate vantage point so that the drone is visible to the flight operator for the entire flight duration. Especially on sunny days, wear proper eye protection when scanning the skies and tracking the drone platform mid-flight. Before conducting flights, perform a series of checks. First, check that the drone platform is ready for operation (e.g., full battery, all attachments secured). Next, check the lake area for swimmers, fishers, other recreators, or watercraft. Before takeoff, conduct appropriate checks for other aircraft traffic (e.g., seaplanes, other drones) and make sure that the skies are clear for operation. Mobile applications such as B4UFLY have been recommended by the FAA to check the operational airspace for other aircraft. The maximum flight altitude allowed by the FAA is 400 feet above ground level. In addition, allow a margin of safety between the water surface and the launch point so that the drone does not land in the water. Manually take over flight operation if automated landings are off course. When landing the drone, verify that the drone platform's propellers are clear of obstacles. Also, consider the use of a self-inflating buoy attached to the drone housing when operating the drone over water.

This will allow the operator to locate and recover the drone in the unlikely event of a drone crash into the lake. Remote pilots are expected to take precautions and practice drone safety.

Insurance and Liability

It is recommended to create and implement a site health and safety plan for drone operation at public access lakes. Safety precautions must be prioritized to ensure the safety of the workers and the public. Review all applicable insurance requirements to operate drones responsibly for this application. Accidents such as drone crashes, incidents with territorial birds, and other unanticipated events can occur. Pierce County, Washington currently has a Drone Program and provides a document discussing prohibited uses and insurance requirements for drones. Pierce County employs drones for a variety of use cases, including for water resource visual assessment, sampling, and monitoring support.

Costs

See the table below for approximate retail equipment and software costs for this pilot research project. For this work, equipment rental costs were subsidized through the University of Washington RAPID facility. It is important to note that other drone platforms, camera sensors, and photo processing programs are available and that equipment costs are subject to change.

Drone Application Summary Cost Table	
Item	**Approximate Cost (USD)**
FAA Part 107 Remote Pilot Certification[1]	$175
FAA Drone Platform Registration[2]	$5
DJI Phantom 4 Pro+ RTK Drone Platform	$6,600
DJI Phantom 4 Series Flight Battery	$185/battery
DJI RTK High-Precision GNSS Mobile Station	$3,600
WB37 Battery (for Phantom 4 Controller and RTK Mobile Station)	$59/battery
DJI Matrice 210 Drone Platform	$12,000
DJI Matrice 200 Series Flight Battery	$480/battery
Micasense Altum Multispectral Sensor	$16,000
Drone GCP Points/Aerial Targets (x10)	$85
Pix4Dmapper Photogrammetry Software	$3,500/year
Notes:	
[1]valid for 24 months and renewed with a free online course to update recency of aeronautical knowledge.	
[2]valid for 3 years	
FAA = Federal Aviation Administration	
RTK = Real Time Kinematic	
GNSS = Global Navigation Satellite System	
GCP = Ground Control Point	

Appendix H. Supplemental Tables and Figures

Table A1. Chlorophyll a Extract and Absorbance Measurements for Dilution Calibration Curves										
Dilution	**Chl-a (µg/L) - Extract 1**	**Chl-a (µg/L) - Extract 2**	**Chl-a (µg/L) - Extract 3**	**Average Chl-a Extract (µg/L)**	**SD**	**Abs 664 nm 1**	**Abs 664 nm 2**	**Abs 664 nm 3**	**Average Abs 664 nm**	**SD**
7-24-23 1st Event										
1:10	2949.77	2961.62	2971.93	2961.11	11.1	0.257	0.258	0.259	0.258	0.001
1:100	310.31	320.62	310.39	313.77	5.9	0.027	0.028	0.027	0.027	0.0006
1:1,000	23.70	33.93	23.70	27.11	5.9	0.002	0.003	0.002	0.002	0.0006
1:10,000	0	0	0	0	0	0	0	0	0	0
1:100,000	0	0	0	0	0	0	0	0	0	0
8-7-23 2nd Event										
1:25	1445.30	1455.61	1445.30	1448.74	6.0	0.126	0.127	0.126	0.126	0.0006
1:50	734.50	732.96	734.50	733.99	0.9	0.064	0.064	0.064	0.064	0
1:100	390.10	378.33	368.02	378.82	11.0	0.034	0.033	0.032	0.033	0.001
1:200	195.13	195.05	195.05	195.08	0.05	0.017	0.017	0.017	0.017	0
1:500	69.54	81.33	81.33	77.40	6.8	0.006	0.007	0.007	0.007	0.0006
8-21-23 3rd Event										
1:25	1480.85	1458.85	1438.39	1459.36	21.2	0.129	0.127	0.125	0.127	0.002
1:50	744.73	724.35	725.89	731.66	11.3	0.065	0.063	0.063	0.064	0.001
1:100	357.87	325.56	325.56	336.33	18.7	0.031	0.028	0.028	0.029	0.002
1:200	142.20	142.20	154.05	146.15	6.8	0.012	0.012	0.013	0.012	0.0006
1:500	47.40	35.55	35.55	39.50	6.8	0.004	0.003	0.003	0.003	0.0006
9-2-23 4th Event										
1:25	1504.55	1494.32	1506.09	1501.65	6.4	0.131	0.130	0.131	0.131	0.0006
1:50	758.12	747.97	747.89	751.33	5.9	0.066	0.065	0.065	0.065	0.0006
1:100	369.64	369.64	369.64	369.64	0	0.032	0.032	0.032	0.032	0
1:200	186.44	184.82	174.59	181.95	6.4	0.016	0.016	0.015	0.016	0.0006
1:500	59.25	69.56	59.25	62.69	6.0	0.005	0.006	0.005	0.005	0.0006
9-11-23 5th Event										
1:25	1560.56	1572.41	1560.56	1564.51	6.8	0.136	0.137	0.136	0.136	0.0006
1:50	780.28	770.05	780.28	776.87	5.9	0.068	0.067	0.068	0.068	0.0006
1:100	401.95	401.95	401.95	401.95	0	0.035	0.035	0.035	0.035	0
1:200	195.13	206.90	206.90	202.98	6.8	0.017	0.018	0.018	0.018	0.0006
1:500	79.79	79.79	91.56	83.71	6.8	0.007	0.007	0.008	0.007	0.0006
10-7-23 6th Event										
1:25	1548.71	1536.86	1525.01	1536.86	11.9	0.135	0.134	0.133	0.134	0.001
1:50	780.28	778.74	768.51	775.84	6.4	0.068	0.068	0.067	0.068	0.0006
1:100	390.18	390.18	400.41	393.59	5.9	0.034	0.034	0.035	0.034	0.0006
1:200	206.90	195.13	195.05	199.03	6.8	0.018	0.017	0.017	0.017	0.0006
1:500	79.79	79.79	79.79	79.79	0	0.007	0.007	0.007	0.007	0
10-23-23 7th Event										
1:25	1538.40	1538.48	1538.40	1538.43	0.05	0.134	0.134	0.134	0.134	0
1:50	770.05	781.82	780.28	777.38	6.4	0.067	0.068	0.068	0.068	0.0006
1:100	401.95	390.18	401.95	398.03	6.8	0.035	0.034	0.035	0.035	0.0006
1:200	195.13	196.67	206.90	199.57	6.4	0.017	0.017	0.018	0.017	0.0006
1:500	81.41	81.33	81.41	81.38	0.05	0.007	0.007	0.007	0.007	0
All Sampling Events										
1:25				1508.26	46.6				0.131	0.004
1:50				757.84	21.7				0.066	0.002
1:100				370.30	33.5				0.032	0.003
1:200				187.46	21.5				0.016	0.002
1:500				70.75	17.02				0.006	0.002

Notes:

Note that averages and standard deviations for the chlorophyll a extract values and absorbance readings are reported within each sample event at the top of the table and are reported across all sample events at the bottom of the table.

Only the 1:100 dilution values from the first sampling event are factored into the average and standard deviation calculations at the bottom of the table.

Each extract and absorbance value represents an independent reading since all dilutions were analyzed in triplicate.

Note that each value is an average of three values analyzed from the spectrophotometer output.

Abs 664 nm = Absorbance (in Absorbance Units) measured at a wavelength of 664 nanometers

SD = standard deviation

µg/L = micrograms per liter

Table A2. Absorption Peak Ratio Data for Acid-Corrected Dilutions			
Dilution	**Abs 664b nm**	**Abs 665a nm**	**Absorption Ratio (664b/665a):**
9-11-23 5th Event			
1:25	0.136	0.077	1.77
1:50	0.068	0.040	1.70
1:100	0.035	0.020	1.75
1:200	0.017	0.010	1.70
1:500	0.007	0.004	1.75
10-7-23 6th Event			
1:25	0.135	0.077	1.75
1:50	0.068	0.039	1.74
1:100	0.034	0.019	1.79
1:200	0.018	0.010	1.80
1:500	0.007	0.004	1.75
10-23-23 7th Event			
1:25	0.134	0.076	1.76
1:50	0.067	0.037	1.81
1:100	0.035	0.020	1.75
1:200	0.017	0.010	1.70
1:500	0.007	0.004	1.75

Notes:

Results are reported here from the first of the three dilutions analyzed in triplicate.

Absorption peak ratios of 1.70 are considered to contain no pheophytin a (i.e., no degradation) for extractions using a 90% acetone solvent; however, higher concentrations of acetone used may result in absoprotion peak ratios closer to 2.0.

Abs = Absorbance (measured in Absorbance Units)

nm = nanometers

664b = turbidity-corrected absorbance at 664 nanometers measured before acidification

665a = turbidity-corrected absorbance at 665 nanometers measured after acidification

Table A3. Chlorophyll a Results for Uncorrected and Acid-Corrected Samples					
Sample	**Chl-a (µg/L) - Whole Sample**	**Chl-a (µg/L) - Average**	**Chl-a (µg/L) - Whole Sample**	**Chl-a (µg/L) - Average**	**Difference (µg/L)**
9-11-23 5th Event Uncorrected			**9-11-23 5th Event Acid-Corrected**		
SW17	9.79	9.79	8.90	8.90	0.89
SW17-DUP	9.78		8.90		
SW18	11.02	10.83	9.79	9.79	1.04
SW18-DUP	10.63		9.79		
SW19	11.71	11.73	10.68	11.13	0.61
SW19-DUP	11.76		11.57		
SW20	7.18	7.75	5.34	5.34	2.41
SW20-DUP	8.31		5.34		
10-7-23 6th Event Uncorrected			**10-7-23 6th Event Acid-Corrected**		
SW21	80.07	80.58	72.09	73.43	7.16
SW21-DUP	81.10		74.76		
SW22	81.10	82.28	74.76	76.10	6.19
SW22-DUP	83.47		77.43		
SW23	23.41	24.56	18.69	21.36	3.20
SW23-DUP	25.70		24.03		
SW24	27.40	27.36	24.03	24.03	3.33
SW24-DUP	27.32		24.03		
10-23-23 7th Event Uncorrected			**10-23-23 7th Event Acid-Corrected**		
SW25	48.44	47.68	44.06	44.06	3.62
SW25-DUP	46.91		44.06		
SW26	35.81	34.49	30.71	31.37	3.12
SW26-DUP	33.17		32.04		
SW27	35.37	34.57	32.04	32.71	1.86
SW27-DUP	33.76		33.38		
SW28	35.30	34.53	32.04	32.04	2.49
SW28-DUP	33.76		32.04		
Notes:					
Acid-corrected chlorophyll a values were only completed for the last three sampling events.					
µg/L = micrograms per liter					

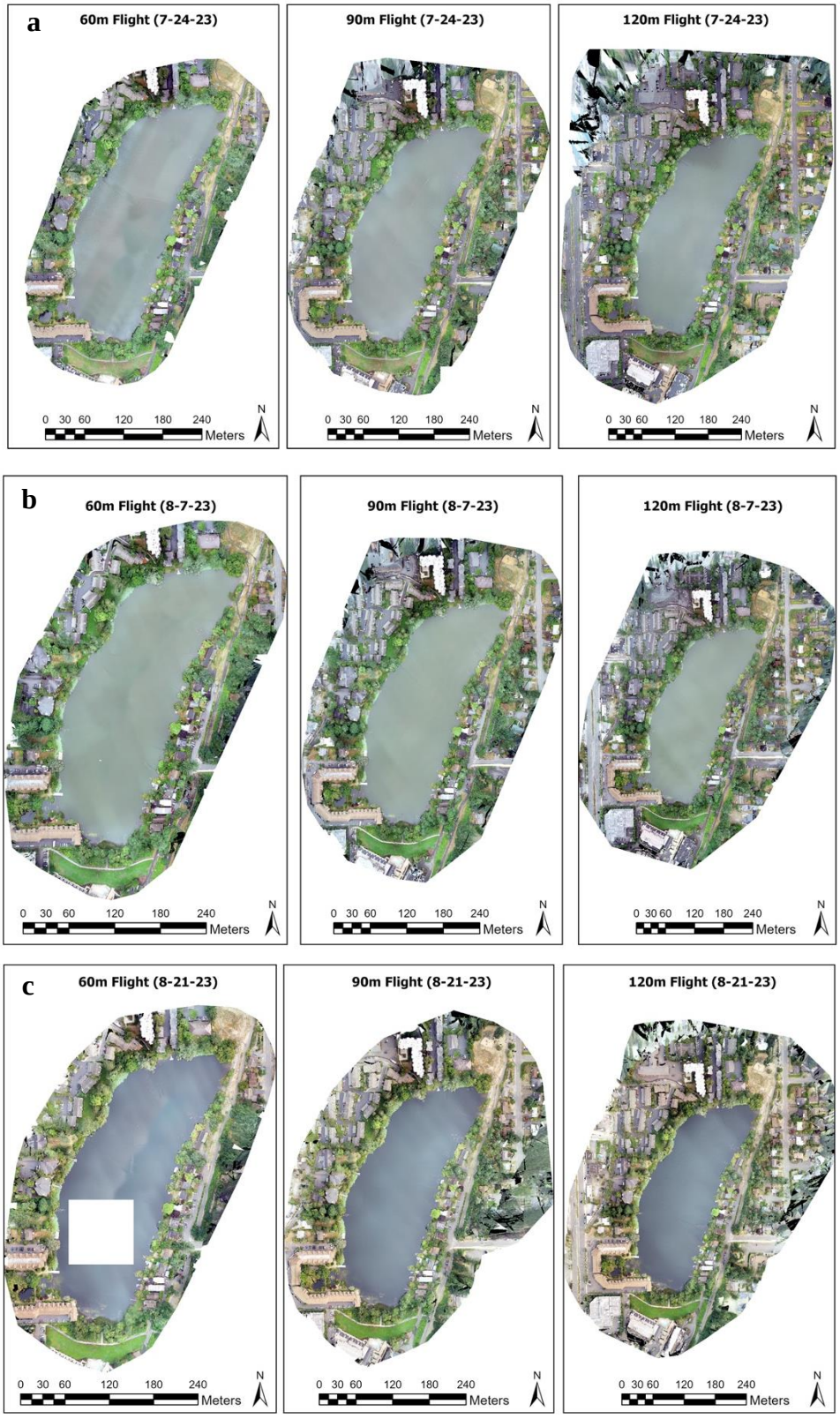

Figure A1a-c. ArcGIS Maps of the First (a), Second (b) and Third (c) Sample Event RGB Orthomosaics.

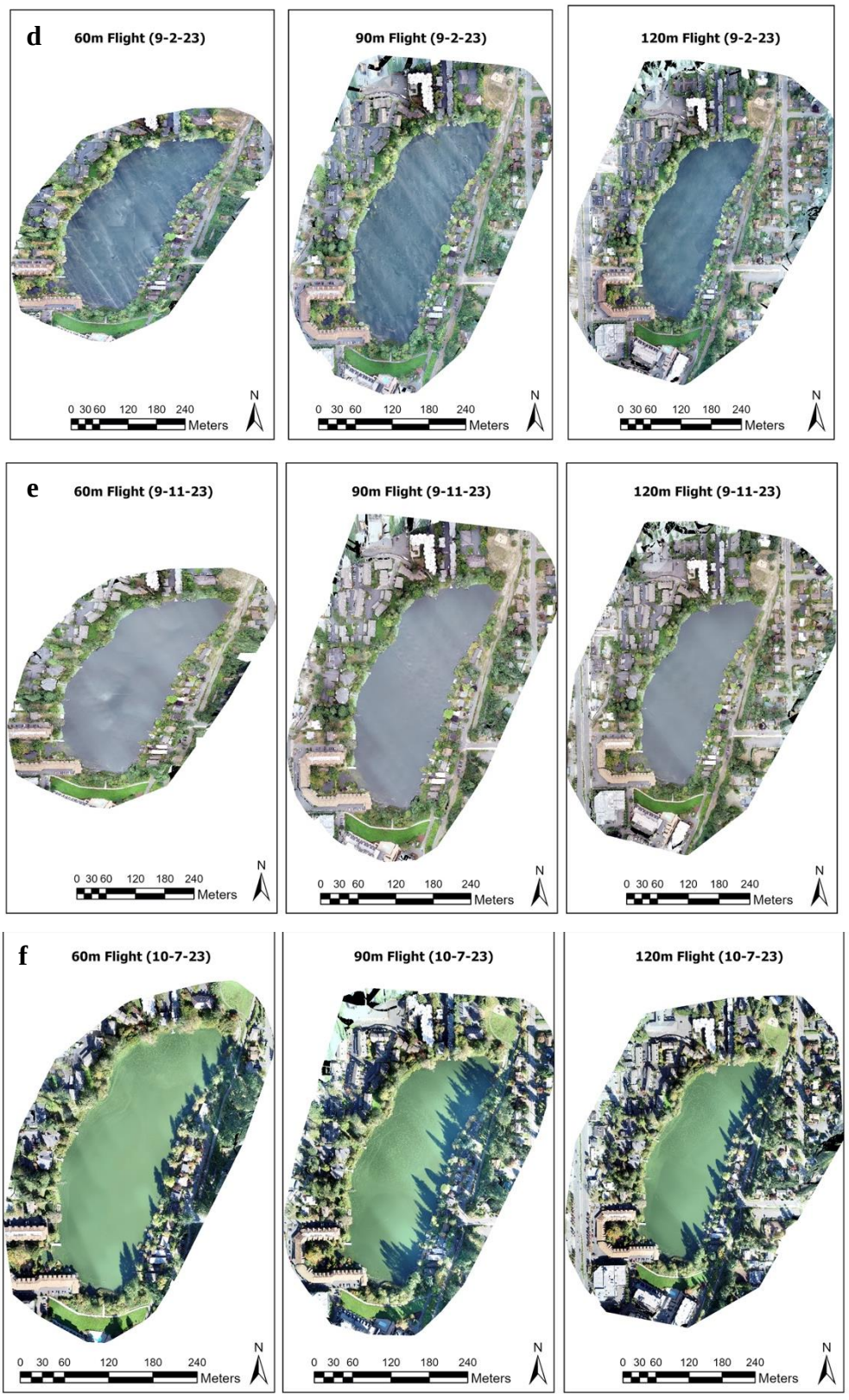

Figure A1d-f. ArcGIS Maps of the Fourth (d), Fifth (e), and Sixth (f) Sample Event RGB Orthomosaics.

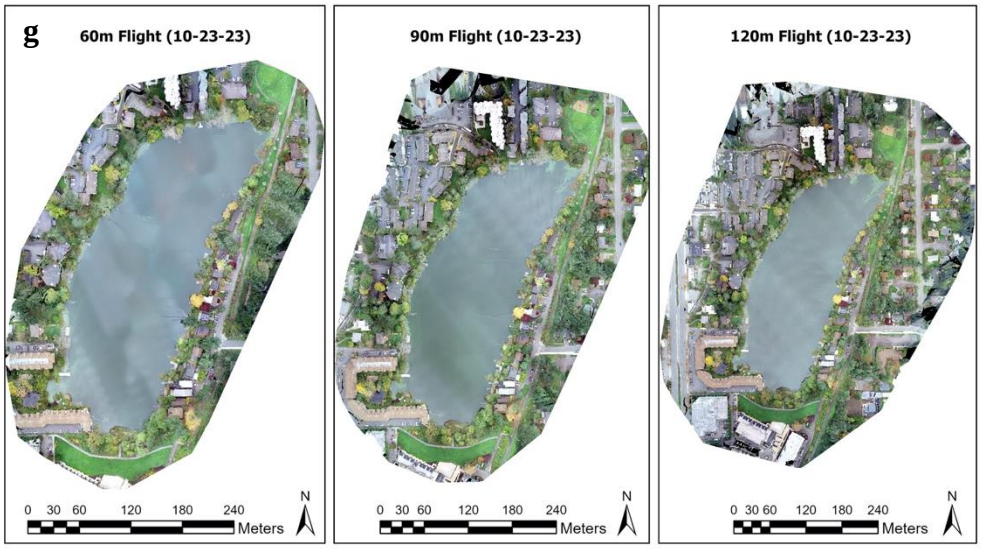

Figure A1g. ArcGIS Maps of the Seventh Sample Event RGB Orthomosaics.

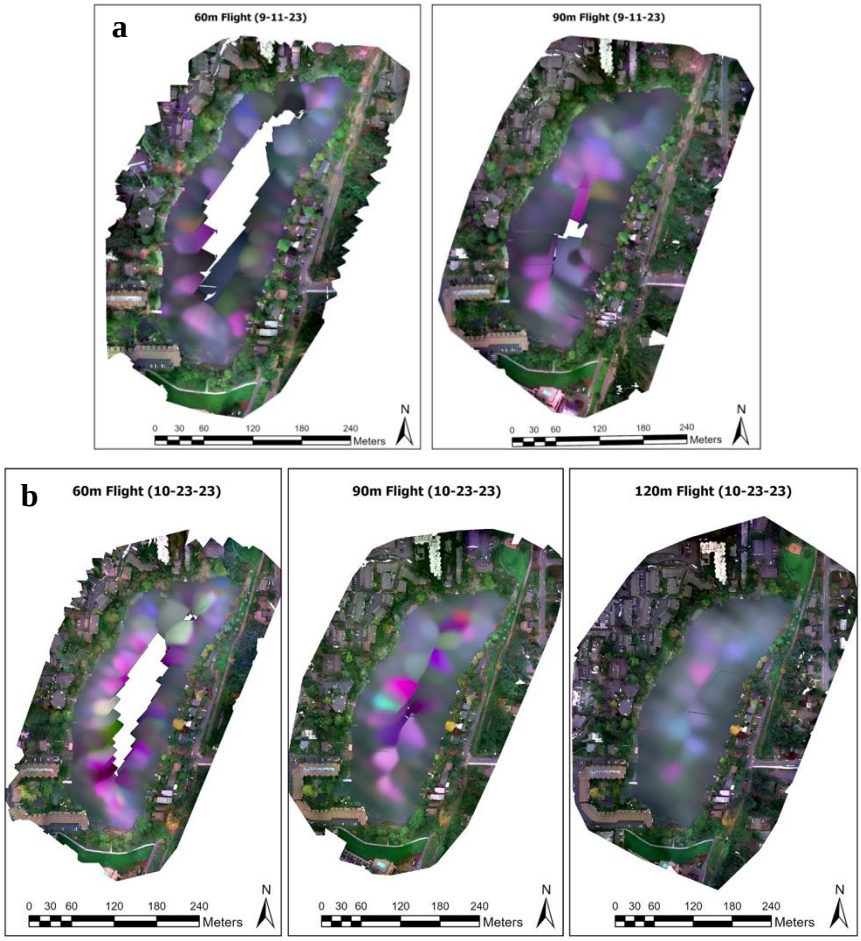

Figure A2a-b. ArcGIS Maps of the Fifth (a) and Seventh (b) Sample Event Multispectral Orthomosaics.

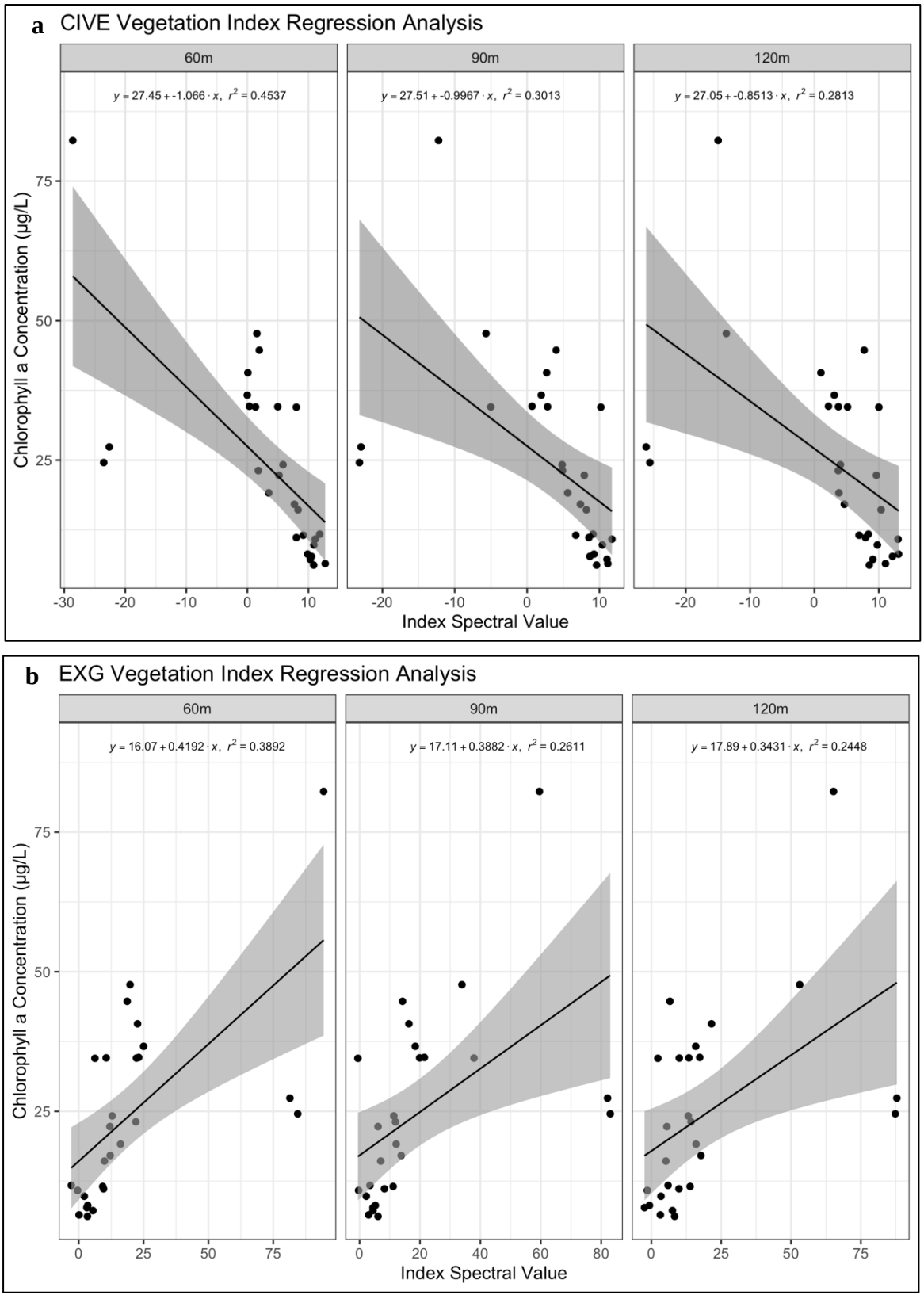

Figure A3a-b. CIVE (a) and EXG (b) Simple Linear Regression Analysis Plots.

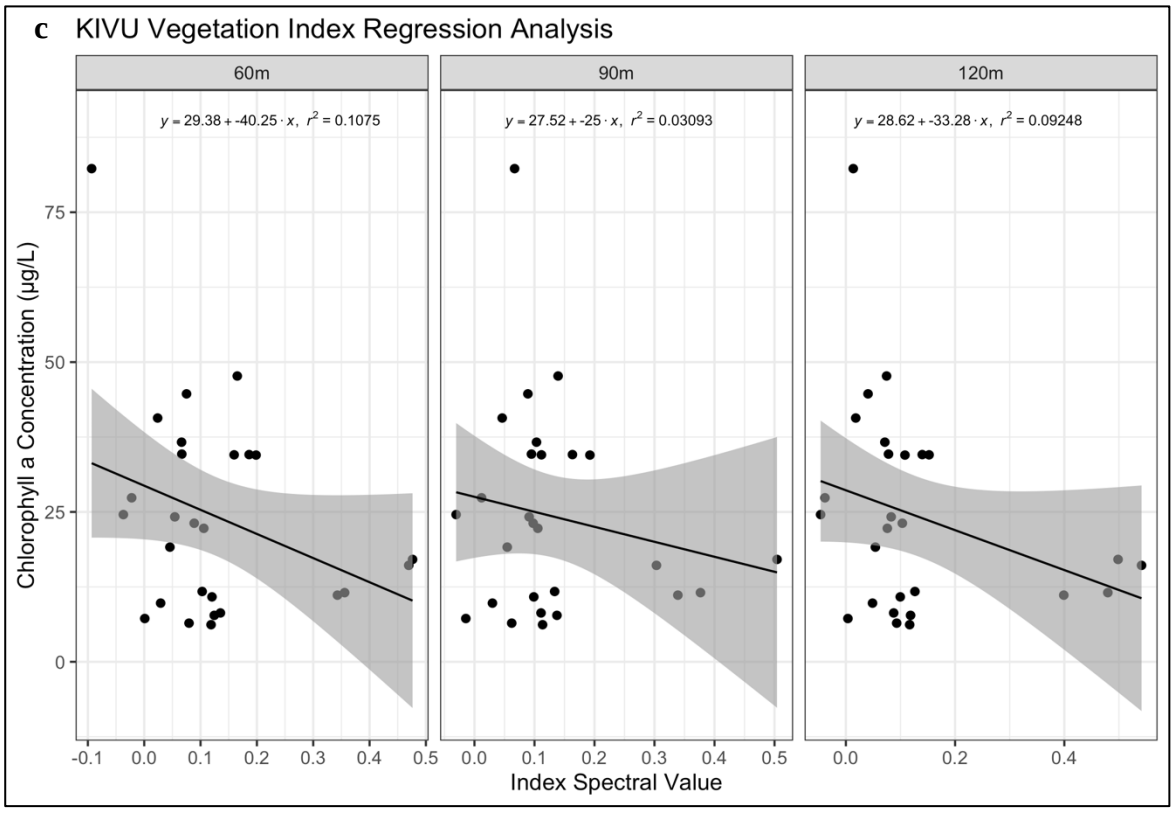

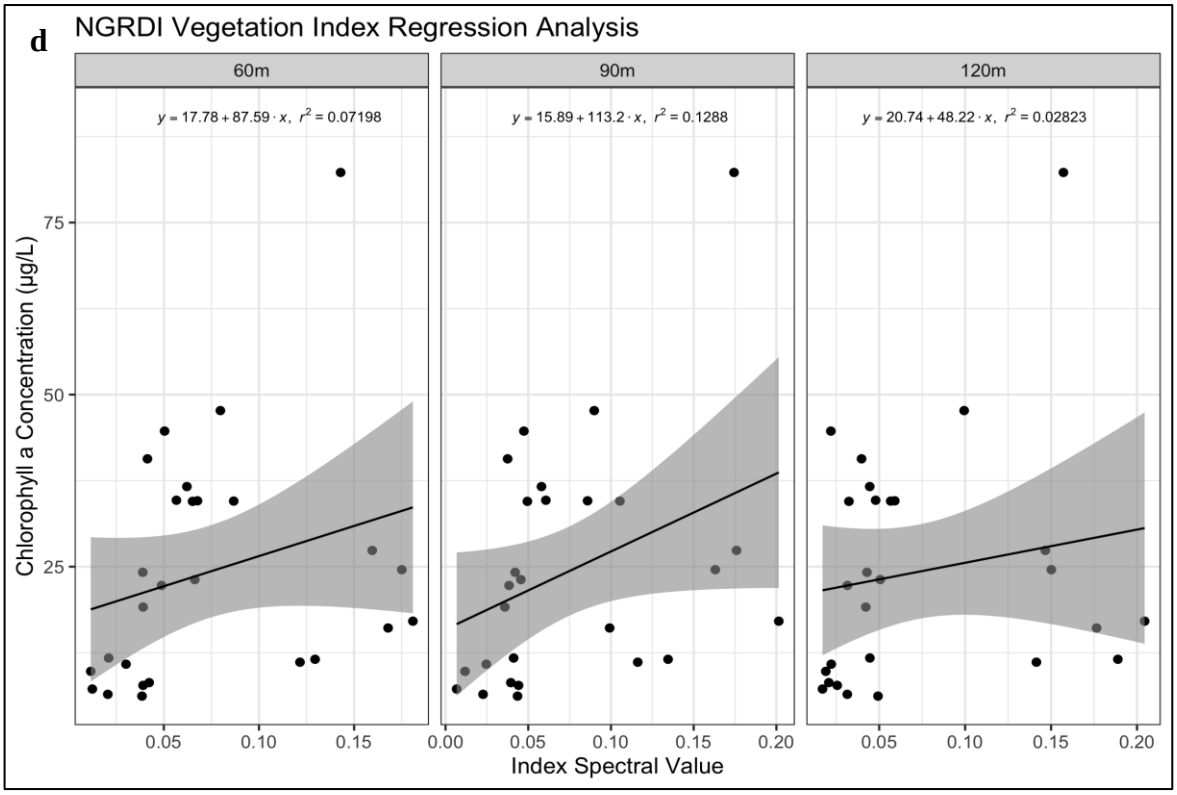

Figure A3c-d. KIVU (c) and NGRDI (d) Simple Linear Regression Analysis Plots.

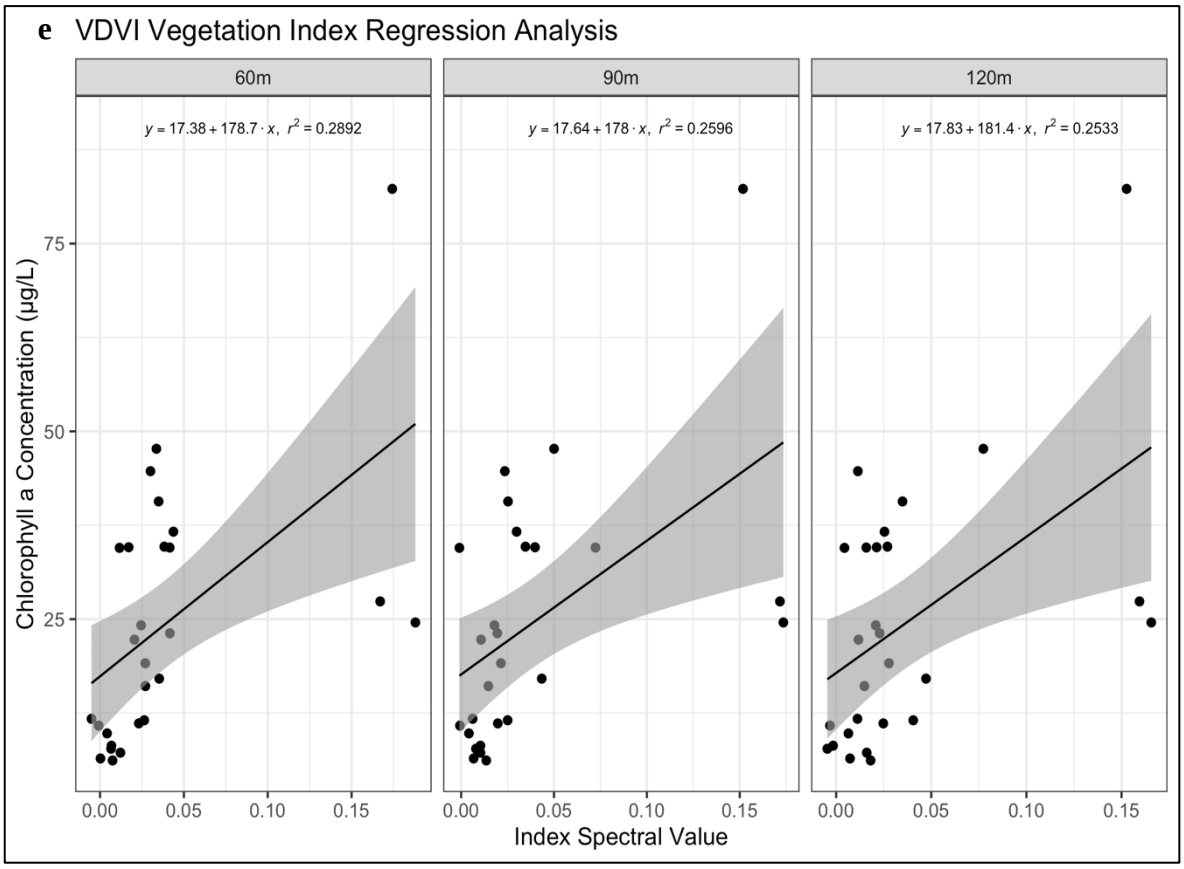

Figure A3e. VDVI Simple Linear Regression Analysis Plots.

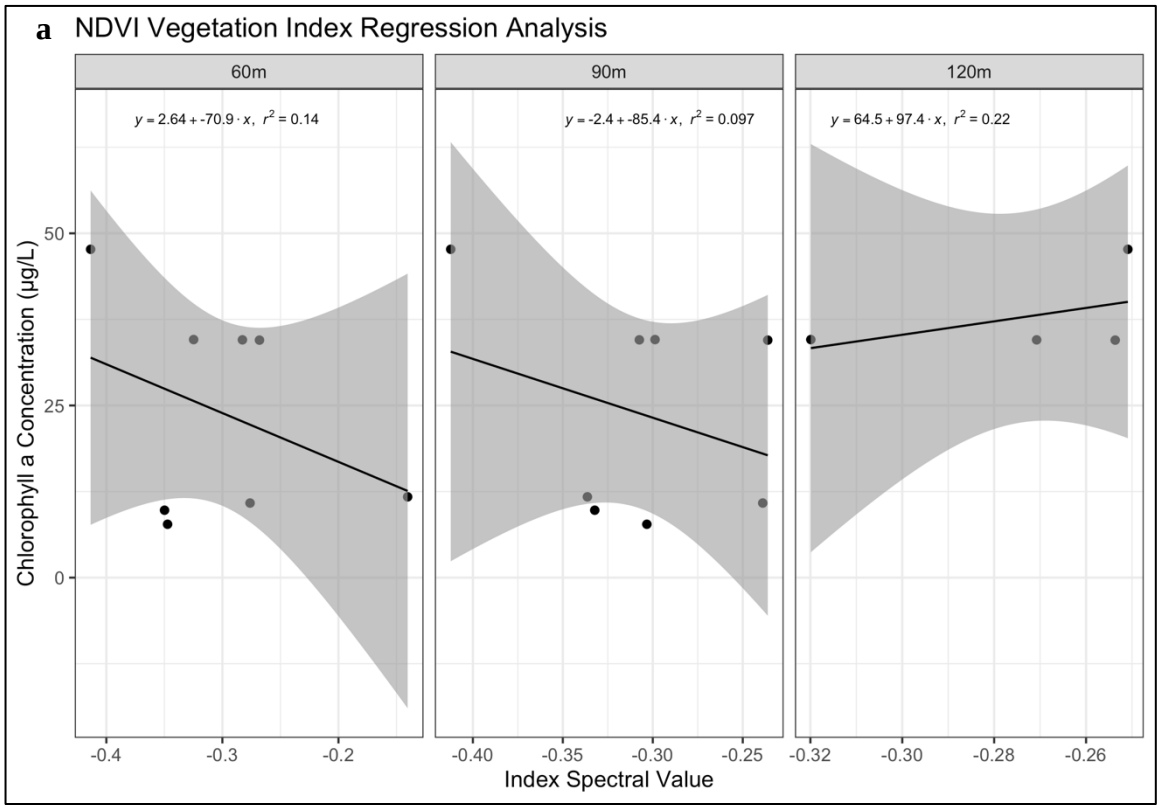

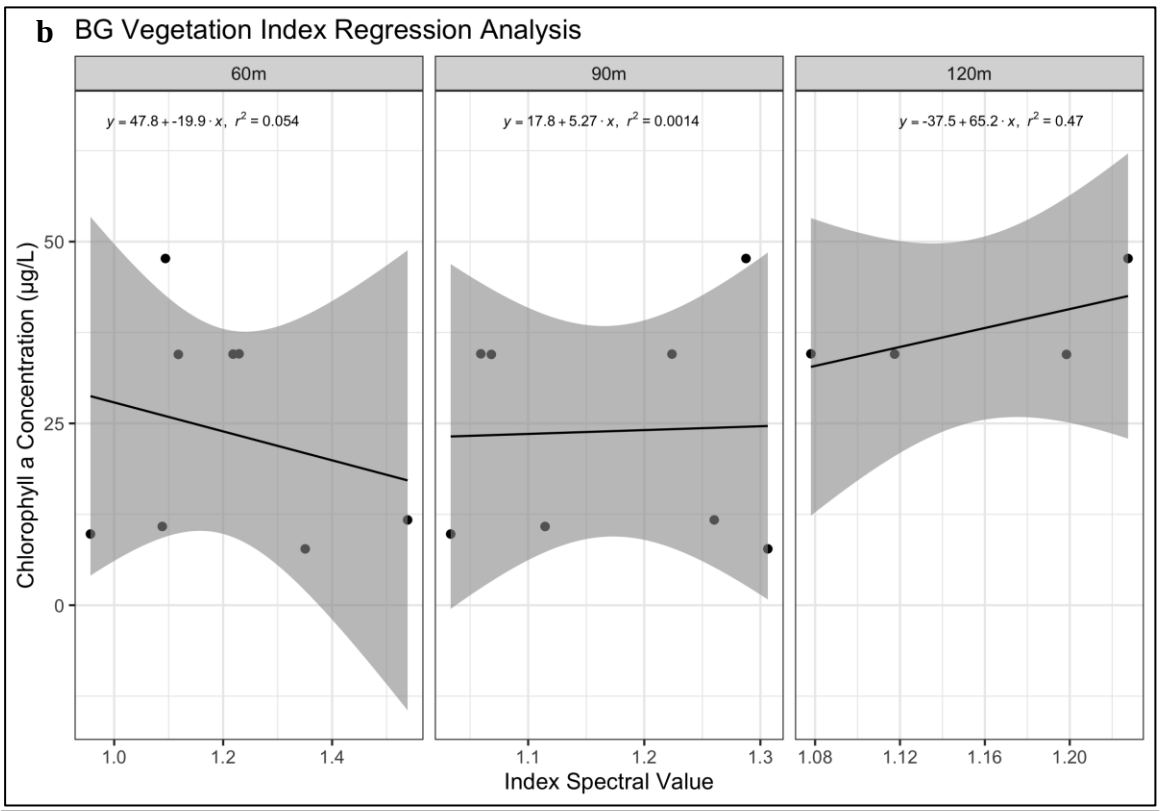

Figure A4a-b. NDVI (a) and B/G (b) Simple Linear Regression Analysis Plots.

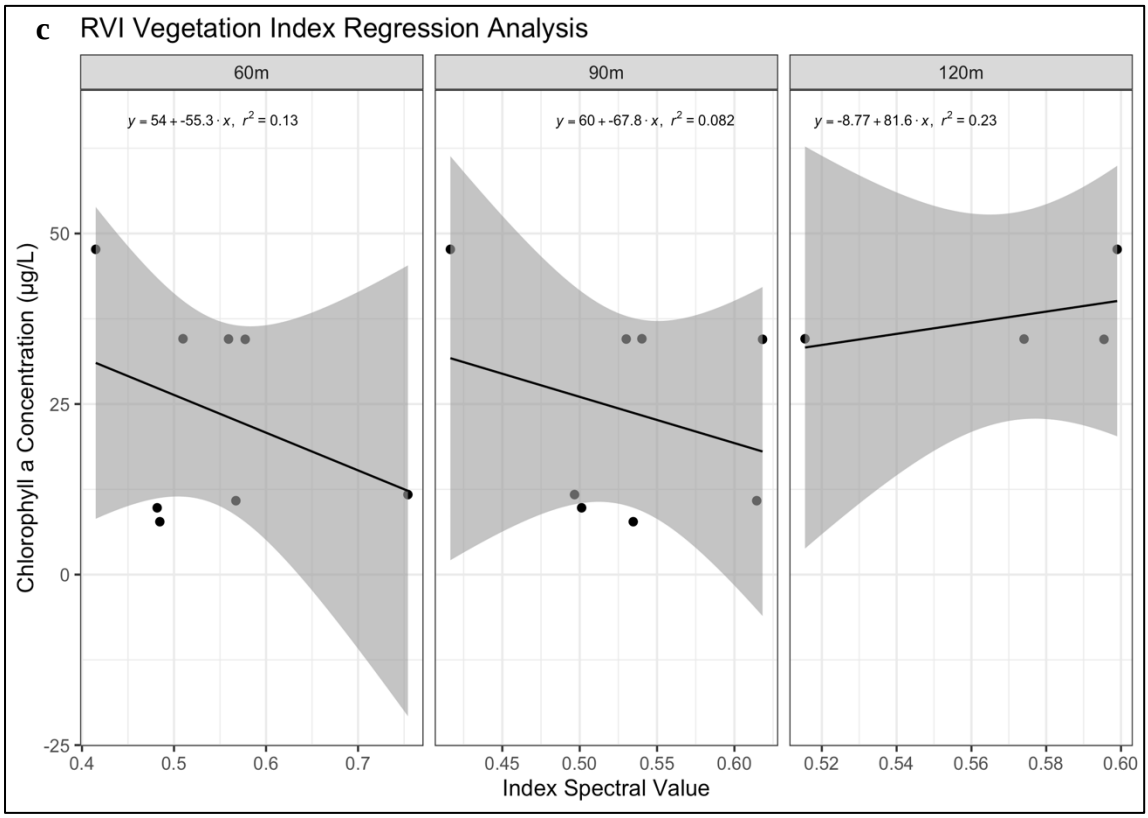

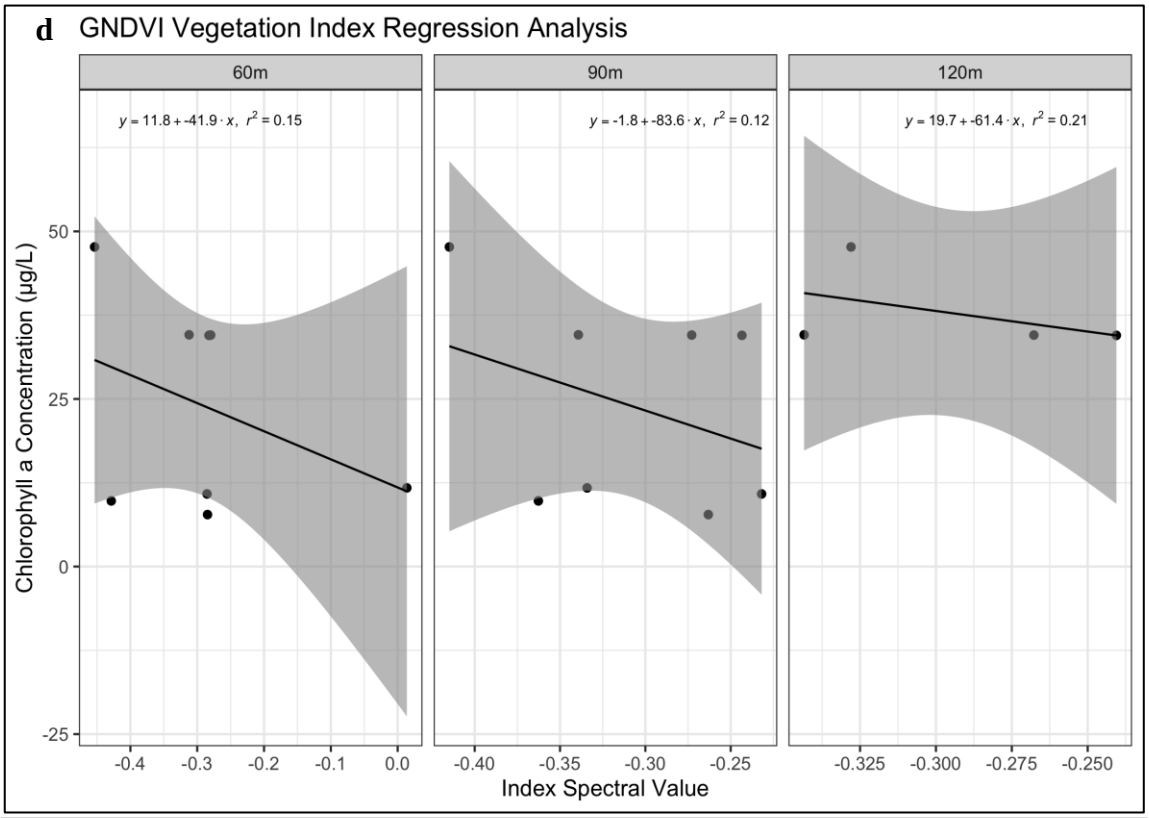

Figure A4c-d. RVI (c) and GNDVI (d) Simple Linear Regression Analysis Plots.

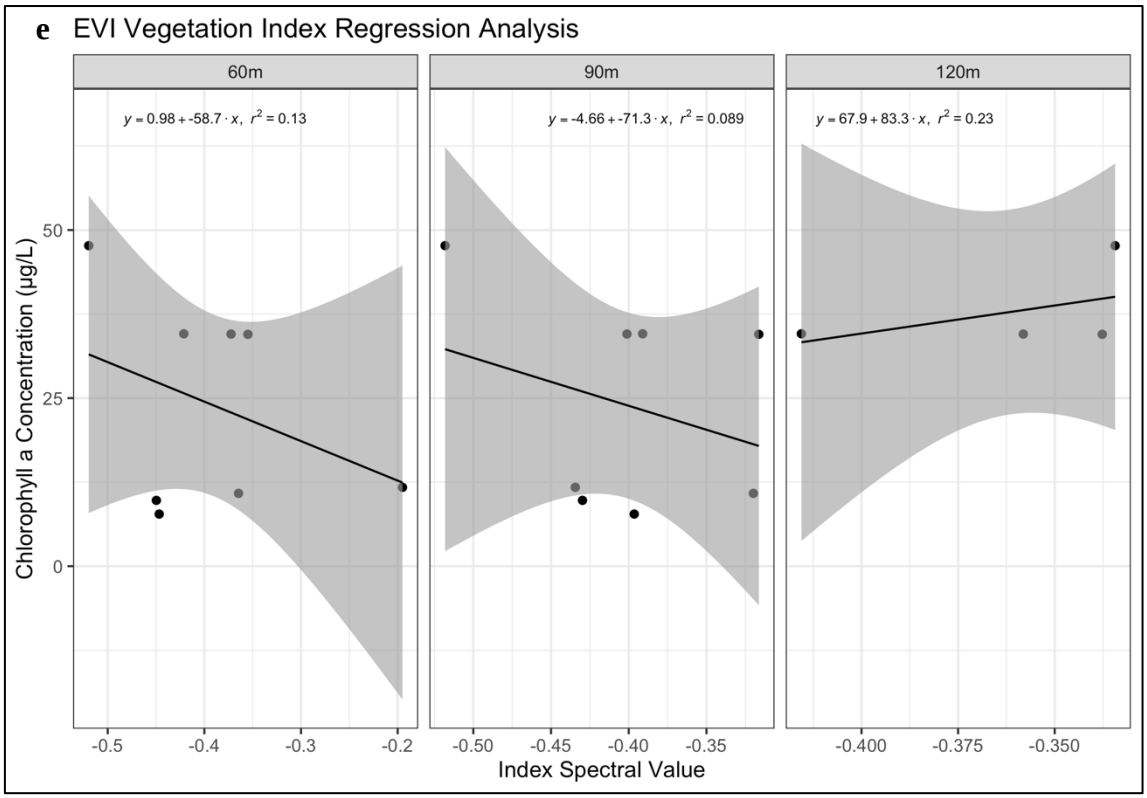

Figure A4e. EVI (also EVI2) Simple Linear Regression Analysis Plots.

Appendix I. Selected Site Photographs

Aerial view of Echo Lake, facing north. Dated 06/23/2023.

Aerial view of Echo Lake during HCB, facing north. Dated 10/07/2023.